frontiers | Research Topics

Novel strategies targeting obesity and metabolic diseases, volume II

Edited by
Xinran Ma, Lingyan Xu, Yan Lu, Dechun Feng,
Nuo Sun and Jiqiu Wang

Published in
Frontiers in Physiology

ISSN 1664-8714
ISBN 978-2-8325-4449-5
DOI 10.3389/978-2-8325-4449-5

About Frontiers

Frontiers is more than just an open access publisher of scholarly articles: it is a pioneering approach to the world of academia, radically improving the way scholarly research is managed. The grand vision of Frontiers is a world where all people have an equal opportunity to seek, share and generate knowledge. Frontiers provides immediate and permanent online open access to all its publications, but this alone is not enough to realize our grand goals.

Frontiers journal series

The Frontiers journal series is a multi-tier and interdisciplinary set of open-access, online journals, promising a paradigm shift from the current review, selection and dissemination processes in academic publishing. All Frontiers journals are driven by researchers for researchers; therefore, they constitute a service to the scholarly community. At the same time, the *Frontiers journal series* operates on a revolutionary invention, the tiered publishing system, initially addressing specific communities of scholars, and gradually climbing up to broader public understanding, thus serving the interests of the lay society, too.

Dedication to quality

Each Frontiers article is a landmark of the highest quality, thanks to genuinely collaborative interactions between authors and review editors, who include some of the world's best academicians. Research must be certified by peers before entering a stream of knowledge that may eventually reach the public - and shape society; therefore, Frontiers only applies the most rigorous and unbiased reviews. Frontiers revolutionizes research publishing by freely delivering the most outstanding research, evaluated with no bias from both the academic and social point of view. By applying the most advanced information technologies, Frontiers is catapulting scholarly publishing into a new generation.

What are Frontiers Research Topics?

Frontiers Research Topics are very popular trademarks of the *Frontiers journals series*: they are collections of at least ten articles, all centered on a particular subject. With their unique mix of varied contributions from Original Research to Review Articles, Frontiers Research Topics unify the most influential researchers, the latest key findings and historical advances in a hot research area.

Find out more on how to host your own Frontiers Research Topic or contribute to one as an author by contacting the Frontiers editorial office: frontiersin.org/about/contact

Novel strategies targeting obesity and metabolic diseases, volume II

Topic editors

Xinran Ma — East China Normal University, China
Lingyan Xu — East China Normal University, China
Yan Lu — Fudan University, China
Dechun Feng — National Institute on Alcohol Abuse and Alcoholism (NIH), United States
Nuo Sun — The Ohio State University, United States
Jiqiu Wang — Shanghai Jiao Tong University, China

Citation

Ma, X., Xu, L., Lu, Y., Feng, D., Sun, N., Wang, J., eds. (2024). *Novel strategies targeting obesity and metabolic diseases, volume II*. Lausanne: Frontiers Media SA. doi: 10.3389/978-2-8325-4449-5

Table of contents

05 Editorial: Novel strategies targeting obesity and metabolic diseases, volume II
Xinran Ma, Dechun Feng, Yan Lu, Nuo Sun, Jiqiu Wang and Lingyan Xu

07 Effect of a 12-Week Concurrent Training Intervention on Cardiometabolic Health in Obese Men: A Pilot Study
Francisco J. Amaro-Gahete, Jesús G. Ponce-González, Juan Corral-Pérez, Daniel Velázquez-Díaz, Carl J. Lavie and David Jiménez-Pavón

17 Pilates for Overweight or Obesity: A Meta-Analysis
Yi Wang, Zehua Chen, Zugui Wu, Xiangling Ye and Xuemeng Xu

30 Association of Metabolic Syndrome With Prevalence of Obstructive Sleep Apnea and Remission After Sleeve Gastrectomy
Yufei Chen, Lijia Chen, Lingxia Ye, Jiabin Jin, Yingkai Sun, Ling Zhang, Shaoqian Zhao, Yifei Zhang, Weiqing Wang, Weiqiong Gu and Jie Hong

38 Adiposity Measurements and Metabolic Syndrome Are Linked Through Circulating Neuregulin 4 and Adipsin Levels in Obese Adults
Dan Guo, Jianfang Liu, Peizhen Zhang, Xiaoyu Yang, Deying Liu, Jiayang Lin, Xueyun Wei, Bingyan Xu, Chensihan Huang, Xuan Zhou, Fei Teng, Hong Zhu and Huijie Zhang

47 Nobiletin Alleviates Non-alcoholic Steatohepatitis in MCD-Induced Mice by Regulating Macrophage Polarization
Si-wei Wang, Tian Lan, Hao Sheng, Fang Zheng, Mei-kang Lei, Li-xia Wang, Hang-fei Chen, Chun-yi Xu and Feng Zhang

59 Myogenetic Oligodeoxynucleotide (myoDN) Recovers the Differentiation of Skeletal Muscle Myoblasts Deteriorated by Diabetes Mellitus
Shunichi Nakamura, Shinichi Yonekura, Takeshi Shimosato and Tomohide Takaya

72 Altered Jagged1-Notch1 Signaling in Enhanced Dysfunctional Neovascularization and Delayed Angiogenesis After Ischemic Stroke in HFD/STZ Induced Type 2 Diabetes Rats
Zhihui Guo, Jia Jia, Yanling Tu, Chang Jin, Cen Guo, Feifei Song, Xuqing Wu, Haifeng Bao and Wei Fan

87 Serum Adropin as a Potential Biomarker for Predicting the Development of Type 2 Diabetes Mellitus in Individuals With Metabolic Dysfunction-Associated Fatty Liver Disease
Na Li, Guomin Xie, Biao Zhou, Aijuan Qu, Hua Meng, Jia Liu and Guang Wang

95 The G2A Receptor Deficiency Aggravates Atherosclerosis in Rats by Regulating Macrophages and Lipid Metabolism
Xueqin Cui, Roumei Xing, Yue Tian, Man Wang, Yue Sun, Yongqian Xu, Yiqing Yang, Yongliang Zhao, Ling Xie, Yufang Xiao, Dali Li, Biao Zheng, Mingyao Liu and Huaqing Chen

108 Liver Zonation – Revisiting Old Questions With New Technologies
Rory P. Cunningham and Natalie Porat-Shliom

frontiers | Frontiers in Physiology

TYPE Editorial
PUBLISHED 30 January 2024
DOI 10.3389/fphys.2024.1342943

OPEN ACCESS

EDITED AND REVIEWED BY
Johannes Van Lieshout,
University of Amsterdam, Netherlands

*CORRESPONDENCE
Lingyan Xu,
lyxu@bio.ecnu.edu.cn

RECEIVED 22 November 2023
ACCEPTED 22 January 2024
PUBLISHED 30 January 2024

CITATION
Ma X, Feng D, Lu Y, Sun N, Wang J and Xu L (2024), Editorial: Novel strategies targeting obesity and metabolic diseases, volume II. *Front. Physiol.* 15:1342943. doi: 10.3389/fphys.2024.1342943

Editorial: Novel strategies targeting obesity and metabolic diseases, volume II

Xinran Ma[1], Dechun Feng[2], Yan Lu[3], Nuo Sun[4], Jiqiu Wang[5] and Lingyan Xu[1]*

[1]Shanghai Key Laboratory of Regulatory Biology, Institute of Biomedical Sciences and School of Life Sciences, East China Normal University, Shanghai, China, [2]National Institute on Alcohol Abuse and Alcoholism (NIAAA), National Institutes of Health (NIH), Bethesda, MD, United States, [3]Institute of Metabolism and Regenerative Medicine, Shanghai Sixth People's Hospital Affiliated to Shanghai Jiao Tong University School of Medicine, Shanghai, China, [4]Wexner Medical Center, The Ohio State University, Columbus, OH, United States, [5]National Key Laboratory for Medical Genomes, Department of Endocrinology and Metabolism, China National Research Center for Metabolic Diseases, Ruijin Hospital, Shanghai Jiao Tong University School of Medicine (SJTUSM), Shanghai, China

KEYWORDS

obesity, metabolic diseases, adipose tissue, liver, muscle

Editorial on the Research Topic
Novel strategies targeting obesity and metabolic diseases, volume II

Obesity and metabolic diseases including type 2 diabetes, cardiovascular disease, atherosclerosis, non-alcoholic fatty liver diseases (NAFLD), and obstructive sleep apnea threaten human health and life quality. In the second volume of this Frontiers Research Topic, we pay special attention to recent clinic advances and focusing on the contribution of previously unappreciated cell types, including macrophages and vascular endothelial cells, to these metabolic diseases.

Firstly, maintaining systemic homeostasis needs the coordination of different organs in the body. Adipose tissue and liver produce and secrete specific organokines such as adipokines and hepatokines in response to nutritional and environmental stimuli, while dysregulation of these organokines causes metabolic diseases, thus making them potential clinical biomarkers and therapeutic targets. As adipokines, Nrg4 increases brown adipose tissue activity, drive the browning of white adipose tissue, prevent lipogenesis in the liver, and improve insulin sensitivity, while adipsin increases adipogenesis and lipid accumulation. Guo et al. indicated that adiposity measurements, including waist circumference, visceral fat level, and muscle mass to visceral fat ratio are closely linked with circulating Nrg4 and adiposin levels in obese adults in a cohort of 1,212 subjects, thus provides clinical relevance of these adipokines with metabolic diseases. Meanwhile, Adropin is a hepatokine that improves glucose homeostasis, dyslipidemia, obesity-associated hyperinsulinemia, and energy homeostasis. Li et al. demonstrated that metabolic dysfunction-associated fatty liver disease (MAFLD) is correlated with adropin levels. Adropin plasma levels in MALFD and type 2 diabetes patients were lower than healthy control subjects. Serum adropin concentrations were negatively correlated with intrahepatic triglyceride, total cholesterol, and NAFLD activity score.

Secondly, external interventions like physical activity, provide valuable therapeutic opportunities to control body weights and reduce the risk of cardiovascular diseases, while different exercise protocols may lead to various outcomes. Amaro-Gahete et al. performed a

pilot study with 12-week concurrent training intervention in 12 obese men and found significant decrease in weight, body mass index, fat mass, blood pressure and cardiometabolic risk. Meanwhile, Wang et al. performed meta-analysis on eleven randomized controlled trials (RCT) with 393 subjects comparing Pilates with other physical exercises or without any intervention. The results showed that Pilates dramatically reduces body weight, BMI, and body fat percentage in adults with overweight or obesity. In addition, Nakamura et al. developed myogenetic oligodeoxynucleotides (myoDNs), which are 18-base single-strand DNAs that promote myoblast differentiation by targeting nucleolin. They applied a myoDN, iSN04, to myoblasts isolated from healthy subjects and patients with type 1 or type 2 diabetes. iSN04 treatment improved differentiation of myoblasts from diabetic patients by downregulating myostatin and interleukin-8. These studies confirmed the importance of exercise in improving metabolic health and possibility of iSN04 as a nucleic acid drug targeting myoblasts for the prevention and treatment of muscle wasting in patients with diabetes.

In addition, bariatric surgery has been shown to effectively reduce weight and obesity-related comorbidities. Obstructive sleep apnea (OSA) is a sleep-related breathing disorder and an independent risk factor for cardiovascular diseases. Chen et al. performed a cross-sectional study involving 123 metabolically healthy obese patients and 200 age- and BMI-matched metabolically unhealthy obese patients to estimate the prevalence of OSA at baseline, as well as a retrospective study including 67 patients who underwent laparoscopic sleeve gastrectomy to evaluate the remission of OSA. The results suggested that, in patients with obesity, metabolic syndrome does not add extra risk for the prevalence or severity of OSA, while both metabolically healthy and unhealthy obese patients could benefit equally from laparoscopic sleeve gastrectomy in terms of weight loss and obstructive sleep apnea remission, suggesting bariatric surgery is a promising surgery for obesity and metabolic diseases.

Thirdly, metabolic organs consist of numerous cell types that play vital roles in the pathogenesis of metabolic diseases. Macrophage is the predominant immune cell type in metabolic tissues and arteries and plays vital roles in the progression of obesity, liver diseases and atherosclerosis. Cui et al. demonstrated that the orphan G protein-coupled receptor G2A modulates lipid metabolism and atherosclerosis in low-density lipoprotein receptor deficient ($Ldlr^{-/-}$) rats as shown by exacerbated atherosclerotic plaques in $G2a^{-/-}Ldlr^{-/-}$ double knockout rats, together with increased oxidative stress and macrophage accumulation due to increased migration and reduced apoptosis via PI3K/AKT pathway. Meanwhile, Non-alcoholic steatohepatitis (NASH) is an inflammatory disorder that is characterized by chronic activation of the hepatic inflammatory response and subsequent liver damage. Wang et al. demonstrated that the Nobiletin, a natural polymethoxylated flavone and a reported retinoic-acid-related orphan receptor α (RORα) activator, reduced the infiltration of macrophages and neutrophils and promoted M1 to M2 macrophage polarization via Krüppel-like factor 4 (KLF4) in the liver in MCD fed mice. In addition, diabetes exacerbates brain damage in cerebral ischemic stroke. Guo et al. found dysfunctional neovascularization with activated Jagged1-Notch1 signaling in the cerebrovasculature before cerebral ischemia in diabetic rats compared with non-diabetic rats, as well as delayed angiogenesis and suppressed Jagged1-Notch1 signaling after ischemic stroke. The dynamic regulation of Jagged1-Notch1 signaling is vital for diabetes-related cerebral microvasculature dysfunction after ischemic stroke. These results revealed the unappreciated roles of macrophages or endothelial cells in metabolic diseases.

Last but not the least, the complexity of physiology and architecture of liver is highly related to spatial compartmentalization known as liver zonation. Cunningham et al. reviewed recent advances in examining liver zonation and elucidating the regulatory mechanisms via single cell analysis and imaging technologies. Understanding the spatial organization of metabolism is vital to extend our knowledge of liver disease and to provide targeted therapeutic avenues.

In conclusion, the current Research Topic provides comprehensive and in-depth understandings on diagnostic biomarkers, clinical advances, unappreciated cell types and molecular mechanisms, thus overall provide latest trends and technique advances towards therapeutic strategies to combat obesity and metabolic diseases.

Author contributions

XM: Writing–original draft, Writing–review and editing. DF: Writing–review and editing. YL: Writing–review and editing. NS: Writing–review and editing. JW: Writing–review and editing. LX: Writing–review and editing, Writing–original draft.

Funding

The author(s) declare that no financial support was received for the research, authorship, and/or publication of this article.

Conflict of interest

The authors declare that the research was conducted in the absence of any commercial or financial relationships that could be construed as a potential conflict of interest.

Publisher's note

frontiers in Physiology

ORIGINAL RESEARCH
published: 11 February 2021
doi: 10.3389/fphys.2021.630831

Effect of a 12-Week Concurrent Training Intervention on Cardiometabolic Health in Obese Men: A Pilot Study

Francisco J. Amaro-Gahete[1,2], Jesús G. Ponce-González[3,4], Juan Corral-Pérez[3,4], Daniel Velázquez-Díaz[3,4], Carl J. Lavie[5] and David Jiménez-Pavón[3,4]**

[1] EFFECTS-262 Research group, Department of Physiology, Faculty of Medicine, University of Granada, Granada, Spain, [2] PROmoting FITness and Health Through Physical Activity Research Group, Department of Physical Education and Sports, Faculty of Sport Sciences, University of Granada, Granada, Spain, [3] MOVE-IT Research Group, Department of Physical Education, Faculty of Education Sciences, University of Cádiz, Cádiz, Spain, [4] Biomedical Research and Innovation Institute of Cádiz Research Unit, Puerta del Mar University Hospital, University of Cádiz, Cádiz, Spain, [5] Department of Cardiovascular Diseases, John Ochsner Heart and Vascular Institute, Ochsner Clinical School, The University of Queensland School of Medicine, New Orleans, LA, United States

OPEN ACCESS

Edited by:
Lingyan Xu,
East China Normal University, China

Reviewed by:
Heikki Kainulainen,
University of Jyväskylä, Finland
Ashril Yusof,
University of Malaya, Malaysia
Idoia Labayen,
Public University of Navarre, Spain

***Correspondence:**
Francisco J. Amaro-Gahete
amarof@ugr.es
David Jiménez-Pavón
david.jimenez@uca.es

Specialty section:
This article was submitted to Clinical and Translational Physiology, a section of the journal Frontiers in Physiology

Received: *18 November 2020*
Accepted: *18 January 2021*
Published: *11 February 2021*

Citation:
Amaro-Gahete FJ, Ponce-González JG, Corral-Pérez J, Velázquez-Díaz D, Lavie CJ and Jiménez-Pavón D (2021) Effect of a 12-Week Concurrent Training Intervention on Cardiometabolic Health in Obese Men: A Pilot Study. Front. Physiol. 12:630831. doi: 10.3389/fphys.2021.630831

The present study aimed to investigate the effects of a 12-week concurrent training intervention on cardiometabolic health in obese men. Twelve obese men (42.5 ± 5.3 years old) participated in the current 12−week randomized controlled trial with a parallel group design. The participants were randomly assigned to a concurrent training group or to a no-exercise control group. Anthropometry and body composition assessment were determined by electrical bio-impedance. Blood samples were obtained and a cardiometabolic risk Z-Score was calculated. Energy metabolism-related parameters [i.e., resting metabolic rate (RMR), respiratory quotient (RQ), and substrate oxidation in both resting conditions and during exercise] were determined by indirect calorimetry. Echocardiographic studies were performed using an ultrasound system equipped with a transducer to measure cardiac function. A significant decrease of weight ($\Delta = -4.21$ kg; i.e., primary outcome), body mass index ($\Delta = -1.32$ kg/m^2), fat mass (FM; $\Delta = -3.27$ kg), blood pressure (BP; $\Delta = -10.81$ mmHg), and cardiometabolic risk Z-Score ($\Delta = -0.39$) was observed in the exercise group compared with the control group (all $P < 0.05$), while no significant changes were noted in waist circumference (WC), lean mass (LM), bone mineral content, glycemic and lipid profiles, liver function, nor in energy metabolism-related parameters (all $P > 0.1$). Moreover, a significant increment of left ventricular (LV) end diastolic diameter ($\Delta = -4.35$ mm) was observed in the exercise group compared with the control group ($P = 0.02$). A 12-week concurrent training intervention is an effective strategy to induce weight and fat loss with simultaneous reductions of BP and cardiometabolic risk, and improving cardiac function in obese men.

Keywords: concurrent training, cardiac function, obesity, body composition, energy metabolism

INTRODUCTION

Globally, obesity has reached epidemic proportions in the current 21st century and is associated with higher risk of premature mortality (Lavie et al., 2018b). Indeed, obesity is an independent risk factor for cardiovascular (CV) disease (CVD, including hypertension, coronary heart disease, heart failure, and sudden cardiac death) (Go et al., 2014; Ng et al., 2014; Jaacks et al., 2019; Jiménez-Pavón et al., 2019), and has been connected with several comorbidities, including dyslipidemia, insulin resistance, diabetes mellitus (DM), low metabolic flexibility, or left ventricular (LV) hypertrophy, among others (Perumareddi, 2019). Health care spending derived from obesity-related diseases has exponentially increased during the last decade and is expected to continue rising (Lavie et al., 2018a). Therefore, the application of cost-effective measures to reduce obesity and its related health burden are of clinical and scientific interest.

Over the past years, different strategies have been found to improve cardiometabolic health in individuals with obesity. Physical activity (PA) is considered an integral approach for obese individuals, not only for weight loss goals but also for reducing the risk of CVD, type 2 DM, and all-cause mortality (Petridou et al., 2018). World Health Organization has recently updated a consensus statement regarding the global recommendations on PA for health promotion (i.e., 150 or 75 min per week of moderate or vigorous intensity aerobic PA/exercise, respectively, plus resistance exercise twice per week; World Health Organization [WHO], 2015; Piercy et al., 2018). The combination of aerobic and resistance training (i.e., concurrent training) has been positioned as a promising tool to improve CV and metabolic profiles in both healthy individuals (Bennie et al., 2018) and patients with cardiometabolic diseases (Álvarez et al., 2019). Concretely, previous studies have reported that concurrent training is an effective antihypertensive (Corso et al., 2016) and anti-inflammatory therapy (Libardi et al., 2012), improving in turn the glycemic and lipid profiles (Braga de Mello et al., 2019) as well as hepatic function (Monteiro et al., 2015). Nevertheless, these previous studies included individuals with different biological characteristics making it necessary for further investigations attaining patients with cardiometabolic disturbances.

To the best of our knowledge, there is a lack of studies in obese persons investigating not only the effects of concurrent training on body composition and cardiometabolic profile, but also on liver function, energy metabolism, or CV function, all of them involved in further obesity-related complications. Concretely, metabolic flexibility (i.e., the ability to respond or adapt to conditional changes in metabolic demand) has been propagated to explain insulin resistance and mechanisms governing fuel selection between glucose and fatty acids, highlighting that patients with obesity and type 2 diabetes suffer from metabolic inflexibility. Similarly, liver function alterations such **a**s non-alcoholic fatty liver disease **are** usually present in patients with metabolic syndrome and central abdominal obesity (Milić et al., 2014). Considering obesity as a multifactorial disease, it would be of clinical interest to understand the specific effects of concurrent training on those parameters which are altered in obese persons. Therefore, the present study aimed to investigate the effects of a 12-week concurrent training intervention on cardiometabolic health (i.e., body composition, glycemic and lipid profiles, liver function, energy metabolism, and cardiac function) in obese men.

MATERIALS AND METHODS

Research Design and Subjects

A 12-week intervention study with a parallel-group design was conducted following the Consolidated Standards of Reporting Trials guidelines (Welch et al., 2017). After the baseline assessment, participants were randomly assigned into two different groups using computer-generated simple randomization: (i) the control group (no exercise—maintaining their habitual lifestyle) and (ii) the concurrent training group. The participant' allocation was blinded to the assessment staff. Participants were instructed to maintain their dietary and PA habits. The same exercise intervention was offered to the participants of the control group after completing the intervention.

Participants were obese sedentary men (35–55 years) with no comorbidities. The experimental design and study protocols were conducted strictly following the last revised ethical guidelines of the Declaration of Helsinki. The current pilot study was approved by the Ethics Committee on Human Research at the University of Leon and all participants signed an informed consent. The participants were recruited from the province of Cadiz (Spain) using social networks and local media. Inclusion criteria were: (i) to have a BMI > 30 kg/m^2; (ii) to be sedentary [less than 150 min/week of moderate-intensity PA (i.e., self-reported) over the last 6 months]; (iii) to present a stable weight over the last 12 weeks; (iv) to be free of any chronic disease that could be aggravated by exercise training; and (v) not to consume any chronic mediation (i.e., self-reported) over the last 6 months. Baseline and follow-up assessment were performed at the same setting (Physical Activity and Exercise physiology Laboratory at the Faculty of Education Sciences, University of Cádiz).

Concurrent Training Intervention

The participants included in the concurrent training group performed a 12-week intervention based on the updated PA recommendations provided by the World Health Organization (World Health Organization [WHO], 2015). All sessions were conducted under the supervision of an accredited exercise physiologist. A training frequency of three sessions/week was selected. Each training session lasted 60 min and consisted of a combination of aerobic and resistance exercises. Aerobic training intensity was fixed at 60–70% of the heart rate reserve, while resistance training intensity was set at 6–7 of their subjective rates of perceived exertion. The participants were instructed to complete three to four sets which included a total of six to eight aerobic and resistance exercises following a circuit training

methodology. The rest between sets was 60–120 s. Treadmill and cycle-ergometer were used to complete the aerobic training, whereas weight bearing and free-weights exercises (i.e., using both dumbbells and bars) were used to perform the resistance training involving the main upper and lower body muscle groups (i.e., lateral pull down, dips, deadlift, squat, or bench press among others). A dynamic standardized warm-up was performed before the beginning of the main part based on mobility and activation exercises, and a cooling-down protocol (i.e., stretching exercises) was conducted at the end of the training session. Exercise' intensity was continuously monitored during all sessions using a Polar team 2 system (Polar Team 2 system, Polar Electro Oy, Kempele, Finland). No adverse events were observed.

Procedures

The baseline and post-intervention measurement were organized on 2 days: (i) day 1: medical examination and fasting blood determinations and (ii) day 2: anthropometry and body composition, blood pressure (BP), energy metabolism-related parameters, cardiorespiratory fitness (CRF), and echocardiography. We also used accelerometers to objectively measure PA and we controlled the dietary intake by three 24 h recalls.

Anthropometry and Body Composition

Anthropometry and body composition assessments were conducted before and after the intervention program. Weight (primary outcome) and height were determined using a validated scale and stadiometer (SECA 225, Hamburg, Germany) without shoes and with light clothing. Subsequently, the BMI was calculated as weight divided by height^2. Waist circumference (WC) was measured at the mid-point between the bottom of the rib cage and the iliac crest at the end of a normal expiration.

Electrical bio-impedance (TANITA-MC780MA, Barcelona, Spain) was used to estimate fat mass (FM), lean mass (LM), and bone mineral content (g) following the manufacturer's recommendations.

Blood Samples

Venous blood samples were obtained from the antecubital vein and collected in ethylenediamine tetra-acetic acid-containing tubes in fasting conditions. All samples were centrifuged at 4000 r/min for 10 min at 4°C, and subsequently stored at −80°C until further analysis. Plasma glucose, insulin, total cholesterol, high-density lipoprotein cholesterol (HDL-C), triglycerides (TGs), glutamic oxaloacetic transaminase (GOT), glutamic-pyruvic transaminase (GPT), γ-glutamyl transferase (γ-GT), C-reactive protein (CRP), and leptin were determined using conventional methods (i.e., spectrophotometry, chemiluminescence assay, and enzyme-linked immunosorbent assay). The homeostatic model assessment of insulin resistance (HOMA-IR) index was then calculated as (*plasma insulin*) × *plasma glucose*/22.5 (Ascaso et al., 2001). Low-density lipoprotein cholesterol (LDL-C) was determined as (*total cholesterol*) – (*HDL-C*) – 0.45 × (*TGs*). Fatty liver index was also calculated using a previously validated equation (Bedogni et al., 2006):

$$\textit{Fatty Liver Index (FLI)} = \left(e^{0.953 * \log e(TGs) + 0.139 * BMI + 0.718 * \log e(\gamma\text{-GT}) + 0.053 * \text{WC} - 15.745)}\right) * 100$$

A cardiometabolic risk Z-score was determined considering the clinical parameters proposed by the International Diabetes Federation to diagnose metabolic syndrome (Carracher et al., 2018) (i.e., WC, BP, plasma glucose, HDL-C, and TGs). These outcomes were standardized as (*value – mean*)/*standard deviation*. HDL-C standardized value was multiplied by −1 since we aimed to reflect a high cardiometabolic risk with higher values. The mean of the five standardized values was considered the cardiometabolic risk Z-score obtaining a standard deviation of 1 and a mean of 0 by definition.

BP

Participants were sitting in a chair, relaxed with their feet firmly on the floor. After 5 min, systolic and diastolic BPs were assessed using an automatic monitor Omron M3 intelligence advice (HEM-7051-E, Kyoto, Japan), which has been previously validated, on the non-dominant arm following the recommendations of the European Heart Society (Whelton and Williams, 2018). A minimum of three measurements were taken 1 min apart, and the mean value was subsequently calculated as:

$$\text{Mean arterial BP (MAP)} = \frac{\textit{Systolic BP} + (2 * \textit{Dyastolic BP})}{3}$$

Energy Metabolism

Resting metabolic rate (RMR) was assessed in the morning after an overnight fast. We instructed the participants to avoid any exertion after waking up the testing day, to refrain from any moderate or vigorous PA before the testing (i.e., 24 and 48 h, respectively), to sleep as usual, to maintain their usual diet and to avoid the intake of alcohol and caffeine the day before. The environmental conditions were strictly controlled (temperature 20–22°C, humidity 60–65%). After their lab arrival, the participants were instructed to lie on a comfortable bed in a supine position for 5 min before the beginning of the RMR test that lasted 30 min (Fullmer et al., 2015). Oxygen consumption and carbon dioxide production were obtained by indirect calorimetry methods using a metabolic cart Jaeger MasterScreen CPX® (CareFusion, San Diego, CA, United States) which was previously calibrated following the manufacturer's guidelines (i.e., gas and volume calibrations). The participants were asked not to sleep, talk, or fidget, and to breath normally. For the calculation of the RMR, we averaged the ventilatory parameters every 20 s. The first 10 min was discarded (Fullmer et al., 2015), and we calculated the coefficients of variance (CV) for oxygen consumption, carbon dioxide production, respiratory quotient (RQ), and minute ventilation every 5 min period (Fullmer et al., 2015; Sanchez-Delgado et al., 2018). Then, the periods that met the steady-state criteria for the ventilatory parameters (i.e., CV < 10%

for oxygen consumption, CV < 10% for carbon dioxide production, CV < 5% for RQ, and CV < 10% for minute ventilation) were chosen, considering the period with the lowest average CV for these ventilatory outcomes for further analysis (Fullmer et al., 2015; Sanchez-Delgado et al., 2018). RMR and substrates oxidation (i.e., fat and carbohydrate oxidation) were determined through the stoichiometry equations of Weir and Frayn, respectively.

Maximal fat oxidation (MFO) and the intensity that elicits MFO (Fat_{max}) were determined through a graded exercise test on cycloergometer (Lode Excalibur, Groningen, Netherlands). This test consisted on cycling at 15 W keeping a constant cadence of 60–80 r/min for 3 min increasing the workload 15 W every step until reaching an RQ of 1.0 (Tsujimoto et al., 2011). Oxygen consumption and carbon dioxide production were determined by indirect calorimetry during the exercise protocol, using a metabolic cart Jaeger MasterScreen CPX® (CareFusion, San Diego, CA, United States), previously calibrated as explained above, and employing a face mask equipped with a metabolic flow sensor (CareFusion, San Diego, CA, United States) for gas data collection. We averaged the ventilatory parameters every 20 s, and fat oxidation values were estimated considering oxygen consumption and carbon dioxide production values averaged over the final 1 min of each 3-min stage (Amaro-Gahete et al., 2019c), using the Frayn stoichiometric equation and considering the urinary nitrogen excretion as negligible. MFO and Fat_{max} were calculated using a third polynomial regression curve with an intersection at 0;0, plotting fat oxidation values obtained in each period of the graded exercise test against the relative exercise intensity (Amaro-Gahete et al., 2019c).

Dietary Intake

Dietary intake was determined by a qualified and trained researcher on diet assessments through three non-consecutive 24 h recalls (including one weekend day). Food consumption was obtained by the DIAL® software for Windows, version 3.7.1.0. Subsequently, food consumption was transformed into energy and macronutrient intakes.

PA and Sedentary Behavior (SB)

Levels of PA and sedentary behavior (SB) were measured with a hip-worn ActiGraph GT3X + accelerometer (ActiGraph, Pensacola, FL, United States). The participants were asked to wear the accelerometer for seven consecutive days during the 24 h. After data collection, the ActiLife v.6.2.2 software (ActiGraph, Pensacola, FL, United States) was used to their processing, excluding those participants that did not wear the accelerometer for at least 16 h/day during at least 4 days (including at least one weekend day).

CRF

Maximum oxygen uptake (VO_{2max}) was determined just after the MFO and Fat_{max} determination. After a short break (≈3 min), the second phase of the graded exercise test was initiated starting with the last step' intensity of the previous phase and increasing the load 15 W each minute. The participants were asked to maintain a constant cadence of 60–80 r/min until they reached voluntary exhaustion. Oxygen consumption and carbon dioxide production were also obtained via indirect calorimetry, gathering data as for MFO and Fat_{max} testing (see above). The criteria for achieving VO_2max were: (i) to attain an RQ higher than 1.1, (ii) to reach a plateau in oxygen consumption (change lower than 100 mL/min in the last 30-s stages), and (iii) to show a heart rate between 10 beats/min of the age-predicted maximal heart rate (Midgley et al., 2007; Amaro-Gahete et al., 2019a). We considered the peak oxygen uptake value during the exercise test when these criteria were not met (Midgley et al., 2007; Amaro-Gahete et al., 2019a).

Echocardiography

Echocardiographic studies were performed by single experienced cardiologist (blinded to the participants' assignment group) using an ultrasound system (Sonosite-Edge, Amsterdam, Netherlands) equipped with a transducer. Cardiac mass, volumes, and dimensions were measured according to the current recommendations. Mitral inflow velocities were determined using pulsed-wave Doppler recording velocities end-expiration. LV diastolic function was measured following the EAE/ASE consensus guidelines (Nagueh et al., 2008) obtaining E wave, A wave, E/A ratio, and E wave deceleration time.

Statistical Analysis

Descriptive and exploratory analyses of all the study outcomes were conducted to check statistical assumptions, distributions, and imbalances between the study groups. Student's *t*-tests for unpaired values were applied to determine intergroup differences (i.e., control vs. intervention group) at the baseline in the study' outcomes. The intervention effects on primary and secondary parameters were assessed through linear mixed-effects models considering individual measures of growth as the function of randomly assigned group, time, and its interaction. We conducted these estimations using the restricted maximum-likelihood method which includes an unstructured covariance matrix to adjust for within-participant clustering resulting from the repeated-measures design. We adjusted the model for the baseline values of each outcome analyzed. Lastly, we also calculated the standardized effect sizes using Cohen's d coefficients. The Statistical Package for the Social Sciences v.22.0, (IBM Corporation, Chicago, IL, United States) was used to perform the analyses.

RESULTS

Twelve obese sedentary men (mean age = 42.5 years) were participated in this trial. Participants attended to ≥ 86% (31 of 36 sessions) of their supervised exercise from baseline to week 12 and they showed a percentage of compliance of ∼90% for exercise' intensity and 100% for exercise' volume. There were no significant differences between groups in any variable at the baseline (all $P \geq 0.09$).

A significant decrease of weight, BMI, and FM was observed in the concurrent training group compared with the control group (all $P < 0.049$; **Table 1**), while no significant changes were noted

TABLE 1 | Changes in cardiometabolic health outcomes after 12-week intervention among control and concurrent training group.

	Control group (n = 6)			Concurrent training group (n = 6)			Net effect	
	Baseline Mean (SD)	**After 12 weeks Mean (SD)**	**Δ (SE)**	**Baseline Mean (SD)**	**After 12 weeks Mean (SD)**	**Δ (SE)**	**Mean difference (95% CI)**	**Standardized mean difference (95% CI)**
Age (years)	43.7 (6.1)			41.3 (4.4)				
Anthropometry and body composition								
Weight (kg)	101.4 (12.9)	103.5 (14.4)	2.13 (0.88)	97.5 (15.4)	95.4 (12.9)	−2.08 (1.33)	4.21 (0.45, 8.37)	1.23 (0.01, 2.45)*
Body mass index (kg/m^2)	32.5 (3.0)	33.2 (3.3)	0.65 (0.26)	32.1 (3.6)	31.4 (2.7)	−0.67 (0.42)	1.32 (0.01, 2.63)	1.23 (0.01, 2.45)*
Waist circumference (cm)	108.0 (6.1)	107.9 (8.0)	−0.05 (1.52)	105.4 (9.4)	104.1 (8.3)	−1.23 (0.98)	1.18 (− 2.79, 5.15)	0.46 (− 1.08, 1.99)
Fat mass (kg)	28.5 (7.3)	30.7 (7.6)	2.15 (0.70)	27.8 (6.6)	26.6 (4.8)	−1.12 (0.83)	3.27 (0.56, 5.97)	1.36 (0.23, 2.48)*
Lean mass (kg)	69.3 (6.9)	69.3 (7.4)	0.00 (0.71)	66.3 (9.3)	65.3 (8.4)	−0.93 (0.51)	0.93 (− 0.69, 2.56)	0.82 (− 0.61, 2.25)
Bone mineral content (kg)	3.60 (0.32)	3.58 (0.36)	−0.03 (0.03)	3.43 (0.46)	3.40 (0.41)	−0.03 (0.33)	0.01 (− 0.98, 0.11)	0.12 (− 1.45, 1.70)
Blood pressure								
Systolic blood pressure (mm Hg)	131.5 (16.9)	130.0 (18.6)	−1.50 (1.21)	131.4 (22.0)	120.2 (14.8)	−11.22 (3.63)	9.72 (0.38, 19.07)	1.15 (0.04, 2.26)*
Diastolic blood pressure (mm Hg)	83.2 (6.3)	86.9 (8.1)	3.75 (1.80)	86.6 (13.9)	79.0 (8.8)	−7.61 (3.40)	11.36 (1.02, 21.70)	1.29 (0.12, 2.47)*
Mean blood pressure (mm Hg)	99.3 (9.2)	101.3 (11.4)	2.00 (1.58)	101.5 (16.5)	92.7 (10.4)	−8.81 (3.45)	10.81 (1.79, 19.84)	1.26 (0.21, 2.30)*
Glycemic profile								
Plasma glucose (mg/dL)	101.5 (3.9)	100.3 (3.8)	−1.25 (2.21)	94.8 (9.1)	93.8 (8.5)	−1.00 (1.52)	−0.25 (− 6.39, 5.89)	−0.07 (− 1.76, 1.63)
Plasma insulin (UI/mL)	13.9 (4.2)	19.6 (11.1)	5.71 (4.00)	8.6 (2.0)	8.3 (3.8)	−0.26 (2.38)	5.97 (− 4.50, 16.44)	0.86 (− 0.65, 2.37)
HOMA-IR	3.47 (1.02)	4.84 (2.75)	1.37 (1.05)	2.00 (0.52)	1.96 (0.98)	−0.04 (0.55)	1.42 (− 1.22, 4.05)	0.82 (− 0.71, 2.35)
Lipid profile								
Total cholesterol (mg/dL)	216.0 (59.8)	212.5 (47.2)	−3.50 (15.09)	198.0 (22.6)	211.8 (42.5)	13.80 (13.4)	−17.30 (− 65.02, 30.42)	0.58 (− 2.19, 1.03)
HDL-C (mg/dL)	48.8 (9.6)	46.8 (1.7)	−2.00 (5.35)	40.8 (5.0)	43.8 (4.9)	3.00 (0.45)	−5.00 (− 16.18, 6.18)	−0.70 (− 2.28, 0.87)
LDL-C (mg/dL)	145.0 (50.3)	142.3 (41.5)	−2.75 (9.29)	130.8 (22.0)	147.6 (37.7)	16.80 (9.07)	−19.55 (− 50.60, 11.50)	−0.93 (− 2.41, 0.55)
Triglycerides (mg/dL)	112.0 (53.9)	118.5 (44.6)	6.50 (16.98)	131.4 (70.5)	102.0 (56.5)	−29.40 (30.55)	35.90 (− 53.28, 125.08)	0.64 (− 0.95, 2.24)
Liver function								
GOT (IU/L)	29.3 (8.5)	33.0 (2.8)	3.75 (2.93)	21.6 (8.1)	21.2 (7.6)	−0.40 (0.68)	4.15 (− 2.19, 10.49)	0.96 (− 0.51, 2.42)
GPT (IU/L)	44.0 (27.5)	46.5 (21.6)	2.50 (3.12)	22.0 (7.2)	23.8 (13.4)	1.80 (3.76)	0.70 (− 11.29, 12.69)	0.10 (− 1.59, 1.79)
γ-GT (IU/L)	68.5 (75.2)	73.3 (62.7)	4.75 (11.28)	27.2 (8.23)	27.2 (13.3)	0.00 (3.56)	4.75 (− 20.55, 30.05)	0.31 (− 1.36, 1.99)
Fatty liver index	90.8 (6.9)	93.6 (5.0)	2.77 (8.40)	67.9 (62.2)	62.2 (16.5)	−5.64 (7.39)	8.42 (− 25.51, 42.34)	0.63 (− 1.91, 3.17)
Cardiovascular risk Z-Score	0.023 (0.525)	0.203 (0.416)	0.180 (0.089)	0.084 (0.506)	−0.136 (0.358)	−0.220 (0.148)	0.39 (0.04, 0.83)	1.30 (0.12, 2.51)*
Other biochemical parameters								
Protein C reactive (mg/dL)	11.7 (18.1)	8.2 (9.4)	−3.53 (4.47)	1.6 (0.8)	1.8 (1.0)	0.18 (0.17)	−3.71 (− 13.01, 5.60)	−0.64 (− 2.23, 0.96)
Leptin (ng/mL)	19.8 (5.1)	21.0 (6.4)	1.18 (1.00)	23.3 (12.1)	15.7 (3.0)	−7.58 (5.03)	8.76 (− 4.89, 22.40)	0.94 (− 0.52, 2.41)

(Continued)

TABLE 1 | Continued

	Control group (n = 6)			Exercise group (n = 6)			Net effect	
	Baseline Mean (SD)	After 12 weeks Mean (SD)	Δ (SE)	Baseline Mean (SD)	After 12 weeks Mean (SD)	Δ (SE)	Mean difference (95% CI)	Standardized mean difference (95% CI)
Energy metabolism								
RMR (kcal/kg/day)	18.78 (1.00)	20.24 (1.75)	1.46 (1.72)	20.13 (2.53)	20.55 (1.77)	0.41 (1.98)	−1.09 (− 2.02, 4.19)	0.57 (− 0.59, 1.72)
RQ	0.867 (0.172)	0.861 (0.173)	−0.006 (0.021)	0.831 (0.194)	0.824 (0.188)	−0.007 (0.028)	−0.001 (− 0.018, 0.014)	−0.04 (− 1.17, 1.09)
RFox (g/min)	0.084 (0.026)	0.102 (0.044)	0.018 (0.014)	0.081 (0.027)	0.082 (0.023)	0.001 (0.008)	0.02 (− 0.02, 0.05)	0.71 (− 0.76, 2.18)
RFox (% RMR)	50.8 (19.3)	60.6 (25.8)	9.76 (11.95)	51.5 (16.6)	50.7 (12.5)	−0.75 (4.92)	10.50 (− 25.27, 46.26)	0.61 (− 1.46, 2.67)
RCHox (g/min)	0.148 (0.065)	0.131 (0.086)	−0.017 (0.045)	0.154 (0.049)	0.153 (0.035)	−0.001 (0.017)	−0.02 (− 0.15, 0.12)	−0.27 (− 2.48, 1.95)
RCHox (% RMR)	46.4 (17.3)	38.8 (25.4)	−7.66 (10.98)	49.1 (17.2)	48.0 (12.5)	−1.12 (4.95)	−6.53 (− 39.24, 26.18)	−0.41 (− 2.46, 1.64)
MFO (g/min)	0.24 (0.03)	0.26 (0.07)	0.019 (0.037)	0.24 (0.05)	0.25 (0.03)	0.010 (0.020)	0.01 (− 0.08, 0.10)	0.17 (− 1.39, 1.75)
Fat_{max} (% VO_2max)	48.8 (9.5)	54.6 (6.9)	5.85 (3.91)	51.5 (6.8)	53.1 (7.3)	1.58 (3.75)	4.28 (− 8.67, 17.24)	0.50 (− 1.02, 2.03)
Dietary intake								
Energy intake (kcal/day)	2868 (972)	2796 (680)	−71.5 (370.9)	2911 (518)	2436 (408)	−474.7 (272.7)	403.2 (− 633.6, 1439.9)	0.59 (− 0.91, 2.09)
Carbohydrate intake (g/day)	281.0 (81.1)	277.8 (121.7)	−3.25 (47.53)	238.3 (47.9)	284.0 (42.6)	45.67 (30.27)	48.92 (− 74.04, 171.88)	0.60 (− 0.90, 2.10)
Sugar intake (g/day)	114.6 (32.6)	84.7 (22.4)	−29.83 (21.31)	111.1 (20.0)	91.5 (19.1)	−19.63 (8.91)	−10.19 (− 73.91, 53.53)	−0.34 (− 2.47, 1.79)
Far intake (g/day)	103.3 (56.1)	116.2 (37.6)	2.93 (25.34)	126.7 (23.8)	104.3 (26.7)	−22.35 (15.95)	25.28 (− 39.91, 90.46)	0.58 (− 0.92, 2.09)
Protein intake (g/day)	130.2 (39.4)	121.6 (38.4)	−8.55 (14.33)	110.5 (23.4)	107.5 (15.2)	−2.97 (8.96)	−5.58 (− 48.26, 37.09)	−0.24 (− 1.80, 1.33)
Alcohol intake (g/day)	13.4 (11.6)	14.1 (13.5)	−0.70 (6.02)	19.3 (23.8)	10.9 (7.6)	−8.40 (10.13)	9.10 (− 22.11, 40.31)	0.45 (− 1.09, 1.98)
Physical activity and sedentary behavior								
Sedentary time (min/day)	7122.5 (1694.2)	6834.3 (1018.9)	−288.25 (754.93)	7323.4 (478.5)	7291.2 (855.9)	−32.20 (205.50)	−256.1 (− 1917.9, 1405.8)	−0.26 (− 1.94, 1.42)
LPA (min/day)	9807.0 (268.9)	9782.5 (89.2)	−24.50 (147.99)	9864.8 (118.6)	9833.4 (47.3)	−31.40 (66.08)	6.90 (− 347.87, 361.67)	0.03 (− 1.66, 1.73)
MPA (min/day)	272.8 (268.9)	296.3 (88.8)	23.50 (147.81)	188.8 (92.9)	239.4 (43.6)	50.60 (45.83)	−27.10 (− 357.76, 303.56)	−0.14 (− 1.83, 1.55)
VPA (min/day)	0.3 (0.5)	0.3 (0.5)	0.00 (0.41)	3.4 (3.1)	25.8 (57.1)	22.40 (25.94)	22.40 (− 47.16, 91.96)	0.52 (− 1.10, 2.15)
MVPA (min/day)	273.0 (268.9)	296.5 (89.2)	23.50 (147.99)	215.2 (118.6)	145.6 (47.27)	30.40 (66.08)	−6.90 (− 361.67, 347.87)	−0.03 (− 1.73, 1.66)
Cardiorespiratory fitness								
VO_2max (mL/min)	2596.3 (472.2)	2876.0 (524.4)	279.75 (95.79)	2620.3 (573.3)	2913.5 (561.4)	293.17 (299.34)	−13.42 (− 893.75, 866.92)	−0.24 (− 1.60, 1.55)
VO_2max (mL/kg/min)	25.6 (2.3)	27.7 (2.6)	2.19 (0.88)	27.4 (7.4)	30.7 (5.5)	3.31 (2.97)	−1.11 (− 8.74, 6.51)	−0.20 (− 1.57, 1.17)
Echocardiography								
Cardiac mass (g)	207.4 (32.0)	181.8 (42.3)	−25.57 (7.08)	192.6 (27.8)	197.5 (21.9)	4.88 (15.3)	−30.45 (− 72.41, 11.51)	−1.01 (− 2.39, 0.38)
Ejection fraction (%)	65.8 (6.2)	61.0 (1.8)	−4.75 (2.69)	66.2 (5.7)	61.6 (7.4)	−4.60 (3.87)	−0.15 (− 11.93, 11.63)	−0.02 (− 1.72, 1.67)
LV end diastolic diameter (mm)	52.5 (5.2)	50.8 (3.5)	−1.75 (1.25)	52.6 (3.2)	55.2 (0.4)	2.60 (1.54)	−4.35 (− 9.22, −0.52)	−1.28 (− 2.50, −0.14)*
LV end systolic diameter (mm)	26.3 (4.0)	30.5 (2.6)	4.25 (1.89)	33.4 (3.6)	34.2 (3.7)	0.80 (0.80)	3.45 (− 2.20, 9.10)	1.08 (0.69, 2.84)
LV end systolic volume (mL)	21.5 (10.3)	28.0 (15.3)	6.50 (5.33)	22.4 (2.4)	34.6 (10.6)	12.20 (4.62)	−5.70 (− 22.31, 10.91)	−0.56 (− 2.18, 1.06)
E wave (cm/s)	87.3 (12.5)	81.8 (23.7)	−5.50 (8.93)	70.2 (20.8)	67.6 (16.3)	−2.60 (6.17)	−2.90 (− 27.75, 21.95)	−0.20 (− 1.88, 1.49)
A wave (cm/s)	55.8 (3.7)	59.8 (2.6)	4.00 (3.16)	65.8 (17.4)	61.8 (8.4)	−4.00 (8.61)	8.00 (− 15.51, 31.51)	−0.55 (− 1.08, 2.18)
E/A	1.57 (0.26)	1.37 (0.38)	−0.20 (0.08)	1.07 (0.13)	1.10 (0.26)	0.04 (0.16)	0.24 (− 0.69, 0.21)	0.81 (− 2.34, 0.71)
E wave deceleration time (ms)	205.0 (20.4)	212.5 (24.7)	7.50 (21.26)	261.0 (43.8)	223.0 (31.3)	−38.00 (25.62)	45.50 (− 36.17, 127.17)	0.85 (− 0.67, 2.36)

Abbreviations: SD, standard deviation; SE, standard error; CI; confidence interval; HOMA, homeostasis model assessment; HDL-C, high-density lipoprotein cholesterol; LDL-C, low-density lipoprotein cholesterol; GOT, Glutamic oxaloacetic transaminase; GPT, glutamic-pyruvic transaminase; γ-GT, γ-glutamyl transferase; RMR, resting metabolic rate; RFox, resting fat oxidation; RCHox, resting carbohydrate oxidation; MFO, maximal fat oxidation during exercise; Fatmax, intensity that elicits MFO; LPA, physical activity levels at light intensity; MPA, physical activity levels at moderate intensity; VPA, physical activity levels at vigorous intensity; MVPA, physical activity levels at moderate-vigorous intensity; VO2max, maximal oxygen uptake; LV, left ventricle.

Analyses were performed using multilevel mixed analysis including group as a fixed variable (control group vs. exercise).

**Significant differences between groups ($P < 0.05$).*

in height, WC, LM, and bone mineral content (all $P > 0.1$; **Table 1**).

Multi-level mixed analyses, adjusting for baseline values, revealed a significant reduction of BP (i.e., systolic, diastolic, and MAP) and CV risk Z-Score in the concurrent training group compared with the control group (all $P < 0.044$; **Table 1**), whereas no significant differences were seen between groups with respect to the change in both glycemic (i.e., plasma glucose, plasma insulin, and HOMA-IR) and lipid profiles (i.e., total cholesterol, HDL-C, LDL-C, and TGs), as well as in liver function (i.e., GOT, GPT, γ-GT, and FLI) and other biochemical parameters, such as CRP and leptin (all $P > 0.17$; **Table 1**).

There were no differences between groups neither in energy metabolism-related parameters (i.e., RMR, RQ, resting substrates oxidation, MFO, and Fat_{max}), dietary intake (i.e., energy, macronutrients, and alcohol intake) and PA levels, and sedentary time nor in VO_{2max} (all $P > 0.2$; **Table 1**).

We observed a significant increment of LV end diastolic diameter in the concurrent training group compared with the control group ($P = 0.02$; **Table 1**), while no significant differences were noted in cardiac mass, ejection fraction, LV end systolic diameter, LV end systolic volume, E wave, A wave, E/A, and E wave deceleration time (all $P > 0.2$; **Table 1**).

DISCUSSION

The current study sought to elucidate whether a 12-week concurrent training intervention improves cardiometabolic health in obese men. As we expected, the main findings of the present work were that compared to the control group, the participants included in the exercise group benefited from a significant improvement in weight management, FM loss, BP, cardiometabolic risk, and cardiac function, while no significant changes were noted in neither liver function nor energy metabolism-related parameters.

Previous studies have reported that concurrent training is an efficient tool to reduce weight and FM while increasing LM (Ferreira et al., 2010; Michell et al., 2014; Amaro-Gahete et al., 2019). Michell et al. (2014) showed an increment of LM and a decrement of FM in response to 24-week concurrent training intervention which consisted of three 40-min sessions/week combining aerobic training (i.e., 55–70% of maximum oxygen uptake intensity) and resistance training (65–85% of one maximum repetition intensity) in sedentary men. Ferreira et al. (2010) found that a 10-week concurrent intervention characterized by three 60-min sessions/week of aerobic and resistance training at moderate intensity also induces FM loss and LM gain in sedentary women. Similarly, a recent study conducted in our laboratory (Amaro-Gahete et al., 2019) revealed a significant decrease of FM and an increase of LM after a 12-week concurrent training intervention based on the minimum PA recommended by the World Health Organization (World Health Organization [WHO], 2015; Piercy et al., 2018) in middle-aged sedentary adults. These results partially concur with those obtained in the current study, since we also observed a significant decrease of both weight and FM in the current cohort. However, we did not observe significant changes in LM after the exercise intervention compared with the control group. The main reasons that could explain this discrepancy among studies are the different duration of the above-mentioned concurrent training intervention (i.e., ranged from 10 to 24 weeks) and the different initial weight status of the participants (i.e., normal-weight vs. obese), which could imply different metabolic, hormonal, and molecular responses to a similar exercise stimulus.

Concurrent training has also been proposed as an excellent method to improve cardiometabolic health through the management of glycemic and lipid profile as well as BP (Kelley and Kelley, 2009; Cornelissen et al., 2011; Umpierre et al., 2011; Greene et al., 2012; Mann et al., 2014; Álvarez et al., 2019; Amaro-Gahete et al., 2019b). In the present study, BP and the CV risk Z-Score decreased in the concurrent training group, which concurs with the results of other studies involving similar concurrent training interventions (Kelley and Kelley, 2009; Cornelissen et al., 2011; Umpierre et al., 2011; Greene et al., 2012; Mann et al., 2014; Álvarez et al., 2019; Amaro-Gahete et al., 2019b). However, our study findings partially disagree with those previously mentioned (Kelley and Kelley, 2009; Cornelissen et al., 2011; Umpierre et al., 2011; Greene et al., 2012; Mann et al., 2014; Álvarez et al., 2019; Amaro-Gahete et al., 2019b) since we showed no significant differences between the concurrent training group and the control group with respect to the change in the glycemic (i.e., plasma glucose and insulin concentration and HOMA-IR) and lipid (total cholesterol, HDL-C, LDL-C, and TGs) profiles, as well as in hepatic function. The different intervention durations could be a potential reason for these discrepancies (i.e., ranged from 8 to 24 weeks). But certainly, the most plausible explanation is that the low sample size of the present study is not enough to detect statistical differences between groups. Further studies with more statistic power are needed to confirm the current results.

The influence of concurrent training on energy metabolism-related parameters has been previously investigated obtaining controversial findings. On the one hand, a significant increase of RMR was observed after a 10-week concurrent training program in physically active men (Dolezal and Potteiger, 1998), whereas no significant changes were noted neither in RMR nor in resting substrates oxidation in response to both a 20- and 12-week concurrent training interventions in sedentary middle-aged women (Byrne and Wilmore, 2001) and in middle-aged sedentary adults (Amaro-Gahete et al., 2020), respectively. On the other hand, there is also controversy regarding the effects of both aerobic and resistance training on MFO. While no change in MFO was observed after either 4 weeks of aerobic training or 12 weeks of concurrent training in middle-aged adults with (Venables and Jeukendrup, 2008) and without obesity (Amaro-Gahete et al., 2020), a significant increase of MFO was reported in overweight men after a 3-month aerobic training intervention (Rosenkilde et al., 2015), and in middle-aged untrained adults after a 1-year aerobic training intervention (Scharhag-Rosenberger et al., 2010). The present results showed no significant differences in RMR, resting nutrients oxidation, and MFO after 12 weeks of concurrent training compared with a no-exercise control group. These findings could be explained by the lack of changes in LM

since this outcome is the most important determinant of RMR (i.e., skeletal muscle is the most metabolically active tissue) (Blundell et al., 2015), and its optimization could improve mitochondrial function/activity and insulin sensitivity modulating in turn substrate oxidation during both resting and exercise conditions (Goodpaster and Sparks, 2017). It is therefore plausible that an increase of LM could be mandatory or determinant to induce changes in energy metabolism-related parameters. In the same line, it is possible that the required exercise duration to guarantee LM and RMR improvements would be longer than 12 weeks.

In the current study, a significant increase of the LV end diastolic diameter was observed following a 12-week concurrent training intervention, which seems logical because this type of exercise training induces subsequent increments of pressure overload to volume overload, as a consequent of the exercise duration and intensity (Hosseini et al., 2012). These findings concurred with those reported by previous studies that revealed LV morphologic adaptations in response to (i) an 8-week concurrent training program in young women (Hosseini et al., 2012), (ii) a 10-week concurrent training intervention in trained men (duManoir et al., 2007), and (iii) a 5-month concurrent training program in rowers (Cavallaro et al., 1993). However, no further changes were observed in other cardiac parameters when both exercise and control groups were compared. This finding could be explained by the relatively short duration of our intervention since previous studies have suggested longer exercise programs to improve cardiac function (Voulgari et al., 2013). Despite the positive changes found only in LV end diastolic diameter, these findings are very relevant due to the particular characteristic of the participants (i.e., obese rather than trained or healthy population) who could especially benefit of the improvement in this morphologic parameter which is known as an indicator of CV health and a risk factor for mortality (Narayanan et al., 2014).

LIMITATIONS

This study had some important limitations that should be noted, and therefore findings of this work should be interpreted with caution. First, the small sample size limits the generalization of the results and might limit the detection of statistical significance. Regardless, the effect size for all outcome measures has been reported. Second, this intervention was conducted in obese men, thus we cannot extrapolate the findings to their women counterparts. Insulin resistance was not assessed by the gold standard method (i.e., the hyperinsulinemic euglycemic glucose clamp technique). However, HOMA (Ascaso et al., 2001) method has been previously validated for assessing insulin resistance. Finally, we observed a reduction of energy intake in the exercise group which could explain the body weight loss of such participants. Nevertheless, it has been suggested in previous studies that the compensatory effect of exercise intervention may be on behavior parameters (e.g., diet and PA) (Stubbs et al., 2004). This phenomenon may have affected our participants but further studies are needed to confirm these findings.

CONCLUSION

In conclusion, the present study shows that a 12-week concurrent training intervention is an effective strategy to induce weight and FM loss with simultaneous reductions of BP and cardiometabolic risk, and improving CV function in obese men. These findings could have important clinical implications since, despite its inherent limitations, they suggest that a combination of aerobic and resistance training intervention is an effective and cost-efficient strategy for the management of obesity and its related complications. Further studies should be conducted to confirm these results with a higher sample size, and to determine whether the same holds true for women and whether longer duration would imply additional benefits.

DATA AVAILABILITY STATEMENT

The raw data supporting the conclusions of this article will be made available by the authors, without undue reservation.

ETHICS STATEMENT

The studies involving human participants were reviewed and approved by the Ethics Committee on Human Research at the University of Leon. The patients/participants provided their written informed consent to participate in this study.

AUTHOR CONTRIBUTIONS

JGP-G, JC-P, and DJ-P contributed to conceptualization. FA-G and DJ-P contributed to data curation. FA-G contributed to formal analysis and writing—original draft. DJ-P contributed to funding acquisition, project administration, resources, and supervision. JGP-G, JC-P, DV-D, CL, and DJ-P contributed to investigation. FA-G, JGP-G, JC-P, and DJ-P contributed to methodology. FA-G, JGP-G, JC-P, DV-D, CL, and DJ-P contributed to writing—review and editing. All authors contributed to the article and approved the submitted version.

FUNDING

Current research activities of DJ-P are supported by a grant from the Spanish Ministry of Science and Innovation—MINECO (RYC-2014-16938) and the Spanish Ministry of Economy and Competitiveness—MINECO/FEDER (DEP2016-76123-R), the Government of Andalusian, Integrated Territorial Initiative 2014–2020 for the province of Cádiz (PI-0002-2017); the European Union's ERASMUS + SPORT program (Grant Agreement: 603121-EPP-1-2018-1-ES-SPO-SCP), and the EXERNET Research Network on Exercise and Health in Special Populations (DEP2005-00046/ACTI). Technology Fund—FEDER funds (R&D&I Operating Program) by

and for the benefit of companies (Technology Fund) INNTERCONECTA (BRISA Contract-University of Cádiz). The results of the study are presented clearly, honestly, and without fabrication, falsification, or inappropriate data manipulation.

SUPPLEMENTARY MATERIAL

The Supplementary Material for this article can be found online at: https://www.frontiersin.org/articles/10.3389/fphys.2021.630831/full#supplementary-material

REFERENCES

Álvarez, C., Ramírez-Vélez, R., Ramírez-Campillo, R., Lucia, A., Alonso-Martinez, A. M., Faúndez, H., et al. (2019). Improvements cardiometabolic risk factors in Latin American Amerindians (the Mapuche) with concurrent training. *Scand. J. Med. Sci. Sports* 29, 886–896. doi: 10.1111/sms.13409

Amaro-Gahete, F. J., De-la-O, A., Jurado-Fasoli, L., Dote-Montero, M., Gutiérrez, Á, Ruiz, J. R., et al. (2019a). Changes in physical fitness after 12 weeks of structured concurrent exercise training, high intensity interval training, or whole-body electromyostimulation training in sedentary middle-aged adults: a randomized controlled trial. *Front. Physiol.* 10:451.

Amaro-Gahete, F. J., De-la-O, A., Jurado-Fasoli, L., Martinez-Tellez, B., Ruiz, J. R., and Castillo, M. J. (2019b). Exercise training as a treatment for cardiometabolic risk in sedentary adults: are physical activity guidelines the best way to improve cardiometabolic health? the fit-ageing randomized controlled trial. *J. Clin. Med.* 8:E2097.

Amaro-Gahete, F. J., De-la-O, A., Jurado-Fasoli, L., Ruiz, J. R., Castillo, M. J., and Gutiérrez, Á (2019). Effects of different exercise training programs on body composition: a randomized control trial. *Scand. J. Med. Sci. Sports* 29, 968–979.

Amaro-Gahete, F. J., De-la-O, A., Jurado-Fasoli, L., Sanchez-Delgado, G., Ruiz, J. R., and Castillo, M. J. (2020). Metabolic rate in sedentary adults, following different exercise training interventions: the fit-ageing randomized controlled trial. *Clin. Nutr.* 39, 3230–3240. doi: 10.1016/j.clnu.2020.02.001

Amaro-Gahete, F. J., Sanchez-Delgado, G., Alcantara, J. M. A., Martinez-Tellez, B., Acosta, F. M., Helge, J. W., et al. (2019c). Impact of data analysis methods for maximal fat oxidation estimation during exercise in sedentary adults. *Eur. J. Sport Sci.* 19, 1230–1239. doi: 10.1080/17461391.2019.1595160

Ascaso, J. F., Romero, P., Real, J. T., Priego, A., Valdecabres, C., and Carmena, R. (2001). [Insulin resistance quantification by fasting insulin plasma values and HOMA index in a non-diabetic population]. *Med. Clin.* 117, 530–533.

Bedogni, G., Bellentani, S., Miglioli, L., Masutti, F., Passalacqua, M., Castiglione, A., et al. (2006). The fatty liver index: a simple and accurate predictor of hepatic steatosis in the general population. *BMC Gastroenterol.* 6:33.

Bennie, J. A., Ding, D., Khan, A., Stamatakis, E., Biddle, S. J., and Kim, J. (2018). Run, lift, or both? associations between concurrent aerobic-muscle strengthening exercise with adverse cardiometabolic biomarkers among Korean adults. *Eur. J. Prev. Cardiol.* 27, 738–748. doi: 10.1177/2047487318817899

Blundell, J. E., Finlayson, G., Gibbons, C., Caudwell, P., and Hopkins, M. (2015). The biology of appetite control: do resting metabolic rate and fat-free mass drive energy intake? *Physiol. Behav.* 152, 473–478. doi: 10.1016/j.physbeh.2015.05.031

Braga de Mello, D., Monteiro-Lago, T., da Silva, Cardoso, M., Henriques, I., et al. (2019). Impact of eight weeks of concurrent training on obesity-related biochemical parameters and cardiometabolic risk factors: a case report. *Adv. Obesity Weight Manag. Control* 9, 98–103. doi: 10.15406/aowmc.2019.09.00281

Byrne, H. K., and Wilmore, J. H. (2001). The effects of a 20-week exercise training program on resting metabolic rate in previously sedentary, moderately obese women. *Int. J. Sport Nutr. Exerc. Metab.* 11, 15–31. doi: 10.1123/ijsnem.11.1.15

Carracher, A. M., Marathe, P. H., and Close, K. L. (2018). International diabetes federation 2017. *J. Diabetes* 10, 353–356. doi: 10.1111/1753-0407.12644

Cavallaro, V., Petretta, M., Betocchi, S., Salvatore, C., Morgano, G., Binachi, V., et al. (1993). Effects of sustained training on left ventricular structure and function in top level rowers. *Eur. Heart J.* 14, 898–903. doi: 10.1093/eurheartj/14.7.898

Cornelissen, V. A., Fagard, R. H., Coeckelberghs, E., and Vanhees, L. (2011). Impact of resistance training on blood pressure and other cardiovascular risk factors. *Hypertension* 58, 950–958. doi: 10.1161/hypertensionaha.111.177071

Corso, L. M. L., Macdonald, H. V., Johnson, B. T., Farinatti, P., Livingston, J., Zaleski, A. L., et al. (2016). Is concurrent training efficacious antihypertensive therapy? a meta-analysis. *Med. Sci. Sport. Exerc.* 48, 2398–2406. doi: 10.1249/mss.0000000000001056

Dolezal, B. A., and Potteiger, J. A. (1998). Concurrent resistance and endurance training influence basal metabolic rate in nondieting individuals. *J. Appl. Physiol.* 85, 695–700. doi: 10.1152/jappl.1998.85.2.695

duManoir, G., Haykowsky, M., Syrotuik, D., Taylor, D., and Bell, G. (2007). The effect of high-intensity rowing and combined strength and endurance training on left ventricular systolic function and morphology. *Int. J. Sports Med.* 28, 488–494. doi: 10.1055/s-2006-955897

Ferreira, F. C., de Medeiros, A. I., Nicioli, C., Nunes, J. E. D., Shiguemoto, G. E., Prestes, J., et al. (2010). Circuit resistance training in sedentary women: body composition and serum cytokine levels. *Appl. Physiol. Nutr. Metab.* 35, 163–171. doi: 10.1139/h09-136

Fullmer, S., Benson-Davies, S., Earthman, C. P., Frankenfield, D. C., Gradwell, E., Lee, P. S. P., et al. (2015). Evidence analysis library review of best practices for performing indirect calorimetry in healthy and non-critically ill individuals. *J. Acad. Nutr. Diet.* 115, 1417–1446.e2.

Go, A. S., Mozaffarian, D., Roger, V. L., Benjamin, E. J., Berry, J. D., Blaha, M. J., et al. (2014). Heart disease and stroke statistics–2014 update: a report from the american heart association. *Circulation* 129, e28–e292.

Goodpaster, B. H., and Sparks, L. M. (2017). Metabolic flexibility in health and disease. *Cell Metab.* 25, 1027–1036. doi: 10.1016/j.cmet.2017.04.015

Greene, N. P., Martin, S. E., and Crouse, S. F. (2012). Acute exercise and training alter blood lipid and lipoprotein profiles differently in overweight and obese men and women. *Obesity* 20, 1618–1627. doi: 10.1038/oby.2012.65

Hosseini, M., Piri, M., Agha-Alinejad, H., and Haj-Sadeghi, S. (2012). The effect of endurance, resistance and concurrent training on the heart structure of female students. *Biol. Sport* 29, 17–21. doi: 10.5604/20831862.979404

Jaacks, L. M., Vandevijvere, S., Pan, A., McGowan, C. J., Wallace, C., Imamura, F., et al. (2019). The obesity transition: stages of the global epidemic. *Lancet. Diabetes Endocrinol.* 7, 231–240. doi: 10.1016/s2213-8587(19)30026-9

Jiménez-Pavón, D., Lavie, C. J., and Blair, S. N. (2019). The role of cardiorespiratory fitness on the risk of sudden cardiac death at the population level: a systematic review and meta-analysis of the available evidence. *Prog. Cardiovasc. Dis.* 62, 279–287. doi: 10.1016/j.pcad.2019.05.003

Kelley, G. A., and Kelley, K. S. (2009). Impact of progressive resistance training on lipids and lipoproteins in adults: a meta-analysis of randomized controlled trials. *Prev. Med.* 48, 9–19. doi: 10.1016/j.ypmed.2008.10.010

Lavie, C. J., Arena, R., Alpert, M. A., Milani, R. V., and Ventura, H. O. (2018a). Management of cardiovascular diseases in patients with obesity. *Nat. Rev. Cardiol.* 15, 45–56.

Lavie, C. J., Laddu, D., Arena, R., Ortega, F. B., Alpert, M. A., and Kushner, R. F. (2018b). Healthy weight and obesity prevention. *J. Am. Coll. Cardiol.* 72, 1506–1531.

Libardi, C. A., De Souza, G. V., Cavaglieri, C. R., Madruga, V. A., and Chacon-Mikahil, M. P. T. (2012). Effect of resistance, endurance, and concurrent training on TNF-α, IL-6, and CRP. *Med. Sci. Sport. Exerc.* 44, 50–56. doi: 10.1249/mss.0b013e318229d2e9

Mann, S., Beedie, C., and Jimenez, A. (2014). Differential effects of aerobic exercise, resistance training and combined exercise modalities on cholesterol and the lipid profile: review, synthesis and recommendations. *Sports Med.* 44, 211–221. doi: 10.1007/s40279-013-0110-5

Michell, V., Samaria, C., Junior Rudy, N., Danyela, V., and Dantas, E. (2014). Effects of a concurrent physical exercise program on aerobic power and body composition in adults. *J. Sports Med. Phys. Fitness* 54, 441–446.

Midgley, A. W., McNaughton, L. R., Polman, R., and Marchant, D. (2007). Criteria for determination of maximal oxygen uptake: a brief critique and recommendations for future research. *Sport. Med.* 37, 1019–1028. doi: 10.2165/00007256-200737120-00002

Milić, S., Lulić, D., and Štimac, D. (2014). Non-alcoholic fatty liver disease and obesity: biochemical, metabolic and clinical presentations. *World J. Gastroenterol.* 20, 9330–9337.

Monteiro, P. A., Chen, K. Y., Lira, F. S., Saraiva, B. T. C., Antunes, B. M. M., Campos, E. Z., et al. (2015). Concurrent and aerobic exercise training promote similar benefits in body composition and metabolic profiles in obese adolescents. *Lipids Health Dis.* 14:153.

Nagueh, S. F., Appleton, C. P., Gillebert, T. C., Marino, P. N., Oh, J. K., Smiseth, O. A., et al. (2008). Recommendations for the evaluation of left ventricular diastolic function by echocardiography. *Eur. J. Echocardiogr.* 10, 165–193.

Narayanan, K., Reinier, K., Teodorescu, C., Uy-Evanado, A., Aleong, R., Chugh, H., et al. (2014). Left ventricular diameter and risk stratification for sudden cardiac death. *J. Am. Heart Assoc.* 3:e001193.

Ng, M., Fleming, T., Robinson, M., Thomson, B., Graetz, N., Margono, C., et al. (2014). Global, regional, and national prevalence of overweight and obesity in children and adults during 1980-2013: a systematic analysis for the global burden of disease study 2013. *Lancet* 384, 766–781.

Perumareddi, P. (2019). Prevention of hypertension related to cardiovascular disease. *Prim. Care* 46, 27–39.

Petridou, A., Siopi, A., and Mougios, V. (2018). Exercise in the management of obesity. *Metabolism* 92, 163–169.

Piercy, K. L., Troiano, R. P., Ballard, R. M., Carlson, S. A., Fulton, J. E., Galuska, D. A., et al. (2018). The physical activity guidelines for Americans. *J. Am. Med. Assoc.* 320, 2020–2028.

Rosenkilde, M., Reichkendler, M. H., Auerbach, P., Bonne, T. C., Sjödin, A., Ploug, T., et al. (2015). Changes in peak fat oxidation in response to different doses of endurance training. *Scand. J. Med. Sci. Sport.* 25, 41–52. doi: 10.1111/sms.12151

Sanchez-Delgado, G., Alcantara, J. M. A., Ortiz-Alvarez, L., Xu, H., Martinez-Tellez, B., Labayen, I., et al. (2018). Reliability of resting metabolic rate measurements in young adults: impact of methods for data analysis. *Clin. Nutr.* 37, 1618–1624. doi: 10.1016/j.clnu.2017.07.026

Scharhag-Rosenberger, F., Meyer, T., Walitzek, S., and Kindermann, W. (2010). Effects of one year aerobic endurance training on resting metabolic rate and exercise fat oxidation in previously untrained men and women. metabolic endurance training adaptations. *Int. J. Sports Med.* 31, 498–504. doi: 10.1055/s-0030-1249621

Stubbs, R. J., Hughes, D. A., Johnstone, A. M., Whybrow, S., Horgan, G. W., King, N., et al. (2004). Rate and extent of compensatory changes in energy intake and expenditure in response to altered exercise and diet composition in humans. *Am. J. Physiol. Integr. Comp. Physiol.* 286, R350–R358.

Tsujimoto, T., Sasai, H., Miyashita, M., Eto, M., So, R., Ohkubo, H., et al. (2011). Effect of weight loss on maximal fat oxidation rate in obese men. *Obes. Res. Clin. Pract.* 6, e111–e119.

Umpierre, D., Ribeiro, P. A. B., Kramer, C. K., Leitão, C. B., Zucatti, A. T. N., Azevedo, M. J., et al. (2011). Physical activity advice only or structured exercise training and association with HbA1c levels in type 2 diabetes: a systematic review and meta-analysis. *JAMA* 305, 1790–1799. doi: 10.1001/jama.2011.576

Venables, M. C., and Jeukendrup, A. E. (2008). Endurance training and obesity: effect on substrate metabolism and insulin sensitivity. *Med. Sci. Sports Exerc.* 40, 495–502. doi: 10.1249/mss.0b013e31815f256f

Voulgari, C., Pagoni, S., Vinik, A., and Poirier, P. (2013). Exercise improves cardiac autonomic function in obesity and diabetes. *Metabolism* 62, 609–621. doi: 10.1016/j.metabol.2012.09.005

Welch, V. A., Norheim, O. F., Jull, J., Cookson, R., Sommerfelt, H., and Tugwell, P. (2017). CONSORT-Equity 2017 extension and elaboration for better reporting of health equity in randomised trials. *BMJ* 359:j5085. doi: 10.1136/bmj.j5085

Whelton, P. K., and Williams, B. (2018). The 2018 european society of cardiology/european society of hypertension and 2017 american college of cardiology/american heart association blood pressure guidelines. *JAMA* 320:1749. doi: 10.1001/jama.2018.16755

World Health Organization [WHO] (2015). *Global Recommendations on Physical Activity for Health*. Geneva: World Health Organization.

Conflict of Interest: The authors declare that the research was conducted in the absence of any commercial or financial relationships that could be construed as a potential conflict of interest.

frontiers in Physiology

SYSTEMATIC REVIEW
published: 11 March 2021
doi: 10.3389/fphys.2021.643455

Pilates for Overweight or Obesity: A Meta-Analysis

Yi Wang[1†], *Zehua Chen*[1†], *Zugui Wu*[1], *Xiangling Ye*[1] *and Xuemeng Xu*[1,2*]

[1] *The Fifth Clinical Medical College of Guangzhou University of Chinese Medicine, Guangzhou, China,* [2] *Guangdong Second Traditional Chinese Medicine Hospital, Guangzhou, China*

Background: Evidence for the efficacy of Pilates for the modulation of body weight and body composition is unclear.

Objective: This meta-analysis aimed to evaluate the effects of Pilates on body weight and body composition in adults with overweight or obesity.

Data Sources: The PubMed, Cochrane Library, Web of Science, China National Knowledge Infrastructure (CNKI), and EMBASE databases were systematically searched from the inception dates to 12 November 2020 for relevant randomized controlled trials (RCTs).

Study Selection: Randomized controlled trials comparing Pilates with other physical exercises or without any intervention were included.

Data Extraction and Synthesis: Three reviewers independently performed the data extraction and assessed study quality. The mean differences (MDs) and 95% confidence intervals (CIs) for pooled data were calculated.

Main Outcomes and Measures: Outcome measures were body weight, body mass index (BMI), body fat percentage, lean body mass, and waist circumference.

Results: Eleven RCTs with 393 subjects were included. This study revealed that Pilates dramatically reduces body weight (MD = −2.40, 95% CI: [−4.04, −0.77], $P = 0.004$, $I^2 = 51\%$), BMI (MD = −1.17, 95% CI: [−1.85, −0.50], $P = 0.0006$, $I^2 = 61\%$), and body fat percentage (MD = −4.22, 95% CI: [−6.44, −2.01], $P = 0.0002$, $I^2 = 88\%$) in adults with overweight or obesity. The reduction in body weight and body fat percentage appears to be more pronounced in studies including participants with obesity only, and the efficacy of Pilates for the improvement of body weight and BMI appears to be more evident in longer intervention duration. However, Pilates has no significant effect on waist circumference (MD = −2.65, 95% CI: [−6.84, 1.55], $P = 0.22$, $I^2 = 0\%$) and lean body mass (MD = −0.00, 95% CI: [−1.40, 1.40], $P = 1.00$, $I^2 = 23\%$).

Conclusions: Pilates dramatically reduces body weight, BMI, and body fat percentage in adults with overweight or obesity. Large-scale and well-designed RCTs with improved methodology and reporting are urgently needed to further confirm these results.

Keywords: Pilates, overweight, obesity, review, meta-analysis

OPEN ACCESS

Edited by:
Nuo Sun,
The Ohio State University Wexner Medical Center, United States

Reviewed by:
Ramon Bossardi Ramos,
Albany Medical College, United States
Lin Zhang,
Hubei University of Chinese Medicine, China

***Correspondence:**
Xuemeng Xu
xuxuemeng@163.com

†These authors have contributed equally to this work

Specialty section:
This article was submitted to Integrative Physiology, a section of the journal Frontiers in Physiology

Received: *18 December 2020*
Accepted: *08 February 2021*
Published: *11 March 2021*

Citation:
Wang Y, Chen Z, Wu Z, Ye X and Xu X (2021) Pilates for Overweight or Obesity: A Meta-Analysis. Front. Physiol. 12:643455. doi: 10.3389/fphys.2021.643455

INTRODUCTION

Overweight and obesity, which are defined as abnormal or excessive body fat accumulation (World Health Organization, 2020), are the leading variable risk factors for chronic diseases and premature death (World Health Organization, 2018). According to the body mass index (BMI) (kg/m^2), for adults, overweight is a BMI $\geq$ 25, whereas obesity is a BMI $\geq$ 30 (World Health Organization, 2020). Statistically, in 2016, 39% of adults aged 18 years and over were overweight, and 13% were obese; the prevalence of overweight and obesity among children and adolescents aged 5–19 was about 18%. Thirty-eight million children under the age of 5 were overweight or obese in 2019 (World Health Organization, 2020). Overweight and obesity have considerable negative socioeconomic impacts due to the high prevalence (Hammond and Levine, 2010). Besides excessive caloric intake, a sedentary lifestyle is also a major factor leading to overweight and obesity (Morgen and Sørensen, 2014). Therefore, regular physical activity has been recommended as one of the most effective prevention and treatment options for people with overweight or obesity (Expert Panel Members et al., 2014; World Health Organization, 2020). Given that some common physical exercises are ineffective in losing weight, and even may damage the musculoskeletal system due to knee joints overload in individuals with overweight or obesity (Girard et al., 2017; Hun-Young et al., 2019), it is necessary to investigate the alternative forms of exercise for treating overweight and obesity.

One such alternative modality of exercise that is widely used for health enhancement and adjuvant treatment in various diseases is Pilates (Sharma et al., 2018; Eliks et al., 2019; Fernández-Rodríguez et al., 2019). Pilates exercise, which was originated in the 1920s, mainly involved isometric contractions of the core muscles (Chen Z. et al., 2020). Moreover, the Pilates exercise system combined practical movement styles and ideas of martial arts, dance, gymnastics, and yoga with philosophical notions and followed six basic principles of centering, concentration, control, precision, flowing movements, and breathing (Latey, 2001). Pilates, although not designed to reduce body weight, can be considered a good option for people with overweight or obesity who have difficulty in adhering to those monotonous traditional physical exercises (Vancini et al., 2017; de Souza Cavina et al., 2020). Furthermore, Pilates does not require high costs to practice and produces high concentration in the muscle core, which could contribute to the implementation of this exercise method in clinical practice to improve body weight and body composition (de Souza Cavina et al., 2020). While the overall effects of physical exercises on body weight in people with overweight or obesity are now well-known, Pilates is not. Despite several studies have been conducted to assess the physical effects of Pilates for individuals with overweight or obesity, the results have been diverse with no clear consensus (Hagner-Derengowska et al., 2015; Rayes et al., 2019; Jung et al., 2020). Additionally, there is no systematic review or meta-analysis on Pilates for treating overweight and obesity to date. Therefore, the aim of this systematic review and meta-analysis of randomized controlled trials (RCTs) was to evaluate the effects of Pilates on body weight and body composition in adults with overweight or obesity.

METHODS

Search Strategy

This review was conducted in accordance with the Preferred Reporting Items for Systematic Reviews and Meta-Analyses (PRISMA) guidelines (Moher et al., 2009). PubMed, the Cochrane Library, Web of Science, the China National Knowledge Infrastructure (CNKI), and EMBASE databases were systematically searched from the inception dates to 12 November 2020. We applied no language restrictions. We used the following combined text and MeSH terms: "Pilates," "overweight and obesity," and "Randomized Controlled Trial." The complete search used for PubMed was: ((((((((((((("Overweight" [Mesh]) OR ("Obesity" [Mesh])) OR (Overweight [Title/Abstract])) OR (Obesity [Title/Abstract])) OR (adipose tissue hyperplasia [Title/Abstract])) OR (adipositas [Title/Abstract])) OR (adiposity [Title/Abstract])) OR (alimentary obesity [Title/Abstract])) OR (body weight, excess [Title/Abstract])) OR (corpulency [Title/Abstract])) OR (fat overload syndrome [Title/Abstract])) OR (nutritional obesity [Title/Abstract])) OR (obesitas [Title/Abstract])) AND (((((((("Exercise Movement Techniques" [Mesh]) OR (Movement Techniques, Exercise [Title/Abstract])) OR (Exercise Movement Technics [Title/Abstract])) OR (Pilates-Based Exercises [Title/Abstract])) OR (Exercises, Pilates-Based [Title/Abstract])) OR (Pilates Based Exercises [Title/Abstract])) OR (Pilates Training [Title/Abstract])) OR (Training, Pilates [Title/Abstract])) OR (Pilates [Title/Abstract]))) AND ((randomized controlled trial[pt] OR controlled clinical trial[pt] OR randomized[tiab] OR placebo[tiab] OR drug therapy[sh] OR randomly[tiab] OR trial[tiab] OR groups[tiab] NOT (animals [mh] NOT humans [mh]))). Additionally, the reference lists of all retrieved articles and relevant reviews were manually screened for potentially eligible studies. Two reviewers (Y Wang and ZH Chen) independently screened and selected papers, a third reviewer (ZG Wu) was consulted to resolve disagreements. The search strategy is detailed in **Supplementary Table 1**.

Selection Criteria

We formulated the study's eligibility criteria using the participants, interventions, comparison, outcomes, and study design (PICOS) description model (Guyatt et al., 2011).

Participants

Inclusion criteria:

- Adult subjects aged 18 or over with overweight or obesity (overweight, BMI $\geq$25.0 kg/m^2; obesity, BMI $\geq$30.0 kg/m^2)

Exclusion criteria:

- Pregnancy
- Participants with any contraindication of exercise therapy
- Participants with eating disorders

Intervention

- Pilates

No restrictions were made in terms of the type of Pilates, the duration, dose, or intensity of the intervention. Furthermore, studies with dietary intervention were excluded.

Comparators

- Pilates vs. other physical exercises
- Pilates vs. without any intervention

Outcomes

The included studies had to assess at least one primary outcome related to body weight or body composition:

- Body weight
- Body mass index
- Body fat percentage
- Lean body mass
- Waist circumference

In addition, the safety of Pilates intervention was considered secondary outcomes.

Study Design

- RCTs
- Published in English or Chinese language

Data Extraction

Two reviewers (Y Wang and ZH Chen) independently extracted the following data from the included studies: participant characteristics (e.g., age, gender, year), study characteristics (e.g., author names, publication year, region, study design, intervention type, intervention characteristics, sample size), and related study outcomes. Any disputes were resolved by discussing with a third reviewer (ZG Wu). If necessary, the corresponding authors were contacted for additional information.

Quality Assessment

The methodological quality of included studies was assessed using the Physiotherapy Evidence Database (PEDro) scale (Maher et al., 2003; Macedo et al., 2010), which is used to assess the quality of RCTs with physical therapist interventions. The PEDro scale includes 10 items on random allocation, concealed allocation, similarly at baseline, subjects blinding, therapists blinding, assessors blinding, dropout rate <15%, intention to treat analysis, between-group statistical analysis, and point and variability measures; the score ranges from 0 to 10. A score $\geq$7 was considered "high quality," a score of 5 or 6 was considered "moderate quality," and $\leq$4 "poor quality" (de Souza Cavina et al., 2020). Moreover, the quality of evidence was assessed using the Grading of Recommendations Assessment, Development, and Evaluation System (GRADEprofiler, version 3.6; GRADE Working Group, 2004; Higgins et al., 2020). The assessment process was also conducted by two independent reviewers (Y Wang and ZH Chen), and the consensus approach was once again adopted.

Statistical Analysis

Review Manager (version 5.3) and Stata (version 13.0) were used to conduct statistical analyses. Data were presented as mean ± standard deviation (SD) or 95% confidence interval (CI). All continuous variables were pooled by mean difference (MD) or MD with 95% CI. Heterogeneity was assessed by Higgins I^2 statistic and 0–25% suggests very low heterogeneity, 25–50% low heterogeneity, 50–75% moderate heterogeneity, and more than 75% high heterogeneity (Higgins and Thompson, 2002; Higgins et al., 2020). The fixed effect models would be enabled if $I^2 <$ 50%; otherwise, a random-effect model was applied. To explore potential sources of heterogeneity between studies, subgroup and meta-regression analyses were conducted based on intervention duration and participant type. Sensitivity analyses were used to test the robustness of significant results. In addition, the visual inspection of funnel plots and statistical asymmetry tests (Begg's and Egger's tests) were used to assess publication bias. Statistical significance was considered for $P < 0.05$.

RESULTS

Study Selection

A total of 2,670 potentially relevant records were acquired *via* electronic and hand search. We imported all the literature into EndNote X9 (Bld,12062) for de-duplication. Then we initially screened out 2,502 articles through title and abstract, and the remaining 60 were considered highly relevant. Finally, we further excluded 49 studies by means of reading full text according to our study selection criteria, leaving 11 studies (Cakmakçi, 2011; Gorji et al., 2014, 2015; Chaudhary, 2016; Savkin and Aslan, 2016; Khormizi and Azarniveh, 2017; Khajehlandi et al., 2018; Chen J. et al., 2020; Jung et al., 2020; Tyagi and Kumar, 2020; Wong et al., 2020) for inclusion in this analysis (**Figure 1**).

Study Characteristics

All included studies were RCTs involving 393 adults with overweight or obesity. The studies were from Korea (Jung et al., 2020), Turkey (Cakmakçi, 2011; Savkin and Aslan, 2016), Iran (Gorji et al., 2014, 2015; Khormizi and Azarniveh, 2017; Khajehlandi et al., 2018), the USA (Wong et al., 2020), India (Chaudhary, 2016; Tyagi and Kumar, 2020), and China (Chen J. et al., 2020). These studies were published between 2011 and 2020, and the intervention duration varied from 8 to 24 weeks, with the sample size ranging from 20 to 61 participants. The participants were mostly female (77.1%). Nine studies (81.8%) only recruited women (Cakmakçi, 2011; Gorji et al., 2014, 2015; Savkin and Aslan, 2016; Khormizi and Azarniveh, 2017; Khajehlandi et al., 2018; Chen J. et al., 2020; Jung et al., 2020; Wong et al., 2020), and another two (18.2%) only recruited men (Chaudhary, 2016; Tyagi and Kumar, 2020). In terms of the definition of overweight and obesity, all 11 studies used BMI. Three studies recruited participants with hypertension (Wong et al., 2020), type 2 diabetes (Khormizi and Azarniveh, 2017), and depression (Chen J. et al., 2020), other studies recruited participants with no reported existing medical conditions. Regarding the measurement method of body composition, four studies (Gorji et al., 2014, 2015; Savkin and Aslan, 2016; Wong et al., 2020) used bioelectric impedance analysis device, three studies (Chaudhary, 2016; Khajehlandi et al., 2018; Tyagi and Kumar, 2020) used body composition analyzer, one study (Jung et al., 2020) used a dual-energy X-ray absorptiometry scanner,

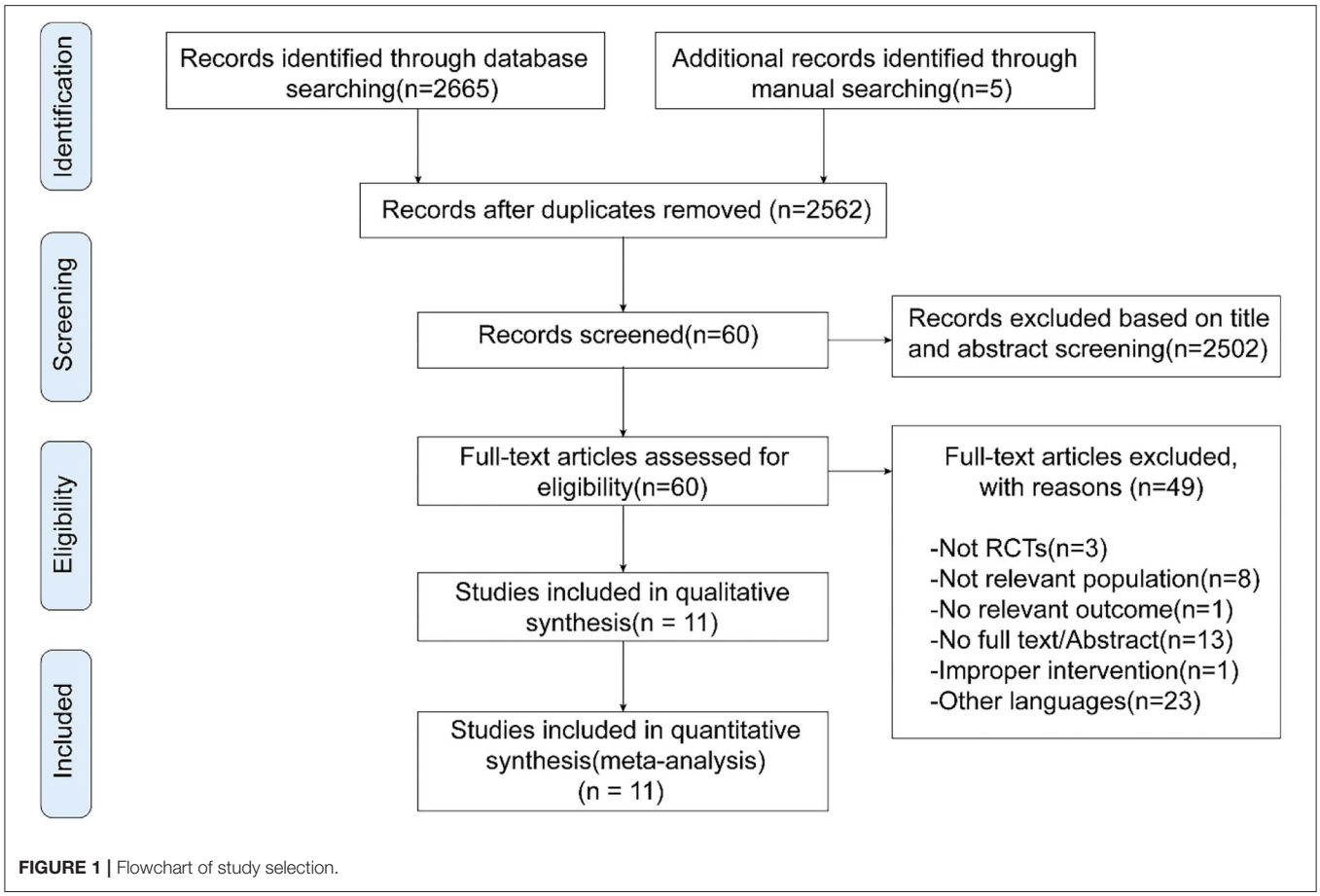

FIGURE 1 | Flowchart of study selection.

two studies (Cakmakçi, 2011; Chen J. et al., 2020) did not specify, and the remaining one (Khormizi and Azarniveh, 2017) did not measure. The characteristics of the included studies are summarized in **Table 1**.

Risk of Bias in Included Studies

The PEDro assessment indicated that the methodological quality of included studies was moderate (mean score = 6.09 ± 0.83; **Table 2**). All studies randomly allocated subjects, but only two studies (Savkin and Aslan, 2016; Wong et al., 2020) used concealed allocation. None of the studies employed subjects blinding and therapists blinding. However, only two studies (Khormizi and Azarniveh, 2017; Wong et al., 2020) used assessor blinding, which could lead to potential limitations. In addition, none of the studies had a loss to follow-up rate of more than 15%, and no study used intention-to-treat analysis.

Analysis of Overall Effect Size

Primary Outcomes

Body Weight

Ten studies recorded body weight outcomes. Meta-analysis results showed that Pilates significantly reduced body weight (MD = −2.40, 95% CI: [−4.04, −0.77], $P = 0.004$). Moderate heterogeneity was detected between studies ($P = 0.03$, $I^2 = 51\%$; **Figure 2**). Therefore, we conducted subgroup analyses for the results. Subgroup analysis based on intervention duration showed that a significant decrease was observed on body weight in studies with more than 10 weeks of duration (MD = −3.30, 95% CI: [−4.67, −1.92], $P < 0.00001$, $I^2 = 34\%$); whereas, no significant effect in studies with duration of 10 weeks or less (MD = −1.17, 95% CI: [−4.91, 2.58], $P = 0.54$, $I^2 = 55\%$). Moreover, the subgroup analysis according to participant type demonstrated that body weight dramatically decreased by Pilates in studies including participants with obesity only (MD = −3.81, 95% CI: [−4.82, −2.81], $P < 0.00001$, $I^2 = 0\%$), and no statistically significant effect in another two groups. The results of subgroup analyses are summarized in **Table 3**. Meta-regression analyses on body weight indicated that the intervention duration ($\beta = -0.612$, $P = 0.189$) and participant type ($\beta = -0.16$, $P = 0.654$) were not related to interstudy heterogeneity.

Body Mass Index

Ten studies recorded outcomes for BMI. Meta-analysis results indicated that Pilates remarkably decreased BMI (MD = −1.17, 95% CI: [−1.85, −0.50], $P = 0.0006$) and a moderate heterogeneity was detected between studies ($P = 0.006$, $I^2 = 61\%$; **Figure 3**). Subgroup analysis based on intervention duration revealed that a significant reduction was observed on BMI in

TABLE 1 | Characteristics of the included studies.

References, country	Study design	Sample: population, sample size, mean age ± SD	Groups: sample size, mean age ± SD	Intervention	Intervention characteristics	Outcome measures	PEDro score
Cakmakçi (2011), Turkey	RCT	Healthy sedentary obese women, $n = 61$	IG: $n = 34$, 36.15 ± 9.59 years CG: $n = 27$, 38.96 ± 10.02 years	(a) IG: Pilates exercise (b) CG: without intervention	8 weeks, 4 sessions/week, 60 min/session	BW BMI BFP LBM WC	6
Gorji et al. (2015), Iran	RCT	Sedentary overweight women aged between 37 and 45 years (BMI > 25 kg/m^2), $n = 60$	IG: $n = 15$, 41.62 ± 2.05 years CG: $n = 15$, 40.62 ± 3.05 years SG: $n = 15$, 40.62 ± 3.05 years SPG: $n = 15$, 39.60 ± 2.70 years	(a) IG: Pilates exercise (b) CG: capsules containing starch powder, without other intervention (c) SG: celery supplement, not included in meta-analysis (d) SPG: celery supplement plus Pilates exercise, not included in meta-analysis	8 weeks, 3 sessions/week, 60 min/session	BW BMI	6
Savkin and Aslan (2016), Turkey	RCT	Sedentary overweight and obese women aged between 30 and 50 years (BMI ≥ 25 kg/m^2), $n = 37$, (43.79 ± 4.88) years	IG: $n = 19$, 43.79 ± 4.88 years CG: $n = 18$, 39.67 ± 6.30 years	(a) IG: Pilates exercise (b) CG: normal lifestyle	8 weeks, 3 sessions/week, 90 min/session	BW BMI BFP LBM WC	6
Wong et al. (2020), USA	RCT	Obese young women with elevated blood pressure aged between 19 and 27 years and BMI (30–40 kg/m^2), $n = 28$	IG: $n = 14$, 22.0 ± 3.74 years CG: $n = 14$, 23.0 ± 3.74 years	(a) IG: Pilates exercise (b) CG: normal lifestyle	12 weeks, 3 sessions/week, 60 min/session	BW BMI BFP LBM	8
Jung et al. (2020), Korea	RCT	Overweight and obese women aged between 34 and 60 years (BMI > 25 kg/m^2), $n = 32$, (47.5 ± 7.5) years	IG: $n = 10$, 43.8 ± 8.6 years CG: $n = 10$, 51.6 ± 6.5 years HPG: $n = 12$, 47.2 ± 6.4 years	(a) IG: normoxic Pilates exercise (b) CG: normal lifestyle (c) HPG: hypoxic Pilates exercise, not included in meta-analysis	12 weeks, 3 sessions/week, 50 min/session	BW BMI BFP	5
Gorji et al. (2014), Iran	RCT	Sedentary overweight women aged between 35 and 45 years (BMI ≥ 25 kg/m^2), $n = 30$	IG: $n = 15$, 39.60 ± 4.7 years CG: $n = 15$, 40.62 ± 3.05 years	(a) IG: Pilates exercise (b) CG: without intervention	8 weeks, 3 sessions/week, 60 min/session	BW BMI BFP	6
Khajehlandi et al. (2018), Iran	RCT	Overweight inactive women aged between 25 and 35 years, BMI (25–29 kg/m^2), $n = 28$	IG: $n = 14$, 30.1 ± 4.0 years CG: $n = 14$, 29.6 ± 3.6 years	(a) IG: Pilates exercise (b) CG: normal lifestyle	12 weeks, 3 sessions/week, 60 min/session	BW BMI	6
Chaudhary (2016), India	RCT	Overweight male people aged between 30 and 45 years, $n = 30$	IG: $n = 15$ CG: $n = 15$	(a) IG: Pilates exercise (b) CG: without intervention	10 weeks, 5–6 sessions/week, 30–40 min/session	BFP	6
Tyagi and Kumar (2020), India	RCT	Obese male people aged between 20 and 45 years, $n = 60$	IG: $n = 30$ CG: $n = 30$	(a) IG: Pilates exercise (b) CG: without intervention	24 weeks	BW BMI BFP	6
Khormizi and Azarniveh (2017), Iran	RCT	Obese women with type 2 diabetes aged between 40 and 60 years (BMI > 30 kg/m^2), $n = 30$, (51.9 ± 5.9) years	IG: $n = 15$, 51.06 ± 2.3 years CG: $n = 15$, 51.2 ± 3.7 years	(a) IG: Pilates exercise (b) CG: without intervention	8 weeks, 3 sessions/week, 60 min/session	BW BMI	7
Chen J. et al. (2020), China	RCT	Obese female college students (BMI ≥ 30 kg/m^2), $n = 39$	IG: $n = 20$ CG: $n = 19$	(a) IG: Pilates exercise (b) CG: normal lifestyle	16 weeks, 3 sessions/week, 60 min/session	BW BMI BFP	5

RCT, randomized controlled trials; SD, standard deviation; IG, intervention group; CG, control group; SG, supplement group; SPG, supplement plus Pilates group; HPG, hypoxic Pilates group; BW, body weight; BMI, body mass index; BFP, body fat percentage; LBM, lean body mass; WC, waist circumference.

TABLE 2 | PEDro scores of the included studies.

References	Eligibility criteria	Random allocation	Concealed allocation	Similar baseline	Blinding subjects	Blinding therapists	Blinding assessors	Dropout <15%	Intention to treat	Between-group statistics	Point measures	Total score
Jung et al. (2020)	Yes	Yes	No	Yes	No	No	No	Yes	No	Yes	Yes	5
Cakmakçi (2011)	Yes	Yes	No	Yes	No	No	No	Yes	Yes	Yes	Yes	6
Gorji et al. (2015)	Yes	Yes	No	Yes	No	No	No	Yes	Yes	Yes	Yes	6
Savkin and Aslan (2016)	Yes	Yes	Yes	Yes	No	No	No	Yes	No	Yes	Yes	6
Wong et al. (2020)	Yes	Yes	Yes	Yes	No	No	Yes	Yes	Yes	Yes	Yes	8
Gorji et al. (2014)	Yes	Yes	No	Yes	No	No	No	Yes	Yes	Yes	Yes	6
Khajehlandi et al. (2018)	Yes	Yes	No	Yes	No	No	No	Yes	Yes	Yes	Yes	6
Chaudhary (2016)	Yes	Yes	No	Yes	No	No	No	Yes	Yes	Yes	Yes	6
Tyagi and Kumar (2020)	Yes	Yes	No	Yes	No	No	No	Yes	Yes	Yes	Yes	6
Khormizi and Azarniveh (2017)	Yes	Yes	No	Yes	No	No	Yes	Yes	Yes	Yes	Yes	7
Chen J. et al. (2020)	Yes	Yes	No	Yes	No	No	No	Yes	No	Yes	Yes	5

PEDro, physiotherapy evidence database scale.

studies with more than 10 weeks of duration (MD = −1.04, 95% Cl: [−1.67, −0.40], $P = 0.001$, $I^2 = 51\%$); however, no significant effect in studies with duration of 10 weeks or less (MD = −1.36, 95% Cl: [−2.95, 0.24], $P = 0.10$, $I^2 = 66\%$). Additionally, the subgroup analysis according to participant type demonstrated that a remarkable decrease on BMI in studies including participants with overweight only or ones with obesity only (**Table 3**), which may be the reason for the excessive individual differences. Meta-regression analyses on BMI showed that the intervention duration ($\beta = -0.142$, $P = 0.761$) and participant type ($\beta = -0.17$, $P = 0.613$) were not correlated to interstudy heterogeneity.

Body Fat Percentage

Eight studies recorded outcomes for body fat percentage (BFP). Meta-analysis results revealed that Pilates significantly reduced BFP (MD = −4.22, 95% CI: [−6.44, −2.01], $P = 0.0002$), but a high heterogeneity was detected between studies ($P < 0.00001$, $I^2 = 88\%$; **Figure 4**). The subgroup analysis according to participant type revealed that a significant reduction on BFP in studies including participants with obesity only (MD = −3.56, 95% CI: [−5.07, −2.04], $P < 0.00001$, $I^2 = 67\%$), and no statistically significant effect in another two groups (**Table 3**).

Lean Body Mass and Waist Circumference

The analysis of three studies indicated that no significant effect on lean body mass (LBM) after Pilates (MD = −0.00, 95% CI: [−1.40, 1.40], $P = 1.00$), and a very low heterogeneity was seen between studies ($P = 0.27$, $I^2 = 23\%$). In addition, the meta-analysis of two studies demonstrated that waist circumference (WC) did not decrease after Pilates (MD = −2.65, 95%CI: [−6.84, 1.55], $P = 0.22$, $I^2 = 0\%$; **Figure 5**).

Secondary Outcomes

We considered safety as secondary outcomes in this study; however, no adverse events following Pilates intervention were reported in the included studies.

Sensitivity Analysis

The leave-one-out approach was used for sensitivity analysis of each outcomes (Patsopoulos et al., 2008; **Supplementary Table 2**). The analysis results indicated that the meta-analysis results for BMI and BFM did not alter when each study was removed in turn, and that the findings were robust. In the meta-analysis of BMI outcome, the removal of studies conducted by Khormizi and Azarniveh (2017) significantly reduced the heterogeneity, suggesting that this study could be the potential source of heterogeneity. Additionally, the meta-analysis results for body weight changed from significant ($P < 0.05$) to non-significant ($P = 0.06$) when the study by Chen J. et al. (2020) was removed, suggesting that this study was primarily responsible for the between-study heterogeneity.

Publication Bias

Visual inspection of funnel plots revealed no asymmetry (**Figure 6**), and the results from Egger's and Begg's test indicated that no evidence for publication bias was detected for body weight (Begg's test, $P = 0.59$; Egger's test, $P = 0.35$) and BMI (Begg's test, $P = 0.37$; Egger's test, $P = 0.55$).

Quality of Evidence

Regarding the assessment of the quality of evidence, there is low to moderate evidence in body weight and BMI, very low to low evidence in BFP, low evidence in lean body mass, and moderate evidence in waist circumference. This indicates that

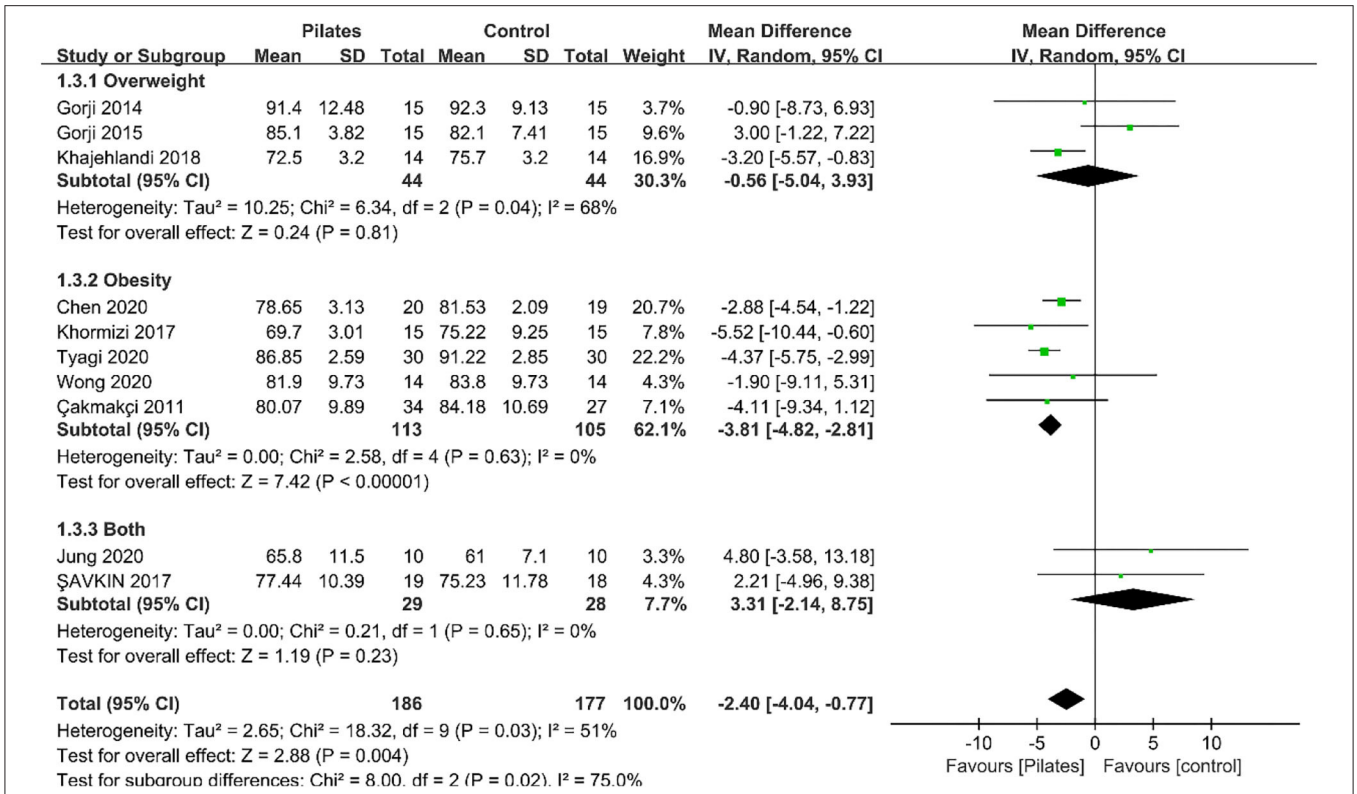

FIGURE 2 | Forest plot of meta-analysis on body weight.

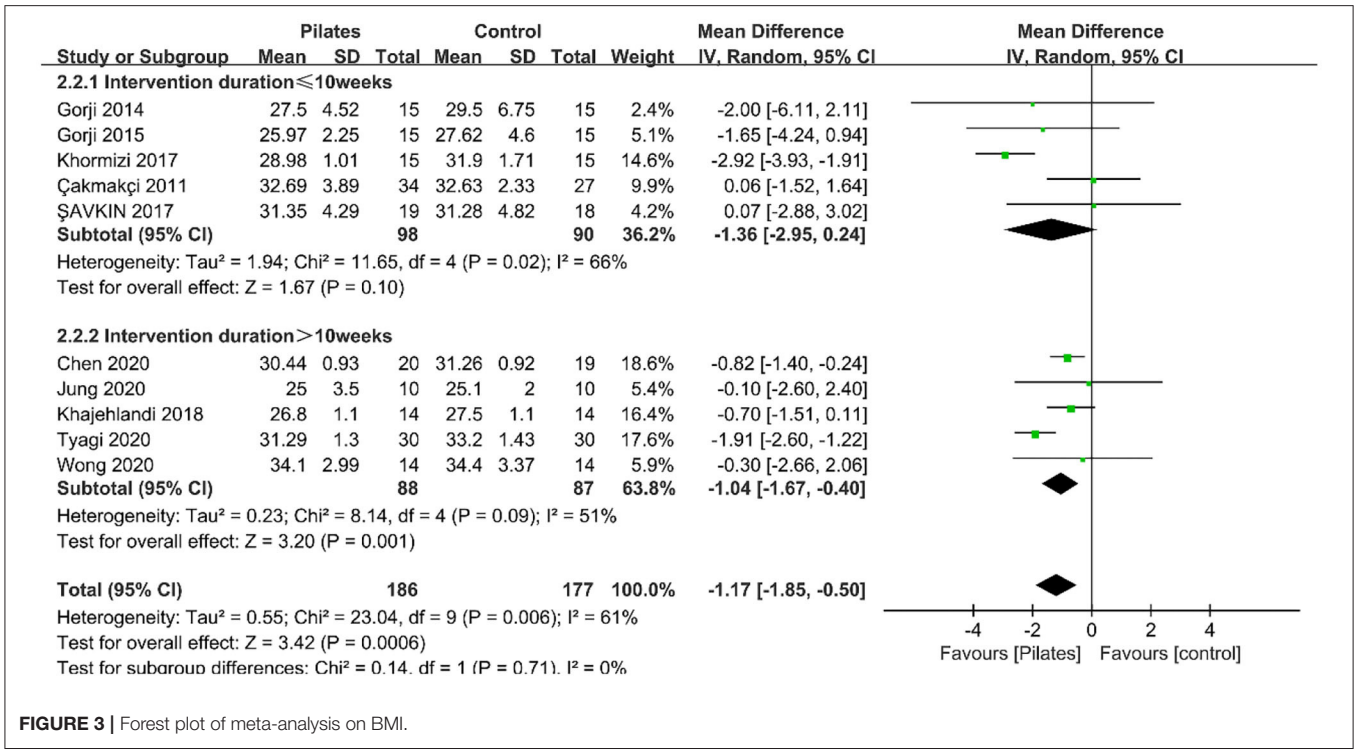

FIGURE 3 | Forest plot of meta-analysis on BMI.

TABLE 3 | Results of the subgroup analyses and overall analyses.

	No. of datasets	No. of subjects	Meta-analysis MD (95% CI)	*P*-value	Heterogeneity *Q* statistic	*P*-value	I^2 (%)	*P* between group
Body weight (kg)								
Overall	10	363	−2.40 (−4.04, −0.77)	0.004	18.32	0.03	51	–
Intervention duration								
≤10 weeks	5	188	−1.17 (−4.91, 2.58)	0.54	8.82	0.07	55	0.29
>10 weeks	5	175	−3.30 (−4.67, −1.92)	<0.00001	6.08	0.19	34	
Participant type								
Overweight	3	88	−0.56 (−5.04, 3.93)	0.81	6.34	0.04	68	0.02
Obesity	5	218	−3.81 (−4.82, −2.81)	<0.00001	2.58	0.63	0	
Both	2	57	3.31 (−2.14, 8.75)	0.23	0.21	0.65	0	
Body mass index (kg/m^2)								
Overall	10	363	−1.17 (−1.85, −0.50)	0.0006	23.04	0.006	61	–
Intervention duration								
≤10 weeks	5	188	−1.36 (−2.95, 0.24)	0.1	11.65	0.02	66	0.71
>10 weeks	5	175	−1.04 (−1.67, −0.40)	0.001	8.14	0.09	51	
Participant type								
Overweight	3	88	−0.83 (−1.59, −0.06)	0.03	0.79	0.67	0	0.44
Obesity	5	218	−1.35 (−2.33, −0.38)	0.007	18.84	0.0008	79	
Both	2	57	−0.03 (−1.93, 1.88)	0.98	0.01	0.93	0	
Body fat percentage (%)								
Overall	8	305	−4.22 (−6.44, −2.01)	0.002	59.72	<0.00001	88	–
Intervention duration								
≤10 weeks	4	158	−6.39 (−10.65, −2.12)	0.003	40.47	<0.00001	93	0.10
>10 weeks	4	147	−2.77 (−3.65, −1.88)	<0.00001	2.35	0.50	0	
Participant type								
Overweight	2	60	−9.82 (−20.16, 0.53)	0.06	28.24	<0.00001	96	0.04
Obesity	4	188	−3.56 (−5.07, −2.04)	<0.00001	9.02	0.03	67	
Both	2	57	−0.12 (−2.82, 2.58)	0.93	0.13	0.72	0	

Both, overweight and obesity; MD, mean difference.

more researches may have a significant impact on the results of the effect estimate and even may change the results. The detailed information was presented in **Supplementary Table 3**.

DISCUSSION

Summary of Main Results

We performed this study to evaluate scientific evidence for the efficacy of Pilates in improving body weight and body composition in adults with overweight or obesity. The analyses combined 11 studies involving a total of 393 adults with overweight or obesity (90 men and 303 women). Outcome measures were body weight, BMI, BFP, lean body mass, and WC. Overall results revealed that Pilates leads to a significant decrease in body weight, BMI, and BFP in adults with overweight or obesity. The reduction in body weight and BFP appears to be more pronounced in studies including participants with obesity only, and the efficacy of Pilates for the improvement of body weight and BMI appears to be more evident in longer intervention duration. These findings could have significant implications for the promotion of exercise interventions for overweight and obesity management. We also found that Pilates has no remarkable effect on WC and lean body mass. However, given the low to moderate overall quality of the evidence, we are still unable to draw a definite conclusion. Furthermore, since no trials reported adverse events, we could not judge the safety of Pilates.

Comparison With Other Reviews

To our knowledge, this is the first systematic review and meta-analysis to investigate the effects of Pilates on body weight and body composition in adults with overweight or obesity. In the previous reviews, few studies systematically analyzed and assessed the effects of Pilates on body weight and body composition. Aladro-Gonzalvo et al. (2012) conducted a systematic review to determine the effects of Pilates on body composition in several populations; the results suggested that there is insufficient evidence indicating a positive effect of Pilates on body weight and body composition. This finding is inconsistent with our review, and the main reason that might explain this is the poor methodological quality of the included studies. In another systematic review (Kamioka et al., 2016),

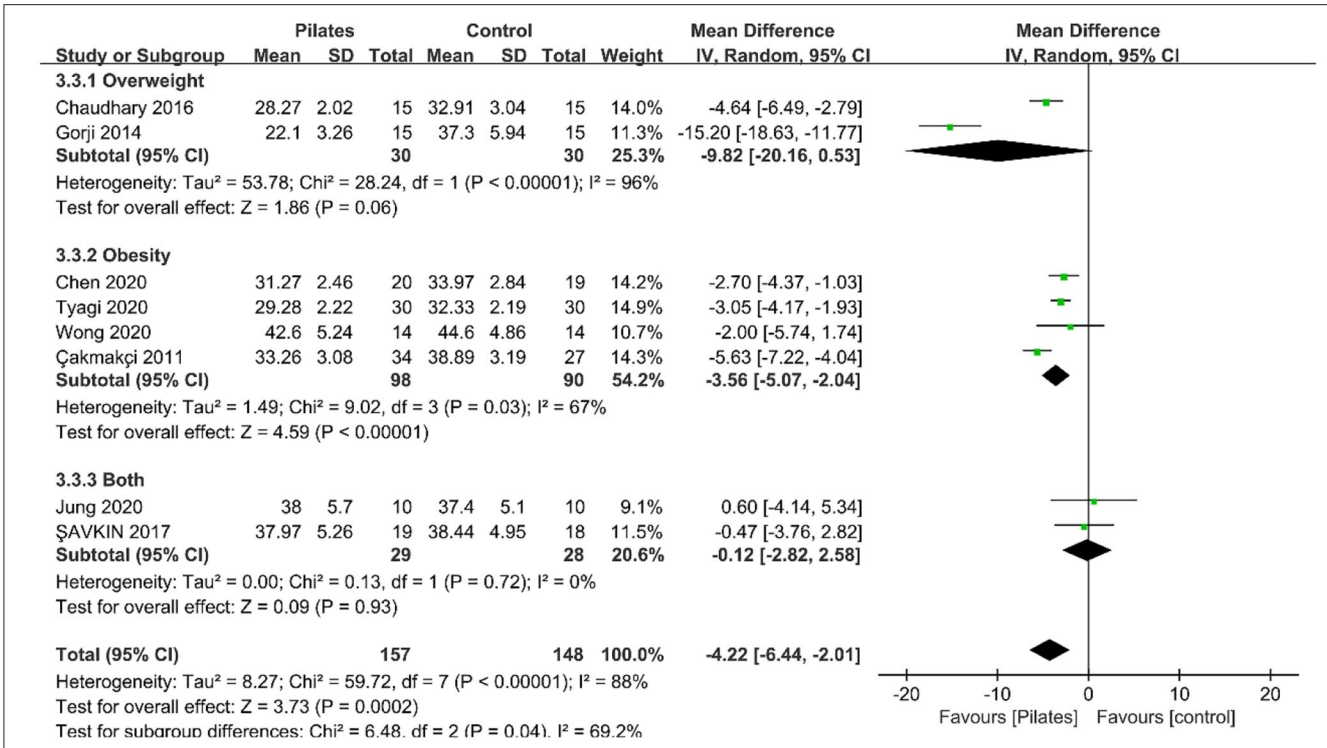

FIGURE 4 | Forest plot of meta-analysis on body fat percentage.

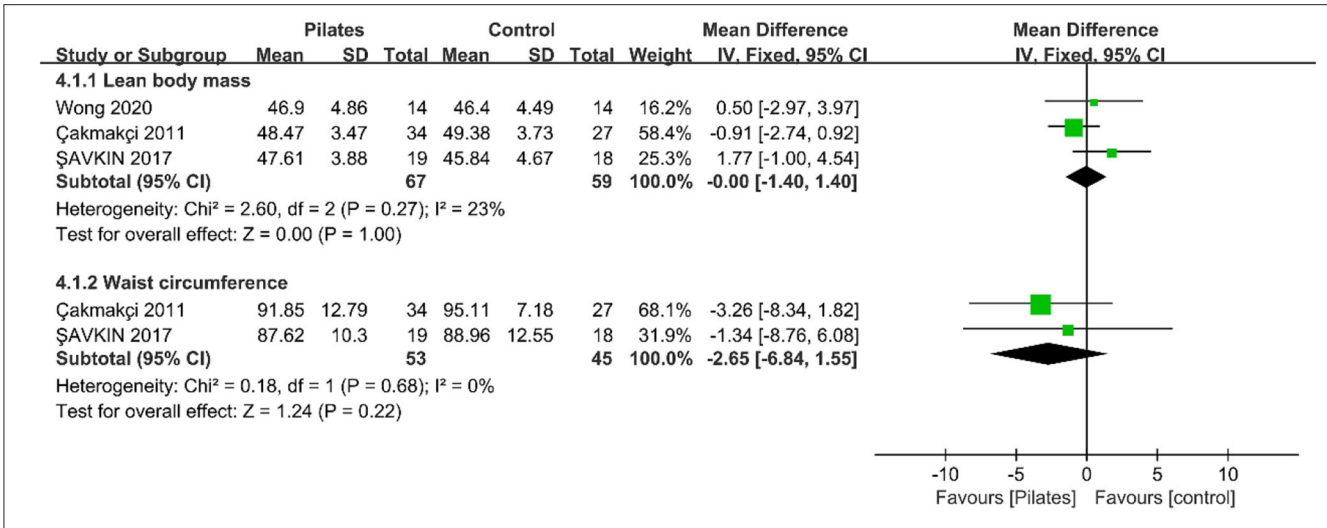

FIGURE 5 | Forest plot of meta-analysis on lean body mass and waist circumference.

there was some evidence that Pilates could reduce body fat and increase fat free mass. Although this is partially consistent with our findings, the authors of this review did not perform a meta-analysis, which limited the comparison with our review. The most recent review (de Souza Cavina et al., 2020) showed no evidence for the efficacy of Pilates in improving body weight and body composition in general population including overweight and obese individuals; the results conflicted with our present review, and insufficient training intensity and not performing diet control could be the main reasons for these results.

How the Intervention Might Work

Overweight and obesity, which are serious public health problems worldwide, are associated with many comorbidities

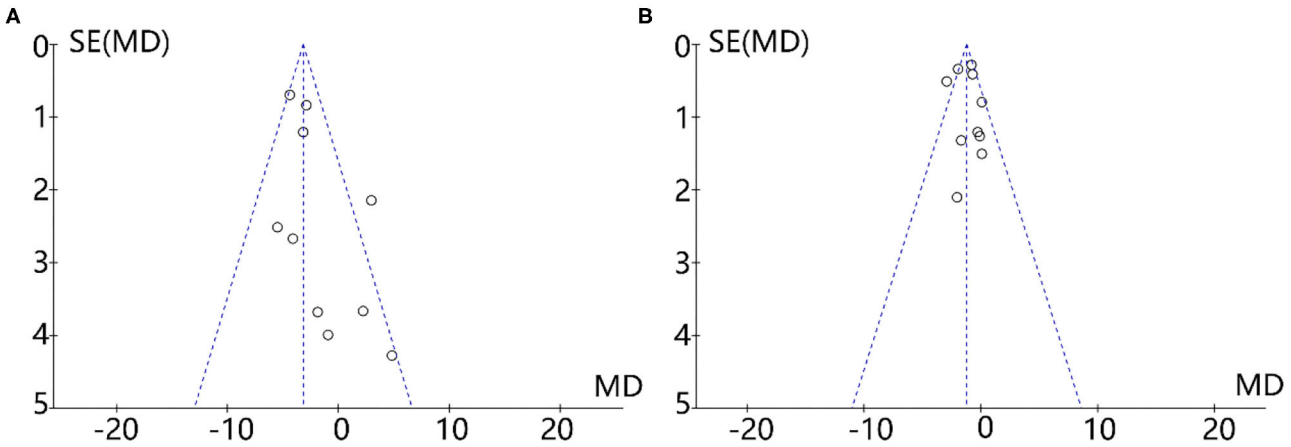

FIGURE 6 | Funnel plots of 10 RCTs recording body weight **(A)** and BMI **(B)** outcomes.

such as insulin resistance and diabetes (Diabetes Prevention Program Research Group, 2002; Look AHEAD Research Group, 2003), hypertension and cardiovascular disease (Ozbey et al., 2002), metabolic syndrome (Frank et al., 2005), depression, and also cancer (Field et al., 2001). While overweight and obesity are being prevented and treated worldwide, they continue to be highly prevalent conditions that impose a substantial economic burden (Kushner and Kahan, 2018). Therefore, growing attention has been poured to the problems of body weight and a mounting number of medical staff have attached importance to develop available and affordable therapies for reducing body weight. Some studies indicated that exercise could improve the functions of several body systems, thereby improving body weight, body composition, cardiometabolic risk factors, and emotional health status (Jakicic et al., 2018; Garber, 2019), so exercise is widely used to reduce body weight in clinical practice. As for Pilates, it is often considered an alternative form of exercise. It was reported that completion of 30–45 min Pilates exercise could produce sufficient stimuli to induce positive changes in energy expenditure, thus reducing body weight (Olson et al., 2004). Moreover, since Pilates exercise involves employing different types of resistance (Lange et al., 2000), it could enhance the muscle strength of upper body parts, lower body parts, and abdomen (Bergamin et al., 2015) and could thus contribute to improving body composition. Besides exercise, Pilates also involves relaxation, concentration, and breath control. Thus, Pilates has been shown to effectively improve depression and anxiety (Vancini et al., 2017; Fleming and Herring, 2018; Aibar-Almazán et al., 2019), which might in turn improve overweight or obesity caused by emotional factors (Jantaratnotai et al., 2017).

Limitations

However, this present review had several potential limitations. Firstly, the overall effect sizes could have been affected by lack of concealed allocation (9 out of 11 studies), inability to use therapists/subjects blinding (all studies) or assessors blinding (9 out of 11 studies). Secondly, publication bias might have been a factor, as this review retrieved only relevant articles in the English and Chinese language within a limited number of electronic databases. Thirdly, given the small size of overall samples, some conclusions should be considered preliminary and even might be biased. Fourthly, there was a moderate to high heterogeneity between studies, while several subgroup analyses could explain the heterogeneity to some extent; however, considerable heterogeneity remained unclear. This may be partially because of the differences in participants (e.g., age, gender, race, lifestyle), Pilates intervention (e.g., exercise modalities, duration, dose, intensity), and the measuring method of outcomes. In addition, it remained unclear whether Pilates was more effective than other exercises for improving body weight and body composition as the included studies did not involve other exercise interventions.

Implications for Clinical Practice

This present meta-analysis showed that Pilates could improve body weight, BMI, and BFP in adults with overweight or obesity. Although the methodological quality of the included RCTs is poor, Pilates could still be preliminarily considered an effective intervention to treat overweight and obesity. It has been shown that people with overweight or obesity find it difficult to adhere to physical activities targeting weight loss (Burgess et al., 2017), mainly due to the monotony of physical activities (Vancini et al., 2017); these people are however more likely to practice Pilates (de Souza Cavina et al., 2020). Therefore, Pilates could be specifically considered an alternative to other forms of physical exercise for overweight or obese people who do not abide by recommended physical exercise regimens.

Implications for Further Research

Given the poor methodological quality of the majority of RCTs and the limited strength of evidence, more rigorous and robust methods are recommended to use in future studies. Firstly, the reporting of future Pilates RCTs should be improved and strictly follow standard reporting guidelines such as CONSORT (Schulz

et al., 2010). Secondly, future RCTs should further ensure the use of concealed allocation, therapists/subjects blinding, intention-to-treat analysis, and assessors blinding. Thirdly, to reduce potential publication bias, the researchers are recommended to register beforehand in the clinical trial registry before recruiting participants. Fourthly, there were no adverse events described in any of the included studies, considering that safety is critical to the evaluation of therapies, future RCTs should improve the reporting of safety. Fifthly, future RCTs should compare Pilates with other interventions (e.g., aerobic exercise, resistance exercise) to evaluate the potential benefits of Pilates for overweight and obesity. In addition, there is evidence that diet and exercise play an important role in weight loss and promoting positive changes in body composition (Clark, 2015). Considering that diet is an uncontrollable factor, in order to eliminate the significant interference of diet on the results, we excluded studies with dietary intervention in this study to determine the effects of Pilates on body weight and body composition in adults with overweight or obesity. Some studies demonstrated that dietary intervention plus exercise resulted in an even greater reduction in body weight and body composition profile parameters than dietary interventions alone (Figueroa et al., 2013; Cheng et al., 2018). In view of this, it remained uncertain whether Pilates plus diet intervention was more effective than Pilates interventions alone in improving body weight and body composition, and further researches are needed to confirm it.

CONCLUSION

In conclusion, this present study indicated that Pilates lead to a remarkable decrease in body weight, BMI, and BFP in adults with overweight or obesity. No significant effect on WC and LBM. Large-scale and well-designed RCTs with improved methodology and reporting are recommended to further elucidate the effectiveness of Pilates for treating overweight and obesity.

DATA AVAILABILITY STATEMENT

The original contributions presented in the study are included in the article/**Supplementary Material**, further inquiries can be directed to the corresponding author/s.

AUTHOR CONTRIBUTIONS

YW and XX conceived and designed the study. YW and ZC performed the literature search, data extraction, and data analysis. ZW and XY helped with the data analysis and reviewed the manuscript for important content. XX supervised the study. All authors have read and approved the final version of the submitted version.

FUNDING

This work was supported by Soft Science Research Project of Guangdong Province (No. 2018B020207009) and Science and Technology Plan Project of Guangdong Province (2019A141401008).

SUPPLEMENTARY MATERIAL

The Supplementary Material for this article can be found online at: https://www.frontiersin.org/articles/10.3389/fphys.2021.643455/full#supplementary-material

REFERENCES

Aibar-Almazán, A., Hita-Contreras, F., Cruz-Díaz, D., de la Torre-Cruz, M., Jiménez-García, J. D., and Martínez-Amat, A. (2019). Effects of Pilates training on sleep quality, anxiety, depression and fatigue in postmenopausal women: a randomized controlled trial. *Maturitas* 124, 62–67. doi: 10.1016/j.maturitas.2019.03.019

Aladro-Gonzalvo, A. R., Machado-Díaz, M., Moncada-Jiménez, J., Hernández-Elizondo, J., and Araya-Vargas, G. (2012). The effect of Pilates exercises on body composition: a systematic review. *J. Bodyw. Mov. Ther*. 16, 109–114. doi: 10.1016/j.jbmt.2011.06.001

Bergamin, M., Gobbo, S., Bullo, V., Zanotto, T., Vendramin, B., Duregon, F., et al. (2015). Effects of a Pilates exercise program on muscle strength, postural control and body composition: results from a pilot study in a group of post-menopausal women. *Age* 37, 1–8. doi: 10.1007/s11357-015-9852-3

Burgess, E., Hassmén, P., Welvaert, M., and Pumpa, K. L. (2017). Behavioural treatment strategies improve adherence to lifestyle intervention programmes in adults with obesity: a systematic review and meta-analysis. *Clin. Obes*. 7, 105–114. doi: 10.1111/cob.12180

Cakmakçi, O. (2011). The effect of 8 week plates exercise on body composition in obese women. *Coll. Anthropol*. 35, 1045–1050.

Chaudhary, S. (2016). Role of Pilates exercises to reduce body fat percentage of overweight people. *Indian J. Phys. Educ. Sports Appl. Sci*. 10.

Chen, J., Li, Y., Wu, Y., and Su, X. (2020). Effects of Pilates exercise on body composition and serum inflammatory factors in obese female college students with depression. *Chin. J. Sch. Health*. 41, 783–786. doi: 10.16835/j.cnki.1000-9817.2020.05.040

Chen, Z., Ye, X., Shen, Z., Chen, G., Chen, W., He, T., et al. (2020). Effect of pilates on sleep quality: a systematic review and meta-analysis of randomized controlled trials. *Front. Neurol*. 11:158. doi: 10.3389/fneur.2020.00158

Cheng, C. C., Hsu, C. Y., and Liu, J. F. (2018). Effects of dietary and exercise intervention on weight loss and body composition in obese postmenopausal women: a systematic review and meta-analysis. *Menopause* 25, 772–782. doi: 10.1097/GME.0000000000001085

Clark, J. E. (2015). Diet, exercise or diet with exercise: comparing the effectiveness of treatment options for weight-loss and changes in fitness for adults (18-65 years old) who are overfat, or obese; systematic review and meta-analysis. *J. Diabetes. Metab. Disord*. 14, 1–28. doi: 10.1186/s40200-015-0204-8

de Souza Cavina, A. P., Junior, E. P., Machado, A. F., Biral, T. M., Lemos, L. K., Rodrigues, C. R. D., et al. (2020). Effects of the mat pilates method on body composition: systematic review with meta-analysis. *J. Phys. Act. Health* 17, 673–681. doi: 10.1123/jpah.2019-0171

Diabetes Prevention Program Research Group (2002). Reduction in the incidence of type 2 diabetes with lifestyle intervention or metformin. *N. Engl. J. Med*. 346, 393–403. doi: 10.1056/NEJMoa012512

Eliks, M., Zgorzalewicz-Stachowiak, M., and Zeńczak-Praga, K. (2019). Application of Pilates-based exercises in the treatment of chronic non-specific low back pain: state of the art. *Postgrad. Med. J*. 95, 41–45. doi: 10.1136/postgradmedj-2018-135920

Expert Panel Members, Jensen, M. D., Ryan, D. H., Donato, K. A., Apovian, C. M., Ard, J. D., et al. (2014). Executive summary: guidelines (2013) for the management of overweight and obesity in adults: a report of the American College of Cardiology/American Heart Association Task Force on Practice Guidelines and the Obesity Society published by the Obesity

Society and American College of Cardiology/American Heart Association Task Force on Practice Guidelines. Based on a systematic review from the The Obesity Expert Panel, 2013. *Obesity* 22, S5–S39. doi: 10.1002/oby.20821

Fernández-Rodríguez, R., Álvarez-Bueno, C., Ferri-Morales, A., Torres-Costoso, A. I., Cavero-Redondo, I., and Martínez-Vizcaíno, V. (2019). Pilates method improves cardiorespiratory fitness: a systematic review and meta-analysis. *J. Clin. Med.* 8:1761. doi: 10.3390/jcm8111761

Field, A. E., Coakley, E. H., Must, A., Spadano, J. L., Laird, N., Dietz, W. H., et al. (2001). Impact of overweight on the risk of developing common chronic diseases during a 10-year period. *Arch. Intern. Med.* 161, 1581–1586. doi: 10.1001/archinte.161.13.1581

Figueroa, A., Vicil, F., Sanchez-Gonzalez, M. A., Wong, A., Ormsbee, M. J., Hooshmand, S., et al. (2013). Effects of diet and/or low-intensity resistance exercise training on arterial stiffness, adiposity, and lean mass in obese postmenopausal women. *Am. J. Hypertens.* 26, 416–423. doi: 10.1093/ajh/hps050

Fleming, K. M., and Herring, M. P. (2018). The effects of Pilates on mental health outcomes: a meta-analysis of controlled trials. *Complement. Ther. Med.* 37, 80–95. doi: 10.1016/j.ctim.2018.02.003

Frank, L. L., Sorensen, B. E., Yasui, Y., Tworoger, S. S., Schwartz, R. S., Ulrich, C. M., et al. (2005). Effects of exercise on metabolic risk variables in overweight postmenopausal women: a randomized clinical trial. *Obes. Res.* 13, 615–625. doi: 10.1038/oby.2005.66

Garber, C. E. (2019). The health benefits of exercise in overweight and obese patients. *Curr. Sport. Med. Rep.* 18, 287–291. doi: 10.1249/JSR.0000000000000619

Girard, O., Malatesta, D., and Millet, G. P. (2017). Walking in hypoxia: an efficient treatment to lessen mechanical constraints and improve health in obese individuals? *Front. Physiol.* 8:73. doi: 10.3389/fphys.2017.00073

Gorji, N. E., Farzanegi, P., Habibian, M., Mahdirejei, H. A., and Abadei, S. F. (2015). Celery as an effective supplement for pilates exercise in weight loss studies. *Int. Med,. J.* 22, 190–193.

Gorji, N. E.,Habibian,M., and Farzanegi, P. (2014). 8Weeks pilates training effects on fetuin-a levels and anthropometric indicators in sedentary overweight women. *Int. Med.* J. 21, 548–551.

GRADE Working Group (2004). Grading quality of evidence and strength of recommendations. *BMJ* 328:1490. doi: 10.1136/bmj.328.7454.1490

Guyatt, G. H., Oxman, A. D., Kunz, R., Atkins, D., Brozek, J., Vist, G., et al. (2011). GRADE guidelines: 2. Framing the question and deciding on important outcomes. *J. Clin. Epidemiol.* 64, 395–400. doi: 10.1016/j.jclinepi.2010.09.012

Hagner-Derengowska, M., Kaluzny, K., Kochanski, B., Hagner, W., Borkowska, A., Czamara, A., et al. (2015). Effects of Nordic Walking and Pilates exercise programs on blood glucose and lipid profile in overweight and obese postmenopausal women in an experimental, nonrandomized, open-label, prospective controlled trial. *Menopause* 22, 1215–1223. doi: 10.1097/GME.0000000000000446

Hammond, R. A., and Levine, R. (2010). The economic impact of obesity in the United States. *Diabetes Metab. Syndr. Obes.* 3:285. doi: 10.2147/DMSO.S7384

Higgins, J. P. T., Thomas, J., Chandler, J., Cumpston, M., Li, T., Page, M. J., et al. (eds.). (2020). *Cochrane Handbook for Systematic Reviews of Interventions version 6.1 (updated September 2020).* Cochrane, 2020. Available online at: www.training.cochrane.org/handbook (accessed December 04, 2020).

Higgins, J. P. T., and Thompson, S. G. (2002). Quantifying heterogeneity in a meta-analysis. *Stat. Med.* 21, 1539–1558. doi: 10.1002/sim.1186

Hun-Young, P., Won-Sang, J., Jisu, K. I. M., and Hyejung, H., Kiwon, L. (2019). Changes in the paradigm of traditional exercise in obesity therapy and application of a new exercise modality: a narrative review article. *Iran J. Public Health.* 48, 1395–1404. doi: 10.18502/ijph.v48i8.2978

Jakicic, J. M., Rogers, R. J., Davis, K. K., and Collins, K. A. (2018). Role of physical activity and exercise in treating patients with overweight and obesity. *Clin. Chem.* 64, 99–107. doi: 10.1373/clinchem.2017.272443

Jantaratnotai, N., Mosikanon, K., Lee, Y., and McIntyre, R. S. (2017). The interface of depression and obesity. *Obes. Res. Clin. Pract.* 11, 1–10. doi: 10.1016/j.orcp.2016.07.003

Jung, K., Kim, J., Park, H. Y., Jung, W. S., and Lim, K. (2020). Hypoxic Pilates intervention for obesity: a randomized controlled trial. *Int. J. Environ. Res. Public Health* 17:7186. doi: 10.3390/ijerph17197186

Kamioka, H., Tsutani, K., Katsumata, Y., Yoshizaki, T., Okuizumi, H., Okada, S., et al. (2016). Effectiveness of Pilates exercise: a quality evaluation and summary of systematic reviews based on randomized controlled trials. *Complement. Ther. Med.* 25, 1–19. doi: 10.1016/j.ctim.2015.12.018

Khajehlandi, M., Bolboli, L., and Siahkuhian, M. (2018). Effect of Pilates Exercise Training on Serum Osteocalcin and Parathormone levels in inactive and overweight women. *Hormozgan. Med. J.* 22, 87–94. doi: 10.29252/hmj.22.2.87

Khormizi, S. A. T., and Azarniveh, M. S. (2017). The effect of Pilates exercise on glycemic control and weight loss in obese women with type2 diabetes. *Int. Sci. J. Kine* 10, 68–73.

Kushner, R. F., and Kahan, S. (2018). Introduction: the state of obesity in 2017. *Med. Clin.* 102, 1–11. doi: 10.1016/j.mcna.2017.08.003

Lange, C., Unnithan, V. B., Larkam, E., and Latta, P. M. (2000). Maximizing the benefits of Pilates-inspired exercise for learning functional motor skills. *J. Bodyw. Mov. Ther.* 4, 99–108. doi: 10.1054/jbmt.1999.0161

Latey, P. (2001). The Pilates method: history and philosophy. *J. Bodyw. Mov. Ther.* 5, 275–282. doi: 10.1054/jbmt.2001.0237

Look AHEAD Research Group (2003). Look AHEAD (Action for Health in Diabetes): design and methods for a clinical trial of weight loss for the prevention of cardiovascular disease in type 2 diabetes. *Control. Clin. Trials* 24, 610–628. doi: 10.1016/S0197-2456(03)00064-3

Macedo, L. G., Elkins, M. R., Maher, C. G., Moseley, A. M., Herbert, R. D., and Sherrington, C. (2010). There was evidence of convergent and construct validity of Physiotherapy Evidence Database quality scale for physiotherapy trials. *J. Clin. Epidemiol.* 63, 920–925. doi: 10.1016/j.jclinepi.2009.10.005

Maher, C. G., Sherrington, C., Herbert, R. D., Moseley, A. M., and Elkins, M. (2003). Reliability of the PEDro scale for rating quality of randomized controlled trials. *Phys. Ther.* 83, 713–721. doi: 10.1093/ptj/83.8.713

Moher, D., Liberati, A., Tetzlaff, J., Altman, D. G., and Prisma Group, M. (2009). Preferred reporting items for systematic reviews and meta-analyses: the PRISMA statement. *PLoS Med.* 6:e1000097. doi: 10.1371/journal.pmed.1000097

Morgen, C. S., and Sørensen, T. I. A. (2014). Global trends in the prevalence of overweight and obesity. *Nat. Rev. Endocrinol.* 10, 513–514. doi: 10.1038/nrendo.2014.124

Olson, M. S., Williford, H. N., Martin, R. S., Ellis, M., Woolen, E., and Esco, M. R. (2004). The energy cost of a basic, intermediate, and advanced Pilates' mat workout. *Med. Sci. Sports Exerc.* 36:S357. doi: 10.1097/00005768-200405001-01711

Ozbey, N., Sencer, E., Molvalilar, S., and Orhan, Y. (2002). Body fat distribution and cardiovascular disease risk factors in pre-and postmenopausal obese women with similar BMI. *Endocr. J.* 49, 503–509. doi: 10.1507/endocrj.49.503

Patsopoulos, N. A., Evangelou, E., and Ioannidis, J. P. A. (2008). Sensitivity of between-study heterogeneity in meta-analysis: proposed metrics and empirical evaluation. *Int. J. Epidemiol.* 37, 1148–1157. doi: 10.1093/ije/dyn065

Rayes, A. B. R., de Lira, C. A. B., Viana, R. B., Benedito-Silva, A. A., and Vancini, R. L. (2019). The effects of Pilates vs. aerobic training on cardiorespiratory fitness, isokinetic muscular strength, body composition, and functional tasks outcomes for individuals who are overweight/obese: a clinical trial. *PeerJ* 7:e6022. doi: 10.7717/peerj.6022

Savkin, R., and Aslan, U. B. (2016). The effect of Pilates exercise on body composition in sedentary overweight and obese women. *J. Sport Med. Phys. Fit* 57, 1464–1470. doi: 10.23736/S0022-4707.16.06465-3

Schulz, K. F., Altman, D. G., and Moher, D. (2010). CONSORT 2010 statement: updated guidelines for reporting parallel group randomised trials. *Trials* 11, 1–8. doi: 10.1186/1745-6215-11-32

Sharma, D., Kaur, J., Rani, M., Bansal, A., Malik, M., and Kulandaivelan, S. (2018). Efficacy of Pilates based mat exercise on quality of life, quality of sleep and satisfaction with life in type 2 diabetes mellitus. *Rom. J. Diabetes Nutr. Metab. Dis.* 25, 149–156. doi: 10.2478/rjdnmd-2018-0017

Tyagi, R., and Kumar, P. (2020). The effects of selected Pilates exercise on the body composition of obese people. *J. Crit. Rev.* 7, 3374–3381.

Vancini, R. L., Rayes, A. B. R., Lira, C. A. B., Sarro, K. J., and Andrade, M. S. (2017). Pilates and aerobic training improve levels of depression, anxiety and quality of life in overweight and obese individuals. *Arq. Neuro-Psiquiatr.* 75, 850–857. doi: 10.1590/0004-282x20170149

Wong, A., Figueroa, A., Fischer, S. M., Bagheri, R., and Park, S. Y. (2020). The effects of mat pilates training on vascular function and body fatness in obese young women with elevated blood pressure. *Am. J. Hypertens.* 33, 563–569. doi: 10.1093/ajh/hpaa026

World Health Organization (2018). *Noncommunicable Diseases.* Available online at: https://www.who.int/zh/news-room/fact-sheets/detail/noncommunicable-diseases (accessed December 18, 2020).

World Health Organization (2020). *Obesity and Overweight.* Available online at: https://www.who.int/en/news-room/fact-sheets/detail/obesity-and-overweight (accessed December 18, 2020).

Conflict of Interest: The authors declare that the research was conducted in the absence of any commercial or financial relationships that could be construed as a potential conflict of interest.

frontiers in Physiology

ORIGINAL RESEARCH
published: 31 March 2021
doi: 10.3389/fphys.2021.650260

Association of Metabolic Syndrome With Prevalence of Obstructive Sleep Apnea and Remission After Sleeve Gastrectomy

Yufei Chen[1,2†], Lijia Chen[1,2†], Lingxia Ye[3], Jiabin Jin[4], Yingkai Sun[1,2], Ling Zhang[1,2], Shaoqian Zhao[1,2], Yifei Zhang[1,2], Weiqing Wang[1,2], Weiqiong Gu[1,2] and Jie Hong[1,2*]*

[1] Department of Endocrine and Metabolic Diseases, Ruijin Hospital Affiliated to Shanghai Jiao Tong University School of Medicine, Shanghai, China, [2] Shanghai Institute of Endocrine and Metabolic Diseases, Shanghai, China, [3] Department of Endocrinology, The Second Affiliated Hospital of Zhejiang University School of Medicine, Hangzhou, China, [4] Department of Pancreatic Surgery, Ruijin Hospital Affiliated to Shanghai Jiao Tong University School of Medicine, Shanghai, China

OPEN ACCESS

Edited by:
Yan Lu,
Fudan University, China

Reviewed by:
Huijie Zhang,
Southern Medical University, China
Chen Ying,
Fudan University, China

***Correspondence:**
Weiqiong Gu
weiqionggu@163.com
Jie Hong
hongjie@medmail.com.cn

[†] These authors have contributed equally to this work and share first authorship

Specialty section:
This article was submitted to Clinical and Translational Physiology, a section of the journal Frontiers in Physiology

Received: 06 January 2021
Accepted: 08 March 2021
Published: 31 March 2021

Citation:
Chen Y, Chen L, Ye L, Jin J, Sun Y, Zhang L, Zhao S, Zhang Y, Wang W, Gu W and Hong J (2021) Association of Metabolic Syndrome With Prevalence of Obstructive Sleep Apnea and Remission After Sleeve Gastrectomy. Front. Physiol. 12:650260. doi: 10.3389/fphys.2021.650260

Obesity is an important risk factor for metabolic syndrome and obstructive sleep apnea (OSA). Bariatric surgery has been shown to effectively reduce weight and obesity-related comorbidities. However, the prevalence and severity of OSA in obese patients with different baseline metabolic states and the improvements of OSA after bariatric surgery remain unknown. The main aims of this study were to ascertain the prevalence of OSA in young Chinese obese patients with different metabolic states and to evaluate their respective OSA remission after laparoscopic sleeve gastrectomy. We first performed a cross-sectional study involving 123 metabolically healthy obese patients and 200 metabolically unhealthy obese patients (who had the same age and BMI ranges) to estimate the prevalence of OSA at baseline. Then we performed a retrospective study, which was registered at ClinicalTrials.gov (ref. NCT02653430) of 67 patients who underwent laparoscopic sleeve gastrectomy to evaluate the remission of OSA. Metabolically healthy and unhealthy obese patients had similar apnea-hypopnea index levels (16.6 ± 22.0 vs. 16.7 ± 18.7 events/h, $P = 0.512$) and prevalence of OSA (66.7% vs. 69.0%, $P = 0.662$). Male sex, age, waist circumference and lower liver-to-spleen ratio were independent risk factors for OSA. After laparoscopic sleeve gastrectomy, no difference was found in the decrease in body mass index (BMI) change (10.8 ± 4.8 vs. 10.8 ± 3.0 kg/m^2, $P = 0.996$) or the decrease in the apnea-hypopnea index (18.9 ± 24.6 vs. 17.0 ± 24.0 events/h, $P = 0.800$). The remission of moderate-to-severe OSA was observed in the MHO (36.3%; 54.5–18.2%, $P = 0.125$) and MUO (32.2%; 66.1–33.9%, $P = 0.001$) patients. These results suggest that, in patients with obesity, metabolic syndrome does not add extra risk for the prevalence or severity of OSA. Both metabolically healthy and unhealthy obese patients could benefit equally from laparoscopic sleeve gastrectomy in terms of weight loss and obstructive sleep apnea remission.

Keywords: metabolically healthy obesity, metabolically unhealthy obesity, metabolic syndrome, obstructive sleep apnea, laparoscopic sleeve gastrectomy

INTRODUCTION

The prevalence of obesity has continued to rise in prevalence at a rapid rate over the past decades. As of 2015, 2.2 billion people were overweight or obese worldwide, accounting for about one-third of the world's total population (Reilly, 2017). It is well recognized that there is an obese phenotype that does not involve the typical metabolic disorders associated with obesity. This unique subset of obese individuals without metabolic syndromes (MetS) has been described as "benign obesity" or "metabolically healthy obesity (MHO)." Previous reports of this special obesity phenotype mostly focused on the risk of all-cause mortality, cardiovascular events, and diabetes, and the conclusions remain controversial. Some studies have suggested that obese individuals have increased risk of adverse outcomes even in the absence of metabolic abnormalities, especially over the long-term (Kramer et al., 2013), while other studies showed that MHO individuals had a lower risk of cardiovascular disease than their unhealthy counterparts (Meigs et al., 2006; Ogorodnikova et al., 2012; Phillips, 2013). As for the impact of MetS on other obesity-related comorbidities, there remains a lack of evidence.

Obstructive sleep apnea (OSA) is a sleep-related breathing disorder that is characterized by repeated episodes of partial or complete obstruction of the upper airway during sleeping. In the general adult population, the prevalence of OSA ranges from 9 to 38% (Senaratna et al., 2016), while in individuals with morbid obesity, it can affect >70% of the group and the prevalence increases with increasing body mass index (BMI) (Lopez et al., 2008). Epidemiological studies have indicated that OSA might also be an independent risk factor for stroke, ischemic heart disease, cardiac arrhythmia, and heart failure (Redline et al., 2010; Gottlieb et al., 2011) via several mechanisms, including oxidative stress, systemic inflammation, intrathoracic pressure changes, sympathetic activation and endothelial dysfunction (Malcolm and Stradling, 2010). Although some studies have indicated that there are higher rates of OSA among individuals with obesity or MetS (Drager et al., 2010; Leong et al., 2013), there are no previous studies comparing the prevalence of OSA in individuals with MHO and those with metabolically unhealthy obesity (MUO).

Bariatric surgery has been shown to be more effective at treating morbid obesity and its comorbidities than medicine and lifestyle changes (Madsbad et al., 2014; Schauer et al., 2017). Limited studies have demonstrated the beneficial effects of bariatric surgery regarding MetS remission (Ibrahim et al., 2017; Guilbert et al., 2018) and OSA remission (Peromaa-Haavisto et al., 2016; Timmerman et al., 2019). However, there are no previous studies comparing the impact of sleeve gastrectomy on weight loss and OSA remission between patients with or without MetS.

The aims of this study were to determine whether the presence of MetS increases the prevalence of OSA in young Chinese obese individuals and also to analyze whether the improvements in weight and OSA after laparoscopic sleeve gastrectomy are related to the preoperative metabolic state.

MATERIALS AND METHODS

Study Population

The initial cross-sectional study included 323 obese patients (aged 14–40 years, BMI $\geq$ 30 kg/m^2) who had been hospitalized at the Ruijin Hospital, Shanghai Jiao Tong University School of Medicine, from September 2011 to July 2019. Individuals with secondary causes of obesity were excluded. All participants were Han Chinese, had not taken antihypertensive, antidiabetic, or lipid-lowering drugs within the 3 months before study enrollment, and had provided informed consent.

Next, a retrospective study was conducted on 67 patients with obesity who had undergone laparoscopic sleeve gastrectomy from August 2013 to May 2019. These patients all met the criteria set out in "Comprehensive clinical practice guidelines for medical care of patients with obesity" published by the American Association of Clinical Endocrinologists and the American College of Endocrinology in 2016 (Garvey et al., 2016). We excluded subjects with serious systemic disease, alcohol or drug addiction, mental illness, and those who with a relatively high surgical risk. Surgeries were performed by the same group, with standardization of the processes and technique. Each patient provided written informed consent for their data to be used in this study. The study was registered at ClinicalTrials.gov (NCT02653430).

Definition of MetS

Based on the National Cholesterol Education Program Adult Treatment Panel III (NCEP ATP III), the diagnosis of MetS was made when patients had $\geq$ 3 of the following components, which include a combination of categorical and borderline components: (1) abdominal obesity defined as waist circumference >102 cm in men or >88 cm in women, (2) triglycerides $\geq$1.7 mmol/L, (3) high-density lipoprotein cholesterol (HDL-C) <1.04 mmol/L in men or <1.30 mmol/L in women, (4) systolic blood pressure $\geq$130 mmHg and/or diastolic blood pressure $\geq$85 mmHg, and (5) fasting plasma glucose $\geq$5.6 mmol/L. Based on these criteria, 123 patients with obesity were classified into the MHO group while 200 patients were classified into the MUO group. Before laparoscopic sleeve gastrectomy, 11 patients were classified into the MHO group while 56 patients were classified into the MUO group.

Diagnosis of OSA

All patients underwent standard overnight polysomnography (PSG) using the Alice-4 or Alice-5 Diagnostic Sleep System (Philips Healthcare/Respironics, Murrysville, Pennsylvania, United States). Apnea-hypopnea index (AHI) $\geq$5 events/h is defined as OSA according to the Clinical Practice Guideline for Diagnostic Testing for Adult Obstructive Sleep Apnea updated in 2016 (Kapur et al., 2017). Regarding the severity, AHI $\geq$ 5, $\geq$15, and $\geq$30 events/h was classified as mild, moderate, and severe, respectively. Postoperative PSG was performed for each patient who underwent sleeve gastrectomy to assess remission or persistence of OSA at a follow-up point between 6 and 12 months after surgery.

Anthropometric and Biochemical Characteristics

A thorough medical history was recorded for each patient. Height, weight, waist, hip, and neck circumference and seated blood pressure were measured by an experienced physician. BMI was calculated as weight in kilograms divided by height in meters squared. Blood samples were taken in the morning (after an overnight fast for at least 10 h) for clinical biochemical analyses of lipid profiles and glycosylated hemoglobin (HbA1c). Additionally, an oral glucose tolerance test was performed (75 g of glucose was administered orally, and plasma glucose levels and serum insulin levels were detected at 0, 30, 60, 120, and 180 min). Homeostasis model assessment-estimated insulin resistance index (HOMA-IR) was calculated as fasting insulin (IU/ml) × fasting glucose (mmol/L)/22.5. Regarding the sleeve gastrectomy patients, data on the anthropometric and biochemical characteristics were collected again after bariatric surgery. Percentage of excess weight loss (%EWL) was calculated as:

$$\%\mathrm{EWL} = \frac{\text{preoperative weight} - \text{followup weight}}{\text{preoperative weight} - \text{ideal weight}} \times 100$$

Abdominal Computed Tomography (CT) Scan

Of the 323 patients in the initial study, 289 underwent general CT scans during a breath-hold at 5.0-mm collimation, 15.0-mm rotation-1 table speed (HQ mode, pitch 1:3), 120 kV(p), and Auto mA (Light speed QXi; GE Healthcare, Pittsburgh, Pennsylvania, United States). Visceral and subcutaneous adipose tissues were calculated using the single image at the L4–L5 vertebral interspace. Fat Scan software (N2 System) was used to determine the total, subcutaneous and visceral abdominal adipose tissue areas according to tissue density, and to calculate the visceral-to-total adipose tissue ratio. The liver-to-spleen ratio was determined by the mean value of the CT values measured in three regions of the liver and spleen, avoiding vessels, bile ducts, calcifications, and artifacts (Zeng et al., 2008).

Statistical Analysis

Data analysis was performed with the statistical package SPSS (version 26.0; IBM, Armonk, New York, United States). Anthropometric, biochemical and PSG data are expressed as mean ± standard deviation or median (interquartile range) for normally or non-normally distributed variables. Categorical variables are expressed in terms of the frequency (and percentage) in each category and were compared using the chi-square test. Normally distributed continuous variables were compared using the independent-samples *t*-test, while non-normally distributed continuous variables were compared using the non-parametric test. To compare preoperative and postoperative data for each patient, the paired-samples *t*-test or Wilcoxon test was used for normally or non-normally distributed continuous variables. McNemar test was used to compare categorical variables before and after surgery. Binary logistic regression was used to identify independent predictors of the presence of OSA. A *P*-value of < 0.05 was considered significant.

RESULTS

Clinical Characteristics and Metabolic Features in MHO and MUO Patients

According to the NCEP ATP III criteria, 323 patients with obesity were classified into the MUO group ($n = 200$) and MHO group ($n = 123$). Men represented 40.7% in the MHO group and 39.5% in the MUO group. The median age was 23 (20–27) years of MHO group and 25 (20–29) years of MUO group, respectively. Therefore, the age and sex distributions in the two groups were comparable. Smoking status was also similar between the two groups. There were no significant differences in body weight, BMI, neck, waist, and hip circumference, or waist-to-hip ratio. The mean BMI in the MHO and MUO groups was 38.0 ± 5.5 and 38.0 ± 4.8 kg/m^2, respectively ($P = 0.495$). As expected, there were significant differences in blood pressure, fasting and 2-h glucose, fasting insulin and HbA1c. HOMA-IR and lipid levels were also higher in the MUO group except for low-density lipoprotein cholesterol (LDL-C) (**Table 1**). The MUO patients had a higher level of visceral abdominal adipose tissue (195.3 ± 127.0 vs. 160.6 ± 62.1 cm^2, $P = 0.002$), a higher visceral-to-total adipose tissue ratio (28.4 ± 8.9% vs. 26.4 ± 7.2%, $P = 0.031$), and a lower liver-to-spleen ratio (0.74 ± 0.36 vs. 0.83 ± 0.32, $P = 0.024$).

PSG Variables and Prevalence of OSA in MHO and MUO Patients

Regarding the PSG results of the 323 patients with obesity, no significant difference was found in total sleeping time. The MHO patients had a similar AHI to the MUO patients (16.6 ± 22.0 events/h vs. 16.7 ± 18.6 events/h, $P = 0.512$). The two groups also had similar minimum and mean oxygen saturation values. The prevalence of OSA was 66.7% ($n = 82$) in MHO and 69.0% ($n = 138$; $P = 0.662$) and the prevalence of moderate-to-severe OSA was 34.1% ($n = 42$) and 40.0% ($n = 80$; $P = 0.292$) in the MHO and MUO groups, respectively (**Table 1**). Moreover, the prevalence of each severity level of OSA did not differ between the two groups (**Figure 1** and **Supplementary Table 1**).

In the stepwise binary logistic regression analysis, the presence of MetS was not an independent predictor of the presence of OSA (odds ratio 0.852, 95% confidence interval 0.487–1.491, $P = 0.575$), after adjusting for other variables (**Table 2**). In model 3, being male (odds ratio 2.491, 95% confidence interval 1.234–4.983, $P = 0.010$), age (odds ratio 1.075, 95% confidence interval 1.017–1.137, $P = 0.010$), waist circumference (odds ratio 1.051, 95% confidence interval 1.006–1.098, $P = 0.025$) and lower liver-to-spleen ratio (odds ratio 0.361, 95% confidence interval 0.156–0.835, $P = 0.017$) were the independent risk factors for the occurrence of OSA.

Changes in MetS Components and Other Clinical Features After Sleeve Gastrectomy

Regarding the follow-up analysis of the 67 sleeve gastrectomy patients, the mean postoperative follow-up time was 9.7 ± 2.8

TABLE 1 | Clinical features and polysomnographic variables of obese patients with and without MetS.

Characteristic	MUO	MHO	*P*-value
Number	200	123	
Male sex n (%)	79 (39.5)	50 (40.7)	0.838
Age (years)	25 (20–29)	23 (20–27)	0.112
Smoker n (%)	21 (10.5)	8 (6.5)	0.223
Body weight (kg)	110.2 ± 19.00	108.8 ± 19.9	0.358
BMI (kg/m^2)	38.0 ± 4.8	38.0 ± 5.5	0.495
Systolic blood pressure (mmHg)	137.1 ± 18.5	124.8 ± 15.5	<0.001
Diastolic blood pressure (mmHg)	85.9 ± 12.3	78.2 ± 9.6	<0.001
Fasting plasma glucose (mmol/L)	5.7 ± 1.4	5.4 ± 1.2	0.020
2-h plasma glucose (mmol/L)	9.1 ± 3.8	8.2 ± 3.1	0.014
Fasting serum insulin (μIU/ml)	26.9 ± 15.5	23.2 ± 12.9	0.015
2-h serum insulin (μIU/ml)	182.6 ± 139.7	180.7 ± 144.8	0.437
HOMA-IR	5.7 (4.2–8.1)	4.8 (3.0–6.7)	0.006
HbA1c (%)	5.7 (5.4–6.2)	5.6 (5.3–6.0)	0.039
Triglycerides (mmol/L)	2.0 (1.6–2.4)	1.2 (0.9–1.5)	<0.001
Total cholesterol (mmol/L)	4.8 ± 1.1	4.6 ± 0.8	0.038
HDL-C (mmol/L)	1.0 ± 0.2	1.2 ± 0.2	<0.001
LDL-C (mmol/L)	3.0 ± 0.8	2.9 ± 0.7	0.158
Total sleep time (min)	393 (340–448)	391 (350–439)	0.808
AHI (/h)	16.7 ± 18.7	16.6 ± 22.0	0.512
Lowest SaO_2 (%)	84.0 (77.0–89.0)	85.0 (76.0–89.0)	0.557
Average SaO_2 (%)	96.0 (94.3–97.0)	96.0 (95.0–97.0)	0.082
OSA	138 (69.0%)	82 (66.7%)	0.662
moderate to severe OSA	80 (40.0%)	42 (34.1%)	0.292

Continuous variables are presented as mean ± standard deviation or median (interquartile range) and categorical variables are presented as N (%).

months after surgery. The mean BMI decreased from 42.6 ± 7.7 to 31.9 ± 5.9 kg/m^2 ($P < 0.001$). Significant improvements in MetS and each component were observed after surgery (**Table 3**). The components that improved most notably were fasting glucose and triglycerides levels, with percentage changes from 58.2 to 10.4% ($P < 0.001$) and 53.7 to 3.0% ($P < 0.001$), respectively. Waist circumference, blood pressure and HDL-C level also improved significantly. The preoperative prevalence of MetS was 83.6%, and there was rapid remission after surgery with a postoperative prevalence of 31.3% ($P < 0.001$).

Additionally, both MHO and MUO patients achieved significant weight loss after surgery and there were no significant between-group differences in change in body weight or BMI (−10.8 ± 4.8 vs. −10.8 ± 3.0 kg/m^2, $P = 0.996$). No statistically significant difference was observed in mean %EWL (63.2 ± 24.5 vs. 76.2 ± 28.9%, $P = 0.124$), indicating that surgery had a similar benefit of weight loss in the two groups (**Table 4**). In terms of surgical safety, 3 patients had severe postoperative complications included gastrointestinal obstruction and fistula. Gallstone disorders were the most common long-term adverse event, occurring in 14 patients.

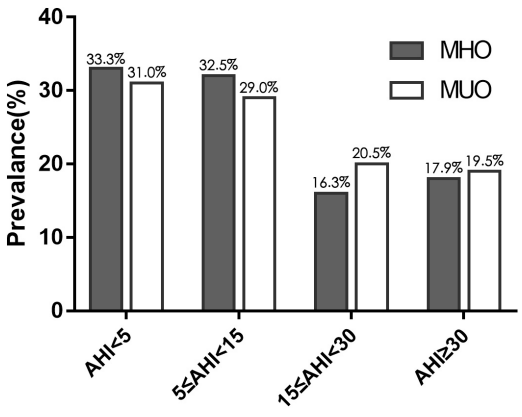

FIGURE 1 | Prevalence of obstructive sleep apnea (OSA), of varying severity, in obese patients with and without MetS. Gray bars correspond to metabolically healthy obese patients and white bars correspond to metabolically unhealthy obese patients. The two groups had similar rates of the varying severities of OSA.

Postoperative Remission of OSA in MHO and MUO Patients

After surgery, AHI was dramatically reduced in the MUO (32.7 ± 29.2 to 13.8 ± 16.0/h, $P < 0.001$) and MHO patients (27.9 ± 26.0 to 10.8 ± 15.3/h, $P < 0.001$) patients, and there was no between-group difference in the decrease in AHI in both groups (18.9 ± 24.6 vs. 17.0 ± 24.0 events/h, $P = 0.800$). The remission of moderate-to-severe OSA was observed in the MHO (36.3%; 54.5–18.2%, $P = 0.125$) and MUO (32.2%; 66.1–33.9%, $P < 0.001$) patients, though there was no statistically significant difference between preoperative and postoperative prevalence of

TABLE 2 | The stepwise binary logistic regression model for predicting OSA.

Model 1			Model 2			Model 3		
Predictors	**OR**	***P***	**Predictors**	**OR**	***P***	**Predictors**	**OR**	***P***
Male sex	3.179	< 0.001***	Male sex	2.438	0.009**	Male sex	2.491	0.010*
Smoker	3.404	0.113	Smoker	3.519	0.105	Smoker	3.004	0.167
Age	1.100	< 0.001***	Age	1.088	0.001**	Age	1.075	0.010*
BMI	1.069	0.018*	BMI	1.032	0.559	BMI	1.029	0.610
MetS	0.975	0.926	MetS	0.993	0.980	MetS	0.852	0.575
			Neck circumference	0.977	0.554	Neck circumference	0.963	0.389
			Waist circumference	1.057	0.008**	Waist circumference	1.051	0.025*
			Hip circumference	0.971	0.244	Hip circumference	0.973	0.310
						Visceral-to-total abdominal adipose ratio	2.001	0.724
						Liver-to-spleen ratio	0.361	0.017*

**P < 0.05, **P < 0.01, ***P < 0.001.*

TABLE 3 | Baseline and postoperative clinical features and evolution of MetS.

Characteristic	Baseline	Follow-up	*P*-value
Body weight (kg)	119.6 ± 24.1	89.6 ± 19.2	< 0.001
BMI (kg/m^2)	42.6 ± 7.7	31.9 ± 5.9	< 0.001
Waist circumference (cm)	123.6 ± 15.3	102.5 ± 14.4	< 0.001
Systolic blood pressure (mmHg)	141.0 ± 24.3	126.8 ± 20.3	< 0.001
Diastolic blood pressure (mmHg)	87.8 ± 15.7	76.5 ± 16.1	< 0.001
Fasting plasma glucose (mmol/L)	6.5 ± 2.0	4.8 ± 0.5	< 0.001
2-h plasma glucose (mmol/L)	10.9 ± 4.7	5.5 ± 2.1	< 0.001
HbA1c (%)	6.1 (5.5–7.0)	5.2 (4.9–5.6)	< 0.001
HOMA-IR	6.9 (4.1–10.9)	1.7 (1.2–2.6)	< 0.001
Triglycerides (mmol/L)	1.8 (1.4–2.1)	0.9 (0.8–1.2)	< 0.001
Total cholesterol (mmol/L)	4.8 ± 0.9	4.5 ± 0.9	0.001
HDL-C (mmol/L)	1.0 (0.9–1.2)	1.2 (1.0–1.4)	< 0.001
LDL-C(mmol/L)	3.0 ± 0.8	2.9 ± 0.8	0.099
AHI (/h)	31.9 ± 28.6	13.3 ± 15.8	< 0.001
Lowest SaO_2 (%)	79.0 (63.0–83.0)	87.0 (82.0–90.0)	< 0.001
Moderate to severe OSA	43 (64.2%)	21 (31.3%)	< 0.001
MetS	56 (83.6%)	21(31.3%)	< 0.001
Abdominal obesity	67 (100.0%)	56 (83.6%)	0.001
High triglycerides level	36 (53.7%)	2 (3.0%)	< 0.001
Low HDL-C level	51 (76.1%)	36 (53.7%)	< 0.001
High blood pressure	44 (65.7%)	29 (43.3%)	0.004
High fasting glucose level	39 (58.2%)	7 (10.4%)	< 0.001
Number of components	3.9	1.7	< 0.001

Continuous variables are presented as mean ± standard deviation or median (interquartile range) and categorical variables are presented as N (%).

OSA in MHO patients (potentially due to the limited sample size in the MHO group). The remission rates of OSA and moderate-to-severe OSA were 37.5% vs. 23.9% and 66.7% vs. 54.1% in the MHO and MUO group, respectively. These results indicated that laparoscopic sleeve gastrectomy can lead to similar improvement in OSA in MHO and MUO patients.

DISCUSSION

In our study, we analyzed the relationship between metabolic state and the prevalence of OSA in obese patients and their remission after laparoscopic sleeve gastrectomy. To focus on the effects of obesity and surgery themselves, we selected a population of young, non-treated obese patients. We found that the prevalence and severity of OSA did not differ between the obese individuals with or without MetS (who had the same age and BMI ranges). Central obesity may play a more critical role in OSA than general obesity and metabolic state. More importantly, preoperative metabolic state did not affect the weight loss or improvement in OSA achieved by sleeve gastrectomy. With a mean interval of 9.6 months between surgery and follow-up assessment, the mean BMI decreased by 10.8 ± 4.8 kg/m^2 and 10.8 ± 3.0 kg/m^2 in the MUO and MHO patients, respectively.

TABLE 4 | Postoperative evolution of clinical features and polysomnographic variables of obese patients with and without MetS.

	MUO (*n* = 56)			MHO (*n* = 11)			
Characteristic	**Baseline**	**Follow-up**	***P*-value**	**Baseline**	**Follow-up**	***P*-value**	***P*-value**
Body weight (kg)	120.9 ± 23.9	90.9 ± 18.4	<0.001	113.0 ± 25.2	83.3 ± 22.8	<0.001	
BMI (kg/m^2)	43.0 ± 7.8	32.2 ± 5.7	<0.001	40.7 ± 7.0	29.9 ± 6.7	<0.001	
δBMI (kg/m^2)	10.8 ± 4.8	10.8 ± 3.0					0.996
Excess weight (kg)	50.5 ± 21.0	20.5 ± 15.6	<0.001	43.9 ± 21.8	14.2 ± 19.4	<0.001	
%EWL	63.2 ± 24.5	76.2 ± 28.9					0.124
AHI (/h)	32.7 ± 29.2	13.8 ± 16.0	<0.001	27.8 ± 26.0	10.8 ± 15.3	<0.001	
Lowest SaO_2 (%)	75.0 (60.0–89.0)	89.0 (79.0–93.0)	<0.001	79.0 (63.3–83.0)	87.0 (82.3–89.8)	<0.001	
NO OSA	10 (17.9%)	20 (35.7%)	0.006	3 (27.3%)	6 (54.5%)	0.453	
Moderate to severe OSA	37 (66.1%)	19 (33.9%)	<0.001	6 (54.5%)	2 (18.2%)	0.125	
δAHI (/h)	18.9 ± 24.6	17.0 ± 24.0					0.800

Continuous variables are presented as mean l' standard deviation or median (interquartile range) and categorical variables are presented as N (%).

AHI decreased by 18.9 ± 24.6 events/h and 17.0 ± 24.0 events/h, respectively.

Although substantial evidence supported the strong association between increased BMI and metabolic disorders, recent studies have described the concept of the so-called "metabolically healthy obese," who are a subpopulation of obese individuals with a normal metabolic phenotypes observed in a group of obese population. Several studies have supported the phenotypical absence of MetS in people with MHO (Bonora et al., 1998; Wildman et al., 2008). However, several obesity-related comorbidities, such as OSA, have not been systematically evaluated in people with MHO, leaving the question whether early intervention is valuable for MHO patients.

OSA is a common comorbidity of obesity. In the general adult population, the prevalence of OSA ranges from 9 to 38% (Senaratna et al., 2016), and obesity increases this number to as high as 70% (Lopez et al., 2008). Furthermore, the presence of other obesity-related metabolic disorders was independently associated with higher AHI (Heinzer et al., 2015), strongly suggesting an important role of OSA in the development of obesity-induced metabolic abnormalities. It is well known that the impaired upper airway anatomy is the primary cause of OSA. Although obesity is a major cause of a narrow pharyngeal airway as it can cause deposition of adipose tissue around the airway, obvious anatomical obstructions were not identified in many patients with obesity (Andrew et al., 2004). In the absence of an abnormal upper airway, the hypothesized mechanisms of obesity contributing to OSA vary widely. Upper airway inflammation seems to be one of the causes of OSA. Studies have shown inflammatory cell accumulation and increased cytokine levels in the upper airways (Marin et al., 2005; Vicente et al., 2016). Also, systemic inflammation augmented by obesity may cause pharyngeal myopathy and influence central control of the upper airway muscles (Hatipoğlu and Rubinstein, 2003). The similar degree of low-grade inflammation in the two groups may partly explain the comparable prevalence of OSA in MHO and MUO patients in our study. Second, many studies have revealed that central obesity is a major predisposing factor for OSA, as increased fat storage in upper airway structures can cause airway collapse (Patil et al., 2004; Francis et al., 2013; Harada et al., 2014). Consistently with these studies, our results also showed important effect of central obesity on the prevalence of OSA as weight circumference and liver/spleen ratio were independent risk factors for OSA. As men tend to gain weight more centrally than do women (Whittle et al., 1999), this may also partly explain why male sex is an important predisposing factor for OSA. These results suggest that the prevalence and severity of OSA in obesity are not influenced by metabolic state, and previous results indicate that OSA is more strongly correlated with central obesity than general obesity or metabolic state. Both MHO and MUO patients had a similar risk of OSA and its related metabolic abnormalities. These results highlight the importance of early screening for OSA and weight management among MHO individuals, to avoid the occurrence of related complications.

Bariatric surgery is the most effective treatment for obesity and also greatly improves the associated comorbidities. Bariatric surgery can lead to rapid and durable weight loss, which is often difficult to achieve with medications, diet, or physical exercises alone. Few studies have analyzed the relationship between bariatric surgery and remission of MetS. In a study performed by Martini et al. (2015), 75.8% of patients achieved remission, while 24.2% of patients showed persistence of MetS 1 year after Roux-en-Y gastric bypass. Guilbert et al. (2018) observed that the prevalence of MetS decreased from 100 to 6.34% 1 year after Roux-en-Y gastric bypass, and this decrease was still maintained at 2 years. Researchers also reported OSA remission in 70–80% patients in short and long-term after bariatric surgery (Casella et al., 2015; Timmerman et al., 2019). However, there are no studies focusing on the difference in weight loss and improvement of OSA in patients with or without MetS before surgery. We found that, after surgery, the prevalence of MetS decreased from 83.6 to 31.3% and all five components of MetS were improved, especially regarding the elevated triglycerides and fasting plasma glucose levels. Notably, sleeve gastrectomy led to a similar degree of weight loss in MHO and MUO patients. Excess weight was significantly decreased after surgery, with no difference was found in postoperative %EWL between the two groups. Additionally, the postoperative

PSG assessments showed that AHI decreased from 32.7 to 13.8 events/h ($P < 0.001$) in MUO patients and from 27.8 to 10.8 events/h ($P < 0.001$) in MHO patients. There was no significant difference in the change in AHI (18.9 ± 24.6 vs. 17.0 ± 24.0 events/h, $P = 0.800$) and remission of moderate to severe OSA was observed in 32.2 and 36.3% of MUO and MHO patients, respectively. These results indicated that patients with obesity can achieve similar weight loss benefits and OSA remission after sleeve gastrectomy regardless of preoperative metabolic state after sleeve gastrectomy.

Recently, growing evidence has challenged the proposed existence of "healthy obese individuals," as several studies found that MHO subjects were at increased risk of cardiovascular disease and type 2 diabetes compared to metabolically healthy normal weight individuals (Guy-Marino et al., 2015; Song et al., 2019). Our recent study also showed that the prevalence of polycystic ovarian syndrome was not influenced by the presence of MetS (Liang et al., 2017). All these results suggest that metabolically healthy obesity is not a benign condition, and that many complications have already developed before apparent changes in the metabolic state. Clinicians should take more initiative when treating MHO patients to avoid their transition to the MUO phenotype. This study also showed that whether or not patients presented with MetS before surgery, they could equally benefit from sleeve gastrectomy both regarding weight loss and OSA remission. Therefore, early bariatric surgery among obese patients with an apparently normal metabolic profile could be beneficial regarding improving OSA and avoiding conversion to the metabolically unhealthy phenotype.

A limitation of our hospital-based study is the small sample size and retrospective design of the follow-up study. Larger prospective studies in the future may provide us more powerful evidence regarding weight loss and remission rates of obesity-related comorbidities among MHO patients.

CONCLUSION

In conclusion, our study illustrated that having a normal metabolic state did not decrease the prevalence or severity of OSA in patients with obesity. Weight management is equally important for both obese phenotypes. Both MHO and MUO patients who underwent laparoscopic sleeve gastrectomy experienced rapid and remarkable improvement in weight and OSA, suggesting that early bariatric surgery could be an higher-priority option when treating MHO patients.

DATA AVAILABILITY STATEMENT

The raw data supporting the conclusions of this article will be made available by the authors, without undue reservation.

ETHICS STATEMENT

The studies involving human participants were reviewed and approved by Ethics committee of Ruijin Hospital Affiliated to Shanghai Jiao Tong University School of Medicine. Written informed consent to participate in this study was provided by the participants' legal guardian/next of kin.

AUTHOR CONTRIBUTIONS

JH and WG contributed to study conception. YC and LC contributed to study design and drafted the manuscript. LZ, SZ, and LY contributed to analysis and interpretation of data. YZ, YS and WW contributed to critical revision. JJ contributed to the surgery. All authors contributed to acquisition of data.

FUNDING

This study was supported by the National Key Technologies R&D Program of China (No. 2018YFC1313800), the National Key Technologies R&D Program of China (No. 2018YFC1314800), the National Natural Science Foundation of China (No. 81870582), and the Program of Shanghai Academic/Technology Research Leader (No. 19XD1403200).

ACKNOWLEDGMENTS

We thank all the patients enrolled in this study for their cooperation and clinical staff for their contributions to the overnight polysomnography assessments.

SUPPLEMENTARY MATERIAL

The Supplementary Material for this article can be found online at: https://www.frontiersin.org/articles/10.3389/fphys.2021.650260/full#supplementary-material

REFERENCES

Andrew, W., Jordan, A. S., Atul, M., Fogel, R. B., Katz, E. S., Karen, S., et al. (2004). Ventilatory control and airway anatomy in obstructive sleep apnea. *Am. J. Respir. Crit. Care Med.* 170, 1225–1232.

Bonora, E., Kiechl, S., Willeit, J., Oberhollenzer, F., Egger, G., Targher, G., et al. (1998). Prevalence of insulin resistance in metabolic disorders: the Bruneck Study. *Diabetes.* 47, 1643–1649. doi: 10.2337/diabetes.47.10.1643

Casella, G., Soricelli, E., Giannotti, D., Collalti, M., and Basso, N. (2015). Long-term results after laparoscopic sleeve gastrectomy in a large monocentric series. *Surg. Obes. Relat. Dis.* 12, 757–762. doi: 10.1016/j.soard.2015.09.028

Drager, L. F., Queiroz, E. L., Lopes, H. F., Genta, P. R., Krieger, E. M., and Lorenzi-Filho, G. (2010). Obstructive sleep apnea is highly prevalent and correlates with impaired glycemic control in consecutive patients with the metabolic syndrome. *J. Cardiom. Synd.* 4, 89–95. doi: 10.1111/j.1559-4572.2008.00046.x

Francis, D., Emilia, S., Virginie, D., Sébastien, C., Arnauld, G., Philippe, C., et al. (2013). Relation of central fat mass to obstructive sleep apnea in the elderly. *Sleep* 36:501. doi: 10.5665/sleep.2532

Garvey, W. T., Mechanick, J. I., Brett, E. M., Garber, A. J., Hurley, D. L., Jastreboff, A. M., et al. (2016). American association of clinical endocrinologists and american college of endocrinology comprehensive clinical practice guidelines

for medical care of patients with obesity. *End. Pract.* 22, 1–203. doi: 10.4158/ep161365.gl

Gottlieb, D. J., Yenokyan, G., Newman, A. B., O'Connor, G. T., Punjabi, N. M., Quan, S. F., et al. (2011). Prospective study of obstructive sleep apnea and incident coronary heart disease and heart failure: the sleep heart health study. *South China J. Cardiol.* 122, 352–360. doi: 10.1161/circulationaha.109.901801

Guilbert, L., Ortiz, C. J., Espinosa, O., Sepúlveda, E. M., Piña, T., Joo, P., et al. (2018). Metabolic syndrome 2 years after laparoscopic gastric bypass. *Int. J. Surg.* 52, 264–268. doi: 10.1016/j.ijsu.2018.02.056

Guy-Marino, H., Sébastien, C., Aline, D., Hermann, N., Brunner, E. J., Mika, K., et al. (2015). Metabolically healthy obesity and the risk of cardiovascular disease and type 2 diabetes: the Whitehall II cohort study. *Eur. Heart J.* 36, 551–559. doi: 10.1093/eurheartj/ehu123

Harada, Y., Oga, T., Chihara, Y., Azuma, M., Murase, K., Toyama, Y., et al. (2014). Differences in associations between visceral fat accumulation and obstructive sleep apnea by sex. *Ann. Am. Thorac. Soc.* 11, 383–391. doi: 10.1513/annalsats.201306-182oc

Hatipoğlu, U., and Rubinstein, I. (2003). Inflammation and obstructive sleep apnea syndrome pathogenesis: a working hypothesis. *Respiration* 70, 665–671. doi: 10.1159/000075218

Heinzer, R., Vat, S., Marques-Vidal, P., Marti-Soler, H., Andries, D., Tobback, N., et al. (2015). Prevalence of sleep-disordered breathing in the general population: the HypnoLaus study. *Lancet Respirat. Med.* 3, 310–318. doi: 10.1016/s2213-2600(15)00043-0

Ibrahim, N., Jaime, A., Beverley, A.-H., Sachin, K., and Nancy, P. (2017). Metabolic syndrome remission after Roux-en-Y gastric bypass or sleeve gastrectomy. *Diab. Metab. Synd. Obes. Targets Ther.* 10, 393–402. doi: 10.2147/dmso.s142731

Kapur, V. K., Auckley, D. H., Chowdhuri, S., Kuhlmann, D. C., Mehra, R., Ramar, K., et al. (2017). Clinical practice guideline for diagnostic testing for adult obstructive sleep apnea: an american academy of sleep medicine clinical practice guideline. *J. Clin. Sleep Med.* 13, 479–504. doi: 10.5664/jcsm.6506

Kramer, C. K., Zinman, B., and Retnakaran, R. (2013). Are metabolically healthy overweight and obesity benign conditions: a systematic review and meta-analysis. *Ann. Int. Med.* 2013, 758–769. doi: 10.7326/0003-4819-159-11-201312030-00008

Leong, W. B., Arora, T., Jenkinson, D., Thomas, A., Punamiya, V., Banerjee, D., et al. (2013). The prevalence and severity of obstructive sleep apnea in severe obesity: the impact of ethnicity. *J. Clin. Sleep Med. Jcsm* 9, 853–858. doi: 10.5664/jcsm.2978

Liang, P., Xi, L., Shi, J., Li, W., Zhao, S., Deng, Y., et al. (2017). Prevalence of polycystic ovary syndrome in Chinese obese women of reproductive age with or without metabolic syndrome. *Fertil. Steril.* 107:1048. doi: 10.1016/j.fertnstert.2016.12.029

Lopez, P. P., Stefan, B., Schulman, C. I., and Byers, P. M. (2008). Prevalence of sleep apnea in morbidly obese patients who presented for weight loss surgery evaluation: more evidence for routine screening for obstructive sleep apnea before weight loss surgery. *Am. Surg.* 74, 834–838. doi: 10.1177/000313480807400914

Madsbad, S., Dirksen, C., and Holst, J. J. (2014). Mechanisms of changes in glucose metabolism and bodyweight after bariatric surgery. *Lancet Diab. Endocrinol.* 2, 152–164. doi: 10.1016/s2213-8587(13)70218-3

Malcolm, K., and Stradling, J. R. (2010). Mechanisms of vascular damage in obstructive sleep apnea. *Nat. Rev. Cardiol.* 7, 677–685. doi: 10.1038/nrcardio.2010.145

Marin, J. M., Carrizo, S. J., Vicente, E., and Agusti, A. G. (2005). Long-term cardiovascular outcomes in men with obstructive sleep apnoea-hypopnoea with or without treatment with continuous positive airway pressure: an observational study. *Dkgest World Latest Med. Inform.* 365, 1046–1053. doi: 10.1016/s0140-6736(05)71141-7

Martini, F., Anty, R., Schneck, A.-S., Casanova, V., Iannelli, A., and Gugenheim, J. (2015). Predictors of metabolic syndrome persistence 1 year after laparoscopic Roux-en-Y gastric bypass. *Surg. Obes. Relat. Dis.* 1054–1060. doi: 10.1016/j.soard.2015.02.019

Meigs, J. B., Wilson, P. W., Fox, C. S., Vasan, R. S., Nathan, D. M., Sullivan, L. M., et al. (2006). Body mass index, metabolic syndrome, and risk of type 2 diabetes or cardiovascular disease. *J. Clin. Endocrinol. Metab.* 91, 2906–2912.

Ogorodnikova, A. D., Mimi, K., Mcginn, A. P., Paul, M., Unab, K., and Wildman, R. P. (2012). Incident cardiovascular disease events in metabolically benign obese individuals. *Obesity.* 20, 651–659. doi: 10.1038/oby.2011.243

Patil, S., Schneider, H., Gladmon, E., Magnuson, T., Smith, P. L., O'Donnell, C. P., et al. (2004). Obesity and upper airway mechanical control during sleep. *Am. J. Respir. Crit. Care Med.* 1:A435.

Peromaa-Haavisto, P., Tuomilehto, H., Kössi, J., Virtanen, J., Luostarinen, M., Pihlajamäki, J., et al. (2016). Prevalence of obstructive sleep apnoea among patients admitted for bariatric surgery. A Prospective multicentre trial. *Obes. Surg.* 26, 1384–1390. doi: 10.1007/s11695-015-1953-7

Phillips, C. M. (2013). Metabolically healthy obesity: definitions, determinants and clinical implications. *Rev. Endocr. Metab. Disord.* 14, 219–227. doi: 10.1007/s11154-013-9252-x

Redline, S., Yenokyan, G., Gottlieb, D. J., Shahar, E., O'Connor, G. T., Resnick, H. E., et al. (2010). Obstructive sleep apnea–hypopnea and incident stroke: the sleep heart health study. *Am. J. Respir. Crit. Care Med.* 182, 1332–1333. doi: 10.1164/ajrccm.182.10.1332b

Reilly, J. J. (2017). Health effects of overweight and obesity in 195 Countries. *N. Engl. J. Med.* 377:1496.

Schauer, P. R., Bhatt, D. L., Kirwan, J. P., Wolski, K., Aminian, A., Brethauer, S. A., et al. (2017). Bariatric surgery versus intensive medical therapy for diabetes — 5-year outcomes. *N. Engl. J. Med.* 376, 641–651. doi: 10.1056/nejmoa1600869

Senaratna, C. V., Perret, J. L., Lodge, C. J., Lowe, A. J., Campbell, B. E., Matheson, M. C., et al. (2016). Prevalence of obstructive sleep apnea in the general population: a systematic review. *Sleep Med. Rev.* 34:70.

Song, J., Jiang, X., Juan, J., Cao, Y., Chibnik, L. B., Hofman, A., et al. (2019). The role of metabolic syndrome and its components as mediators of the genetic effect on type 2 diabetes: a family-based study in China. *J. Diab.*11, 552–562. doi: 10.1111/1753-0407.12882

Timmerman, M., Basille, D., Basille-Fantinato, A., Baud, M. E., Rebibo, L., Andrejak, C., et al. (2019). Short-term assessment of obstructive sleep apnea syndrome remission rate after sleeve gastrectomy: a cohort study. *Obes. Surg.*29, 3690–3697. doi: 10.1007/s11695-019-04110-0

Vicente, E., Marin, J. M., Carrizo, S. J., Osuna, C. S., Gonzalez, R., Marin-Oto, M., et al. (2016). Upper airway and systemic inflammation in obstructive sleep apnoea. *Eur. Respir. J.* 48, 1108–1117.

Whittle, A. T., Marshall, I., Mortimore, I. L., Wraith, P. K., Sellar, R. J., and Douglas, N. J. (1999). Neck soft tissue and fat distribution: comparison between normal men and women by magnetic resonance imaging. *Thorax* 54, 323–328. doi: 10.1136/thx.54.4.323

Wildman, R. P., Muntner, P., Reynolds, K., Mcginn, A. P., Rajpathak, S., Wylie-Rosett, J., et al. (2008). The obese without cardiometabolic risk factor clustering and the normal weight with cardiometabolic Risk factor clustering prevalence and correlates of 2 phenotypes among the US population (NHANES 1999–2004). *Obstetr. Gynecol. Survey* 63, 783–784. doi: 10.1097/01.ogx.0000338100.83483.58

Zeng, M. D., Fan, J. G., Lu, L. G., Li, Y. M., and Mao, Y. M. (2008). Guidelines for diagnosis and treatment of nonalcoholic fatty liver diseases. *J. Digest. Dis.* 9, 108–112.

Conflict of Interest: The authors declare that the research was conducted in the absence of any commercial or financial relationships that could be construed as a potential conflict of interest.

frontiers in Physiology

ORIGINAL RESEARCH
published: 04 May 2021
doi: 10.3389/fphys.2021.667330

Adiposity Measurements and Metabolic Syndrome Are Linked Through Circulating Neuregulin 4 and Adipsin Levels in Obese Adults

Dan Guo[1†], Jianfang Liu[1†], Peizhen Zhang[1†], Xiaoyu Yang[1], Deying Liu[1], Jiayang Lin[1], Xueyun Wei[1], Bingyan Xu[1], Chensihan Huang[1], Xuan Zhou[2], Fei Teng[1], Hong Zhu[3] and Huijie Zhang[1,2,4]**

[1] Department of Endocrinology and Metabolism, Nanfang Hospital, Southern Medical University, Guangzhou, China, [2] Department of Endocrinology and Diabetes, The First Affiliated Hospital, Xiamen University, Xiamen, China, [3] Nanfang Hospital, Southern Medical University, Guangzhou, China, [4] School of Public Health, Southern Medical University, Guangzhou, China

OPEN ACCESS

Edited by:
Yan Lu,
Fudan University, China

Reviewed by:
Yan Zheng,
Fudan University, China
Liqiang Zheng,
ShengJing Hospital of China Medical University, China

***Correspondence:**
Huijie Zhang
huijiezhang2005@126.com
Hong Zhu
zhnfyy@yeah.net

[†] These authors have contributed equally to this work

Specialty section:
This article was submitted to Clinical and Translational Physiology, a section of the journal Frontiers in Physiology

Received: 12 February 2021
Accepted: 06 April 2021
Published: 04 May 2021

Citation:
Guo D, Liu J, Zhang P, Yang X, Liu D, Lin J, Wei X, Xu B, Huang C, Zhou X, Teng F, Zhu H and Zhang H (2021) Adiposity Measurements and Metabolic Syndrome Are Linked Through Circulating Neuregulin 4 and Adipsin Levels in Obese Adults. Front. Physiol. 12:667330. doi: 10.3389/fphys.2021.667330

Background: Adiposity and adipokines are associated with metabolic disorders, but little is known regarding that whether adiposity measurements link metabolic syndrome (MetS) through circulating neuregulin 4 (Nrg4) and adipsin levels.

Materials and Methods: A total of 1212 subjects with a waist circumference greater than 90 cm for men or 80 cm for women were enrolled from a Chinese community. Circulating Nrg4 and adipsin levels were measured using commercial kits. Mediation analyses of circulating Nrg4 and adipsin were performed in the study using linear and logistic regression.

Results: Subjects with MetS had higher waist circumference, visceral fat level, and circulating adipsin level, and lower levels of circulating Nrg4 and muscle mass to visceral fat (MVF) ratio (all $P < 0.05$). In multivariable logistic regression analyses, after adjusting for confounding variables, per standard deviation (SD) increase in waist circumference and visceral fat level were significantly associated with increased odds of MetS [OR (95% CI), 1.42 (1.22–1.64); 2.20 (1.62–2.99); respectively]; and per SD reduction in MVF ratio was significantly associated with reduced odds of MetS [OR (95% CI), 0.65 (0.55–0.77)]. In the mediation analyses, both circulating Nrg4 and adipsin levels mediated the association between waist circumference (8.31% and 18.35%, respectively), visceral fat level (7.50% and 9.98%, respectively), and MVF ratio (5.80% and 9.86%, respectively) and MetS after adjustments.

Conclusion: These findings indicate that adiposity measurements and MetS are linked through circulating Nrg4 and adipsin levels in obese adults, suggesting that circulating Nrg4 and adipsin levels might be potential predictors for management of MetS.

Keywords: neuregulin 4, adipsin, adiposity, metabolic syndrome, metabolism, mediation analysis

INTRODUCTION

Metabolic syndrome (MetS) is a constellation of medical conditions, including central obesity, hypertension, hyperglycemia, and dyslipidemia, which are associated with increased risk of cardiometabolic diseases such as cardiovascular diseases (CVD) and type 2 diabetes (Lorenzo et al., 2003; Alberti et al., 2005; Park et al., 2019). MetS has an increasing prevalence worldwide owing to energy-dense dietary intake, sedentary lifestyles, and consequently excess visceral fat accumulation (Cameron et al., 2008; Hirode and Wong, 2020). Although the pathogenesis of MetS has not been fully elucidated, low-grade inflammation induced by central obesity through adipokine dysregulation has been established as one of the significant underlying mechanisms of MetS (Saltiel and Olefsky, 2017; Francisco et al., 2019).

Adipose tissue is recognized as not only an energy storage site but also an endocrine organ secreting a series of adipokines, which are identified to play important roles in metabolic disorders and CVD (Kahn et al., 2019; Sanidas et al., 2020). For instance, it has been documented that Neuregulin 4 (Nrg4) primarily secreted from brown adipose tissue (BAT) and adipsin mainly synthesized in the white adipose tissue (WAT) are associated with metabolic diseases (Saleh et al., 2019; Tutunchi et al., 2020). Nrg4 is a newly identified adipokine and play a role in obesity, diabetes, non-alcoholic fatty liver disease (NAFLD), and CVD in human subjects (Wang et al., 2014; Dai et al., 2015; Jiang et al., 2016; Chen et al., 2017; Yan et al., 2019). Moreover, our previous study found that serum Nrg4 levels were negatively associated with MetS (Cai et al., 2016). The key mechanistic link for Nrg4 in protecting from metabolic disturbances is to regulate BAT activity, drive the browning of WAT, prevent lipogenesis in the liver, and improve insulin sensitivity (Tutunchi et al., 2020). Adipsin has been documented to regulate adipocyte differentiation and increased lipid accumulation, which might be a potential reason for the association between adipsin and metabolic disorders (Song et al., 2016). Clinical evidences indicated that circulating adipsin were positively associated with adiposity, polycystic ovary syndrome (PCOS), insulin resistance (IR), and the development of coronary artery disease (Derosa et al., 2013; Gursoy Calan et al., 2016; Guo et al., 2019; Ohtsuki et al., 2019).

As mentioned above, both Nrg4 and adipsin secreted from adipose tissue have impacts on metabolic abnormalities. However, whether adiposity measurements link MetS through Nrg4 and adipsin remains unknown in humans. In this study, we aimed to explore whether the associations of adiposity measurements with MetS are mediated by circulating Nrg4 and adipsin levels and further quantify the degree of the mediation effects in obese subjects.

SUBJECTS AND METHODS

Study Participants

Obese subjects living in the Lianqian community, Xiamen, China were recruited between April 2011 and December 2013. Adults with central obesity (waist circumference ≥90 cm for men or 80 cm for women) were eligible if they were aged 18 or older. Subjects with viral hepatitis, liver cirrhosis, any secondary chronic liver diseases (e.g., alcoholic fatty liver, autoimmune hepatitis, and/or drug-induced hepatitis), biliary obstructive diseases, cancer, or known hyper- or hypothyroidism were excluded. In brief, a total of 1529 obese subjects were included, of which 1212 (79.3%) participants with complete data were left for further analysis. All participants completed a physical examination and a uniform questionnaire covered social demographic status, family history, past medical history, and lifestyle habits such as smoking status, alcohol consumption, and physical activity. Written informed consent was provided by participants. The methods were carried out in accordance with the approved guidelines.

Clinical and Biochemical Measurements

Basic anthropometric measurements used in the analysis included height, weight, waist circumference, blood pressure (BP). Body mass index (BMI) was calculated as the weight in kilograms divided by the square of the height in meters. Waist circumference was measured at the level of the umbilicus. Each measurement was repeated for three times, and the results were averaged. BP was assessed in triplicate after at least 5 minutes of rest using an electronic sphygmomanometer (OMRON Company), and the mean values were used for analysis. Visceral fat level and muscle mass were determined using the whole body dual-energy X-ray absorptiometry (DXA) system (Hologic Inc., Bedford, MA, United States). Muscle mass to visceral fat (MVF) ratio was calculated as the muscle mass divided by visceral fat level.

All blood samples were obtained after 12 h of fasting or 2 h after 75-g oral glucose tolerance test which was performed to assess glucose tolerance status. Fasting plasma glucose concentrations (FPG) and 2-h plasma glucose concentrations (2-h PG) were determined using the glucose oxidase method. Fasting plasma insulin concentrations and 2-h plasma insulin concentrations were determined using an electrochemiluminescence immunoassay (Roche Elecsys Insulin Test, Roche Diagnostics, Mannheim, Germany). Serum lipid profiles, including triglycerides (TG), total cholesterol (TC), and high-density lipoprotein cholesterol (HDL-c) were measured by enzymatic colorimetric methods with a Hitachi 7450 analyzer (Hitachi, Tokyo, Japan). Low-density lipoprotein cholesterol (LDL-c) was calculated by Friedewald's formula. The homeostasis model assessment of insulin resistance (HOMA-IR) was calculated as the product of fasting serum insulin (mU/L) and FPG (mmol/L) concentrations, divided by 22.5.

Measurements of Circulating Nrg4 and Adipsin Concentrations

Circulating Nrg4 concentrations were measured using enzyme-linked immunosorbent assay (ELISA) kits (Aviscera Biosciences, Santa Clara, CA, United States), following the manufacturer's protocol. The assay had a detection sensitivity of 0.25 ng/mL. The

linear range of the standard was 0.5–32.0 ng/mL, and the intra- and inter-assay variations were both less than 10%.

Circulating adipsin concentrations were assayed by using ELISA kits (AssayPro, St. Charles, MO, United States). The assay had a detection sensitivity of 2.1 ng/mL. The linear range of the standard was 1.875–120 ng /mL, and the intra- and inter-assay variations were both less than 10%.

Definition of Metabolic Syndrome

MetS was defined using the criteria proposed by International Diabetes Federation diagnostic criteria (Alberti et al., 2005), which consisted of central obesity (waist circumference ≥90 cm for Chinese men or ≥80 cm for Chinese women) and the presence of any two of four risk factors: (1) elevated BP (≥130/85 mmHg or drug treatment of previously diagnosed hypertension), (2) elevated fasting plasma glucose (≥5.6 mmol/L or previously diagnosed type 2 diabetes), (3) elevated triglyceride (≥1.7 mmol/L, or drug treatment for this lipid abnormality), or (4) reduced HDL-c (<1.03 mmol/L for men or <1.29 mmol/L for women, or drug treatment for this lipid abnormality). The latter two risk factors, elevated triglyceride level and reduced HDL-c, were collectively referred to as dyslipidemia in the present study.

Statistical Analysis

Statistical analyses were performed with SAS version 9.4 (SAS Institute, Cary, NC, United States). All data are presented as proportions for categorical variables or means ± standard deviations (SD) for continuous variables, except for skewed variables, which are presented as medians (interquartile range). Data that were not normally distributed were logarithmically transformed prior to analysis. The subjects were classified into two groups according to different metabolic status. The $\chi 2$-test was used for comparison of categorical variables between groups. Analyses of covariance were performed using general linear models (GLM) to compare the differences in study variables between groups. For adiposity measurements, circulating Nrg4 and adipsin, standardized values (Z-scores) were calculated to allow direct comparison of their effect sizes in the regression analyses. Logistic regression analyses were used to examine the association between adiposity measurements and MetS or components of MetS. The results of the analyses are presented as odds ratio (OR) with a 95% confidence interval (CI).

General causal mediation analysis models previously proposed by VanderWeele and Sobel (Sobel, 1982; VanderWeele, 2016) were constructed to explore whether Nrg4 or adipsin mediated the effect of adiposity measurements on MetS. Linear and logistic regression models were used to estimate standardized regression coefficients (βs). In the mediation models, the predictor variables (X) were waist circumstance, visceral fat level, or MVF ratio; the mediator variables (M) were Nrg4 or adipsin; the outcome variable (Y) was MetS. The mediation model is presented in **Supplementary Figure 1**. Four steps of the mediation analysis were involved in the calculation of the mediating effect:

Step 1: Showing that the predictor variable determines the outcome (Model $Y = \beta_{Tot}X$) [β_{Tot} is the coefficient relating the predictor variable to the outcome variable (total effect)].

Step 2: Showing that the predictor variable affects the mediator (Model $M = \beta_1 X$) [β_1 is the coefficient relating the predictor variable to the mediator variable (indirect effect 1)].

Step 3: Showing that the mediator determines the outcome controlling for the predictor (Model $Y = \beta_2 M + \beta_{Dir}X$) [$\beta_2$ is the coefficient relating the mediator variable to the outcome variable adjusted for the predictor variable (indirect effect 2); β_{Dir} is the coefficient relating the predictor variable to the outcome variable adjusted for the mediator variable (direct effect)].

Step 4: Calculating the proportion of mediation effect (%) by $(\beta_1 \times \beta_2 / \beta_{Tot}) \times 100\%$.

The total indirect effect (β_{Ind}) was calculated by multiplying the regression coefficients $\beta_1 \times \beta_2$. In mediation analyses, testing the significance of the mediation effect is equivalent to testing the null hypothesis H_0: $\beta_1 \times \beta_2 = 0$ versus the alternative hypothesis H_a: $\beta_1 \times \beta_2 \neq 0$, by using the Sobel test. Two-sided values of $P < 0.05$ were considered statistically significant.

RESULTS

Table 1 summarizes the mean levels of study variables according to different components of MetS. Of the 1212 eligible obese subjects, 781 (64.4%) had the MetS, 707 (58.3%) had elevated BP, 715 (60.0%) had elevated fasting glucose, and 704 (58.1%) had dyslipidemia. Female and older people are more likely to have MetS and elevated BP. As expected, subjects with each components of metabolic disorders had an adverse metabolic profile, including significantly higher levels of BMI, waist circumference, visceral fat level, systolic and diastolic BP, fasting plasma glucose and insulin, postprandial glucose and insulin, triglyceride, total cholesterol, and HOMA-IR, and lower levels of HDL-c and MVF ratio. The circulating adipsin level was markedly higher in subjects with MetS ($P = 0.019$) and elevated BP ($P = 0.001$); meanwhile, it was not significantly associated with elevated fasting glucose and dyslipidemia. The circulating Nrg4 level was significantly lower in subjects with MetS ($P < 0.001$), elevated BP ($P = 0.010$), elevated fasting glucose ($P = 0.002$), and dyslipidemia ($P = 0.034$). Furthermore, female subjects with MetS had a higher level of circulating adipsin and a lower level of circulating Nrg4, while the difference of these two adipokines were not statistically significant in male subjects between groups (**Supplementary Table 1**).

Table 2 presents the total effect of adiposity measurements on different components of MetS. Waist circumstance, visceral fat level, and MVF ratio were significantly associated with odds of metabolic components. The ORs for the association of waist circumstance with MetS, elevated BP, elevated fasting glucose, and dyslipidemia were 1.48 (95% CI, 1.29–1.69), 1.58 (95% CI, 1.39–1.80), 1.21 (95% CI, 1.08–1.37), and 1.20 (95% CI, 1.07–1.35), respectively. Furthermore, the adiposity measurements were significantly associated with MetS and elevated BP in both male and female subjects (**Supplementary Figure 2**). The associations between adiposity measurements and different components of MetS remained significant after additional adjustments of age, gender, smoking status, alcohol assumption, and physical activity, and even further adjustments of total

TABLE 1 | Characteristics of obese subjects according to components of metabolic syndrome.

Variables	Metabolic syndrome			Elevated blood pressure			Elevated Fasting Glucose			Dyslipidemia		
	Yes	No	*P*-value	Yes	No	*P*-value	Yes	No	*P*-value	Yes	No	*P*-value
Sample size	781	431		707	505		715	497		704	508	
Age (years)	54.3 ± 7.2	51.6 ± 7.2	<0.001	54.7 ± 7.0	51.4 ± 7.2	<0.001	54.6 ± 6.9	51.5 ± 7.4	<0.001	53.5 ± 7.3	53.2 ± 7.3	0.496
Female (n,%)	530 (67.9)	335 (77.7)	<0.001	457 (64.6)	408 (80.8)	<0.001	509 (71.2)	356 (71.6)	0.867	480 (68.1)	385 (75.8)	0.004
BMI (kg/m^2)	27.8 ± 3.2	26.8 ± 2.7	<0.001	27.9 ± 3.2	26.8 ± 2.8	<0.001	27.7 ± 3.2	27.1 ± 2.8	0.003	27.7 ± 3.0	27.1 ± 3.1	<0.001
Waist circumference (cm)	94.7 ± 7.4	92.2 ± 6.6	<0.001	95.0 ± 7.7	92.1 ± 6.2	<0.001	94.4 ± 7.4	93.0 ± 7.0	0.002	94.3 ± 7.0	93.1 ± 7.5	0.002
Current smokers (n, %)	104 (13.3)	54 (12.5)	0.697	110 (15.6)	48 (9.5)	0.002	94 (13.2)	64 (12.9)	0.891	87 (12.4)	71 (14.0)	0.409
Systolic BP (mmHg)	139.2 ± 16.4	122.6 ± 14.2	<0.001	144.1 ± 14.4	118.2 ± 7.6	<0.001	136.4 ± 17.2	128.9 ± 17.1	<0.001	135.5 ± 17.1	130.3 ± 17.7	<0.001
Diastolic BP (mmHg)	82.3 ± 10.3	73.7 ± 8.7	<0.001	84.7 ± 9.7	71.7 ± 6.4	<0.001	80.6 ± 10.4	77.3 ± 10.6	<0.001	80.7 ± 10.4	77.2 ± 10.6	<0.001
Fasting glucose (mmol/L)	6.49 ± 1.91	5.49 ± 0.87	<0.001	6.37 ± 1.93	5.80 ± 1.18	<0.001	6.76 ± 1.95	5.23 ± 0.26	<0.001	6.34 ± 1.97	5.85 ± 1.13	<0.001
2-h glucose (mmol/L)	9.91 ± 4.38	7.23 ± 2.28	<0.001	9.60 ± 4.30	8.05 ± 3.28	<0.001	10.23 ± 4.56	7.12 ± 1.75	<0.001	9.66 ± 4.48	7.97 ± 2.90	<0.001
Fasting insulin (mU/L)	14.86 ± 13.64	10.05 ± 4.64	<0.001	14.21 ± 14.01	11.68 ± 6.37	<0.001	14.68 ± 14.09	10.96 ± 5.53	<0.001	14.63 ± 14.02	11.11 ± 6.14	<0.001
2-h insulin (mU/L)	94.43 ± 71.21	61.70 ± 46.69	<0.001	89.50 ± 70.52	73.41 ± 56.40	<0.001	91.70 ± 72.73	69.98 ± 50.71	<0.001	92.57 ± 70.46	69.25 ± 55.11	<0.001
HOMA-IR	3.47 (2.54–4.89)	2.19 (1.56–2.99)	<0.001	3.23 (2.33–4.63)	2.60 (1.77–3.89)	<0.001	3.54 (2.59–5.11)	2.28 (1.60–3.10)	<0.001	3.33 (2.40–4.74)	2.54 (1.74–3.53)	<0.001
Triglyceride (mmol/L)	1.97 (1.37–2.67)	1.13 (0.85–1.41)	<0.001	1.78 (1.18–2.52)	1.33 (0.93–1.96)	<0.001	1.66 (1.16–2.39)	1.40 (0.95–2.03)	<0.001	2.12 (1.72–2.88)	1.09 (0.85–1.34)	<0.001
Total cholesterol (mmol/L)	6.01 ± 1.13	5.70 ± 0.97	<0.001	6.03 ± 1.13	5.71 ± 0.99	<0.001	6.04 ± 1.11	5.70 ± 1.02	<0.001	5.97 ± 1.18	5.81 ± 0.94	<0.001
LDL-c (mmol/L)	3.68 ± 1.04	3.65 ± 0.90	0.533	3.74 ± 1.04	3.57 ± 0.91	0.003	3.76 ± 1.03	3.55 ± 0.92	<0.001	3.60 ± 1.06	3.77 ± 0.89	0.004
HDL-c (mmol/L)	1.29 ± 0.27	1.51 ± 0.28	<0.001	1.34 ± 0.29	1.40 ± 0.29	0.001	1.35 ± 0.29	1.39 ± 0.30	0.020	1.23 ± 0.22	1.56 ± 0.27	<0.001
Adipsin (μg/ml)	5.02 (4.05–6.34)	4.84 (3.93–6.16)	0.019	5.13 (4.05–6.44)	4.79 (3.97–6.03)	0.001	4.96 (3.97–6.18)	4.90 (4.06–6.34)	0.794	4.98 (4.05–6.31)	4.90 (3.93–6.23)	0.149
Nrg4 (ng/ml)	3.24 (2.40–4.52)	3.55 (2.60–5.29)	<0.001	3.26 (2.37–4.59)	3.47 (2.60–5.05)	0.010	3.21 (2.38–4.58)	3.53 (2.60–5.05)	0.002	3.32 (2.50–4.65)	3.41 (2.41–5.02)	0.034
Visceral fat level	10 (8–14)	8 (7–11)	<0.001	10 (8–15)	8 (7–10.5)	<0.001	9 (8–14)	9 (8–13)	0.013	9 (8–14)	9 (7–12)	<0.001
MVF ratio	4.22 ± 0.80	4.64 ± 0.93	<0.001	4.17 ± 0.79	4.66 ± 0.90	<0.001	4.28 ± 0.85	4.51 ± 0.89	<0.001	4.28 ± 0.83	4.51 ± 0.92	<0.001

Data are presented as the mean ± SD or median (interquartile range).

BMI, body mass index; BP, blood pressure; HOMA-IR, homeostasis model assessment of insulin resistance; LDL-c, low-density lipoprotein cholesterol; HDL-c, high -density lipoprotein cholesterol; MVF, muscle mass to visceral fat; Nrg4, neuregulin 4.

cholesterol and LDL-c. Of note, per SD increase of visceral fat level was markedly associated with the increased odds of MetS [OR (95% CI), 2.20 (1.62–2.99); $P < 0.001$], elevated BP [OR 95% CI), 2.04 (1.52–2.75); $P < 0.001$], elevated fasting glucose [OR (95% CI), 1.50 (1.13–1.98); $P < 0.01$], and dyslipidemia [OR (95% CI), 1.75 (1.31–2.34); $P < 0.01$] in the final model.

Figure 1 shows the mediation effects of circulating Nrg4 and adipsin levels on the association between waist circumference and MetS. The total effect of waist circumference on MetS was measured as a standardized regression coefficient ($\beta_{Tot} = 0.391$, $P < 0.001$). The waist circumference was inversely correlated with circulating Nrg4 and was positively correlated with circulating adipsin ($\beta_1 = -0.087$, $P < 0.01$; $\beta_1 = 0.156$, $P < 0.001$, respectively). The total indirect effect ($\beta_{Ind} = 0.014$, $P < 0.05$) through circulating Nrg4 level defined as the product of indirect effect 1 (β_1) and indirect effect 2 (β_2) was significant (**Figure 1A**). The mediation effect of circulating Nrg4 level on the waist circumference-MetS association was 3.61%. After adjusting for fasting insulin and postprandial glucose (**Figure 1B**, model a), the mediation effect of circulating adipsin and Nrg4 levels on the waist circumference-MetS association was estimated at 16.87%, 7.66%, respectively. Both the mediation effects were increased from 7.66% to 8.31% for circulating Nrg4 and from 16.87% to 18.35% for circulating adipsin with further adjustment of HOMA-IR (Model b).

Figure 2 presents the mediation effects of circulating Nrg4 and adipsin levels on the association between visceral fat level and MetS. The total effect of visceral fat level on MetS was notable ($\beta_{Tot} = 0.406$, $P < 0.001$). The visceral fat level had a negative correlation with circulating Nrg4 and a positive correlation with circulating adipsin ($\beta_1 = -0.154$, $P < 0.001$; $\beta_1 = 0.184$, $P < 0.001$, respectively). Circulating Nrg4 had a significant mediation effect on the association of visceral fat level and MetS (percent mediated effect, 5.73%), and the mediation effect increased to 7.60% and 7.50% in model a and model b, respectively (**Figure 2A**). After adjusting for several confounding factors, visceral fat level was linked to MetS through circulating adipsin with a mediation effect of 9.45% in model a and a mediation effect of 9.98% in model b (**Figure 2B**).

Figure 3 shows the mediation effects of circulating Nrg4 and adipsin levels on the association between MVF ratio and MetS. The MVF ratio had a significant effect on MetS ($\beta_{Tot} = 0.491$, $P < 0.001$). The MVF ratio was positively correlated with circulating Nrg4 and negatively correlated with circulating adipsin ($\beta_1 = 0.109$, $P < 0.001$; $\beta_1 = -0.174$, $P < 0.001$; respectively). Similarly, circulating Nrg4 also partially mediated the effect of MVF ratio on MetS with a mediation effect of 3.54%, which was elevated to 5.72% and 5.80% with further adjustments (**Figure 3A**). A significant mediation effect of circulating adipsin was presented after adjusting the confounders (percent mediated effect, 9.36% and 9.86% respectively in two models, **Figure 3B**). In addition, the interaction effects of circulating Nrg4 and adipsin by gender on the association between adiposity measurements and MetS were not significant (all $P > 0.05$; **Supplementary Figures 3**, **4**, respectively).

TABLE 2 | Effect of adiposity measurements on the components of metabolic syndrome.

	Metabolic syndrome	Elevated blood pressure	Elevated fasting glucose	Dyslipidemia
	OR (95%CI)	OR (95%CI)	OR (95%CI)	OR (95%CI)
Model 1				
Waist circumference	1.48 (1.29–1.69)***	1.58 (1.39–1.80)***	1.21 (1.08–1.37)**	1.20 (1.07–1.35)**
Visceral fat level	1.50 (1.32–1.71)***	1.74 (1.52–1.98)***	1.16 (1.03–1.31)*	1.29 (1.14–1.45)***
MVF ratio	0.61 (0.54–0.69)***	0.55 (0.48–0.63)***	0.76 (0.68–0.86)***	0.76 (0.68–0.86)***
Model 2				
Waist circumference	1.39 (1.21–1.61)***	1.40 (1.22–1.61)***	1.22 (1.07–1.39)**	1.15 (1.01–1.30)*
Visceral fat level	1.99 (1.48–2.68)***	1.94 (1.45–2.60)***	1.44 (1.09–1.90)*	1.56 (1.18–2.06)**
MVF ratio	0.66 (0.56–0.78)***	0.68 (0.58–0.81)***	0.81 (0.69–0.95)*	0.76 (0.65–0.89)***
Model 3				
Waist circumference	1.42 (1.22–1.64)***	1.41 (1.23–1.62)***	1.22 (1.07–1.39)**	1.18 (1.03–1.34)*
Visceral fat level	2.20 (1.62–2.99)***	2.04 (1.52–2.75)***	1.50 (1.13–1.98)**	1.75 (1.31–2.34)**
MVF ratio	0.65 (0.55–0.77)***	0.68 (0.57–0.80)***	0.81 (0.69–0.96)*	0.73 (0.62–0.87)***

OR, odds ratio; CI, confidence interval; MVF, muscle mass to visceral fat.
**P < 0.05; **P < 0.01; ***P < 0.001.*
Model 1: without adjustment. Model 2: adjusted for age, gender, smoking, alcohol assumption, and physical activity. Model 3: adjusted for model 2 + total cholesterol, LDL- cholesterol.

DISCUSSION

As an endocrine organ, adipose tissue regulates metabolic homeostasis by releasing a large number of adipokines (Kahn et al., 2019). Recently, several novel proteins secreted from adipocytes, such as Nrg4 and adipsin have been identified to play a role in modulate systemic metabolic homeostasis and are associated with MetS and cardiovascular disease (Saleh et al., 2019; Tutunchi et al., 2020). However, it was unclear whether and to what extent adiposity affects MetS through circulating Nrg4 and adipsin levels in humans. In the present study, our findings highlighted that adiposity measurements, including waist circumference, visceral fat level, and MVF ratio, were significantly associated with MetS through circulating Nrg4 and adipsin levels. This study provides strong evidence that the effect of adiposity on the development of MetS is mediated by secretory adipokines.

It has been generally accepted that adiposity is associated with MetS. Several studies have indicated waist circumference, visceral fat level, and MVF ratio were useful measurements for the detection of MetS (Unno et al., 2012; Yu et al., 2016; Ramírez-Vélez et al., 2018). Consistently, we found that waist circumference and visceral fat level were significantly associated

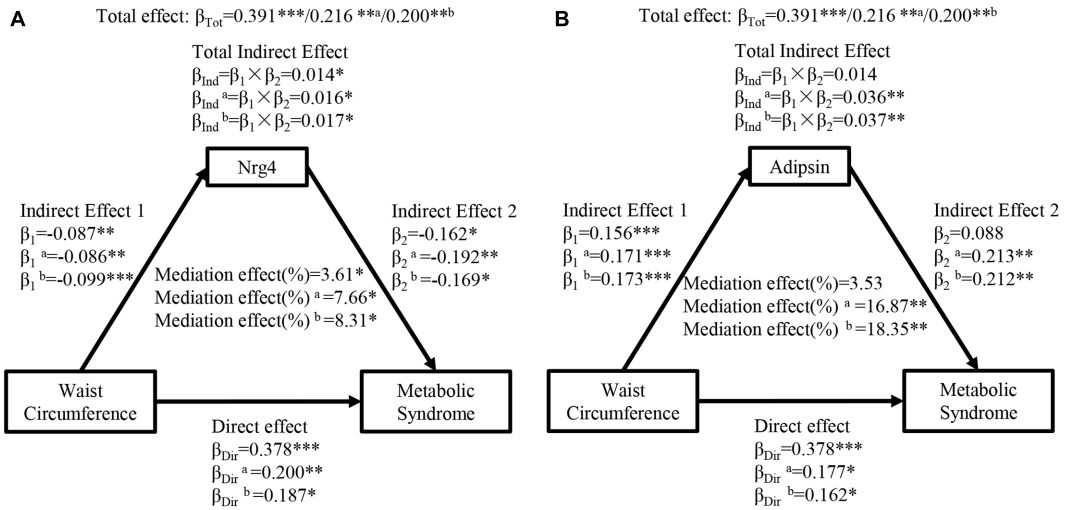

FIGURE 1 | Ngr 4 and adipsin mediate the effect of waist circumference on metabolic syndrome. **(A)** Mediation analysis of Nrg4. **(B)** Mediation analysis of adipsin. β, standardized regression coefficient; β_1, indirect effect 1; β_2, indirect effect 2; β_{Ind}, total indirect effect; β_{Dir}, direct effect; β_{Tot}, total effect; Nrg4, neuregulin 4. $^*P < 0.05$; $^{**}P < 0.01$; $^{***}P < 0.001$. Model a: adjusted for fasting insulin, 2-h glucose. Model b: adjusted for model a + HOMA-IR.

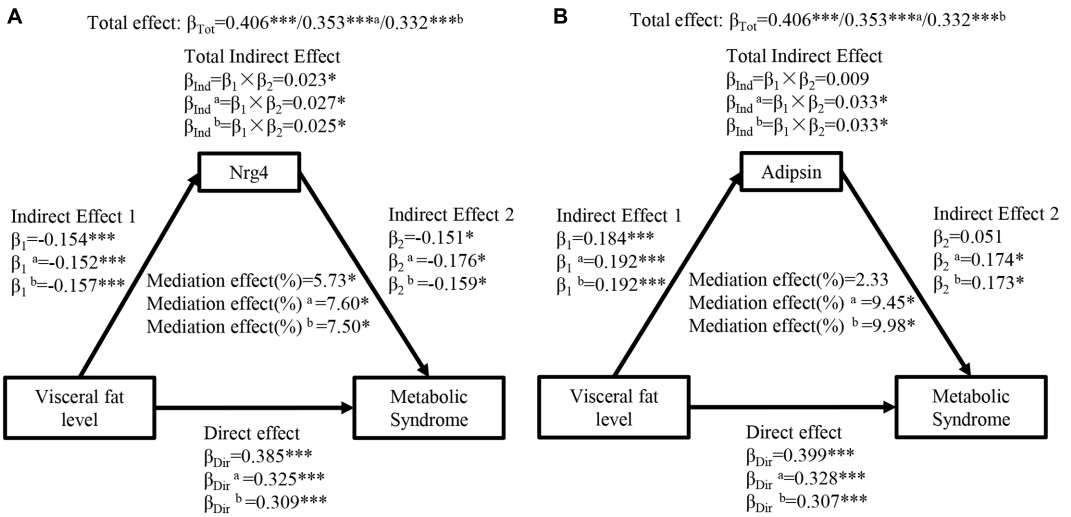

FIGURE 2 | Ngr 4 and adipsin mediate the effect of visceral fat level on metabolic syndrome. **(A)** Mediation analysis of Nrg4. **(B)** Mediation analysis of adipsin. β, standardized regression coefficient; β_1, indirect effect 1; β_2, indirect effect 2; β_{Ind}, total indirect effect; β_{Dir}, direct effect; β_{Tot}, total effect; Nrg4, neuregulin 4. Model a: adjusted for fasting insulin, 2-h glucose. Model b: adjusted for model a + HOMA-IR. $^*P < 0.05$; $^{***}P < 0.001$.

with increased odds of MetS and its each component. Besides, our study also found that increased MVF ratio was associated with lower odds of MetS.

It has been established that adiposity is inversely correlated to BAT mass or activity in adult human, which protects against obesity and related metabolic disorders by promoting energy expenditure via the activity of uncoupling protein 1 (UCP1) (Kahn et al., 2019). Nrg4 is identified a brown-fat-enriched endocrine factor with therapeutic potential for the treatment of obesity-associated disorders (Tutunchi et al., 2020). Evidence has suggested that Nrg4 was inversely correlated with adiposity (Jiang et al., 2016; Chen et al., 2017; Yan et al., 2019) and might be a protective factor in the development of MetS (Cai et al., 2016). However, it was unclear to whether adiposity affects MetS through circulating Nrg4 level. Our results showed that adiposity measurements were significantly associated with MetS through decreased circulating Nrg4 level. Furthermore, we quantified the mediation effect of circulating Nrg4 level in the association of waist circumference, visceral fat level, and MVF ratio with MetS was 8.31%, 7.50%, and 5.80%, respectively. These observations provided additional, stronger evidence to support previous findings from our (Cai et al., 2016) and other studies (Wang et al., 2014; Dai et al., 2015; Jiang et al., 2016; Chen et al., 2017; Yan et al., 2019) that brown fat-enriched

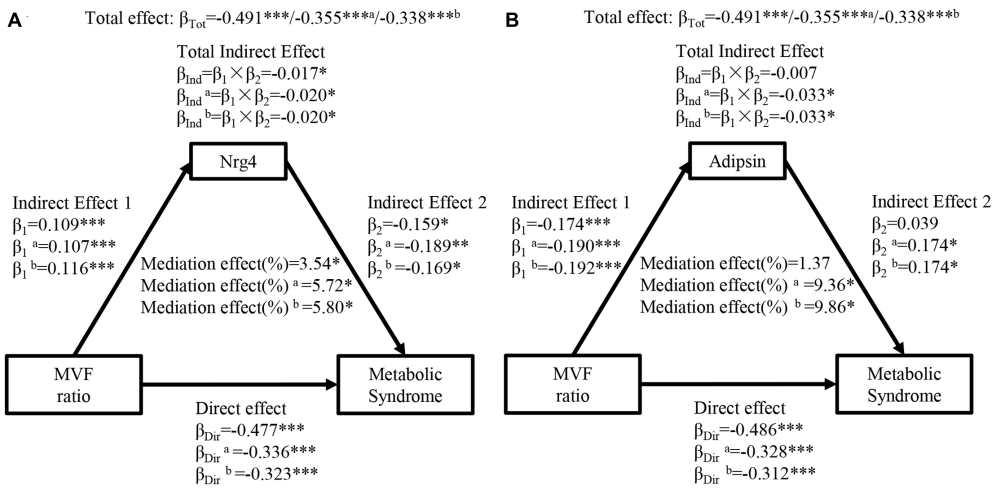

FIGURE 3 | Ngr 4 and adipsin mediate the effect of MVF ratio on metabolic syndrome. **(A)** Mediation analysis of Nrg4. **(B)** Mediation analysis of adipsin. β, standardized regression coefficient; β_1, indirect effect 1; β_2, indirect effect 2; β_{Ind}, total indirect effect; β_{Dir}, direct effect; β_{Tot}, total effect; MVF, muscle mass to visceral fat; Nrg4, neuregulin 4. Model a: adjusted for fasting insulin, 2-h glucose. Model b: adjusted for model a + HOMA-IR. *$P < 0.05$; **$P < 0.01$; ***$P < 0.001$.

secreted factor Nrg4 is involve in crosstalk between adiposity and metabolic disorders.

Adiposity is characterized by a substantial increase in WAT mass and is associated with increased risk of MetS. Adipsin mainly synthesized and secreted from WAT, plays a role in modulating lipid and glucose metabolism (Lo et al., 2014; Gómez-Banoy et al., 2019). Several clinical studies reported that elevated serum adipsin levels was observed in obese subjects and positively associated with BMI and visceral adipose tissue (Abu-Farha et al., 2014; Gursoy Calan et al., 2016; Schrover et al., 2018; Ohtsuki et al., 2019). Schrover et al. (2018) reported that adipsin was not significant associated with MetS in patients with clinically manifest vascular disease. Consistently, our data indicated that circulating adipsin was positively correlated with waist circumference and visceral fat level, and negatively associated with MVF ratio. Besides, our results also demonstrated that subjects with MetS had a higher level of circulating adipsin. Of note, our mediation analyses showed that increased adiposity had an adverse effect on MetS which was partially mediated through circulating adipsin levels, with a mediation effect of 18.35% accounting for waist circumference-MetS association and 9.98% accounting for visceral fat level-MetS association. The mediation effect might be explained by the function of adipsin, which increases lipid accumulation and adipocyte differentiation through inducing the peroxisome proliferator-activated receptor γ (Pparγ) and releasing complement component 3a (C3a) (Song et al., 2016; Saleh et al., 2019). Our data suggests that the expansion of WAT increased the level of circulating adipsin which might have a potential impact on the development of MetS.

Of note, the mediation effects of circulating Nrg4 and adipsin remained significant after adjusting several variables related to IR, suggesting that the potential mechanism of circulating Nrg4 and adipsin mediating the association between adiposity and MetS is independent of IR. Similarly, recent study carried out in the Netherlands also reported that the association between abdominal adiposity and HOMA-IR was mediated by leptin and adiponectin (Noordam et al., 2020). These observations provided stronger evidence that adipokines secreted by adipocytes is involved in crosstalk between adiposity and metabolic disorders. However, the underlying mechanism of different adipokines in the pathogenesis of obesity-induced MetS needs to be further studied in *vivo* and in *vitro*.

The novelty of this community-based, cross-sectional study is that we examined and quantified the degree of the mediation effect of circulating Nrg4 and adipsin on the association between adiposity and MetS. We found that the path from adiposity and MetS was protectively mediated Nrg4 but adversely mediated by adipsin, suggesting that elevating circulating Nrg4 levels and inhibiting adipsin secreting might be therapeutic potentials for protecting obesity from MetS. These findings indicate that adipokines could be used as predictors of metabolic phenotype and monitoring markers for lifestyle intervention and weight management in the future. However, there are several limitations to the current study. First, given its cross-sectional design, we cannot exclude the pathways of associations may exist an inverse direction. Second, the visceral fat in the study was measured using DXA which is not a gold standard tool. However, studies have demonstrated that DXA is comparable with computed tomography (CT) and magnetic resonance imaging (MRI) with R^2 ranging between 0.82 to 0.96, as a result, DXA is considered as a feasible alternative (Browning et al., 2011; Neeland et al., 2018, 2019). Third, our study population focus on the Chinese adults and therefore the findings may not be generalizable to other ethnicities or geographic regions. Therefore, the pathways of the association should be further evaluated in prospective studies with larger sample sizes, different ethnicities, and long follow-up periods.

CONCLUSION

Our study indicated that the association between adiposity measurements and MetS was linked through circulating Nrg4 and adipsin levels. The quantification of the mediation effects of circulating Nrg4 and adipsin levels may facilitate the development of novel prevention and intervention strategies for controlling the progression from adiposity to MetS.

DATA AVAILABILITY STATEMENT

The raw data supporting the conclusions of this article will be made available by the authors, without undue reservation.

ETHICS STATEMENT

The studies involving human participants were reviewed and approved by the Institutional Review Board of The First Affiliated Hospital of Xiamen University. The patients/participants provided their written informed consent to participate in this study.

AUTHOR CONTRIBUTIONS

All authors listed have made a substantial, direct and intellectual contribution to the work, and approved it for publication.

FUNDING

This study was supported by the National Key Research and Development Project (Nos. 2018YFA0800404 and 2020YFC2006400), Natural Science Foundation and Key-Area Research and Development Program of Guangdong Province (Nos. 2018B030311031 and 2019B020227004), and the National Natural Science Foundation of China (No. 81970736). HZ was partially supported by Distinguished Young Scholars Training Program of Nanfang Hospital.

SUPPLEMENTARY MATERIAL

The Supplementary Material for this article can be found online at: https://www.frontiersin.org/articles/10.3389/fphys.2021.667330/full#supplementary-material

REFERENCES

Alberti, K. G., Zimmet, P., and Shaw, J. (2005). The metabolic syndrome–a new worldwide definition. *Lancet*. 366, 1059–1062.

Park, S., Lee, S., Kim, Y., Lee, Y., Kang, M. W., Han, K., et al. (2019). Altered Risk for Cardiovascular Events With Changes in the Metabolic Syndrome Status: A Nationwide Population-Based Study of Approximately 10 Million Persons. *Annals of internal medicine.* 171, 875–884.

Lorenzo, C., Okoloise, M., Williams, K., Stern, M. P., and Haffner, S. M. (2003). The metabolic syndrome as predictor of type 2 diabetes: the San Antonio heart study. *Diabetes Care.* 26, 3153–3159.

Hirode, G., and Wong, R. J. (2020). Trends in the Prevalence of Metabolic Syndrome in the United States, 2011-2016. *JAMA.* 323, 2526–2528.

Cameron, A. J., Boyko, E. J., Sicree, R. A., Zimmet, P. Z., Söderberg, S., Alberti, K. G., et al. (2008). Central obesity as a precursor to the metabolic syndrome in the AusDiab study and Mauritius. *Obesity (Silver Spring).* 16, 2707–2716.

Francisco, V., Ruiz-Fernández, C., Pino, J., Mera, A., González-Gay, M. A., Gómez, R., et al. (2019). Adipokines: Linking metabolic syndrome, the immune system, and arthritic diseases. *Biochemical pharmacology.* 165, 196–206.

Saltiel, A. R., and Olefsky, J. M. (2017). Inflammatory mechanisms linking obesity and metabolic disease. *J Clin Invest.* 127, 1–4.

Sanidas, E., Velliou, M, Papadopoulos, D., Iliopoulos, D., and Barbetseas, J. (2020). Healthy and non healthy obese patients. The truth lies in the adipose tissue. *Eur J Intern Med.* 82, 133–134.

Kahn, C. R., Wang, G., and Lee, K. Y. (2019). Altered adipose tissue and adipocyte function in the pathogenesis of metabolic syndrome. *J Clin Invest.* 129, 3990–4000.

Tutunchi, H., Ostadrahimi, A., Hosseinzadeh-Attar, M. J., Miryan, M., Mobasseri, M., and Ebrahimi-Mameghani, M. (2020). A systematic review of the association of neuregulin 4, a brown fat-enriched secreted factor, with obesity and related metabolic disturbances. *Obesity reviews : an official journal of the International Association for the Study of Obesity.* 21, e12952.

Saleh, J., Al-Maqbali, M., and Abdel-Hadi, D. (2019). Role of Complement and Complement-Related Adipokines in Regulation of Energy Metabolism and Fat Storage. *Comprehensive Physiology.* 9, 1411–1429.

Yan, P., Xu, Y., Zhang, Z., Gao, C., Zhu, J., Li, H., et al. (2019). Decreased plasma neuregulin 4 levels are associated with peripheral neuropathy in Chinese patients with newly diagnosed type 2 diabetes: A cross-sectional study. *Cytokine.* 113, 356–364.

Chen, Z., Wang, G. X., Ma, S. L., Jung, D. Y., Ha, H., Altamimi, T., et al. (2017). Nrg4 promotes fuel oxidation and a healthy adipokine profile to ameliorate diet-induced metabolic disorders. *Molecular metabolism.* 6, 863–872.

Jiang, J., Lin, M., Xu, Y., Shao, J., Li, X., Zhang, H., et al. (2016). Circulating neuregulin 4 levels are inversely associated with subclinical cardiovascular disease in obese adults. *Sci Rep.* 6, 36710.

Dai, Y. N., Zhu, J. Z., Fang, Z. Y., Zhao, D. J., Wan, X. Y., Zhu, H. T., et al. (2015). A case-control study: Association between serum neuregulin 4 level and non-alcoholic fatty liver disease. *Metabolism.* 64, 1667–1673.

Wang, G. X., Zhao, X. Y., Meng, Z. X., Kern, M., Dietrich, A., Chen, Z., et al. (2014). The brown fat-enriched secreted factor Nrg4 preserves metabolic homeostasis through attenuation of hepatic lipogenesis. *Nature medicine.* 20, 1436–1443.

Cai, C., Lin, M., Xu, Y., Li, X., Yang, S., and Zhang, H. (2016). Association of circulating neuregulin 4 with metabolic syndrome in obese adults: a cross-sectional study. *BMC medicine.* 14:165.

Song, N. J., Kim, S., Jang, B. H., Chang, S. H., Yun, U. J., Park, K. M., et al. (2016). Small Molecule-Induced Complement Factor D (Adipsin) Promotes Lipid Accumulation and Adipocyte Differentiation. *PLoS One.* 11:e0162228.

Ohtsuki, T., Satoh, K., Shimizu, T., Ikeda, S., Kikuchi, N., Satoh, T., et al. (2019). Identification of Adipsin as a Novel Prognostic Biomarker in Patients With Coronary Artery Disease. *J Am Heart Assoc.* 8, e013716.

Guo, D., Yuan, Y., Huang, R., Tian, S., Wang, J., Lin, H., et al. (2019). Association between plasma adipsin level and mild cognitive impairment in Chinese patients with type 2 diabetes: a cross-sectional study. *BMC endocrine disorders.* 19:108.

Gursoy Calan, O., Calan, M., Yesil Senses, P., Unal Kocabas, G., Ozden, E., Sari, K. R., et al. (2016). Increased adipsin is associated with carotid intima media thickness and metabolic disturbances in polycystic ovary syndrome. *Clinical endocrinology.* 85, 910–917.

Derosa, G., Fogari, E., D'Angelo, A., Bianchi, L., Bonaventura, A., Romano, D., et al. (2013). Adipocytokine levels in obese and non-obese subjects: an observational study. *Inflammation.* 36, 914–920.

Sobel, E. (1982). Asymptotic confidence intervals for indirect effects in structural equation models. *Sociological Methodology.* 13, 290–312.

VanderWeele, T. J. (2016). Mediation Analysis: A Practitioner's Guide. *Annual review of public health.* 37, 17–32.

Ramírez-Vélez, R., Garcia-Hermoso, A., Prieto-Benavides, D. H., Correa-Bautista, J. E., Quino-Ávila, A. C., Rubio-Barreto, C. M., et al. (2018). Muscle mass to

visceral fat ratio is an important predictor of the metabolic syndrome in college students. *Br J Nutr.* 1–10. **volQ,

Yu, J., Tao, Y., Tao, Y., Yang, S., Yu, Y., Li, B., et al. (2016). Optimal cut-off of obesity indices to predict cardiovascular disease risk factors and metabolic syndrome among adults in Northeast China. *BMC public health.* 16:1079. doi: 10.1186/s12889-016-3694-5

Unno, M., Furusyo, N., Mukae, H., Koga, T., Eiraku, K., and Hayashi, J. (2012). The utility of visceral fat level by bioelectrical impedance analysis in the screening of metabolic syndrome - the results of the Kyushu and Okinawa Population Study (KOPS). *Journal of atherosclerosis and thrombosis.* 19, 462–470.

Gómez-Banoy, N., Guseh, J. S., Li, G., Rubio-Navarro, A., Chen, T., Poirier, B., et al. (2019). Adipsin preserves beta cells in diabetic mice and associates with protection from type 2 diabetes in humans. *Nature medicine.* 25, 1739–1747.

Lo, J. C., Ljubicic, S., Leibiger, B., Kern, M., Leibiger, I. B., Moede, T., et al. (2014). Adipsin is an adipokine that improves β cell function in diabetes. *Cell.* 158, 41–53.

Schrover, I. M., van der Graaf, Y., Spiering, W., and Visseren, F. L. (2018). The relation between body fat distribution, plasma concentrations of adipokines and the metabolic syndrome in patients with clinically manifest vascular disease. *European journal of preventive cardiology.* 25, 1548–1557.

Abu-Farha, M., Behbehani, K., and Elkum, N. (2014). Comprehensive analysis of circulating adipokines and hsCRP association with cardiovascular disease risk factors and metabolic syndrome in Arabs. *Cardiovascular diabetology.* 13, 76.

Noordam, R., Boersma, V., Verkouter, I., le Cessie, S., Christen, T., Lamb, H. J., et al. (2020). The role of C-reactive protein, adiponectin and leptin in the association between abdominal adiposity and insulin resistance in middle-aged individuals. *Nutr Metab Cardiovasc Dis.* 30, 1306–1314.

Neeland, I. J., Ross, R., Després, J. P., Matsuzawa, Y., Yamashita, S., Shai, I., et al. (2019). Visceral and ectopic fat, atherosclerosis, and cardiometabolic disease: a position statement. *Lancet Diabetes Endocrinol.* 7, 715–725.

Neeland, I. J., Poirier, P., and Després, J. P. (2018). Cardiovascular and Metabolic Heterogeneity of Obesity: Clinical Challenges and Implications for Management. *Circulation.* 137, 1391–1406.

Browning, L. M., Mugridge, O., Dixon, A. K., Aitken, S. W., Prentice, A. M., and Jebb, S. A. (2011). Measuring abdominal adipose tissue: comparison of simpler methods with MRI. *Obesity facts.* 4, 9–15.

Conflict of Interest: The authors declare that the research was conducted in the absence of any commercial or financial relationships that could be construed as a potential conflict of interest.

frontiers in Physiology

ORIGINAL RESEARCH
published: 20 May 2021
doi: 10.3389/fphys.2021.687744

Nobiletin Alleviates Non-alcoholic Steatohepatitis in MCD-Induced Mice by Regulating Macrophage Polarization

Si-wei Wang[1†], Tian Lan[2†], Hao Sheng[3], Fang Zheng[1], Mei-kang Lei[4], Li-xia Wang[5], Hang-fei Chen[6], Chun-yi Xu[6] and Feng Zhang[1,3,6]*

[1] Core Facility, The Quzhou Affiliated Hospital of Wenzhou Medical University, Quzhou People's Hospital, Quzhou, China, [2] Department of Pharmacy, The Quzhou Affiliated Hospital of Wenzhou Medical University, Quzhou People's Hospital, Quzhou, China, [3] Zhejiang University School of Medicine, Hangzhou, China, [4] Department of Analytical Testing Center, Quzhou Customs, Quzhou, China, [5] Agriculture and Rural Bureau of Changshan County, Quzhou, China, [6] Zhejiang Chinese Medical University, Hangzhou, China

OPEN ACCESS

Edited by:
Dechun Feng,
National Institute on Alcohol Abuse and Alcoholism (NIAAA), United States

Reviewed by:
Weina Zhao,
University of Texas Health Science Center at Houston, United States
Zhu-Jun Mao,
Zhejiang Chinese Medical University, China

***Correspondence:**
Feng Zhang
felix.f.zhang@outlook.com

[†] These authors have contributed equally to this work

Specialty section:
This article was submitted to Clinical and Translational Physiology, a section of the journal Frontiers in Physiology

Received: 30 March 2021
Accepted: 26 April 2021
Published: 20 May 2021

Citation:
Wang S-w, Lan T, Sheng H, Zheng F, Lei M-k, Wang L-x, Chen H-f, Xu C-y and Zhang F (2021) Nobiletin Alleviates Non-alcoholic Steatohepatitis in MCD-Induced Mice by Regulating Macrophage Polarization. Front. Physiol. 12:687744. doi: 10.3389/fphys.2021.687744

Non-alcoholic steatohepatitis (NASH) is an inflammatory disorder that is characterized by chronic activation of the hepatic inflammatory response and subsequent liver damage. The regulation of macrophage polarization in liver is closely related to the progression of NASH. The orphan nuclear receptor retinoic-acid-related orphan receptor α (RORα) and Krüppel-like factor 4 (KLF4) are key regulators which promote hepatic macrophages toward M2 phenotype and protect against NASH in mice. Nobiletin (NOB), a natural polymethoxylated flavone, is previously reported as a RORα regulator in diet-induced obese mice. However, it is still unclear whether NOB has the protective effect on NASH. In this study, we investigated the role of NOB in NASH using a methionine and choline deficient (MCD)-induced NASH mouse model. Our results showed that NOB ameliorated hepatic damage and fibrosis in MCD fed mice. NOB treatment reduced the infiltration of macrophages and neutrophils in the liver in MCD-fed mice. Of importance, NOB significantly increased the proportion of M2 macrophages and the expression of anti-inflammatory factors *in vivo* and *in vitro*. Meanwhile, NOB also decreased the population of M1 macrophages and the expression of proinflammatory cytokines. Mechanistically, NOB elevated KLF4 expression in macrophages. Inhibition of KLF4 abolished NOB regulated macrophage polarization. Furthermore, the regulation of NOB in KLF4 expression was dependent on RORα.

Keywords: nobiletin, NASH, RORα, macrophage polarization, KLF4

INTRODUCTION

Non-alcoholic steatohepatitis (NASH), the progressive form of non-alcoholic fatty liver disease (NAFLD), is an inflammatory disorder that is characterized by liver inflammation, fibrosis and hepatocellular injury (Han et al., 2017; Kong et al., 2019; Xu et al., 2020). It has been known that macrophage plays a critical role in hepatic immune homeostasis by releasing cytokines and modulating immune cell response in NASH (Han et al., 2019). Macrophages, which can be activated

in a number of ways, can be categorized as two main groups, designated M1 and M2 (Wang et al., 2019). The M1 macrophage phenotype is characterized by the production of high levels of pro-inflammatory cytokines such as tumor necrosis factor α (TNF-α) and interleukin 1β (IL-1β). In contrast, phenotypically M2 macrophages have been characterized as anti-inflammatory cytokines such as interleukin 10 (IL-10) and arginase-1 (Arg-1) (Murray, 2017). Increasing evidence has suggested that targeting M1/M2 polarization of macrophages could be effective strategy to alleviate NASH (Wan et al., 2014; Han et al., 2017, 2019; Kong et al., 2019).

Nuclear receptor retinoic-acid-related orphan receptor α (RORα), as a transcriptional factor, is involved in the regulation of various target genes related to lipid metabolism and inflammation (Jetten, 2009). It has been reported that RORα can directly regulate M1/M2 polarization switch of liver macrophages under the pathological conditions of NASH (Han et al., 2017). Importantly, RORα was low expression in liver of patients with NASH (Ou et al., 2013), and treatment with RORα activator could alleviate NASH (Han et al., 2014, 2017). These findings suggest that regulation of macrophage polarization by targeting RORα will provide an attractive strategy to limit NASH.

Nobiletin (5,6,7,8,3′,4′-hexamethoxyflavone, NOB) (**Figure 1A**) is a natural polymethoxylated flavone extracted exclusively in citrus fruits (Di Donna et al., 2013). It has a wide range of beneficial properties, including anti-obesity (Morrow et al., 2020), anti-diabetic (Mulvihill et al., 2011), anti-inflammatory (Rong et al., 2021), anti-aging (Yang et al., 2020), and anti-tumor (Feng et al., 2020) activities. Previous studies have shown that NOB is a RORα regulator. It can activate RORα to protect against metabolic dysfunctions (He et al., 2016; Nohara et al., 2019). However, the direct effect of NOB on NASH has not been reported, and it is also unclear that whether NOB could regulate macrophage polarization to alleviate NASH by activating RORα .

In current study, we thus evaluated the effect of NOB on NASH using a methionine and choline deficient (MCD)-induced mouse model, and we investigated its effects and molecular mechanism on macrophage polarization *in vivo* and *in vitro*.

MATERIALS AND METHODS

Chemicals and Reagents

Nobiletin (NOB, CAS# 478-01-3, HPLC ≥ 98%), and SR3335 (CAS# 293753-05-6) were purchased from Shanghai Yuanye Biological Technology, China. Recombinant Murine Interleukin-4 (IL-4, #C600050) was purchased from Sangon Biotech, Shanghai, China. Lipopolysaccharide (#L2630) was purchased from Sigma, United States.

Animal Experiments

All animal experiments were performed in accordance with the Experimental Animal Center of Zhejiang University of Traditional Chinese Medicine, China. Experimental procedures were approved by the Ethics Committee of Animal Experiments of Quzhou people's hospital, China. Male C57BL/6 mice (6–8 weeks, specified pathogen free) were purchased from GemPharmatech Co., Ltd., Jiangsu, China (license number of animal production: SYXK2015-0001). All animals were housed in room temperature, allowed free access to distilled water and common pelleted food, and placed under a 12-h/12-h dark/light cycle.

After 1 week of adaptation, the mice were randomly divided into four groups (n = 8/group).

- NCD group: These mice were fed with a control diet for methionine and choline deficient L-Amino acid diet (Research diet A02082003B, Research Diet, NJ) and received intragastrically administered distilled water.
- NCD + NOB group: These mice were fed with a control diet for methionine and choline deficient L-Amino acid diet (Research diet A02082003B, Research Diet, NJ) and treated with 50 mg/kg per day of intragastrically administered NOB.
- MCD group: These mice were received a methionine and choline deficient L-Amino acid diet (Research diet A02082002BR, Research Diet, NJ) and received intragastrically administered distilled water.
- MCD + NOB group: These mice were fed with a methionine and choline deficient L-Amino acid diet (Research diet A02082002BR, Research Diet, NJ) and treated with 50 mg/kg per day of intragastrically administered NOB.

As described, the NOB administration started from the third week and the experiment lasted for 8 weeks in total (**Figure 1B**).

Biochemical Testing

Serum alanine aminotransferase (ALT), and aspartate aminotransferase (AST) were detected by biochemical analyzer according to the manufacturer's instruction (DiaSys Diagnostic Systems, Shanghai, China).

Histopathological Analysis

Liver tissues were fixed with 10% formalin, embedded in paraffin, sectioned, and stained with hematoxylin and eosin (H&E) and Sirius red. NAFLD activity score (NAS) was graded in a blinded manner according to our previously described (Wang et al., 2020a). Mean scores were evaluated through calculating 5 different 400 × microscopic fields per mouse section by two independent trained observers.

Fibrosis score based on the Kleiner/Brunt criteria adapted to rodents (0, no fibrosis; 1, focal pericellular fibrosis in zone 3; 2, perivenular and pericellular fibrosis confined to zones 2 and 3; 3, bridging fibrosis; 4, cirrhosis) (Amrutkar et al., 2016). The area of Sirius red stained was calculated in 5 randomly selected 200 × microscopic fields per mouse section using ImageJ software (U.S. National Institutes of Health, Bethesda, MD).

Immunohistochemical Staining

Deparaffinized and blocked 5 μm sections were incubated with anti-α-SMA (1: 200, # 19245, Cell Signaling Technology), anti-F4/80 (1: 200, # 2370, Cell Signaling Technology) and anti-CD68 (1: 100, ab125212, Abcam) using MaxVision HRP-Polymer

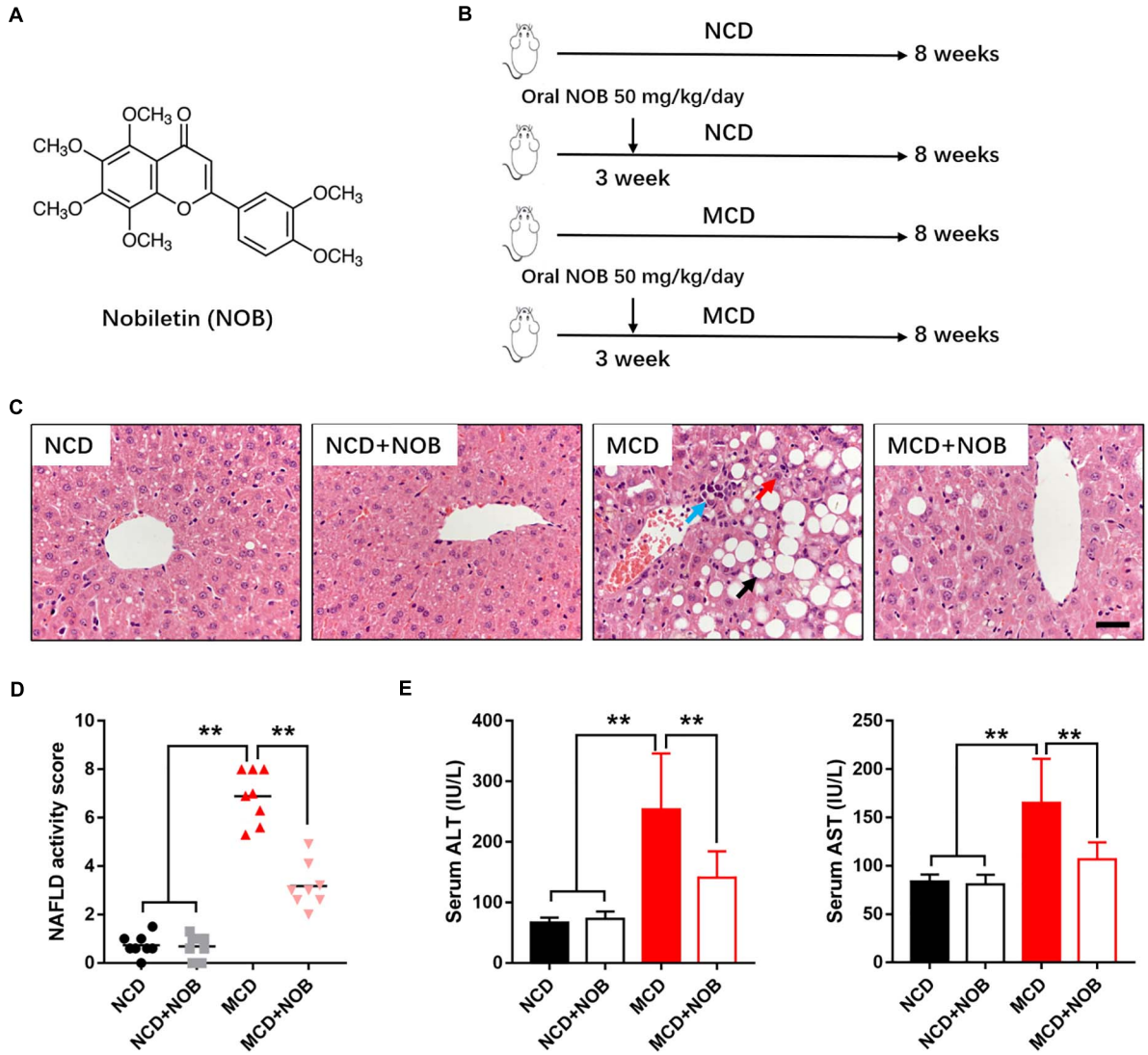

FIGURE 1 | NOB ameliorates liver function in MCD fed mice. **(A)** The chemical structure of NOB. Its molecular weight is 402.39. **(B)** The schematic diagram for MCD-induced NASH and NOB administration. C57BL/6 mice were fed either a chow diet as normal control (NCD) or the MCD diet for 8 weeks to induce NASH (MCD). Mice were treated with daily oral doses of NOB (50 mg/kg) from the third week of MCD diet feeding. Water was gavaged as control. **(C)** The representative images of H&E staining in livers from each group. Scale bar = 300 μm. Black arrow denotes macrovesicular steatosis; red arrow denotes hepatocellular ballooning; blue arrow denotes lobular inflammation. **(D)** The NAFLD activity score was shown. **(E)** Serum alanine aminotransferase (ALT) and aspartate aminotransferase (AST) levels from each group. Data were expressed as the mean ± SD (n = 8). $^{**}P < 0.01$.

anti-Rabbit IHC Kit (MXB Biotechnologies, Fuzhou, China) to develop signal. The area of positive stained was calculated in 5 randomly selected 200× or 400× microscopic fields per mouse section using ImageJ software (U.S. National Institutes of Health, Bethesda, MD).

Immunofluorescence Staining and Analysis

Deparaffinized and blocked 5 μm sections were permeabilized in 0.2% Triton X-100 for 15 min and blocked at room temperature with 3% BSA for 1 h. Primary antibodies used were CD32 (1: 200, cat. no. sc-166711, Santa Cruz Biotechnology) and CD206 (1: 200, cat. no. ab8918, Abcam). After three washes with PBS, the sections incubated with Alexa Fluor 488 goat anti-rabbit IgG for 1 h at room temperature. The fluorescence was visualized by a SUNNY RX50 fluorescence microscope. The number of immunofluorescent positive cells was counted using ImageJ software (U.S. National Institutes of Health, Bethesda, MD).

Cell Culture

RAW 264.7 and 293T cell line were all obtained from the Shanghai Bank of Cell Lines (Shanghai, China). RAW 264.7 cells were cultured in RPMI-1640, and 293T cells were in DMEM. All these were supplemented with 10% fetal bovine serum (FBS,

Gibco, United States), 100 U/mL penicillin, and 100 U/mL streptomycin at 37°C in a humidified atmosphere with 5% CO_2. The source of the cell line was identified by STR profiling and tested for mycoplasma contamination.

RNA Isolation and Quantitative RT-PCR

Total RNA was extracted from liver tissues and cells using TRIzol reagent (#DP424, Tiangen Biotech Co., Ltd., Beijing, China). cDNA was synthesized by reverse transcriptase kits (ThermoFisher Scientific, Waltham, MA) according to the manufacturer's instructions. Quantitative real-time PCR was performed using SGExcel FastSYBR Mixture (#B532955-0005, Sangon Biotech Co., Ltd., Shanghai, China) on Roche LightCycler^R 480 Quantitative PCR System (Indianapolis, United States). The relative gene expression levels were calculated using the $2^{-\Delta\Delta Ct}$ method. Primers used are listed in **Table 1**.

ChIP Assay

For ChIP assay, we used enzymatic ChIP kit from Cell Signaling (Cat. #9003) according to the manufacturer's instruction. Briefly, cells were crosslinked with 1% formaldehyde for 10 min at room temperature. Then, the reaction was stopped using 125 mM glycine. The chromatin was enzymatically digested by micrococcal nuclease at 37°C for 20 min. The digested chromatin was then briefly sonicated to break nuclear membranes. After preclearing, chromatin (500 μg) was subjected to immunoprecipitation with anti-RORα (1: 50, PA1-812, ThermoFisher Scientific) antibody or with anti-IgG as negative control at 4°C overnight. The protein-DNA complexes were then separated by incubation with protein G beads. The magnetic beads were then washed using buffers supplied with the kit to acquire chromatin. The eluted DNA was purified and analyzed by real-time PCR with specific primers: Sense, 5′- CAGAGTTAAACTGGCCTAGTTCCA-3′; Antisense, 5′-CTTTCTCTTGGTTTTGGCAGAGGA-3′. The primer sequences for ChIP-qPCR were obtained from previous publication (Han et al., 2017).

siRNA and Transfection

siRNAs used for KLF4 knockdown were ordered from GenePharma (Shanghai, China). Transfection of siRNAs to Raw264.7 was performed using Lipofectamine RNAiMAX (#13778-075, ThermoFisher Scientific) according to manufacturer's instruction.

Statistical Analysis

GraphPad Prism 7 software (GraphPad Software, La Jolla, CA) was used for all statistical analyses. All results are presented as means ± SD. Student's unpaired two-tailed *t*-test was using for comparisons between two groups. The one-way or two-way analysis of variance (ANOVA) followed by Tukey's multiple comparison's test was applied for comparisons between more than two groups. Differences were considered to be statistically significant at $P < 0.05$and highly significant at $P < 0.01$.

RESULTS

NOB Ameliorates Liver Function in MCD Fed Mice

To estimate the effect of NOB on NASH, we established MCD-induced NASH mouse model (**Figure 1B**). Microscopic examination of H&E-stained liver sections revealed that MCD diet triggered marked macrovesicular steatosis, hepatocellular ballooning and lobular inflammation in mice; however, administration of NOB ameliorates these pathological changes (**Figure 1C**). NOB also reduced NAFLD activity score (NAS) (**Figure 1D**). In addition, NOB treatment decreased serum ALT and AST levels in MCD fed mice (**Figure 1E**), suggesting improved liver function.

NOB Attenuates Liver Fibrosis in MCD-Induced Mice

NASH is a progressive form of NAFLD where inflammation causes liver damage and fibrosis (Wattacheril et al., 2018). Next, we explored the impact of NOB treatment in hepatic fibrosis of MCD-fed mice. Our result showed that NOB reduced MCD-induced perivenular fibrosis, as revealed by picrosirius red staining for collagen fibers (**Figures 2A,B**). Immunohistochemical staining for α-SMA, a marker for activated hepatic stellate cells (HSCs), showed that NOB treatment obviously decreased activated HSCs in MCD fed mice (**Figures 2A,C**). Furthermore, the administration of NOB obviously lowered the fibrosis score in MCD fed mice compared to their counterparts (**Figure 2D**).

NOB Suppresses the Infiltration of Macrophages and Neutrophils in MCD Fed Mice

Inflammation is a key feature of NASH and has been found to be crucial for fibrogenesis (Browning and Horton, 2004; Bataller and Brenner, 2005). Macrophages and neutrophils are important inflammatory cells in NASH (Wattacheril et al., 2018). F4/80 is frequently used marker for identification of macrophage population (Wang et al., 2019, 2020b), and neutrophils are characterized by high expression of myeloperoxidase (MPO) (Klebanoff, 2005; Wang et al., 2020a). Feeding with MCD diet induced overt gathering of F4/80 positive macrophages, which was reduced by NOB treatment (**Figures 3A,B**). Administration of NOB also significantly reduced the elevated hepatic MPO^+ cells in mice fed with MCD diet (**Figures 3C,D**). Notably, it was obvious that the population of neutrophils was smaller than the macrophages in MCD-induced mice (**Figures 3A,C**), suggesting a dominant role of macrophages in this model of NASH.

NOB Decreases M1 Macrophages and the Expression of Proinflammatory Cytokines *in vivo* and *in vitro*

Macrophages are heterogeneous population and include two major subsets: "proinflammatory" M1 and "immunoregulatory" M2 macrophages, according to their phenotype and functions

TABLE 1 | The primers used in this study for real time PCR.

Description	Sense primer (5′→3′)	Antisense primer (5′→3′)
Il-6	CTGCAAGAGACTTCCATCCAG	AGTGGTATAGACAGGTCTGTTGG
Il-1β	TTCAGGCAGGCAGTATCACTC	GAAGGTCCACGGGAAAGACAC
Tnf-α	CTGAACTTCGGGGTGATCGG	GGCTTGTCACTCGAATTTTGAGA
Klf4	GGCGAGTCTGACATGGCTG	GCTGGACGCAGTGTCTTCTC
Cyp7b1	GGAGCCACGACCCTAGATG	GCCATGCCAAGATAAGGAAGC
Glut2	TCAGAAGACAAGATCACCGGA	GCTGGTGTGACTGTAAGTGGG
Gck	TGAGCCGGATGCAGAAGGA	GCAACATCTTTACACTGGCCT
Gapdh	TGAGGCCGGTGCTGAGTATGT	CAGTCTTCTGGGTGGCAGTGAT

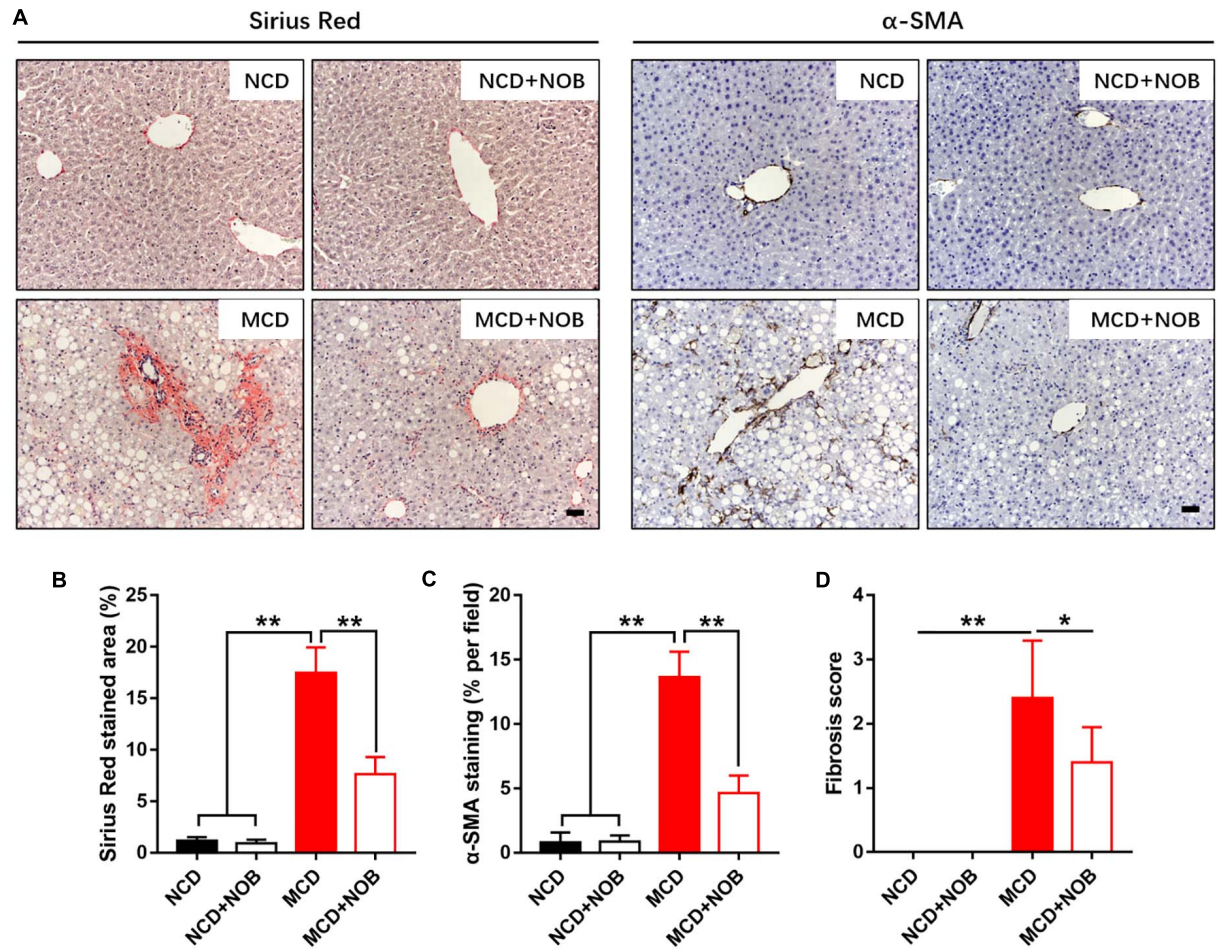

FIGURE 2 | The effect of NOB on liver fibrosis in MCD-induced mice. The deposited collagen and activated HSCs were shown by Sirius red and α-SMA staining, respectively. **(A)** The representative images of Sirius red staining and α-SMA immunohistochemical staining in liver from each group. Scale bar = 300 μm. **(B)** Quantification and statistical analysis of sirius red-stained areas was shown. **(C)** Quantification and statistical analysis of α-SMA-stained areas was shown. **(D)** Quantification of fibrosis score was shown. Data were expressed as the mean ± SD (n = 8). $^{*}P < 0.05$, $^{**}P < 0.01$.

in inflammatory responses (Wan et al., 2014; Kong et al., 2019). Polarization of macrophages toward the M1 phenotype would accelerate disease progression of NASH (Kong et al., 2019). As shown in **Figures 4A–C**, MCD diet increased hepatic M1 macrophages in mice, as detected by immunofluorescence staining with antibodies against the M1 macrophage marker CD32 and CD68 (Wang et al., 2019). NOB treatment markedly decreased the number of CD32 or CD68-postive M1 macrophages in MCD fed mice (**Figures 4A–C**). Consistently, NOB significantly inhibited the expression of proinflammatory cytokines associated with M1 macrophage such as *Il-6*, *Il-1*β, and *Tnf*-α in livers of MCD fed mice and LPS treated RAW 264.7 cells (**Figures 4D,E**). These results indicate that NOB inhibits macrophage polarization toward M1 subtype.

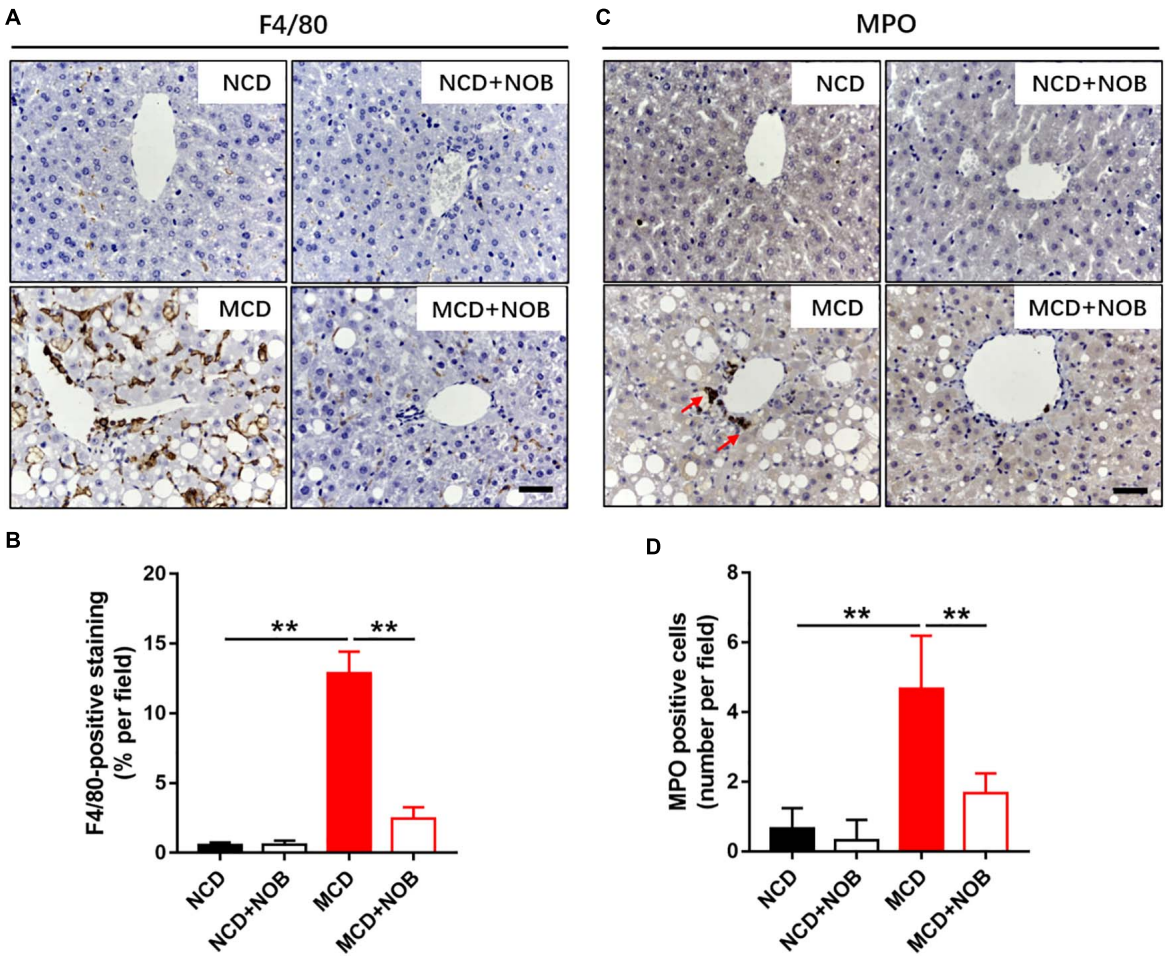

FIGURE 3 | The effect of NOB on the infiltration of macrophages and neutrophils in MCD fed mice. **(A)** The representative images of F4/80 immunohistochemical staining in liver from each group. Scale bar = 300 μm. **(B)** Quantification and statistical analysis of F4/80-stained areas was shown. Data were expressed as the mean ± SD (n = 8). **(C)** The representative images of myeloperoxidase (MPO) immunohistochemical staining in liver from each group. Scale bar = 300 μm. Red arrow points to MPO-positive cells. **(D)** Quantification and statistical analysis of MPO-positive cells in liver from each group. Data were expressed as the mean ± SD (n = 8). $^{**}P < 0.01$.

NOB Increases the Population of M2 Macrophages and the Expression of Anti-inflammatory Factors *in vivo* and *in vitro*

M2 macrophages promote resolution of inflammation and protect hepatocytes against NASH (Wan et al., 2014). CD206 is considered as a marker of M2 macrophages (Han et al., 2017; Wang et al., 2019). As shown in **Figures 5A,B**, the number of M2 macrophages was significantly increased after NOB treatment in the livers of MCD fed mice by CD206 immunofluorescence staining, compared to their MCD-diet-only counterparts. Additionally, the results of RT-qPCR also confirmed that NOB increased the expression of M2 markers *Cd206*, *Il-10* and *Arg-1* in liver of MCD-induced mice (**Figure 5C**). IL-4 is a strong inducer of M2 polarity in macrophages (Patel et al., 2017). Our results showed that NOB enhanced M2 polarization and the expression of M2 markers *Cd206*, *Il-10*, and *Arg-1* in IL-4 free or treated RAW 264.7 cells (**Figure 5D**).

KLF4 Is Required for the Regulation of NOB on Macrophage Polarization

Krüppel-like factor 4 (KLF4) is a critical regulator of macrophage polarization (Liao et al., 2011). It cooperated with STAT6 to induce an M2 genetic program and inhibit M1 polarization. Macrophage KLF4 expression was robustly induced in M2 macrophages and strongly reduced in M1 macrophages (Liao et al., 2011; Murray, 2017). We found that NOB treatment increased *Klf4* expression both in NCD and MCD fed mice, especially in MCD group (**Figure 6A**). Furthermore, NOB treatment elevated *Klf4* expression *in vitro* in a dose dependent manner (**Figure 6B**). NOB also reversed the LPS induced inhibition on *Klf4* expression and further enhanced IL-4-induced *Klf4* expression in RAW 264.7 (**Figure 6C**). To determine

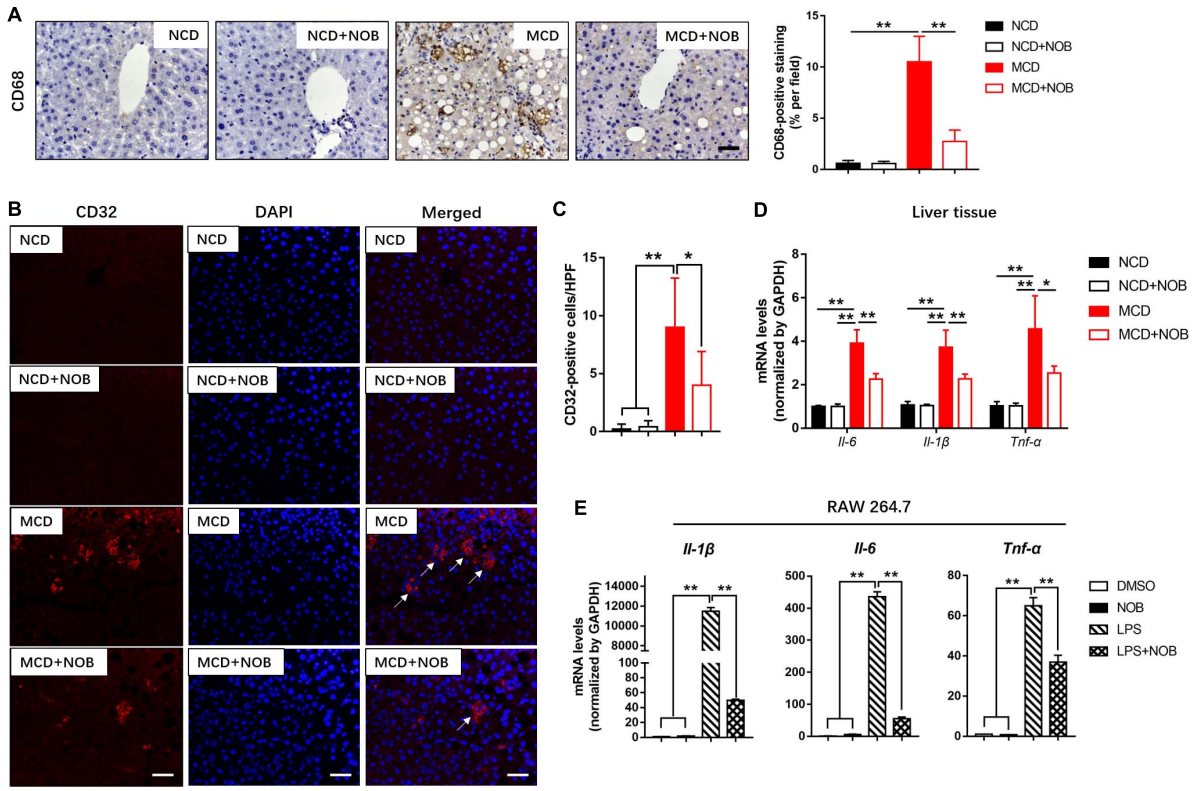

FIGURE 4 | The effect of NOB on M1 macrophage polarization and expression of inflammatory properties in liver tissue and RAW 264.7 cells. **(A)** Left, the representative images of CD68 immunohistochemical staining in liver from each group. Scale bar = 300 μm. Right, quantification and statistical analysis of CD68-stained areas. Data were expressed as the mean ± SD (n = 8). **(B)** Representative fluorescence microscopic images of CD16/32-stained liver sections. Scale bar = 300 μm. **(C)** Quantification and statistical analysis of CD16/32-positive cells in liver tissue. We measured the number of CD16/32-positive membranes from at least five high power fields (HPF, original magnification, 400×). **(D)** The mRNA levels of *Il-6*, *Il-1*β and *Tnf-*α in livers of MCD-induced mice were evaluated using RT-qPCR. Data were expressed as the mean ± SD (n = 5). **(E)** RAW 264.7 cells were pretreated with DMSO, NOB (100 μM), LPS (200 ng/mL), or LPS (200 ng/mL) + NOB (100 μM) for 16 h. The expression of proinflammatory factors *Il-6*, *Il-1*β, and *Tnf-*α determined by RT-qPCR. Values are expressed as mean ± SD (n = 3). $^{*}P < 0.05$, $^{**}P < 0.01$.

whether KLF4 is indispensable to NOB mediated polarization of macrophages, we depleted KLF4 via siRNA in RAW 264.7 cells (**Figure 6D**). As shown in **Figure 6D**, NOB induced expression of *Il-10* and *Arg-1* was completely abolished by siKLF4. Knockdown of KLF4 also reduced the expression of NOB upregulated M2 marker genes (*Cd206*, *Il-10,* and *Arg-1*) in IL-4-treated RAW 264.7 cells (**Figure 6E**). Conversely, the inhibitory effect of NOB on the expression of M1 markers (*Il-1*β and *Tnf-*α) in LPS induced RAW 264.7 cells was counteracted by KLF4 knockdown (**Figure 6F**). These results indicate that NOB-mediated macrophage polarization is dependent on KLF4.

The NOB-Induced Klf4 Expression and Macrophage Polarization Are RORα Dependent

It is reported that the expression of KLF4 is regulated by orphan nuclear receptor retinoic-acid-related orphan receptor α (RORα) in hepatic macrophages (Han et al., 2017). In addition, NOB is known as an RORα activator (He et al., 2016; Nohara et al., 2019). Therefore, we investigated whether RORα is involved in NOB-mediated Klf4 expression and macrophage polarization. First, we found that NOB induced the expression of RORα target genes (*Cyp7b1*, *Glut2*, and *Gck*) in the livers of both NCD and MCD fed mice, implying RORα was activated by NOB *in vivo* (**Figure 7A**). To further explore the underlying mechanism, we expressed luciferase reporters driven by mouse Klf4 promotor in 293T cells. As shown in **Figure 7B**, NOB efficiently induced luciferase activity in cells transfected with wild type but not RORE deleted Klf4 promotor, suggesting the binding of RORα to ROR element in *Klf4* promotor was required to NOB mediated *Klf4* expression. Furthermore, we determined whether NOB promoted the transcriptional activity of endogenous RORα by ChIP-qPCR using RORα specific antibody. As expected, NOB treatment largely enhanced the binding of RORα to *Klf4* promotor in RAW 264.7 cells (**Figure 7C**). Moreover, NOB-induced Klf4 expression in RAW 264.7 cell was significantly inhibited by SR3335, an inverse agonist of RORα (Han et al., 2017; **Figure 7D**). SR3335 also abolished NOB-mediated upregulation of M2 markers (*Il-10* and *Arg-1*) in IL-4 treated RAW 264.7 (**Figure 7E**). Furthermore, the inhibition of M1 markers (*Il-6*, *Il-1*β, and *Tnf-*α) after NOB treatment in LPS challenged

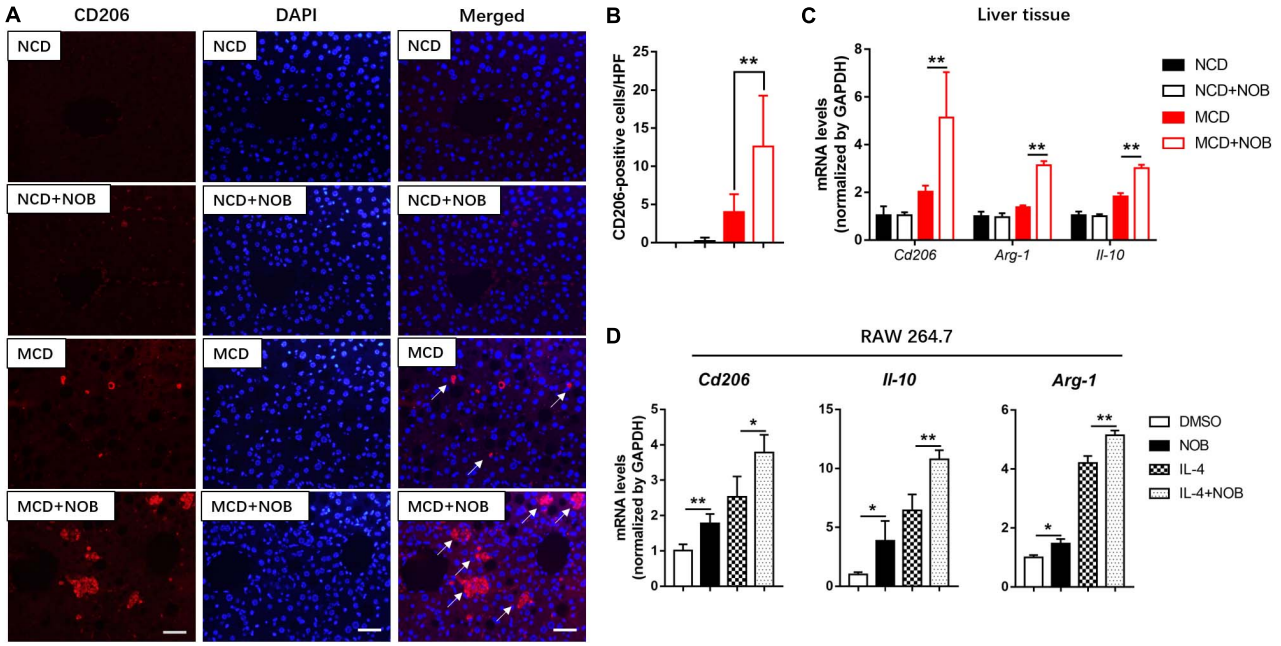

FIGURE 5 | The effect of NOB on M2 macrophage polarization and the expression of anti-inflammatory factors in liver tissue and RAW 264.7 cells. **(A)** Representative fluorescence microscopic images of CD206-stained liver sections. Scale bar = 300 μm. **(B)** Quantification and statistical analysis of CD206-positive cells in liver tissue. We measured the number of CD206-positive membranes from at least five high power fields (HPF, original magnification, 400×). **(C)** The mRNA levels of *Cd206*, *Arg-1,* and *Il-10* in the livers of MCD-induced mice were evaluated using RT-qPCR. Data were expressed as the mean ± SD (n = 5). **(D)** RAW 264.7 cells were pretreated with DMSO, NOB (100 μM), LPS (200 ng/mL), or LPS (200 ng/mL) + NOB (100 μM) for 16 h. The mRNA levels of *Cd206*, *Arg-1,* and *Il-10* were determined by RT-qPCR. Values are expressed as mean ± SD (n = 3). $^*P < 0.05$, $^{**}P < 0.01$.

RAW 264.7 was partially reversed by SR3335 (**Figure 7F**). In general, these results suggest that NOB-mediated macrophage polarization is RORα dependent.

DISCUSSION

In current study, we evaluated the effect of NOB on NASH using MCD-induced mouse model. We observed that NOB administration ameliorated hepatic inflammation, reduced activated hepatic stellate cells and liver fibrosis. Besides, we found M2 type macrophages were significantly increased in the livers of NOB treated NASH mice accompanied by elevated expression of anti-inflammatory cytokine IL-10. Mechanistically, the activation of RORα by NOB was required for the enhanced M2 polarization. Inhibition of RORα activity by small molecular inhibitor abolished the effects of NOB on the induction of *Klf4* and *Il-10* expression in RAW 264.7 cells.

Previous study has shown that activating RORα can promote the M2 polarization of macrophages by up-regulating the expression of *Klf4* (Odegaard et al., 2008). In this study, we found that NOB promoted the M2 alternative activation of RAW 264.7 by activating RORα *in vitro*. Although we could not determine whether it is the case *in vivo* by tracing the fate of individual macrophage, our data still provided some hints. The population of F4/80-positive macrophages in the livers of MCD fed mice was obviously reduced after NOB treatment, even in this case, the macrophages with M2 markers were remarkably increased compared to the control group, suggesting enhanced M2 polarization also occurred *in vivo*.

In the experiments in mouse model of NASH, M1 macrophages with a pro-inflammatory phenotype seem to worsen the disease. Different mouse strains are innately prone to different immune responses after feeding with NASH diet (Mills et al., 2000). M1-prone C57BL/6 mice fed the MCD diet showed an increased tendency toward steatosis and hepatic inflammation compared to the M2 prone BALB/c mice (Maina et al., 2012; Kazankov et al., 2019). In contrast to M1 macrophages, M2 macrophages with an anti-inflammatory phenotype have been associated with ameliorated hepatic injury in NAFLD and improved insulin sensitivity (Odegaard et al., 2008; Wan et al., 2014). Pharmacological alteration of macrophage polarization toward an M2 phenotype could partially reverse hepatic steatosis and hepatocyte apoptosis induced by HFD feeding (Kazankov et al., 2019). Of interest, the conditioned medium from IL-4 induced M2-type macrophages promotes apoptosis of M1-type macrophages *in vitro*. Mechanistically, IL-10 released from M2 macrophages induces high inducible nitric oxide synthase-expressing M1 Kupffer cell (KC) death through paracrine activation of the enzyme arginase (Wan et al., 2014).

In this study, we observed that in mice fed with MCD diet, administration of NOB also reduced MPO positive monocytes. Although the relative number of monocytes is significantly different between NOB treated and the control group, the

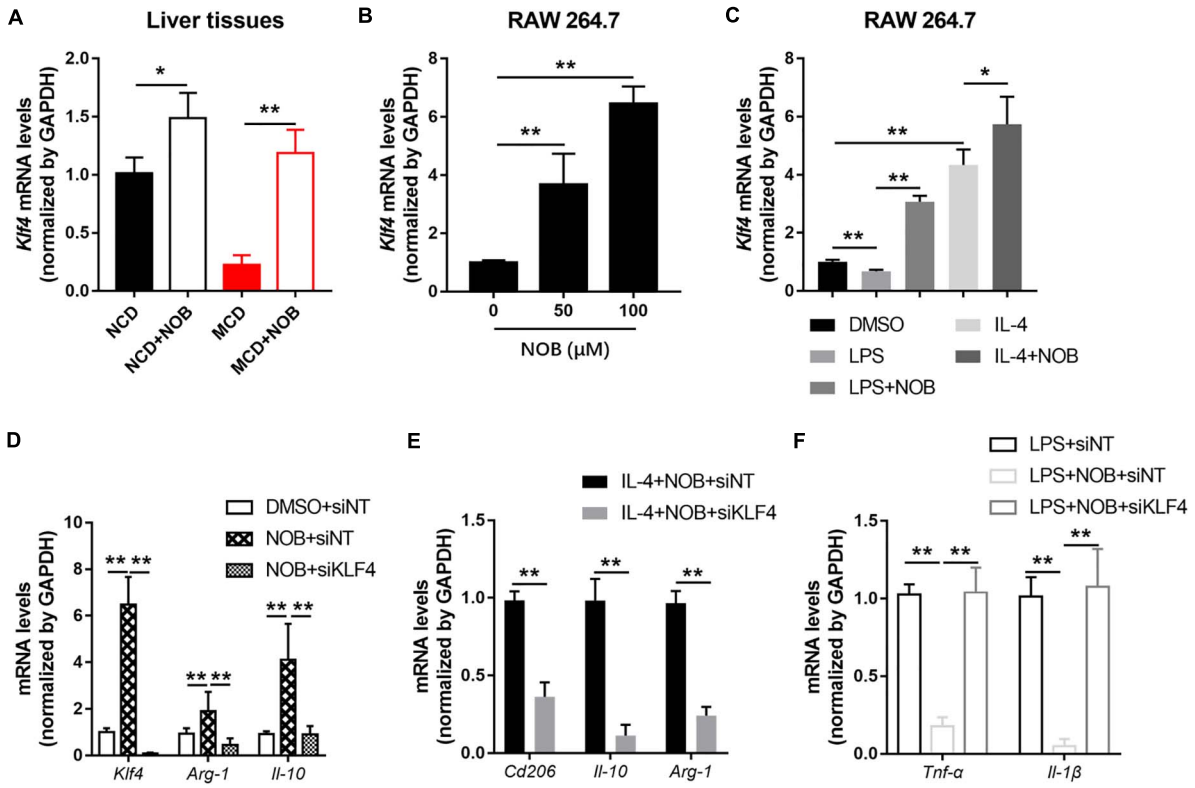

FIGURE 6 | NOB promotes M2 polarization through increasing *Klf4* expression. **(A)** The mRNA expression of *Klf4* in the livers of MCD-fed mice was evaluated by RT-qPCR. Data were expressed as the mean ± SD (n = 5). **(B)** RAW 264.7 cells were treated with DMSO, NOB (50 μM) or NOB (100 μM) for 16 h. The mRNA expression of *Klf4* was determined by RT-qPCR. **(C)** RAW 264.7 cells were pretreated with DMSO, LPS (200 ng/mL), LPS (200 ng/mL) + NOB (100 μM), IL-4 (20 ng/mL), or IL-4 (20 ng/mL) + NOB (100 μM) for 16 h. The mRNA expression of *Klf4* was measured by RT-qPCR. **(D)** RAW 264.7 cells were transiently transfected with control (siNT) or KLF4 (siKLF4) siRNA and treated with either DMSO or NOB for 16 h as indicated. The mRNA levels of *Klf4*, *Arg-1,* and *Il-10* were determined by RT-qPCR. **(E)** The siRNA-NT or siRNA-KLF4 cells were treated with IL-4 (20 ng/mL) + NOB (100 μM) for 16 h. The mRNA levels of *Cd206*, *Arg-1,* and *Il-10* were measured by RT-qPCR. **(F)** The siRNA-NT cells were treated with LPS (2,00 ng/mL) or LPS (200 ng/mL) + NOB (100 μM). The siRNA-KLF4 cells were treated with LPS (200 ng/mL) + NOB (100 μM) for 16 h. The mRNA levels of *Il-1*β and *Tnf-*α were quantified by RT-qPCR. Values are expressed as mean ± SD (n = 3). $^*P < 0.05$, $^{**}P < 0.01$.

absolute number of monocytes even in the control group feeding with MCD diet is far less than that of macrophages. It is supposed that most monocytes are transformed into macrophages in this case. It is well established that in addition to liver-resident Kupffer cells, monocyte derived macrophages have a major role in the pathogenesis of NAFLD and NASH. Whether NOB have different effects on these two types of macrophages derived from different sources is an open question worthy of attention in the follow-up research.

In our previous study, we reported another bioactive flavone hesperetin could inhibits hepatic inflammation via AMPK/CREB/SIRT1 pathway (Wang et al., 2020b). We found hesperetin increased SIRT1 expression through activating AMPK. Besides, AMPK can also elevate SIRT1 activity by enhancing the mitochondrial metabolism and thereafter increasing the abundance of intracellular NAD^+ (Canto et al., 2009). In current study, we observed that NOB effectively activated AMPK like hesperetin (data not shown). It raised a possibility that NOB may ameliorate inflammation in NASH by regulating AMPK or SIRT1 activity in immune cells in liver. To exclude this possibility, we treated LPS induced RAW 264.7 with Compound C (AMPK inhibitor) and EX-527 (SIRT1 inhibitor). In contrast to the re-elevation of inflammatory cytokines by RORα inhibitor SR3335, inhibition of AMPK and SIRT1 didn't abolish the suppressive effect of NOB on the expression of these cytokines (**Supplementary Figure 1**), suggesting NOB induced AMPK activation was not involved in this process.

Among the polyphenols, in addition to NOB, there are other substances that have a regulatory effect on the polarization of macrophage. As a representative polyphenol, resveratrol-treated mice fed alcohol or a high-fat diet displayed preponderant M2 KC polarization, M1 KC apoptosis, and resistance to hepatocyte steatosis and apoptosis, as compared to control mice (Wan et al., 2014). Although the underlying mechanisms involved in NOB and resveratrol induced M2 polarization may be different, our current study combined with the previous study provide new perspectives to the exploration of anti-inflammatory mechanisms of polyphenols, especially in metabolic diseases associated chronic inflammation.

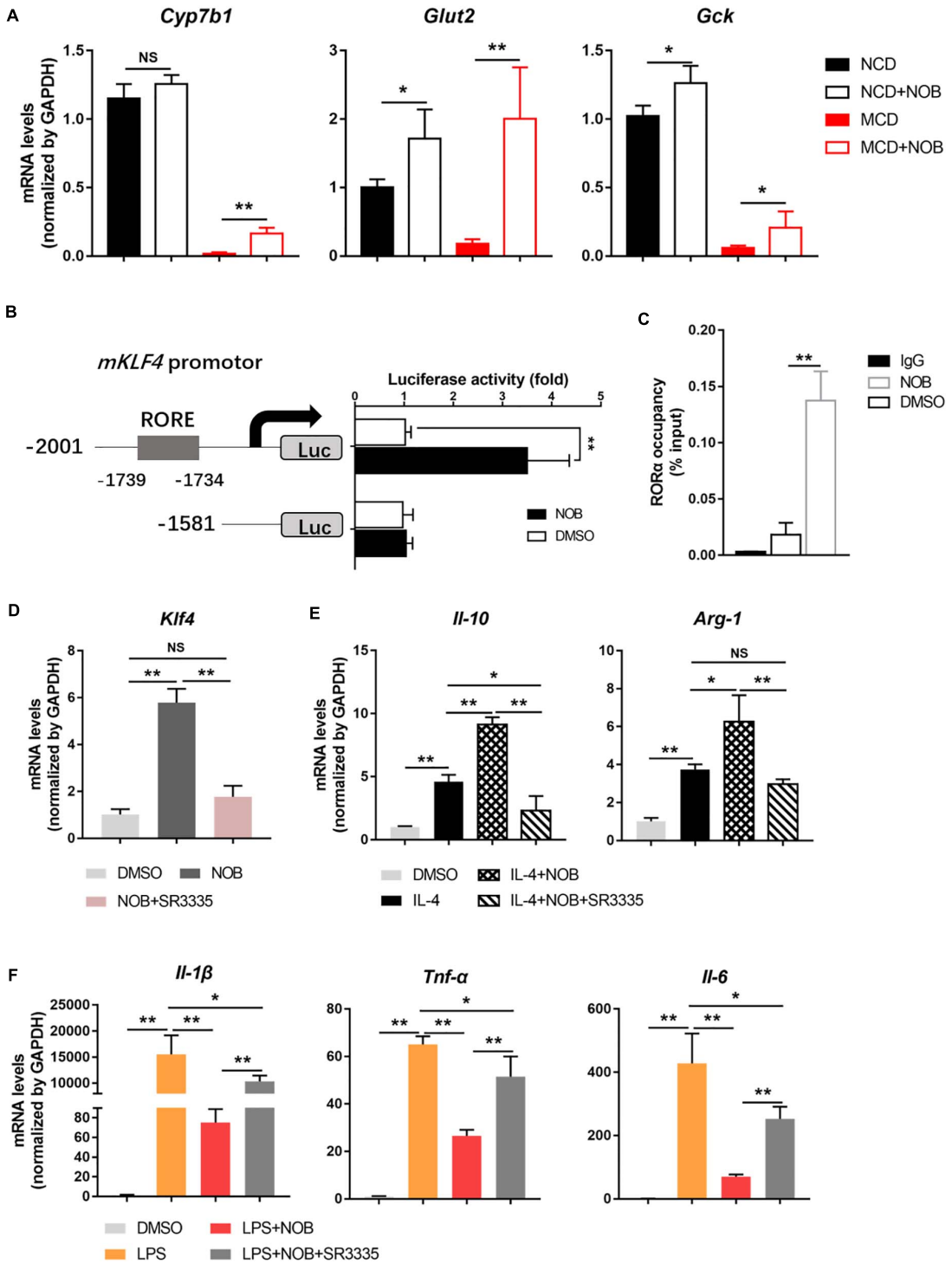

FIGURE 7 | NOB induces *Klf4* expression and macrophage polarization through activiting RORα. **(A)** RT-qPCR analysis of RORα target genes *Cyp7b1*, *Glut2,* and *Gck* in the livers of MCD-fed mice. Data were expressed as the mean ± SD (n = 5). **(B)** Schematic diagram of the mouse Klf4 promoter with the RORα binding element (RORE) shown as gray box. 293T cells were transfected with luciferase reporters driven by Klf4 promoter with or without RORE and treated with DMSO or NOB (100 μM) for 8 h. **(C)** RAW 264.7 cells were treated with DMSO or NOB (100 μM) for 16 h. The binding of RORα to *Klf4* promotor was assessed by ChIP-qPCR. **(D)** RAW 264.7 cells were treated with DMSO, NOB (100 μM) or SR3335 (10 μM) for 16 h. The mRNA level of *Klf4* determined by RT-qPCR. **(E)** RAW 264.7 cells were treated with DMSO, IL-4 (20 ng/mL), IL-4 (20 ng/mL) + NOB (100 μM) or IL-4 (20 ng/mL) + NOB (100 μM) + SR3335 (10 μM) for 16 h. The mRNA levels of *Arg-1* and *Il-10* determined by RT-qPCR. **(F)** RAW 264.7 cells were pretreated with DMSO, LPS (200 ng/mL), LPS (200 ng/mL) + NOB (100 μM) or LPS (200 ng/mL) + NOB (100 μM) + SR3335 (10 μM) for 16 h. Proinflammatory factors *Il-6*, *Il-1*β, and *Tnf-*α determined by RT-qPCR. Values are expressed as mean ± SD (n = 3). *P < 0.05, **P < 0.01.

DATA AVAILABILITY STATEMENT

The original contributions presented in the study are included in the article/**Supplementary Material**, further inquiries can be directed to the corresponding author/s.

ETHICS STATEMENT

The animal study was reviewed and approved by the Ethics Committee of Animal Experiments of Quzhou people's hospital, China.

AUTHOR CONTRIBUTIONS

FZ and SW participated in research design. SW, TL, HS, FZ, ML, LW, HC, and CX conducted experiments. SW, TL, FZ, and HS performed data analysis. FZ and SW wrote or contributed to the writing of the manuscript. All authors contributed to the article and approved the submitted version.

FUNDING

This work was supported by the National Natural Science Foundation of China (81903873), Medical and Health Technology Projects of Zhejiang Province, China (2020PY087 and 2019PY089), the Chinese medicine science foundation of Zhejiang Province, China (2021ZB328), Quzhou technology projects, China (2019K34 and 2018K20), and Natural Science Foundation of Hubei Province (2017CFB767).

ACKNOWLEDGMENTS

We thank Dr. Ping Wu for technical assistance and financial support for this project.

SUPPLEMENTARY MATERIAL

The Supplementary Material for this article can be found online at: https://www.frontiersin.org/articles/10.3389/fphys.2021.687744/full#supplementary-material

REFERENCES

Amrutkar, M., Chursa, U., Kern, M., Nunez-Duran, E., Stahlman, M., Sutt, S., et al. (2016). STK25 is a critical determinant in nonalcoholic steatohepatitis. *Faseb. J.* 30, 3628–3643. doi: 10.1096/fj.201600562r

Bataller, R., and Brenner, D. A. (2005). Liver fibrosis. *J. Clin. Invest.* 115, 209–218.

Browning, J. D., and Horton, J. D. (2004). Molecular mediators of hepatic steatosis and liver injury. *J. Clin. Invest.* 114, 147–152. doi: 10.1172/jci200422422

Canto, C., Gerhart-Hines, Z., Feige, J. N., Lagouge, M., Noriega, L., Milne, J. C., et al. (2009). AMPK regulates energy expenditure by modulating NAD+ metabolism and SIRT1 activity. *Nature* 458, 1056–1060. doi: 10.1038/nature07813

Di Donna, L., Taverna, D., Mazzotti, F., Benabdelkamel, H., Attya, M., Napoli, A., et al. (2013). Comprehensive assay of flavanones in citrus juices and beverages by UHPLC-ESI-MS/MS and derivatization chemistry. *Food Chem.* 141, 2328–2333. doi: 10.1016/j.foodchem.2013.05.034

Feng, S., Zhou, H., Wu, D., Zheng, D., Qu, B., Liu, R., et al. (2020). Nobiletin and its derivatives overcome multidrug resistance (MDR) in cancer: total synthesis and discovery of potent MDR reversal agents. *Acta Pharm. Sin. B* 10, 327–343. doi: 10.1016/j.apsb.2019.07.007

Han, Y. H., Kim, H. J., Kim, E. J., Kim, K. S., Hong, S., Park, H. G., et al. (2014). RORalpha decreases oxidative stress through the induction of SOD2 and GPx1 expression and thereby protects against nonalcoholic steatohepatitis in mice. *Antioxid. Redox Signal.* 21, 2083–2094. doi: 10.1089/ars.2013.5655

Han, Y. H., Kim, H. J., Na, H., Nam, M. W., Kim, J. Y., Kim, J. S., et al. (2017). RORalpha Induces KLF4-mediated M2 polarization in the liver macrophages that protect against nonalcoholic steatohepatitis. *Cell Rep.* 20, 124–135. doi: 10.1016/j.celrep.2017.06.017

Han, Y. H., Shin, K. O., Kim, J. Y., Khadka, D. B., Kim, H. J., Lee, Y. M., et al. (2019). A maresin 1/RORalpha/12-lipoxygenase autoregulatory circuit prevents inflammation and progression of nonalcoholic steatohepatitis. *J. Clin. Invest.* 129, 1684–1698. doi: 10.1172/jci124219

He, B., Nohara, K., Park, N., Park, Y. S., Guillory, B., Zhao, Z., et al. (2016). The small molecule nobiletin targets the molecular oscillator to enhance circadian rhythms and protect against metabolic syndrome. *Cell Metab.* 23, 610–621. doi: 10.1016/j.cmet.2016.03.007

Jetten, A. M. (2009). Retinoid-related orphan receptors (RORs): critical roles in development, immunity, circadian rhythm, and cellular metabolism. *Nucl. Recept. Signal.* 7:e003.

Kazankov, K., Jorgensen, S. M. D., Thomsen, K. L., Moller, H. J., Vilstrup, H., George, J., et al. (2019). The role of macrophages in nonalcoholic fatty liver disease and nonalcoholic steatohepatitis. *Nat. Rev. Gastroenterol. Hepatol.* 16, 145–159.

Klebanoff, S. J. (2005). Myeloperoxidase: friend and foe. *J. Leukoc. Biol.* 77, 598–625. doi: 10.1189/jlb.1204697

Kong, Q., Li, N., Cheng, H., Zhang, X., Cao, X., Qi, T., et al. (2019). HSPA12A is a novel player in nonalcoholic steatohepatitis via promoting nuclear PKM2-mediated M1 macrophage polarization. *Diabetes* 68, 361–376. doi: 10.2337/db18-0035

Liao, X., Sharma, N., Kapadia, F., Zhou, G., Lu, Y., Hong, H., et al. (2011). Kruppel-like factor 4 regulates macrophage polarization. *J. Clin. Invest.* 121, 2736–2749. doi: 10.1093/nar/gkf400

Maina, V., Sutti, S., Locatelli, I., Vidali, M., Mombello, C., Bozzola, C., et al. (2012). Bias in macrophage activation pattern influences non-alcoholic steatohepatitis (NASH) in mice. *Clin. Sci.* 122, 545–553. doi: 10.1042/cs20110366

Mills, C. D., Kincaid, K., Alt, J. M., Heilman, M. J., and Hill, A. M. (2000). M-1/M-2 macrophages and the Th1/Th2 paradigm. *J. Immunol.* 164, 6166–6173. doi: 10.4049/jimmunol.164.12.6166

Morrow, N. M., Burke, A. C., Samsoondar, J. P., Seigel, K. E., Wang, A. D., Telford, E., et al. (2020). The citrus flavonoid nobiletin confers protection from metabolic dysregulation in high-fat-fed mice independent of AMPK. *J. Lipid Res.* 61, 387–402. doi: 10.1194/jlr.ra119000542

Mulvihill, E. E., Assini, J. M., Lee, J. K., Allister, E. M., Sutherland, B. G., Koppes, J. B., et al. (2011). Nobiletin attenuates VLDL overproduction, dyslipidemia, and atherosclerosis in mice with diet-induced insulin resistance. *Diabetes* 60, 1446–1457. doi: 10.2337/db10-0589

Murray, P. J. (2017). Macrophage polarization. *Annu. Rev. Physiol.* 79, 541–566.

Nohara, K., Mallampalli, V., Nemkov, T., Wirianto, M., Yang, J., Ye, Y., et al. (2019). Nobiletin fortifies mitochondrial respiration in skeletal muscle to promote healthy aging against metabolic challenge. *Nat. Commun.* 10:3923.

Odegaard, J. I., Ricardo-Gonzalez, R. R., Red Eagle, A., Vats, D., Morel, C. R., Goforth, M. H., et al. (2008). Alternative M2 activation of kupffer cells by PPARdelta ameliorates obesity-induced insulin resistance. *Cell Metab.* 7, 496–507. doi: 10.1016/j.cmet.2008.04.003

Ou, Z., Shi, X., Gilroy, R. K., Kirisci, L., Romkes, M., Lynch, C., et al. (2013). Regulation of the human hydroxysteroid sulfotransferase (SULT2A1) by RORalpha and RORgamma and its potential relevance to human liver diseases. *Mol. Endocrinol.* 27, 106–115. doi: 10.1210/me.2012-1145

Patel, U., Rajasingh, S., Samanta, S., Cao, T., Dawn, B., and Rajasingh, J. (2017). Macrophage polarization in response to epigenetic modifiers during infection and inflammation. *Drug Discov. Today* 22, 186–193. doi: 10.1016/j.drudis.2016.08.006

Rong, X., Xu, J., Jiang, Y., Li, F., Chen, Y., Dou, Q. P., et al. (2021). Citrus peel flavonoid nobiletin alleviates lipopolysaccharide-induced inflammation by activating IL-6/STAT3/FOXO3a-mediated autophagy. *Food Funct.* 12, 1305–1317. doi: 10.1039/d0fo02141e

Wan, J., Benkdane, M., Teixeira-Clerc, F., Bonnafous, S., Louvet, A., Lafdil, F., et al. (2014). M2 kupffer cells promote M1 Kupffer cell apoptosis: a protective mechanism against alcoholic and nonalcoholic fatty liver disease. *Hepatology* 59, 130–142. doi: 10.1002/hep.26607

Wang, S. W., Bai, Y. F., Weng, Y. Y., Fan, X. Y., Huang, H., Zheng, F., et al. (2019). Cinobufacini ameliorates dextran sulfate sodium-induced colitis in mice through inhibiting M1 macrophage polarization. *J. Pharmacol. Exp. Ther.* 368, 391–400. doi: 10.1124/jpet.118.254516

Wang, S. W., Sheng, H., Bai, Y. F., Weng, Y. Y., Fan, X. Y., Lou, L. J., et al. (2020a). Neohesperidin enhances PGC-1alpha-mediated mitochondrial biogenesis and alleviates hepatic steatosis in high fat diet fed mice. *Nutr. Diabetes* 10:27.

Wang, S. W., Wang, W., Sheng, H., Bai, Y. F., Weng, Y. Y., Fan, X. Y., et al. (2020b). Hesperetin, a SIRT1 activator, inhibits hepatic inflammation via AMPK/CREB pathway. *Int. Immunopharmacol.* 89:107036. doi: 10.1016/j.intimp.2020.107036

Wattacheril, J., Issa, D., and Sanyal, A. (2018). Nonalcoholic Steatohepatitis (NASH) and Hepatic Fibrosis: emerging therapies. *Annu. Rev. Pharmacol. Toxicol.* 58, 649–662. doi: 10.1146/annurev-pharmtox-010617-052545

Xu, F., Guo, M., Huang, W., Feng, L., Zhu, J., Luo, K., et al. (2020). Annexin A5 regulates hepatic macrophage polarization via directly targeting PKM2 and ameliorates NASH. *Redox Biol.* 36:101634. doi: 10.1016/j.redox.2020.101634

Yang, X., Wang, H., Li, T., Chen, L., Zheng, B., and Liu, R. H. (2020). Nobiletin delays aging and enhances stress resistance of caenorhabditis elegans. *Int. J. Mol. Sci.* 21:341. doi: 10.3390/ijms21010341

Conflict of Interest: The authors declare that the research was conducted in the absence of any commercial or financial relationships that could be construed as a potential conflict of interest.

frontiers in Physiology

ORIGINAL RESEARCH
published: 24 May 2021
doi: 10.3389/fphys.2021.679152

Myogenetic Oligodeoxynucleotide (myoDN) Recovers the Differentiation of Skeletal Muscle Myoblasts Deteriorated by Diabetes Mellitus

*Shunichi Nakamura[1], Shinichi Yonekura[2,3], Takeshi Shimosato[1,2,3] and Tomohide Takaya[1,2,3]**

[1] Department of Agriculture, Graduate School of Science and Technology, Shinshu University, Nagano, Japan, [2] Department of Agricultural and Life Sciences, Faculty of Agriculture, Shinshu University, Nagano, Japan, [3] Department of Biomolecular Innovation, Institute for Biomedical Sciences, Shinshu University, Nagano, Japan

Skeletal muscle wasting in patients with diabetes mellitus (DM) is a complication of decreased muscle mass and strength, and is a serious risk factor that may result in mortality. Deteriorated differentiation of muscle precursor cells, called myoblasts, in DM patients is considered to be one of the causes of muscle wasting. We recently developed myogenetic oligodeoxynucleotides (myoDNs), which are 18-base single-strand DNAs that promote myoblast differentiation by targeting nucleolin. Herein, we report the applicability of a myoDN, iSN04, to myoblasts isolated from patients with type 1 and type 2 DM. Myogenesis of DM myoblasts was exacerbated concordantly with a delayed shift of myogenic transcription and induction of interleukins. Analogous phenotypes were reproduced in healthy myoblasts cultured with excessive glucose or palmitic acid, mimicking hyperglycemia or hyperlipidemia. iSN04 treatment recovered the deteriorated differentiation of plural DM myoblasts by downregulating myostatin and interleukin-8 (IL-8). iSN04 also ameliorated the impaired myogenic differentiation induced by glucose or palmitic acid. These results demonstrate that myoDNs can directly facilitate myoblast differentiation in DM patients, making them novel candidates for nucleic acid drugs to treat muscle wasting in patients with DM.

Keywords: myogenetic oligodeoxynucleotide, skeletal muscle, myoblast, myogenic differentiation, diabetes mellitus

OPEN ACCESS

Edited by:
Xinran Ma,
East China Normal University, China

Reviewed by:
Alexander E. Berezin,
Zaporizhzhia State Medical University, Ukraine
Ayman A. Mohamed,
University of Illinois at Urbana-Champaign, United States

***Correspondence:**
Tomohide Takaya
ttakaya@shinshu-u.ac.jp

Specialty section:
This article was submitted to Clinical and Translational Physiology, a section of the journal Frontiers in Physiology

Received: *11 March 2021*
Accepted: *03 May 2021*
Published: *24 May 2021*

Citation:
Nakamura S, Yonekura S, Shimosato T and Takaya T (2021) Myogenetic Oligodeoxynucleotide (myoDN) Recovers the Differentiation of Skeletal Muscle Myoblasts Deteriorated by Diabetes Mellitus. Front. Physiol. 12:679152. doi: 10.3389/fphys.2021.679152

INTRODUCTION

The skeletal muscle is the largest organ (30–40% of total body weight) in human (Janssen et al., 2000), the primary thermogenic tissue producing heat by muscular contraction (Rowland et al., 2015), the main energy storage holding 500 g of glycogen (Jensen et al., 2011), and carries 80% of insulin-responsive glucose uptake (Periasamy et al., 2017). Therefore, a decrease in skeletal muscle mass disturbs systemic homeostasis and increases mortality in chronic diseases. Skeletal muscle wasting is present in around 30% of patients with heart failure and is associated with poor prognosis, probably

in part, by increased inflammation and oxidative stress (Bielecka-Dabrowa et al., 2020). Loss of skeletal muscle mass is present in up to 50% of cancer patients and is a predictor for lower survival during chemotherapy as it increases treatment toxicity (Gibson et al., 2015). Low skeletal muscle mass is also observed in patients with diabetes mellitus (DM). Protein synthesis in skeletal muscle is decreased by type 1 DM (T1DM) due to loss of insulin signaling, and protein degradation is enhanced with myostatin-mediated autophagy in type 2 DM (T2DM) (Sala and Zorzano, 2015). Particularly, an age-adjusted study reported that muscle wasting is an independent risk for all-cause mortality in patients with T2DM (Miyake et al., 2019). Prevention of DM-associated muscle loss is an important subject but there is no efficacious drugs, because it is still a complicated pathology and underlying mechanism has not been fully understood.

The skeletal muscle is composed of a large number of myofibers, which are multinuclear fused myocytes. Each myofiber has dozens of stem cells, termed satellite cells, between the basal lamina and plasma membrane of the fibers. During myogenesis, satellite cells are activated to myogenic precursor cells, called myoblasts. Following this, myoblasts differentiate into mononuclear myocytes expressing myosin heavy chain (MHC), and mutually fused to form multinuclear myotubes (Dumont et al., 2015). Importantly, the satellite cell- and myoblast-driven myogenesis is impaired by DM, which is considered a predisposing factor for skeletal muscle loss. Both T1DM and T2DM deteriorate the functions of satellite cells and myoblasts owing to oxidative stress, chronic inflammation, extracellular matrix defects, and transcriptional disorders (D'Souza et al., 2013; Teng and Huang, 2019). In patients with T1DM, the number of satellite cells decreases with the upregulation of the Notch ligand DLL1 (D'Souza et al., 2016). Myoblasts isolated from patients with T2DM show impaired myogenic differentiation with lower miR-23b/27b levels (Henriksen et al., 2017) and autophagy dysregulation (Henriksen et al., 2019). Even after differentiation, myotubes derived from T2DM-patient myoblasts retain an altered myokine secretion distinct from that of non-diabetic myotubes (Ciaraldi et al., 2016). Although the mechanisms underlying the deteriorated function of myoblasts in DM have not been fully elucidated, several factors have been reported to inhibit myogenic differentiation. Co-culture with adipocytes increases interleukin (IL)-6 expression in myoblasts and attenuates their differentiation into myotubes (Seo et al., 2019). High ambient glucose suppresses the myogenesis of myoblasts by increasing the repressive myokine, myostatin, and decreasing myogenic transcription factors, MyoD and myogenin (Grzelkowska-Kowalczyk et al., 2013). Palmitic acid, a saturated fatty acid, blocks myotube formation by downregulating MyoD and myogenin (Saini et al., 2017). These findings demonstrate that diabetic factors including adipokines, glucose, and fatty acids are inhibitory factors for myoblast differentiation.

We recently identified myogenetic oligodeoxynucleotides (myoDNs), which are 18-base single-strand nucleotides that promote myoblast differentiation (Nihashi et al., 2020; Shinji et al., 2021). One of the myoDNs, iSN04, is directly incorporated into myoblasts and serves as an aptamer that physically interacts with nucleolin (Shinji et al., 2021). Nucleolin has been known to target the untranslated region of p53 mRNA to interfere with its translation (Takagi et al., 2005; Chen et al., 2012). In myoblasts, iSN04 antagonizes nucleolin, rescues p53 protein levels, and eventually facilitates myotube formation (Shinji et al., 2021). In this study, we aimed to determine that iSN04 recovers the deteriorated differentiation of myoblasts isolated from patients with DM. This study presents iSN04 as a potential nucleic acid drug targeting myoblasts for the prevention and therapy of muscle wasting in patients with DM.

MATERIALS AND METHODS

Chemicals

All phosphodiester bonds of iSN04 (5′-AGA TTA GGG TGA GGG TGA-3′) were phosphorothioated to increase resistance to nucleases. Phosphorothioated iSN04 was synthesized and HPLC-purified (GeneDesign, Osaka, Japan), then was dissolved in endotoxin-free water as previously reported (Shinji et al., 2021). Palmitic acid (Wako, Osaka, Japan), which is the most abundant (occupying 20–30%) saturated fatty acid in human (Gesteiro et al., 2019), was dissolved in chloroform to prepare a high concentration stock (600 mM) to decrease treatment volume to myoblasts (Aguer et al., 2010). An equal volume of endotoxin-free water or chloroform, without the test chemicals, served as negative controls.

Cell Culture

We purchased and used commercially available human myoblast (hMB) stocks (Lonza, Walkersville, MD, United States) isolated from healthy subjects (CC-2580) including a 26-year-old male (H26M; lot 18TL211617, August 2018), a 35-year-old female (H35F; lot 0000483427, June 2015), and a 35-year-old male (H35M; lot 0000650386, August 2017), from patients with T1DM (CC-2900) including an 81-year-old male (I81M; lot 0000211092, November 2010) and an 89-year-old female (I89F; lot 0000191810, August 2010), and from patients with T2DM (CC-2901) including a 68-year-old male (II68M; lot 0000211384, November 2010) and an 85-year-old female (II85F; lot 0000219206, January 2011). Detailed information of each hMB is described in certificate of analysis[1]. The hMBs were maintained in Skeletal Muscle Growth Media-2 (CC-3245; Lonza) as a growth medium for hMBs (hMB-GM). The murine myoblast cell line C2C12 (DS Pharma Biomedical, Osaka, Japan) was maintained in a growth medium for C2C12 cells (C2-GM) consisting of DMEM (Nacalai, Osaka, Japan) with 10% fetal bovine serum and a mixture of 100 units/ml penicillin and 100 μg/ml streptomycin (PS) (Nacalai). hMBs and C2C12 cells were differentiated in a differentiation induction medium (DIM) consisting of DMEM with 2% horse serum (HyClone; GE Healthcare, Salt Lake City, UT, United States) and PS (Nihashi et al., 2019b; Shinji et al., 2021).

hMB-GM, C2-GM, and DIM with 5.6 mM D-glucose and 19.4 mM mannitol (hMB-GM-NG, C2-GM-NG, and DIM-NG)

[1]https://bioscience.lonza.com/lonza_bs/CH/en/coa/search

were used for normal-glucose culture, and those with 25 mM D-glucose (hMB-GM-HG, C2-GM-HG, and DIM-HG) were used for high-glucose culture as previously described (La Sala et al., 2015). In the experiments using high-glucose culture, hMBs were maintained in hMB-GM-HG for a total of 6 days with passage every 3 days. The cells were then seeded on fresh dishes and differentiated in DIM-HG for 2 days. C2C12 cells were maintained in C2-GM-HG for a total of 4 days with passage every 2 days. The cells were then seeded on fresh dishes and differentiated in DIM-HG for 4 days. In the palmitic acid experiments, hMBs were maintained in hMB-GM-NG; then, the cells were seeded on fresh dishes and differentiated in DIM-NG with palmitic acid at an optimal concentration of 200 μM (for H26M) or 600 μM (for H35M) for 2 days, according to a previous study (Aguer et al., 2010).

All cells were cultured in dishes or plates coated with collagen type I-C (Cellmatrix; Nitta Gelatin, Osaka, Japan) at 37°C with 5% CO_2 throughout the experiments.

Immunocytochemistry

hMBs in hMB-GM ($1.5–2.5 \times 10^5$ cells/dish optimized for 70% confluency in each cell stock) or C2C12 cells in C2-GM (10×10^5 cells/dish) were seeded on 30-mm dishes. The following day, the medium was replaced with DIM containing iSN04 at an optimal concentration of 1 μM (for H26M in hMB-DIM), 3 μM (C2C12 cells), 10 μM (for H26M in GM, H35M, and II85M), or 30 μM (for H35F, I81M, I89F, and II68M). Optimal iSN04 concentration for each MB was defined as indicating the highest ratio of MHC^+ cells without affecting cell number because the sensitivities to iSN04 differ among MBs. Immunocytochemistry of myoblasts was performed as previously described (Takaya et al., 2017; Nihashi et al., 2019a; Shinji et al., 2021). The myoblasts were fixed with 2% paraformaldehyde, permeabilized with 0.2% Triton X-100, and immunostained with 0.5 μg/ml mouse monoclonal anti-MHC antibody (MF20; R&D Systems, Minneapolis, MN, United States) and 1.0 μg/ml rabbit polyclonal anti-nucleolin antibody (ab22758; Abcam, Cambridge, United Kingdom). 0.1 μg/ml each of Alexa Fluor 488-conjugated donkey polyclonal anti-mouse IgG antibody and Alexa Fluor 594-conjugated donkey polyclonal anti-rabbit IgG antibody (Jackson ImmunoResearch, West Grove, PA, United States) were used as secondary antibodies. Cell nuclei were stained with DAPI (Nacalai). Fluorescent images were captured using EVOS FL Auto microscope (AMAFD1000; Thermo Fisher Scientific, Waltham, MA, United States). The ratio of MHC^+ cells was defined as the number of nuclei in the MHC^+ cells divided by the total number of nuclei, and the fusion index was defined as the number of nuclei in the multinuclear MHC^+ myotubes divided by the total number of nuclei; these were determined using ImageJ software (National Institutes of Health, United States).

Quantitative Real-Time RT-PCR (qPCR)

Total RNA of the myoblasts was isolated using NucleoSpin RNA Plus (Macherey-Nagel, Düren, Germany) and reverse transcribed using ReverTra Ace qPCR RT Master Mix (TOYOBO, Osaka, Japan). qPCR was performed using GoTaq qPCR Master Mix (Promega, Madison, WI, United States) with StepOne Real-Time PCR System (Thermo Fisher Scientific). The amount of each transcript was normalized to that of human glyceraldehyde 3-phosphate dehydrogenase gene (*GAPDH*) and murine 18S ribosomal RNA (*Rn18s*). Results are presented as fold-change. The primer sequences are described in **Supplementary Tables 1**, **2**.

Statistical Analyses

Results are presented as the mean ± standard error. Statistical comparisons were performed using unpaired two-tailed Student's *t*-test or multiple comparison test with Tukey–Kramer test following one-way analysis of variance. Statistical significance was set at $p < 0.05$.

RESULTS

DM Deteriorates Myoblast Differentiation

The hMBs isolated from healthy subjects (H26M, H35F, and H35M), patients with T1DM (I81M and I89F), and patients with T2DM (II68M and II85F) were cultured in the hMB-GM-NG (**Supplementary Figure 1**). These hMBs varied in cell size and morphology, but DM-dependent hallmarks were not observed. The hMBs induced myogenic differentiation in DIM-NG, followed by immunostaining for MHC, a terminal differentiation marker of muscle cells. The ratio of MHC^+ cells and multinuclear myotubes was quantified on days 0, 2, and 4 of differentiation (**Supplementary Figure 2**). On day 2 (**Figure 1**), the ratio of MHC^+ cells of H35M was lower than that of H26M and H35F, indicating the individuality of myogenesis among healthy subjects. I81M differentiated to the same extent as H26M and H35F, but I89F, II68M, and II85F exhibited deteriorated differentiation. In particular, I89F and II85F were exacerbated in myotube formation compared to all healthy subjects. These results indicate that myoblast differentiation is aggravated in patients with DM.

Gene expression patterns in hMBs were examined using qPCR (**Figure 2A**). Among undifferentiated myoblast markers, *PAX7* was expressed 2–3 times higher in T2DM myoblasts throughout differentiation, but *PAX3* and *MYF5* were not. A myogenic transcription factor, *MYOD1*, was highly induced in T1DM myoblasts, but a terminal transcription factor, myogenin (*MYOG*), was not. The mRNA levels of embryonic MHC (*MYH3*) were not significantly different among hMBs. The transcription levels of these genes frequently vary among patients, which reflects individual differences. During myogenic differentiation, the ratios of Pax7, MyoD, and myogenin are critically important. Proliferating myoblasts express both Pax7 and MyoD, but not myogenin. At the initial stage of differentiation, Pax7 disappears, and MyoD drives myogenin transcription. In terminally differentiated myocytes, MyoD decreases, and myogenin becomes a dominant transcription factor (Dumont et al., 2015). qPCR data indicated that *MYOD1*/*PAX7* and *MYOG*/*MYOD1* ratios

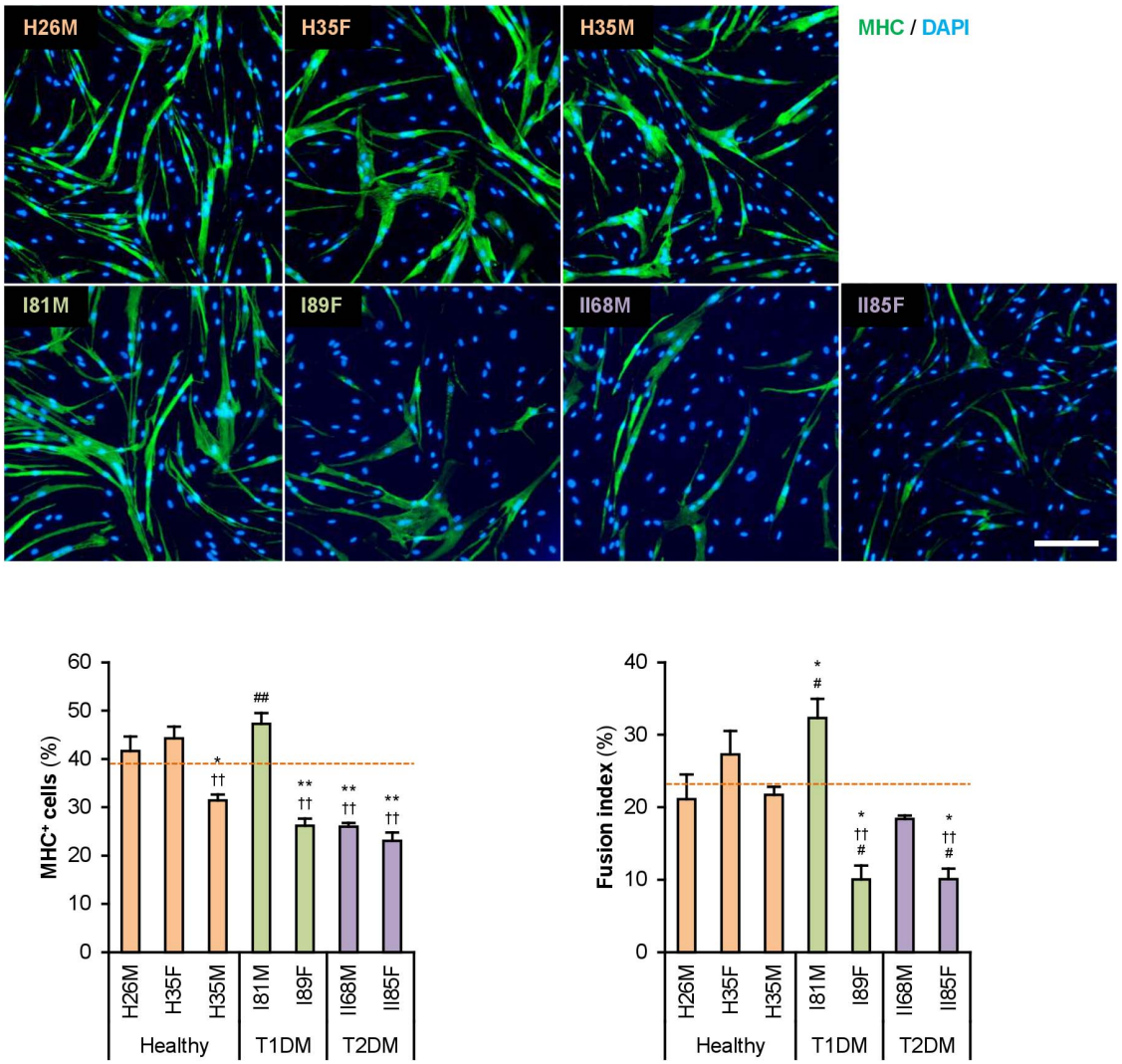

FIGURE 1 | Attenuated myogenic differentiation of DM myoblasts. Representative immunofluorescent images of the hMBs differentiated in DIM-NG for 2 days. Scale bar, 200 μm. Ratio of MHC$^+$ cells and multinuclear myotubes were quantified. Orange dashed lines indicate the mean values of H26M, H35F, and H35M. $^*p < 0.05$, $^{**}p < 0.01$ vs. H26M; $^{\dagger\dagger}p < 0.01$ vs. H35F; $^{\#}p < 0.05$, $^{\#\#}p < 0.01$ vs. H35M (Tukey–Kramer test); $n = 6$.

were lower in T2DM and T1DM myoblasts than those in healthy myoblasts (**Figure 2B**), demonstrating a delayed shift of myogenic transcription factors in DM patients. This may be one of the reasons for the deteriorated differentiation of DM myoblasts.

ILs Are Induced in T2DM Myoblasts

The mRNA levels of atrogin-1 (*FBXO32*), MuRF-1 (*TRIM63*), myostatin (*MSTN*), and myostatin receptor (*ACVR2B*), which are involved in ubiquitin-proteasome-mediated muscle atrophy (Bodine et al., 2001; Lokireddy et al., 2011), were not different among the hMBs. In contrast, transcription of the myostatin antagonist, follistatin (*FST*), was flat in T1DM myoblasts during differentiation (**Supplementary Figure 3**).

Sterol regulatory element-binding proteins (*SREBF1* and *SREBF2*), fatty acid synthase (*FASN*), insulin receptor substrates (*IRS1* and *IRS2*), glucose transporter 4 (*SLC2A4*), mitochondrial carnitine palmitoyltransferase 2 (*CPT2*), and thioredoxin interacting protein (*TXNIP*) are insulin resistance-related factors and involved in differentiation and fatty acid metabolism of muscle cells (Parikh et al., 2007; Kato et al., 2008; Lecomte et al., 2010; Boufroura et al., 2018). However, their mRNA levels were not significantly altered in T2DM myoblasts (**Supplementary Figure 4**).

Type 2 DM myoblasts have been reported to display abnormal inflammatory responses (Green et al., 2011). Indeed, mRNA levels of *IL1B* were 6–7 times higher in T2DM myoblasts than those in healthy myoblasts on days 2 and 4 (**Figure 2C**). In contrast, inflammatory factors, NF-κB p50 (*NFKB1*) and p65 (*RELA*) subunits, TNF-α (*TNF*), interferon γ (*IFNG*), and *IL6* were not upregulated in T2DM myoblasts. Although *IL8* (*CXCL8*) levels were high in H26M on day 0, T2DM

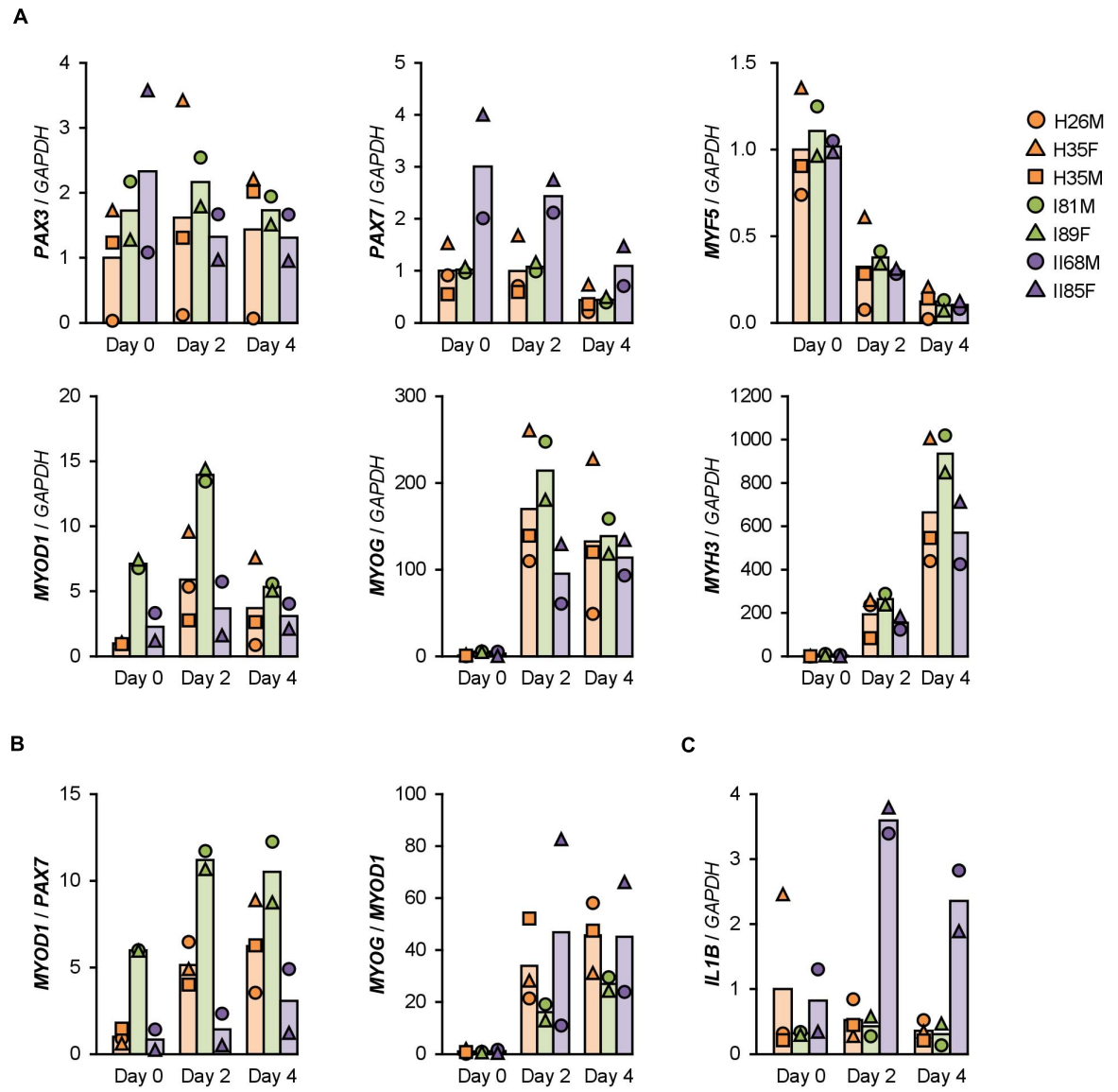

FIGURE 2 | Gene expression patterns altered in DM myoblasts. **(A–C)** qPCR results of gene expression in the hMBs differentiated in DIM-NG on days 0, 2, and 4. Bars indicate mean values of each group. The mean value of healthy myoblasts on day 0 was set to 1.0 for each gene.

myoblasts exhibited higher *IL8* mRNA levels than those did healthy myoblasts (**Supplementary Figure 5**). It has been reported that IL-1β inhibits insulin-like growth factor (IGF)-dependent myoblast differentiation (Broussard et al., 2004), and interleukin-8 (IL-8) is secreted from insulin-resistant myotubes (Bouzakri et al., 2011). Thus, the upregulation of IL-1β and IL-8 potentially impaired the shift in myogenic transcription factors and subsequent differentiation of T2DM myoblasts.

myoDN Recovers Differentiation of DM Myoblasts

We recently identified the single-strand myogenetic oligodeoxynucleotides (myoDNs) that promote myoblast differentiation by antagonizing nucleolin (Shinji et al., 2021). To assess the applicability of myoDN to DM myoblasts, the hMBs used in this study were treated with iSN04, which exhibits the highest myogenetic activity among the myoDNs. iSN04 significantly facilitated the differentiation and myotube formation of H35F, H35M, I81M, I89F, and II85F (**Figure 3**). In particular, iSN04 recovered the attenuated differentiation of II85F to almost the same extent as that of healthy myoblasts. iSN04 did not affect the differentiation of H26M in DIM, but significantly promoted myotube formation in hMB-GM (**Supplementary Figure 6**). In contrast, differentiation of II68M was not altered by iSN04, suggesting the distinct sensitivity or efficacy of iSN04 among individuals. These results indicate that iSN04 is able to recover the deteriorated differentiation of DM

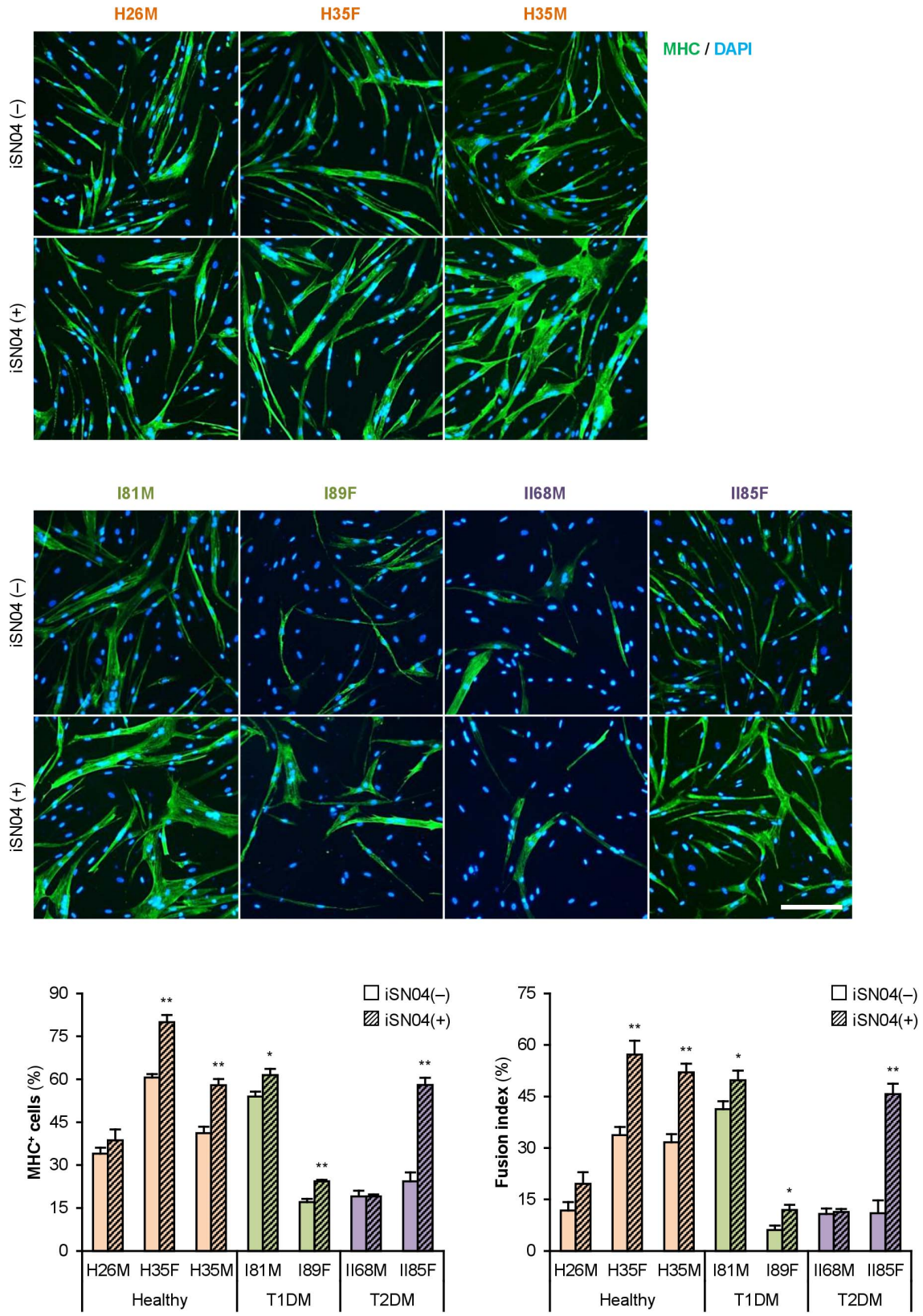

FIGURE 3 | iSN04 recovers the differentiation of DM myoblasts. Representative immunofluorescent images of the hMBs differentiated in DIM-NG with iSN04 for 2 days. Scale bar, 200 μm. Ratio of MHC^+ cells and multinuclear myotubes were quantified. $^*p < 0.05$, $^{**}p < 0.01$ vs. iSN04(–) in each group (Student's *t*-test); $n = 4–6$.

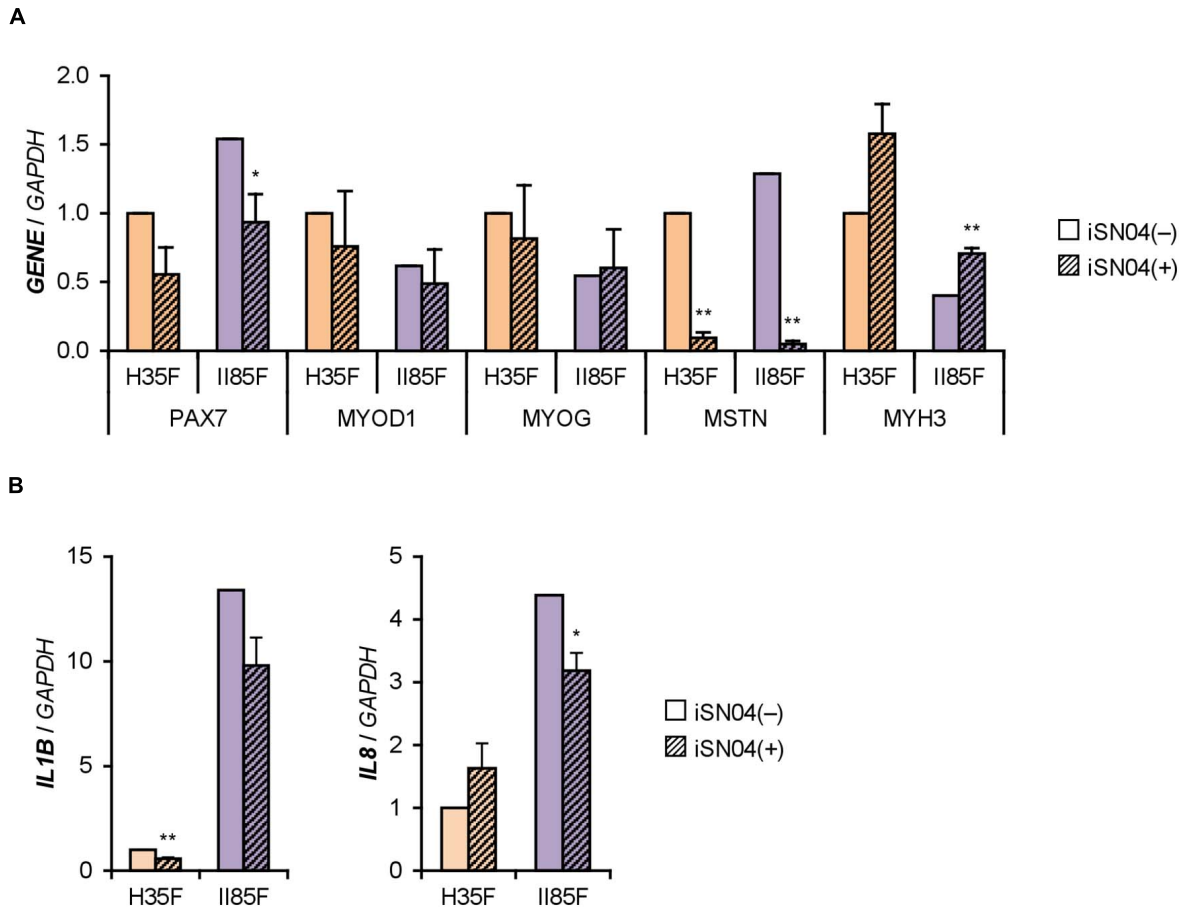

FIGURE 4 | iSN04 suppresses myostatin expression. **(A,B)** qPCR results of gene expression in the H35F and II85F myoblasts differentiated in DIM-NG with iSN04 for 2 days. Mean value of H35F-iSN04(–) group was set to 1.0 for each gene. $^{*}p < 0.05$, $^{**}p < 0.01$ vs. iSN04(–) in each myoblast (Student's *t*-test); $n = 3$.

myoblasts. qPCR revealed that iSN04 treatment significantly reduced *PAX7* and *MSTN* mRNA levels in II85F, resulting in the recovery transcription of *MYH3* (**Figure 4A**). An iSN04-dependent decrease in *MSTN* expression was also detected in H35F. Furthermore, iSN04 significantly suppressed the *IL1B* levels in H35F and the *IL8* levels induced in II85F (**Figure 4B**). These results indicate that iSN04 facilitates the differentiation in both healthy and diabetic myoblasts, in part, by modulating the expression of cytokines including myostatin and ILs.

myoDN Recovers the Myoblast Differentiation Impaired by Excessive Glucose

The DM myoblasts used in this study were isolated from elderly patients (68, 81, 85, and 89-year-old) whose ages were significantly higher than those of the healthy subjects (26, 35, and 35-year-old) ($p < 0.01$; Student's *t*-test). Aging is a factor that compromises myoblast function (Fukada, 2018; McCormick and Vasilaki, 2018). Aged myoblasts are impaired to differentiate into myogenic lineage and induced to fibrogenic lineage due to the activated canonical Wnt signaling pathway (Brack et al., 2007). Therefore, aging possibly affected the deteriorated differentiation of the DM myoblasts used in this study. To investigate the impact of DM without aging on myogenesis, we cultured and differentiated C2C12 myoblast cell line in a high glucose concentration mimicking hyperglycemia. C2C12 cells maintained in high-glucose media exhibited a decreased ratio of MHC^{+} cells and myotubes (**Figure 5A**). qPCR revealed that high-glucose culture significantly induced *Mstn* and suppressed *Myog* and *Myh3* expression in C2C12 cells on differentiation day 1 (**Figure 5B**). It is noteworthy that *Il1b* mRNA levels were not elevated by excessive glucose. High-glucose culture also significantly abrogated the myogenesis of H26M and H35F (**Figure 5A**). These data demonstrated that excessive glucose is one of the age-independent factors for the deterioration of myoblast differentiation.

Importantly, iSN04 treatment significantly recovered myogenic differentiation and myotube formation in C2C12 cells exposed to high glucose concentrations (**Figure 6**). This result corresponds well with the phenotype of the iSN04-treated T2DM myoblasts, indicating that myoDNs are potential candidates for nucleic acid drugs that activate myoblasts in hyperglycemic patients.

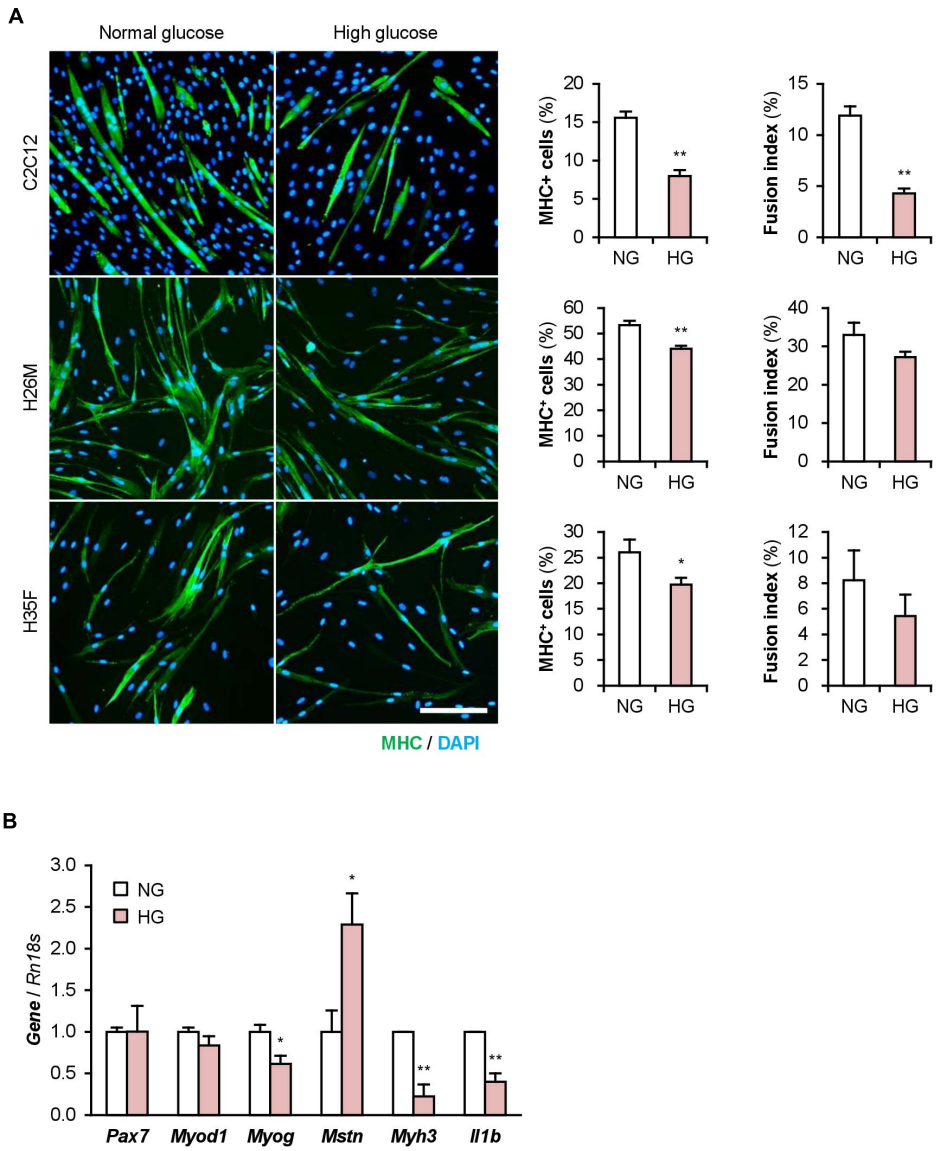

FIGURE 5 | High glucose concentration deteriorates myoblast differentiation. **(A)** Representative immunofluorescent images of the C2C12, H26M, and H35F myoblasts differentiated in DIM-NG or -HG. Scale bar, 200 μm. Ratio of MHC$^+$ cells and multinuclear myotubes were quantified. *$p < 0.05$, **$p < 0.01$ vs. NG (Student's *t*-test); $n = 4$–6. **(B)** qPCR results of myogenic gene expression in the C2C12 cells differentiated in DIM for 1 day. Mean value of NG group was set to 1.0 for each gene. *$p < 0.05$, **$p < 0.01$ vs. NG (Student's *t*-test); $n = 3$.

myoDN Recovers the Myoblast Differentiation Impaired by Palmitic Acid

Patients with T2DM are frequently present with hyperlipidemia. Palmitic acid is the most abundant intravital fatty acid, which is involved in insulin resistance and C2C12 cell differentiation (Yang et al., 2013; Saini et al., 2017). To examine the impact of excessive fatty acids on hMBs, H26M and H35M were induced to differentiate in DIM-NG with palmitic acid. In both hMBs, palmitic acid significantly impaired myogenic differentiation and myotube formation (**Figure 7A**). qPCR showed that palmitic acid decreased the *MYOG*/*MYOD1* ratio, resulting in lower *MYH3* expression in H35M (**Figure 7B**). Palmitic acid also upregulated *IL1B* and *IL8* mRNA levels without altering *NFKB1*, *RELA*, and *TNF* (**Figure 7C**), which recapitulated the phenotype of T2DM myoblasts. These results indicate that excessive fatty acids is another age-independent factor to inhibit myoblast differentiation by inducing inflammatory cytokines.

iSN04 treatment significantly improved the differentiation into MHC$^+$ cells from palmitic acid-treated H35M (**Figure 8A**). As shown in **Figure 8B**, iSN04 induced *MYOD1* and *MYOG* expression under basal conditions, but not in the presence of palmitic acid. In contrast, iSN04 significantly reduced *MSTN* mRNA levels regardless of the presence of palmitic

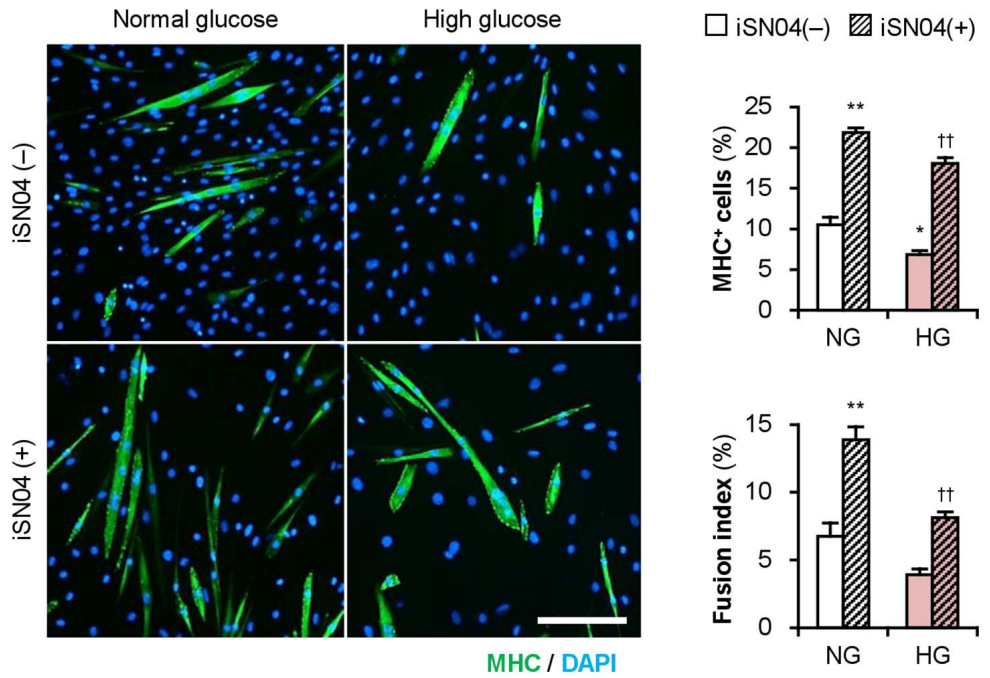

FIGURE 6 | iSN04 recovers the myoblast differentiation impaired by excessive glucose. Representative immunofluorescent images of the C2C12 cells differentiated in DIM with iSN04 for 4 days. Scale bar, 200 μm. Ratio of MHC$^+$ cells and multinuclear myotubes were quantified. $^*p < 0.05$, $^{**}p < 0.01$ vs. NG-iSN04(–); $^{††}p < 0.01$ vs. HG-iSN04(–) (Tukey–Kramer test); $n = 4$.

acid. iSN04 further suppressed palmitic acid-induced *IL8* transcription. These results show that myoDNs conceivably recover myoblast differentiation attenuated by excessive fatty acids in hyperlipidemic patients.

DISCUSSION

This study provides evidence that the myoDN, iSN04, ameliorates the differentiation of DM myoblasts, and presents a novel therapeutic strategy for muscle wasting in patients with DM. Dysfunction of DM myoblasts is caused by various pathophysiological factors such as inflammation and transcriptional disorders (D'Souza et al., 2013; Teng and Huang, 2019), and impaired myogenesis can be one of the reasons for muscle atrophy. A decreased number of satellite cells has been reported in patients with T1DM (D'Souza et al., 2016). Our results further showed the impaired myogenic ability of T1DM myoblasts with a delayed shift to myogenin-dominant transcription. A similar attenuation of myogenesis has been reported in T2DM myoblasts (Henriksen et al., 2017, 2019). The T2DM myoblasts used in this study exhibited a diminished ratio of MyoD/Pax7 and elevated levels of IL-1β and IL-8, which may contribute to the incompetent differentiation. As many patients with T2DM are accompanied by hyperlipidemia in addition to hyperglycemia, surplus glucose and fatty acids are considered the major molecules that interfere with myoblast differentiation. In this study, excessive glucose upregulated myostatin and downregulated myogenin and MHC in C2C12 cells, which is consistent with that reported in previous studies (Grzelkowska-Kowalczyk et al., 2013; Jeong et al., 2013). Similarly, high-glucose culture inhibited myogenesis of plural healthy hMBs. This demonstrates that glucose is an independent factor for myoblast dysfunction, which modulates myogenic gene expression. However, high-glucose culture did not induce IL-1β. Palmitic acid inhibits myokine expression and C2C12 cell differentiation (Yang et al., 2013; Saini et al., 2017). We showed that palmitic acid abrogates the differentiation of healthy hMBs by upregulating IL-1β and IL-8. IL-1β is known to inhibit IGF-induced myogenin expression and myogenesis (Broussard et al., 2004). IL-8 is a chemokine that contributes to insulin resistance in patients with T2DM (Kim et al., 2006; Samaras et al., 2010) and is also a myokine released from skeletal muscle cells. Insulin-resistant human myotubes secrete higher levels of IL-8 (Bouzakri et al., 2011). The role of IL-8 in myoblast differentiation remains controversial. IL-8-neutralizing antibody impairs the differentiation of hMBs (Polesskaya et al., 2016). In contrast, IL-8 treatment decreases the myogenin/MyoD ratio and embryonic MHC expression in rat myoblasts (Milewska et al., 2019). An appropriate level of IL-8 is important for normal myogenesis. Perturbation of IL-8 in T2DM and palmitic acid-cultured myoblasts may be linked to deteriorated differentiation. The mechanism of IL induction in myoblasts remains unclear. NF-κB p65 and TNF-α have been reported to be elevated in T2DM myoblasts (Green et al., 2011). However, in this study, mRNA levels of these genes were not altered by T2DM or palmitic acid. The signaling pathway of fatty acid-dependent IL induction needs to be clarified in further studies.

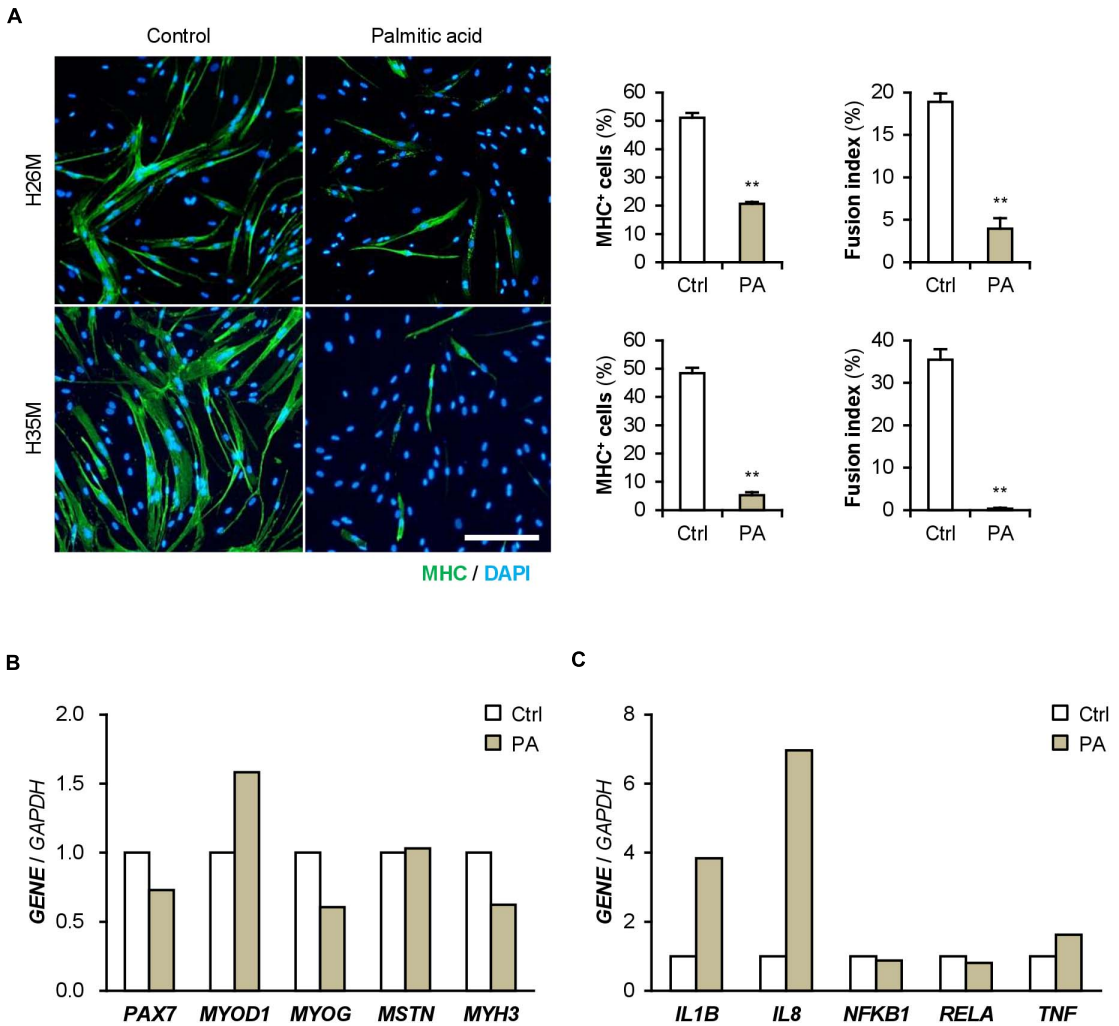

FIGURE 7 | Palmitic acid (PA) deteriorates myoblast differentiation. **(A)** Representative immunofluorescent images of the H26M and H35F myoblasts differentiated in DIM-NG with PA for 2 days. Scale bar, 200 μm. Ratio of MHC$^+$ cells and multinuclear myotubes were quantified. $^{**}p < 0.01$ vs. control (Student's *t*-test); $n = 4$–6. **(B,C)** qPCR results of gene expression in the H35M myoblasts differentiated in DIM-NG with palmitic acid for 2 days. Mean value of control group was set to 1.0 for each gene; $n = 1$.

In addition to inflammation, abnormal protein metabolism is another important factor for diabetic skeletal muscle wasting. In skeletal muscle tissue, T1DM decreases protein synthesis and T2DM enhances autophagy-mediated protein degradation (Sala and Zorzano, 2015). A recent study reported the dysregulated autophagy in T2DM myoblasts (Henriksen et al., 2019). However in this study, expression of proteasome-related genes such as atrogin-1 and MuRF-1 were not altered between healthy and DM myoblasts during short-term differentiation. The effects of T2DM on protein degradation might emerge in the fully maturated myofibers, suggesting the limitation of cultured myoblasts as a model of muscle wasting in patients with DM. Present results need to be carefully interpreted in clinical settings.

This study proved that iSN04 can recover the deteriorated myogenesis of DM myoblasts, in addition to facilitating the differentiation of healthy myoblasts. Although myoDNs, including iSN04, can be potential drug seeds for muscle wasting in patients with DM, the effect of iSN04 should be established using extensive patient-derived myoblasts for clinical application. For instance, the sensitivities to iSN04 were individually different among hMBs. iSN04 is incorporated into the cytoplasm and physically interacts with and interfere with a multifunctional phosphoprotein, nucleolin (Shinji et al., 2021). Nucleolin (*NCL*) mRNA levels were similar among the hMBs used in this study (**Supplementary Figure 7A**), and subcellular localization of nucleolin was not different between insensitive H26M and sensitive H35F throughout differentiation (**Supplementary Figure 7B**). Post-translational phosphorylation or glycosylation is indispensable for nucleolin function (Barel et al., 2001; Losfeld et al., 2009). This suggests that the modification of nucleolin may vary among individuals and may be related to iSN04 sensitivity. The precise role of nucleolin in myoblasts remains unclear. One

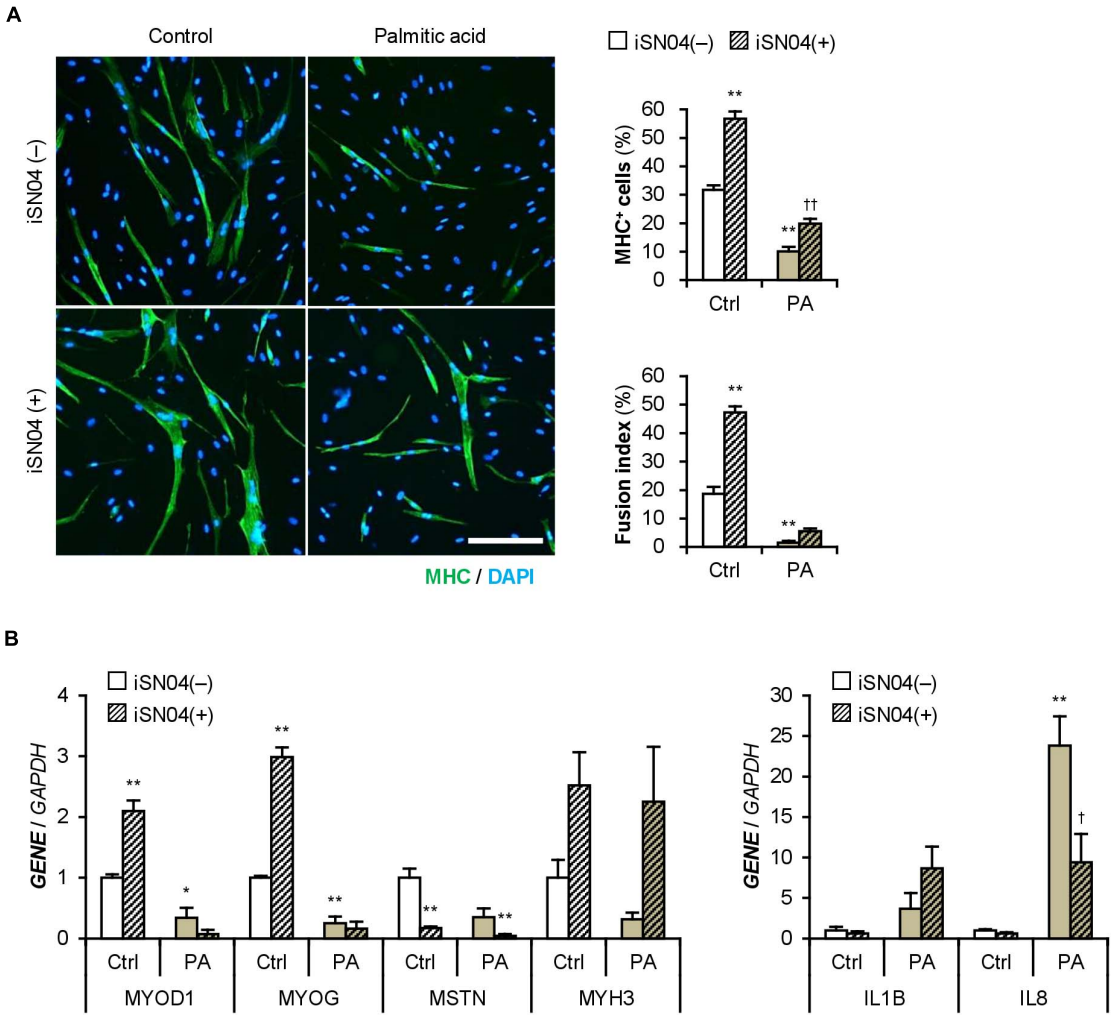

FIGURE 8 | iSN04 recovers the myoblast differentiation impaired by excessive palmitic acid. **(A)** Representative immunofluorescent images of the H35M myoblasts differentiated in DIM-NG with palmitic acid and iSN04 for 2 days. Scale bar, 200 μm. Ratio of MHC$^+$ cells and multinuclear myotubes were quantified. $^{**}p < 0.01$ vs. control-iSN04(–); $^{\dagger\dagger}p < 0.01$ vs. PA-iSN04(–) (Tukey–Kramer test); $n = 6$. **(B)** qPCR results of gene expression in the H35M myoblasts differentiated as in panel **(A)**. Mean value of control-iSN04(–) group was set to 1.0 for each gene. $^{*}p < 0.05$, $^{**}p < 0.01$ vs. control-iSN04(–); $^{\dagger}p < 0.05$ vs. palmitic acid-iSN04(–) (Tukey–Kramer test); $n = 3$.

study reported that a moderate knockdown of nucleolin by miR-34b promotes myoblast differentiation (Tang et al., 2017). We found that iSN04 serves as a nucleolin antagonist and increases p53 protein levels to promote myoblast differentiation (Shinji et al., 2021) because nucleolin binds to p53 mRNA to inhibit its translation (Takagi et al., 2005; Chen et al., 2012). However, inhibition of p53 translation is considered to be a part of the multifunction of nucleolin in myoblasts. In cancer cells, nucleolin competitively interacts with NF-κB essential modulator (NEMO), resulting in the downregulation of NF-κB activity. The established nucleolin aptamer AS1411 forms the NEMO-nucleolin-AS1411 complex to block the transcriptional activity of NF-κB (Girvan et al., 2006). We have already confirmed that AS1411 promotes myoblast differentiation as well as iSN04 (Shinji et al., 2021). Thus, iSN04 possibly inhibits NF-κB activity by associating the NEMO-nucleolin-iSN04 complex. NF-κB has been known to impair myogenesis by upregulating Pax7 and myostatin (Wang et al., 2007; He et al., 2013; Ono and Sakamoto, 2017). Inactivation of NF-κB by iSN04 can be assumed to downregulate myostatin and IL-8 in T2DM and palmitic acid-cultured myoblasts. Investigation of anti-inflammatory effects of iSN04 and AS1411 in myoblasts should be an important subject to reveal their action mechanism and to establish the myoDNs as nucleic acid drugs for skeletal muscle loss in patients with DM.

CONCLUSION

The differentiation abilities of myoblasts deteriorated with dysregulation of myogenic and inflammatory gene expression due to DM, glucose, or palmitic acid. A myoDN, iSN04, recovered impaired myogenesis by modulating gene expression, especially

by decreasing myostatin and IL-8. iSN04 could be a potential drug candidate for muscle wasting in patients with DM by directly targeting myoblasts.

DATA AVAILABILITY STATEMENT

The raw data supporting the conclusions of this article will be made available by the authors, without undue reservation.

AUTHOR CONTRIBUTIONS

TT and SN designed the study. TT wrote the manuscript. SN performed the experiments and analyses. SY and TS provided the materials and supervised the study. All authors contributed to the article and approved the submitted version.

FUNDING

This study was supported in part by a Grant-in-Aid from the Japan Society for the Promotion of Science (19K05948) to TT.

ACKNOWLEDGMENTS

The preprint has been posted on bioRxiv (Nakamura et al., 2021).

SUPPLEMENTARY MATERIAL

The Supplementary Material for this article can be found online at: https://www.frontiersin.org/articles/10.3389/fphys.2021.679152/full#supplementary-material

REFERENCES

Aguer, C., Mercier, J., Man, C. Y., Metz, L., Bordenave, S., Lambert, K., et al. (2010). Intramyocellular lipid accumulation is associated with permanent relocation ex vivo and in vitro of fatty acid translocase (FAT)/CD36 in obese patients. *Diabetologia* 53, 1151–1163. doi: 10.1007/s00125-010-1708-x

Barel, M., Le Romancer, M., and Frade, R. (2001). Activation of the EBV/C3d receptor (CR2, CD21) on human B lymphocyte surface triggers tyrosine phosphorylation of the 95-kDa nucleolin and its interaction with phosphatidylinositol 3 kinase. *J. Immunol.* 166, 3167–3173. doi: 10.4049/jimmunol.166.5.3167

Bielecka-Dabrowa, A., Ebner, N., Dos Santos, M. R., Ishida, J., Hasenfuss, G., and von Haehling, S. (2020). Cachexia, muscle wasting, and frailty in cardiovascular disease. *Eur. J. Heart Fail.* 22, 2314–2326. doi: 10.1002/ejhf.2011

Bodine, S. C., Latres, E., Baumhueter, S., Lai, V. K., Nunez, L., Clarke, B. A., et al. (2001). Identification of ubiquitin ligases required for skeletal muscle atrophy. *Science* 294, 1704–1708. doi: 10.1126/science.1065874

Boufroura, F. Z., Le Bachelier, C., Tomkiewicz-Raulet, C., Schlemmer, D., Benoist, J. F., Grondin, P., et al. (2018). A new AMPK activator, GSK773, corrects fatty acid oxidation and differentiation defect in CPT2-deficient myotubes. *Hum. Mol. Genet.* 27, 3417–3433. doi: 10.1093/hmg/ddy254

Bouzakri, K., Plomgaard, P., Berney, T., Donath, M. Y., Pedersen, B. K., and Halban, P. A. (2011). Bimodal effect on pancreatic beta-cells of secretory products from normal or insulin-resistant human skeletal muscle. *Diabetes* 60, 1111–1121. doi: 10.2337/db10-1178

Brack, A. S., Conboy, M. J., Roy, S., Lee, M., Kuo, C. J., Keller, C., et al. (2007). Increased Wnt signaling during aging alters muscle stem cell fate and increases fibrosis. *Science* 317, 807–810. doi: 10.1126/science.1144090

Broussard, S. R., McCusker, R. H., Novakofski, J. E., Strle, K., Shen, W. H., Johnson, R. W., et al. (2004). IL-1β impairs insulin-like growth factor I-induced differentiation and downstream activation signals of the insulin-like growth factor I receptor in myoblasts. *J. Immunol.* 172, 7713–7720. doi: 10.4049/jimmunol.172.12.7713

Chen, J., Guo, K., and Kastan, M. B. (2012). Interactions of nucleolin and ribosomal protein L26 (RPL26) in translational control of human p53 mRNA. *J. Biol. Chem.* 287, 16467–16476. doi: 10.1074/jbc.M112.349274

Ciaraldi, T. P., Ryan, A. J., Mudaliar, S. R., and Henry, R. R. (2016). Altered myokine secretion is an intrinsic property of skeletal muscle in type 2 diabetes. *PLoS One* 11:e0158209. doi: 10.1371/journal.pone.0158209

D'Souza, D. M., Al-Sajee, D., and Hawke, T. J. (2013). Diabetic myopathy: impact of diabetes mellitus on skeletal muscle progenitor cells. *Front. Physiol.* 4:379. doi: 10.3389/fphys.2013.00379

D'Souza, D. M., Zhou, S., Rebalka, I. A., MacDonald, B., Moradi, J., Krause, M. P., et al. (2016). Decreased satellite cell number and function in humans and mice with type 1 diabetes is the result of altered Notch signaling. *Diabetes* 65, 3053–3061. doi: 10.2337/db15-1577

Dumont, N. A., Bentzinger, C. F., Sincennes, M. C., and Rudnicki, M. A. (2015). Satellite cells and skeletal muscle regeneration. *Compr. Physiol.* 5, 1027–1059. doi: 10.1002/cphy.c140068

Fukada, S. I. (2018). The roles of muscle stem cells in muscle injury, atrophy and hypertrophy. *J. Biochem.* 163, 353–358. doi: 10.1093/jb/mvy019

Gesteiro, E., Guijarro, L., Sanchez-Muniz, F. J., Vidal-Carou, M. D. C., Troncoso, A., Venanci, L., et al. (2019). Palm oil on the edge. *Nutrients* 11:2008. doi: 10.3390/nu11092008

Gibson, D. J., Burden, S. T., Strauss, B. J., Todd, C., and Lal, S. (2015). The role of computed tomography in evaluating body composition and the influence of reduced muscle mass on clinical outcome in abdominal malignancy: a systematic review. *Eur. J. Clin. Nutr.* 69, 1079–1086. doi: 10.1038/ejcn.2015.32

Girvan, A. C., Teng, Y., Casson, L. K., Thomas, S. D., Juliger, S., Ball, M. W., et al. (2006). AGRO100 inhibits activation of nuclear factor-κB (NF-κB) by forming a complex with NF-κB essential modulator (NEMO) and nucleolin. *Mol. Cancer Ther.* 5, 1790–1799. doi: 10.1158/1535-7163.MCT-05-0361

Green, C. J., Pedersen, M., Pedersen, B. K., and Scheele, C. (2011). Elevated NF-κB activation is conserved in human myocytes cultured from obese type 2 diabetic patients and attenuated by AMP-activated protein kinase. *Diabetes* 60, 2810–2819. doi: 10.2337/db11-0263

Grzelkowska-Kowalczyk, K., Wieteska-Skrzeczynska, W., Grabiec, K., and Tokarska, J. (2013). High glucose-mediated alterations of mechanisms important in myogenesis of mouse C2C12 myoblasts. *Cell Biol. Int.* 37, 29–35. doi: 10.1002/cbin.10004

He, W. A., Berardi, E., Cardillo, V. M., Acharyya, S., Aulino, P., Thomas-Ahner, J., et al. (2013). NF-κB-mediated Pax7 dysregulation in the muscle microenvironment promotes cancer cachexia. *J. Clin. Invest.* 123, 4821–4835. doi: 10.1172/JCI68523

Henriksen, T. I., Davidsen, P. K., Pedersen, M., Schultz, H. S., Hansen, N. S., Larsen, T. J., et al. (2017). Dysregulation of a novel miR-23b/27b-p53 axis impairs muscle stem cell differentiation of humans with type 2 diabetes. *Mol. Metab.* 6, 770–779. doi: 10.1016/j.molmet.2017.04.006

Henriksen, T. I., Wigge, L. V., Nielsen, J., Pedersen, B. K., Sandri, M., and Scheele, C. (2019). Dysregulated autophagy in muscle precursor cells from humans with type 2 diabetes. *Sci. Rep.* 9:8169. doi: 10.1038/s41598-019-44535-2

Janssen, I., Heymsfield, S. B., Wang, Z. M., and Ross, R. (2000). Skeletal muscle mass and distribution in 468 men and women aged 18-88 yr. *J. Appl. Physiol.* 89, 81–88. doi: 10.1152/jappl.2000.89.1.81

Jensen, J., Rustad, P. I., Kolnes, A. J., and Lai, Y. C. (2011). The role of skeletal muscle glycogen breakdown for regulation of insulin sensitivity by exercise. *Front. Physiol.* 2:112. doi: 10.3389/fphys.2011.00112

Jeong, J., Conboy, M. J., and Conboy, I. M. (2013). Pharmacological inhibition of myostatin/TGF-beta receptor/pSmad3 signaling rescues muscle regenerative responses in mouse model of type 1 diabetes. *Acta Pharmacol. Sin.* 34, 1052–1060. doi: 10.1038/aps.2013.67

Kato, T., Shimano, H., Yamamoto, T., Ishikawa, M., Kumadaki, S., Matsuzaka, T., et al. (2008). Palmitic acid impairs and eicosapentaenoate restores insulin secretion through regulation of SREBP-1c in pancreatic islets. *Diabetes* 57, 2382–2392. doi: 10.2337/db06-1806

Kim, C. S., Park, H. S., Kawada, T., Kim, J. H., Lim, D., Hubbard, N. E., et al. (2006). Circulating levels of MCP-1 and IL-8 are elevated in human obese subjects and associated with obesity-related parameters. *Int. J. Obes.* 30, 1347–1355. doi: 10.1038/sj.ijo.0803259

La Sala, L., Pujadas, G., De Nigris, V., Canivell, S., Novials, A., Genovese, S., et al. (2015). Oscillating glucose and constant high glucose induce endoglin expression in endothelial cells: the role of oxidative stress. *Acta Diabetol.* 52, 505–512. doi: 10.1007/s00592-014-0670-3

Lecomte, V., Meugnier, E., Euthine, V., Durand, C., Freyssenet, D., Nemoz, G., et al. (2010). A new role for sterol regulatory element binding protein 1 transcription factors in the regulation of muscle mass and muscle cell differentiation. *Mol. Cell. Biol.* 30, 1182–1198. doi: 10.1128/MCB.00690-09

Lokireddy, S., Mouly, V., Butler-Browne, G., Gluckman, P. D., Sharma, M., Kambadur, R., et al. (2011). Myostatin promotes the wasting of human myoblast cultures through promoting ubiquitin-proteasome pathway-mediated loss of sarcomeric proteins. *Am. J. Physiol. Cell Physiol.* 301, C1316–C1324. doi: 10.1152/ajpcell.00114.2011

Losfeld, M. E., Khoury, D. E., Mariot, P., Carpentier, M., Krust, B., Briand, J. P., et al. (2009). The cell surface expressed nucleolin is a glycoprotein that triggers calcium entry into mammalian cells. *Exp. Cell Res.* 315, 357–369. doi: 10.1016/j.yexcr.2008.10.039

McCormick, R., and Vasilaki, A. (2018). Age-related changes in skeletal muscle: changes to life-style as a therapy. *Biogerontology* 19, 519–536. doi: 10.1007/s10522-018-9775-3

Milewska, M., Domoradzki, T., Majewska, A., Blaszczyk, M., Gajewska, M., Hulanicka, M., et al. (2019). Interleukin-8 enhances myocilin expression, Akt-FoxO3 signaling and myogenic differentiation in rat skeletal muscle cells. *J. Cell. Physiol.* 234, 19675–19690. doi: 10.1002/jcp.28568

Miyake, H., Kanazawa, I., Tanaka, K. I., and Sugimoto, T. (2019). Low skeletal muscle mass is associated with the risk of all-cause mortality in patients with type 2 diabetes mellitus. *Ther. Adv. Endocrinol. Metab.* 10:2042018819842971. doi: 10.1177/2042018819842971

Nakamura, S., Yonekura, S., Shimosato, T., and Takaya, T. (2021). Myogenetic oligodeoxynucleotide (myoDN) recovers the differentiation of skeletal muscle myoblasts deteriorated by diabetes mellitus. *bioRxiv* 2021:434717. doi: 10.1101/2021.03.10.434717

Nihashi, Y., Ono, T., Kagami, H., and Takaya, T. (2019a). Toll-like receptor ligand-dependent inflammatory responses in chick skeletal muscle myoblasts. *Dev. Comp. Immunol.* 91, 115–122. doi: 10.1016/j.dci.2018.10.013

Nihashi, Y., Umezawa, K., Shinji, S., Hamaguchi, Y., Kobayashi, H., Kono, T., et al. (2019b). Distinct cell proliferation, myogenic differentiation, and gene expression in skeletal muscle myoblasts of layer and broiler chickens. *Sci. Rep.* 9:16527. doi: 10.1038/s41598-019-52946-4

Nihashi, Y., Shinji, S., Umezawa, K., Shimosato, T., Ono, T., Kagami, H., et al. (2020). Myogenetic oligodeoxynucleotide (myoDN) complexed with berberine promotes differentiation of chicken skeletal muscle myoblasts. *bioRxiv* 2020:4236122. doi: 10.1101/2020.12.19.423622

Ono, Y., and Sakamoto, K. (2017). Lipopolysaccharide inhibits myogenic differentiation of C2C12 myoblasts through the Toll-like receptor 4-nuclear factor-κB signaling pathway and myoblast-derived tumor necrosis factor-α. *PLoS One* 12:e0182040. doi: 10.1371/journal.pone.0182040

Parikh, H., Carlsson, E., Chutkow, W. A., Johansson, L. E., Storgaard, H., Poulsen, P., et al. (2007). TXNIP regulates peripheral glucose metabolism in humans. *PLoS Med.* 4:e158. doi: 10.1371/journal.pmed.0040158

Periasamy, M., Herrera, J. L., and Reis, F. C. G. (2017). Skeletal muscle thermogenesis and its role in whole body energy metabolism. *Diabetes Metab. J.* 41, 327–336. doi: 10.4093/dmj.2017.41.5.327

Polesskaya, A., Pinna, G., Sassi, Y., Vandamme, M., Bigot, A., Mouly, V., et al. (2016). Post-transcriptional modulation of interleukin 8 by CNOT6L regulates skeletal muscle differentiation. *Biochim. Biophys. Acta* 1863, 263–270. doi: 10.1016/j.bbamcr.2015.11.018

Rowland, L. A., Bal, N. C., and Periasamy, M. (2015). The role of skeletal-muscle-based thermogenic mechanisms in vertebrate endothermy. *Biol. Rev. Camb. Philos. Soc.* 90, 1279–1297. doi: 10.1111/brv.12157

Saini, A., Sharples, A. P., Al-Shadai, N., and Stewart, C. E. (2017). Omega-3 fatty acid EPA improves regenerative capacity of mouse skeletal muscle cells exposed to saturated fat and inflammation. *Biogerontology* 18, 109–129. doi: 10.1007/s10522-016-9667-3

Sala, D., and Zorzano, A. (2015). Differential control of muscle mass in type 1 and type 2 diabetes mellitus. *Cell. Mol. Life Sci.* 72, 3803–3817. doi: 10.1007/s00018-015-1954-7

Samaras, K., Botelho, N. K., Chisholm, D. J., and Lord, R. V. (2010). Subcutaneous and visceral adipose tissue gene expression of serum adipokines that predict type 2 diabetes. *Obesity* 18, 884–889. doi: 10.1038/oby.2009.443

Seo, K., Suzuki, T., Kobayashi, K., and Nishimura, T. (2019). Adipocytes suppress differentiation of muscle cells in a co-culture system. *Anim. Sci. J.* 90, 423–434. doi: 10.1111/asj.13145

Shinji, S., Umezawa, K., Nihashi, Y., Nakamura, S., Shimosato, T., and Takaya, T. (2021). Identification of the myogenetic oligodeoxynucleotides (myoDNs) that promote differentiation of skeletal muscle myoblasts by targeting nucleolin. *Front. Cell Dev. Biol.* 8:616706. doi: 10.3389/fcell.2020.616706

Takagi, M., Absalon, M. J., McLure, K. G., and Kastan, M. B. (2005). Regulation of p53 translation and induction after DNA damage by ribosomal protein L26 and nucleolin. *Cell* 123, 49–63. doi: 10.1016/j.cell.2005.07.034

Takaya, T., Nihashi, Y., Kojima, S., Ono, T., and Kagami, H. (2017). Autonomous xenogenic cell fusion of murine and chick skeletal muscle myoblasts. *Anim. Sci. J.* 88, 1880–1885. doi: 10.1111/asj.12884

Tang, Z., Qiu, H., Luo, L., Liu, N., Zhong, J., Kang, K., et al. (2017). miR-34b modulates skeletal muscle cell proliferation and differentiation. *J. Cell. Biochem.* 118, 4285–4295. doi: 10.1002/jcb.26079

Teng, S., and Huang, P. (2019). The effect of type 2 diabetes mellitus and obesity on muscle progenitor cell function. *Stem Cell Res. Ther.* 10:103. doi: 10.1186/s13287-019-1186-0

Wang, H., Hertlein, E., Bakkar, N., Sun, H., Acharyya, S., Wang, J., et al. (2007). NF-κB regulation of YY1 inhibits skeletal myogenesis through transcriptional silencing of myofibrillar genes. *Mol. Cell. Biol.* 27, 4374–4387. doi: 10.1128/MCB.02020-06

Yang, M., Wei, D., Mo, C., Zhang, J., Wang, X., Han, X., et al. (2013). Saturated fatty acid palmitic acid-induced insulin resistance is accompanied with myotube loss and the impaired expression of health benefit myokine genes in C2C12 myotubes. *Lipids Health Dis.* 12:104. doi: 10.1186/1476-511X-12-104

Conflict of Interest: Shinshu University has been assigned the invention of iSN04 by TT, Koji Umezawa, and TS, and Japan Patent Application 2018-568609 has been filed on February 15, 2018.

The remaining authors declare that the research was conducted in the absence of any commercial or financial relationships that could be construed as a potential conflict of interest.

frontiers in Physiology

ORIGINAL RESEARCH
published: 08 July 2021
doi: 10.3389/fphys.2021.687947

Altered Jagged1-Notch1 Signaling in Enhanced Dysfunctional Neovascularization and Delayed Angiogenesis After Ischemic Stroke in HFD/STZ Induced Type 2 Diabetes Rats

Zhihui Guo[1†], Jia Jia[2†], Yanling Tu[3], Chang Jin[1], Cen Guo[4], Feifei Song[1], Xuqing Wu[1], Haifeng Bao[1*] and Wei Fan[1*]*

[1] Department of Neurology, Zhongshan Hospital, Fudan University, Shanghai, China, [2] Department of Neurology, Shanghai Xuhui District Central Hospital, Shanghai, China, [3] Department of Neurology, Zhongshan Hospital, Xiamen University, Xiamen, China, [4] Department of Neurology, Yueyang Hospital of Integrated Traditional Chinese and Western Medicine, Shanghai University of Traditional Chinese Medicine, Shanghai, China

OPEN ACCESS

Edited by:
Xinran Ma,
East China Normal University, China

Reviewed by:
Huang Dongya,
Tongji University, China
Jianliang Fu,
Shanghai Jiao Tong University, China

***Correspondence:**
Xuqing Wu
wu.xuqing@zs-hospital.sh.cn
Haifeng Bao
bao.haifeng@zs-hospital.sh.cn
Wei Fan
Fan.Wei@zs-hospital.sh.cn

[†] These authors have contributed equally to this work and share first authorship

Specialty section:
This article was submitted to Clinical and Translational Physiology, a section of the journal Frontiers in Physiology

Received: 30 March 2021
Accepted: 14 June 2021
Published: 08 July 2021

Citation:
Guo Z, Jia J, Tu Y, Jin C, Guo C, Song F, Wu X, Bao H and Fan W (2021) Altered Jagged1-Notch1 Signaling in Enhanced Dysfunctional Neovascularization and Delayed Angiogenesis After Ischemic Stroke in HFD/STZ Induced Type 2 Diabetes Rats. Front. Physiol. 12:687947. doi: 10.3389/fphys.2021.687947

Diabetes exacerbates brain damage in cerebral ischemic stroke. Our previous study has demonstrated that after cerebral ischemia, type 2 diabetes rats displayed worse neurological outcomes, larger cerebral infarction and severer blood-brain barrier disruption. However, our knowledge of the mechanisms of how diabetes impacts the cerebrovascular repair process is limited. This study was aimed to characterize structural alterations and potential mechanisms in brain microvessels before and after ischemic stroke in type 2 diabetic rats treated with high-fat diet and streptozotocin (HFD/STZ). Furtherly, we tested our hypothesis that dysregulated intercellular Jagged1-Notch1 signaling was involved in the dysfunctional cerebral neovascularization both before and after ischemic stroke in HFD/STZ rats. In our study, we found increased yet dysfunctional neovascularization with activated Jagged1-Notch1 signaling in the cerebrovasculature before cerebral ischemia in HFD/STZ rats compared with non-diabetic rats. Furthermore, we observed delayed angiogenesis as well as suppressed Jagged1-Notch1 signaling after ischemic stroke. Our results elucidate the potential mechanisms underlying diabetes-related cerebral microvasculature dysfunction after ischemic stroke.

Keywords: Jagged1, Notch1, neovascularization, angiogenesis, cerebral ischemia, T2DM

Abbreviations: T2DM, type 2 diabetes mellitus; pMCAO, permanent middle cerebral artery occlusion; ECs, endothelial cells; Hif-1a, hypoxia-inducible factor-1 alpha; VEGF-A, vascular endothelial growth factor A; Ang-2, Angiopoietin-2; Ang-1, Angiopoietin-1; PDGF-β, platelet derived growth factor beta; TGF-β, transforming growth factor beta; TG, Triglyceride; TC, Total cholesterol; LDL-C, low density lipoprotein cholesterol; HDL-C, high density lipoprotein cholesterol; STZ, streptozotocin; HFD, high fat diet; RBG, random blood glucose; OGTT, oral glucose tolerance test; NC, non-diabetic control; DC, diabetic control; NS, non-diabetic sham; NDI, non-diabetic cerebral ischemia; DS, diabetic sham; DI, diabetic cerebral ischemia; GK, Goto-Kakisaki Wistar rats; CCA, common carotid artery; ICA, internal carotid artery; ECA, external carotid artery; MCA, middle cerebral artery; CBF, cerebral blood flow; ROI, regions of interest.

INTRODUCTION

As of 2019, the global estimate of diabetes prevalence is 9.3% (463 million people), with type 2 diabetes mellitus (T2DM) accounting for approximately 90% of the total (Saeedi et al., 2019). Substantial burden is imposed on both the individual and society as it is associated with multiple complications healthcare management including ischemic stroke (Cannon et al., 2018). Diabetes poses a about four times increase on risk of ischemic stroke (Tun et al., 2017) and ultimately leads to worse long-term functional recovery after stroke (Megherbi et al., 2003) and independently doubles the risk of recurrent stroke (Palacio et al., 2014; Pan et al., 2016).

Due to atherosclerotic lesions of intracranial and extracranial arteries in T2DM, ischemic stroke is generally regarded as a macrovascular complication of diabetes. However, recent evidence has also revealed severe cerebral microvasculature impairment in diabetic patients (Guo et al., 2021). According to previous studies focusing on T2DM patients, diffuse brain atrophy, white matter lesions, microbleeds, and asymptomatic lacunar infarcts have been shown on brain magnetic resonance imaging (MRI) or in postmortem studies (Sima, 2010). These lesions may be clinically asymptomatic if they are single, but more and more single lesion and combinations of lesion types are associated with cognitive and mood disorder, and more impressively, higher risk and poorer prognosis of stroke (Wardlaw et al., 2019). Moreover, altered cerebral microcirculation such as increased blood-brain barrier permeability (Yu et al., 2016), diminished baseline regional cerebral blood flow (CBF), and impaired vasoreactivity have been proposed in diabetes patients (Last et al., 2007; Cui et al., 2017). Collectively, emerging evidence indicates that cerebral microvascular dysfunction in T2DM is one of the key underlying mechanisms of stroke, dementia, and depression (van Sloten et al., 2020).

The clinical evidence mentioned above highlights the demand for basic research focusing on the effect of diabetes on cerebral microvasculature in ischemic stroke. It has been shown that Goto-Kakizaki (GK) rats (Li et al., 2010; Prakash et al., 2012) and db/db mouse (Prakash et al., 2013a) developed enhanced, yet immature, neovascularization in the brain, which may cause the diabetic vessels more vulnerable to reperfusion injury, resulting in greater hemorrhagic transformation (Ergul et al., 2007; Prakash et al., 2012). Furthermore, according to recent reports, cerebrovasculature in peri-infarct regions after an ischemic event was significantly declined in diabetes animals, while controls had compensatory neovascularization (Prakash et al., 2013b). In addition, type 1 diabetes mice exhibited delayed angiogenesis after ischemic stroke (Poittevin et al., 2015), which may also explain why diabetes aggravates ischemic brain injury.

The underlying mechanisms by which diabetes damages the cerebral microvascular network are unclear and may be multi-factorial. The disturbed process of angiogenesis which relies on a variety of signaling pathways may play a major role, since it has been shown that elevated Angiopoietin-2 (Ang-2) with declined Angiopoietin-1 (Ang-1) expression (Cui et al., 2011; Ye et al., 2011) and decreased vascular endothelial growth factor (VEGF) with increased angiostatin signaling (Zhu et al., 2010) are involved in dysfunctional cerebral neovascularization in diabetes. Among angiogenic regulators, accumulating data has led to the conclusion that Notch signaling plays a pivotal role in the control of vascular morphogenesis during development and in tumor angiogenesis (Phng and Gerhardt, 2009). A recent study has shown the implication of Jagged1-Notch1 pathway in stroke-induced angiogenesis (Ren et al., 2018). Specifically, another study revealed that Notch signaling was affected by diabetes mellitus associated with the retinal capillary regression, a potentially novel mechanism of diabetes-induced microvasculopathy at an early phase (Yoon et al., 2016). Hence, we suspect that Notch signaling pathway may play a part in the specific pathology where diabetes aggravates ischemic brain injury.

There exists a surplus of animal models in the study of T2DM, for example, genetic models namely GK rat and db/db mouse which develop spontaneous T2DM and show features resembling human pathology. The general development of T2DM in them is principally determined by gene unlike in humans, of which the etiology is characterized by both genetic background and multiple environmental components. Furthermore, the observations obtained from these genetically homogenous strains may not always be extended to the human population because of the large heterogeneity in the latter (Srinivasan et al., 2005). Therefore, our study focused on a suitable animal model with a combination of high fat diet (HFD) and low dose of streptozotocin (STZ) to not only share similar metabolic characteristics but mimic the natural development of human T2DM.

Building upon the above discoveries, our research sought to answer the following issues: (1) Are the cerebral microvasculopathy observed in the GK rat and db/db mice present in HFD/STZ-treated model of T2DM rats; (2) whether the Jagged1-Notch1 pathway is involved in the impaired baseline cerebral neovascularization and angiogenesis both before and after diabetic cerebral ischemia, by which brain injury is aggravated.

MATERIALS AND METHODS

Animal

Male Sprague-Dawley rats (160 ± 10 g) were obtained from Shanghai JieSiJie Laboratory Animal Co., Ltd. and housed in Fudan University animal care facility, with approvement from our University Animal Care and Use Committee. All experiments followed the National Institute of Health guidelines for care and use of animals in research and were under protocols approved by the Committee on the Ethics of Animal Experiments of our university. All rats were randomly assigned to six groups: non-diabetic control (NC) group (n = 9), diabetic control (DC) group (n = 12), non-diabetic sham (NS) group (n = 9), diabetic sham (DS) group (n = 9), non-diabetic cerebral ischemic (NDI) group (n = 24), and diabetic cerebral ischemic (DI) group (n = 24). The rats were sacrificed on days 1, 3, 5, and 7 after cerebral ischemia.

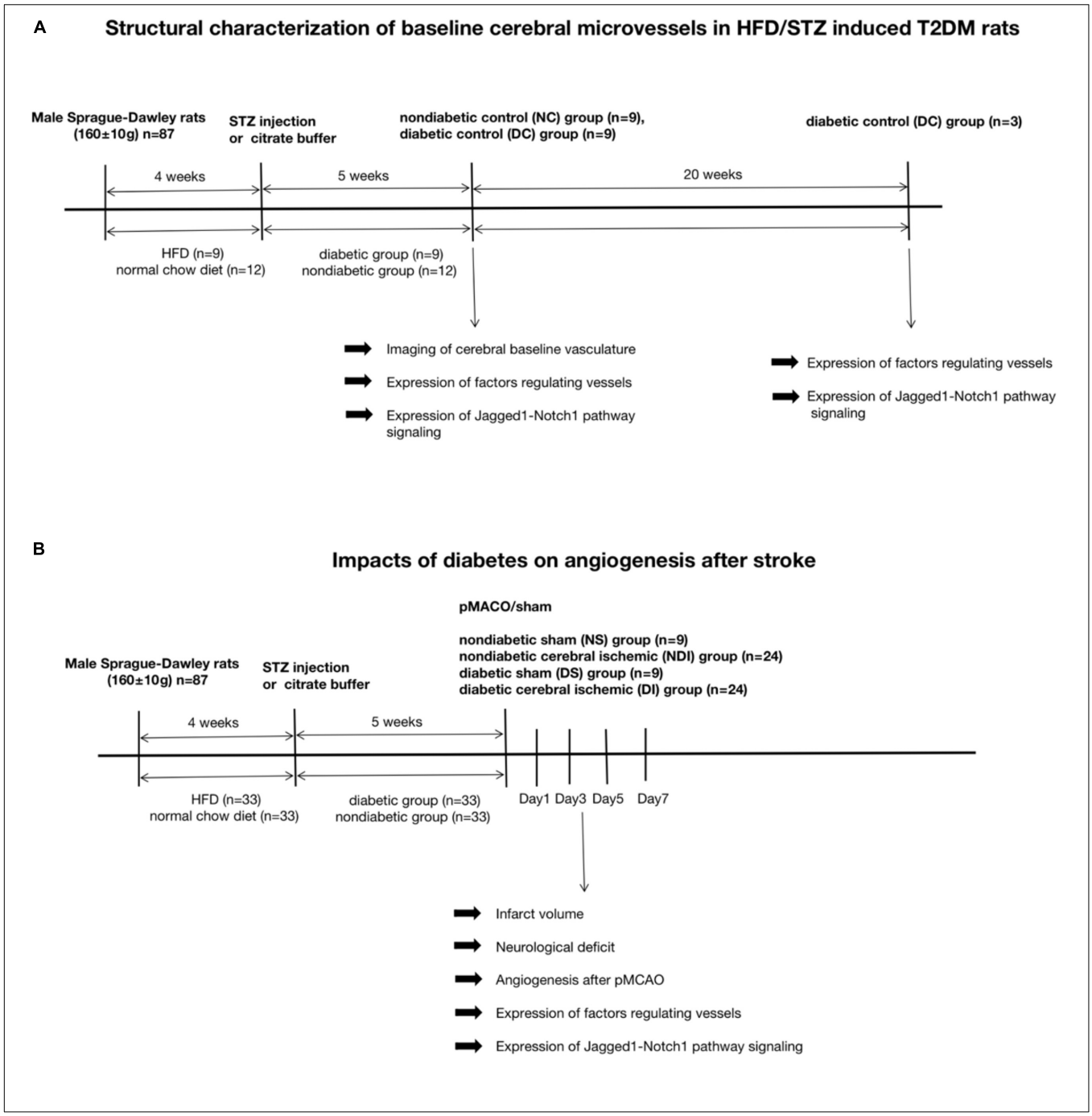

T2DM Model

Since the combination of HFD-fed and low-dose STZ-treated rat serves as an alternative animal model for T2DM (Reed et al., 2000; Srinivasan et al., 2005; Gheibi et al., 2017), in our study, diabetes mellitus was induced in 4-week HFD (Slacom, China; 40% calories as fat) feeding male rats by injection of 35 mg/kg STZ (Sigma, United States) intraperitoneally. Control animals were fed with normal chow diet for 4 weeks, and received only citrate buffer. 3 and 7 days after injection, the HFD rats were considered as T2DM when their random blood glucose (RBG) levels exceeded 300 mg/dL. The RBG level of each rat was measured once a week after STZ injection using an ACCU-CHEK Performa blood glucose meter (Roche, Germany) until euthanasia.

The levels of serum lipids profile including total cholesterol (TC) [TC assay kit (A111-1-1, Jiancheng, China)], high-density lipoprotein cholesterol (HDL-C) [HDL-C assay kit (A112-1-1, Jiancheng, China)], low-density lipoprotein cholesterol (LDL-C) [LDL-C assay kit (A113-1-1, Jiancheng, China)], and triglycerides (TG) [TG assay kit (A110-1-1, Jiancheng, China)] were tested

after euthanasia using commercially available colorimetric quantitation kits.

Permanent Middle Cerebral Artery Occlusion (pMCAO) Model

After 5 weeks of diabetes induction, cerebral ischemia was induced by suture pMCAO as was described (Tu et al., 2019). Briefly, animals were anesthetized with an injection of 10% chloral hydrate (0.35 ml/100 g) intraperitoneally. Following exposure of the surgical field, the right common carotid artery (CCA), external carotid artery (ECA), and internal carotid artery (ICA) were isolated from the vagus nerve and these arteries were ligated temporarily using a cotton thread. The suture (Cinontech Co., China) was introduced into ICA and advanced until the tip occluded the middle cerebral artery (MCA), resulting in a cessation of blood flow. Laser Doppler flowmetry (Perimed, Sweden) monitoring the CBF value dynamically was used to confirm occlusion.

Behavioral Assessment

Sensorimotor test, Garcia test, was performed (Garcia et al., 1995) in a blinded manner on days 1, 3, 5, and 7 after cerebral ischemia. The Garcia test, a composite neurological test used to evaluate various sensorimotor deficits, includes 6 examinations: spontaneous activity, symmetry in the movement of four limbs, forepaw outstretching, climbing, body proprioception, and response to vibrissae touch (Garcia et al., 1995). The score ranges between 3 and 18 and the lower the score, the worse the neurological function.

Measurement of the Volume of Cerebral Infarction and Brain Edema

On 3rd day post-pMCAO, the rats were sacrificed. To quantify experimental cerebral infarction and brain edema volume, cryostat-cuts of coronal brain sections (30 μm) every 360 μm from antiunion were performed, and 15 sections were stained with cresyl violet totally (Sangong, China) and an image analysis system ImageJ was used to evaluate the lesion. The injury volume was calculated as a percentage of the contralateral non-lesioned area in each section (Swanson et al., 1990).

Imaging of Cerebral Baseline Vasculature

To visualize cerebral baseline cortex vessels as previously described (Prakash et al., 2012, 2013a), animals of NC/DC groups received injection of 500 μL of 50 mg/mL fluorescein isothiocyanate (FITC)-dextran (molecular weight 2,000,000; Sigma-Aldrich) via jugular vein after deeply anesthetized with chloral hydrate. After 10 min, brains were isolated and immersed in 4% paraformaldehyde (24 h) followed by 30% sucrose in phosphate-buffered saline (PBS). Z-stacked confocal three-dimensional images were collected from 100 μm thick sections using OLYMPUS FLUOVIEW FV3000 confocal microscope. Z-step was defined as 1.984 μm, image size 512 × 512 pixels, 20 × lens. The mean value of three separate cortical images from three 100 μm apart sections were calculated to reduce variability. Image stacks were imported into FIJI and reconstructed three dimensionally. Vascular density is defined as the density of FITC-stained vasculature from the merged planes over the total section (Prakash et al., 2012).

Angiogenesis After pMCAO

Angiogenesis detected by double immunolabeling of anti-CD31 [endothelial cells (ECs)] and anti-Ki67 (proliferating cells) was evaluated on days 1, 3, 5, and 7 after cerebral ischemia. Coronal 10-μm-thick sections were incubated with primary antibody (1:200, Abcam, United Kingdom) overnight at 4°C followed by appropriate Alexa Fluor 594 or 488–labeled secondary antibodies (1:1,000, Yishan, China) for 1 h at room temperature. Cell counts of the average number of $Ki67^+$ and $CD31^+$ cells in three regions of interest (ROI) located in the peri-infarct area were performed at three coronal brain levels (+ 0.80, -0.80, and -1.20 mm relative to bregma) that consistently contained the infarct area (Poittevin et al., 2015).

Western Blot

The ischemic penumbra was collected as described previously (Ashwal et al., 1998). Equally 40 μg of protein was loaded in each well and resolved by SDS-PAGE electrophoresis. The membranes were immunoblotted with primary antibody: Ang-2 (1:5,000, Abcam, United Kingdom), VEGF-A (1:100, Santa Cruz, United States), Jagged1 (1:100, Santa Cruz, United States), Notch1 (1:1,000, CST, United States), NICD (1:1000, CST, United States), Hes1 (1:1,000, Abcam, United Kingdom), β-actin (1:1,000, Yishan, China) overnight at 4°C, then incubated with appropriate secondary antibody (1:4,000, Yishan, China) and finally visualized with an ECL kit (Epizyme, China).

RNA Isolation and qRT-PCR

The total RNA was extracted by Trizol Reagent (Sigma, United States) and reverse transcription was performed with a cDNA Synthesis Kit (Takara, Japan). The resultant cDNAs were amplified with SYBR-Green Master Kits (Yeasen, China). The primers were as follows:

Hif-1a: forward: 5′-TTCTCCAAGCCCTCCGAGTG TG-3′
reverse: 5′-GCGGTGGCAGTGACAGTGA TG-3′
VEGF-A: forward: 5′-TACTGCTGTACCTCCACCATG CC-3′
reverse: 5′-GCAATAGCTGCGCTGGTAGA CG-3′
Ang-2: forward: 5′-TCCAGACTGACGCACATCAC-3′
reverse: 5′-ATTTCTCCAGACCCGCAGTG-3′
Ang-1: forward: 5′-TTCTTCGCTGCCATTCTGACTC AC-3′
reverse: 5′-CGCACTCTCACGGCAGTTCC-3′
PDGF-β: forward: 5′-CTTGTTCTGGGACGCACTCTT GG-3′
reverse: 5′-GCTTCTCACTGCTTCTGGCTGT AG-3′
TGF-β: forward: 5′-GCAACAATTCCTGGCGTTACC TTG-3′

reverse: 5′-TGTATTCCGTCTCCTTGGTTCAGC-3′
Jagged1: forward: 5′- GAGCCCAACCCTTGCCAGAATG-3′,
reverse: 5′-AGTTCTTGCCCTCGTAGTCCTCAG-3′
Notch1: forward: 5′-TGCCGAGTGTGAGTGGGATGG-3′
reverse: 5′-AAGTGGAAGGAGTTGTTGCGTAGC-3′
Hes1: forward: 5′-TCCTGACGGCCAATTTGCTTTCC-3′
reverse : 5′-CTGGAAGGCGACACTGCGTTAG-3′
Hes5: forward: 5′-GACCGCATCAACAGCAGCATTG-3′
reverse: 5′-TCTCCAGGATGTCGGCCTTCTC-3′

Immunofluorescence Staining

These procedures were performed as previously described (Tu et al., 2019). Serial 10 μm-thick coronal sections of the rat brain after fixation and dehydration were immersed in primary antibodies: Jagged1 (1:100, Santa Cruz, United States), Notch1 (1:1,000, CST, United States), Hes1 (1:100, Santa Cruz, United States), and CD31 (1:200, Abcam, United Kingdom)/CD31 (1:200, Affinity Biosciences, OH, United States) overnight at 4°C, followed by fluorescein-conjugated secondary antibodies (1:1,000, Yishan, China), and observed with fluorescence microscope (Olympus, Japan).

Statistics

SPSS 25 was employed. Data were presented as mean ± standard error of the mean (SEM) if they conformed to normal distribution, and median ± IQR if not. $P < 0.05$ was considered statistically significant. Differences between groups was determined by a one-way ANOVA followed by Tukey test.

RESULTS

General Conditions, Body Weight, Biochemical Analysis, and Mortality Rate

During the first 4 weeks of HFD, the rats fed the HFD weighed significantly heavier than rats fed the normal chow diet ($p < 0.05$), while the serum glucose concentrations of the two groups were similar ($p > 0.05$) (**Table 1**). Oral glucose tolerance test (OGTT) after 4-week HFD (**Figure 1C**) showed elevated serum glucose concentrations of HFD-fed rats compared with chow-fed rats ($p < 0.05$). After 4 weeks of dietary manipulation, injection of STZ significantly ($p < 0.0001$) increased serum glucose concentrations in HFD rats (**Figure 1B** and **Table 1**), which displayed the symptoms of polyuria, polydipsia, and polyphagia as compared to chow-fed control rats. In addition, STZ produced reduction in the body weights of the HFD-fed rats, which were still slightly higher than chow-fed rats on week 1 after injection and were significantly lower than chow-fed rats on week 3 after injection ($p < 0.05$) (**Figure 1A** and **Table 1**).

The diabetic group also displayed higher levels of TC, LDL-C and TG and lower level of HDL-C than the non-diabetic group ($P < 0.01$) (**Table 1**).

The mortality rates were 7/52 in diabetic group, 0/9 in DS group, 5/29 in DI group, 0/9 in NS group, 4/28 in NDI group.

The Enhanced Yet Dysfunctional Baseline Neovascularization in HFD/STZ Rat Model Before Cerebral Ischemia

In the diabetic group, the total cerebral microvasculature (**Figure 1D**) in the cortex was relatively greater than controls ($P < 0.0001$) (**Figure 1E**). In accordance with the FIJI data, there was also more CD31 staining (**Figures 1F,G**) ($P < 0.0001$), implying more non-productive newly formed microvessels. The VEGF-A detected ∼25 kDa (**Figure 2A**) was greater in the cortex of the diabetic group ($P < 0.01$) (**Figure 2B**). Moreover, the expression of VEGF-A in 24 w diabetic rats was much greater than 5 w diabetic rats, and similar changes were observed in the expression of Ang-2 (**Figures 2A,B**). Also, hypoxia-inducible

TABLE 1 | The body weight/random blood glucose/serum lipid level in different groups.

		Non-diabetic group	Diabetic group
Body weight (g)	Baseline	161.75 ± 2.58	161.13 ± 0.83
	(HFD)D1	183.88 ± 1.22	185.30 ± 1.33
	(HFD)W1	243.88 ± 3.73	258.70 ± 2.62*
	(HFD)W2	306.50 ± 6.24	326.06 ± 4.20*
	(HFD)W2	363.00 ± 8.00	392.45 ± 5.77*
	(HFD)W4	405.88 ± 7.83	443.03 ± 7.04*
	(STZ)W1	408.13 ± 9.67	428.70 ± 8.30
	(STZ)W2	452.00 ± 10.85	440.04 ± 9.53
	(STZ)W3	479.50 ± 9.36	416.74 ± 9.90*#
	(STZ)W4	503.50 ± 10.37	431.50 ± 10.30**
	(STZ)W5	512.00 ± 18.88	441.37 ± 11.41*
Blood glucose (mmol/L)	(HFD)D1	6.64 ± 0.14	7.12 ± 0.12
	(HFD)W4	6.36 ± 0.19	6.61 ± 0.17
	(STZ)D1	6.64 ± 0.14	25.86 ± 0.72****
	(STZ)W1	6.27 ± 0.30	25.48 ± 1.16****
	(STZ)W2	5.60 ± 0.16	27.24 ± 1.68****
	(STZ)W3	6.06 ± 0.17	25.75 ± 1.66****
	(STZ)W4	6.19 ± 0.27	29.09 ± 1.35****
	(STZ)W5	5.19 ± 0.24	25.78 ± 1.77****
Serum lipid (mmol/L)	TC	1.87 ± 0.15	4.25 ± 0.45****
	TG	0.33 ± 0.06	0.78 ± 0.14**
	LDL-C	0.52 ± 0.07	1.68 ± 0.22****
	HDL-C	0.45 ± 0.07	0.20 ± 0.02**

*$p < 0.05$ vs. non-diabetic group, **$p < 0.01$ vs. non-diabetic group, ****$p < 0.0001$ vs. non-diabetic group, #$p < 0.05$ vs. diabetic group (non-diabetic group n = 42, diabetic group n = 45).*

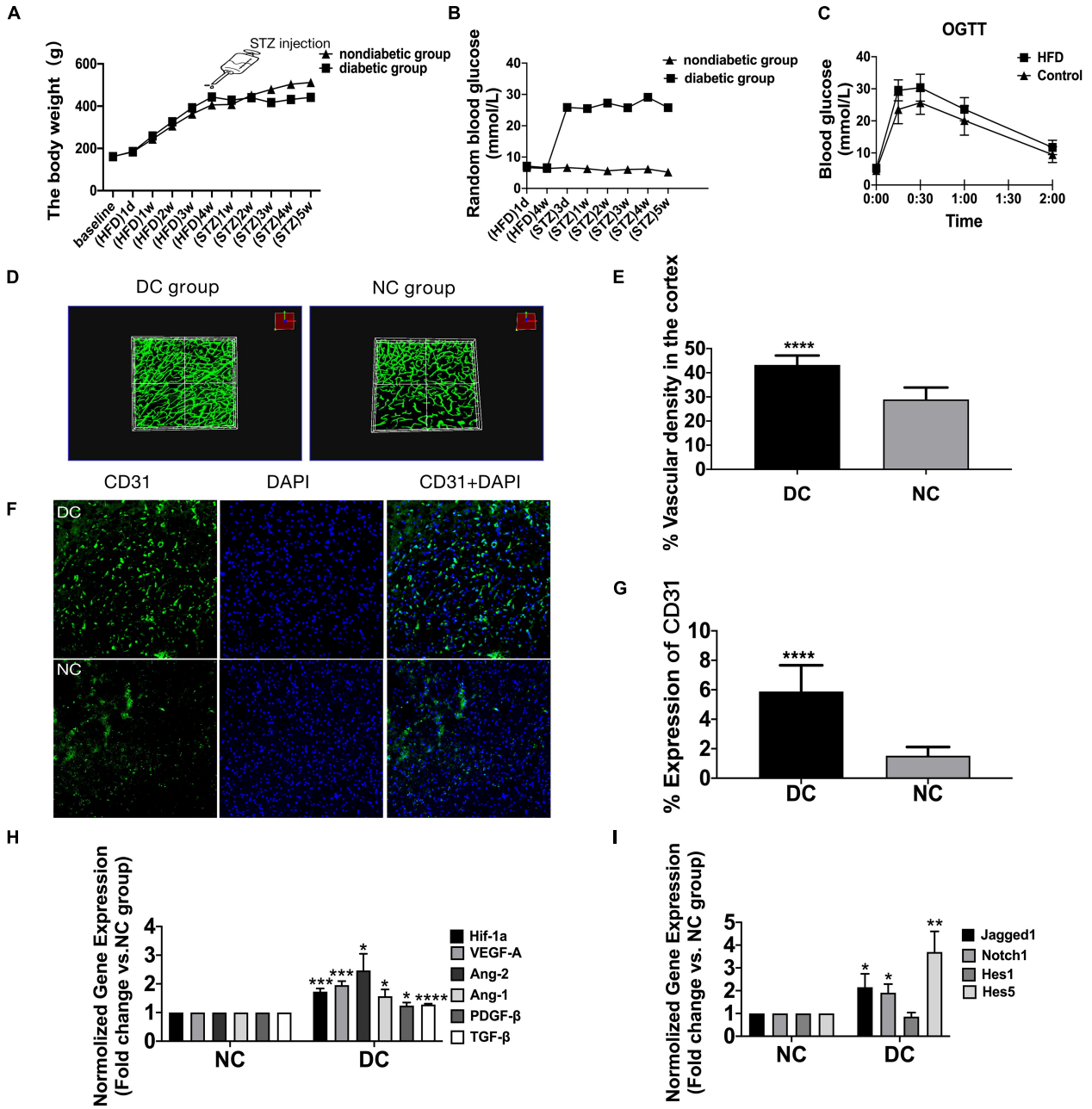

FIGURE 1 | The enhanced yet dysfunctional baseline neovascularization in HFD/STZ rat model before cerebral ischemia. **(A)** Mean body weight changes during the time of high-fat diet and after the STZ treatment (n = 42 in each group). **(B)** Mean plasma glucose concentration changes during the time of high-fat diet and after the STZ treatment (n = 42 in each group). **(C)** Mean plasma glucose concentration in response to an oral glucose challenge in chow-fed and HFD-fed rats (n = 42 in each group). **(D)** Representative FITC-perfused cerebrovascular images from non-diabetic control and diabetic control rats showing differences in neovascularization in the cerebral cortex (Z-step was defined as 1.984 μm, image size 512 × 512 pixels, 20 × lens). **(E)** Significant differences in vascular density were observed in the cortex in both non-diabetic control and diabetic control groups. **(F)** The staining of ECs in the cerebral cortex of diabetic control and non-diabetic control. Magnification ×200. Scale bar = 100 μm. **(G)** ECs were markedly increased in the cortex of the diabetic control group compared with non-diabetic control group. **(H)** The gene expression of Hif-1a, VEGF-A, Ang-2, Ang-1, TGF-β, and PDGF-β was increased in diabetic control group compared with non-diabetic control group. **(I)** The gene expression of Jagged1, Notch1, Hes1, and Hes5 was increased in diabetic control group compared with non-diabetic control group. *p < 0.05 vs. NC group, **p < 0.01 vs. NC group, ***p < 0.001 vs. NC group, ****p < 0.0001 vs. NC group.

factor-1 alpha (Hif-1a) mRNA, VEGF-A mRNA, and Ang-2 mRNA were significantly upregulated in the cortex in the diabetic group (**Figure 1H**). In addition, mRNAs for Ang-1, transforming growth factor-β (TGF-β), and platelet-derived growth factor-β (PDGF-β) were slightly increased in the diabetic group (**Figure 1H**).

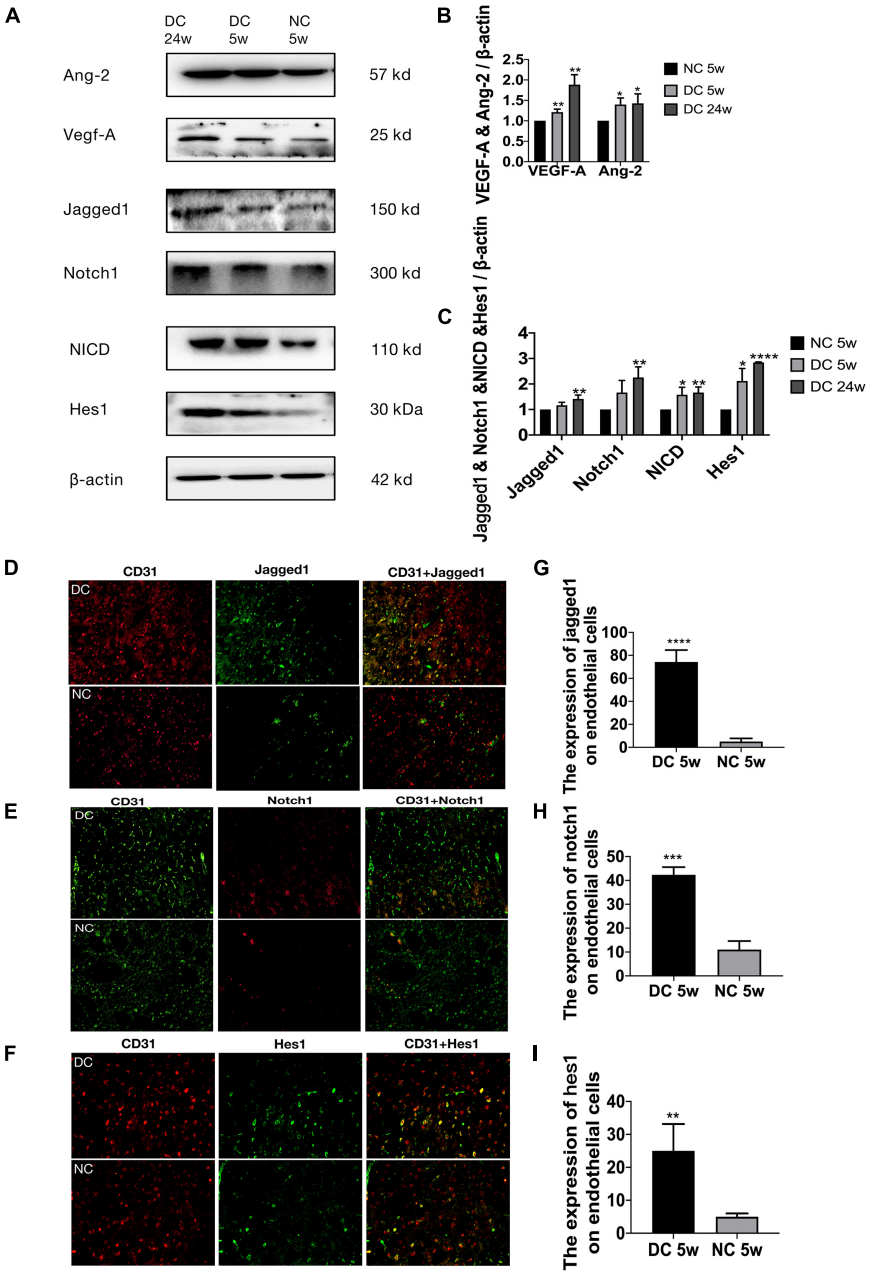

FIGURE 2 | Altered Jagged1-Notch1 signaling with baseline neovascularization in T2DM. **(A–C)** The expression of VEGF-A, Ang-2, Jagged1, Notch1, NICD, and Hes1 in the cortex was assessed by Western blot (n = 3 per group). **(D–I)** The expression of Jagged1/Notch1/Hes1 and CD31 was assessed by immunofluorescence staining in the cortex (Magnification ×200. Scale bar = 100 μm) and the positive cells of Jagged1/Notch1/Hes1 and CD31 were calculated (n = 3 per group). *p < 0.05 vs. NC group, **p < 0.01 vs. NC group, ***p < 0.001 vs. NC group, ****p < 0.0001 vs. NC group.

Altered Jagged1-Notch1 Signaling With Baseline Neovascularization in T2DM

Jagged1/Notch1/Hes1 was expressed on CD31-positive cells in the diabetic group but barely expressed on CD31-positive cells in the non-diabetic group (P < 0.01) (**Figures 2D–I**). In addition, we found increased expression of mRNA of Jagged1, Notch1, and Hes5 (**Figure 1I**) and protein of Jagged1, Notch1, NICD, and Hes1 (**Figures 2A,C**) in the diabetic group (P < 0.05).

Larger Cerebral Infarction, Severer Brain Edema and Poorer Neurological Function in T2DM

Compared with NS group, NDI group had larger cerebral infarction and severer brain edema (p < 0.01), while DI group had larger cerebral infarction (p < 0.05) and brain edema (p < 0.001) than NDI group (**Figures 3A,B**). In the Garcia test, NDI group scored significantly lower than NS group from days 1

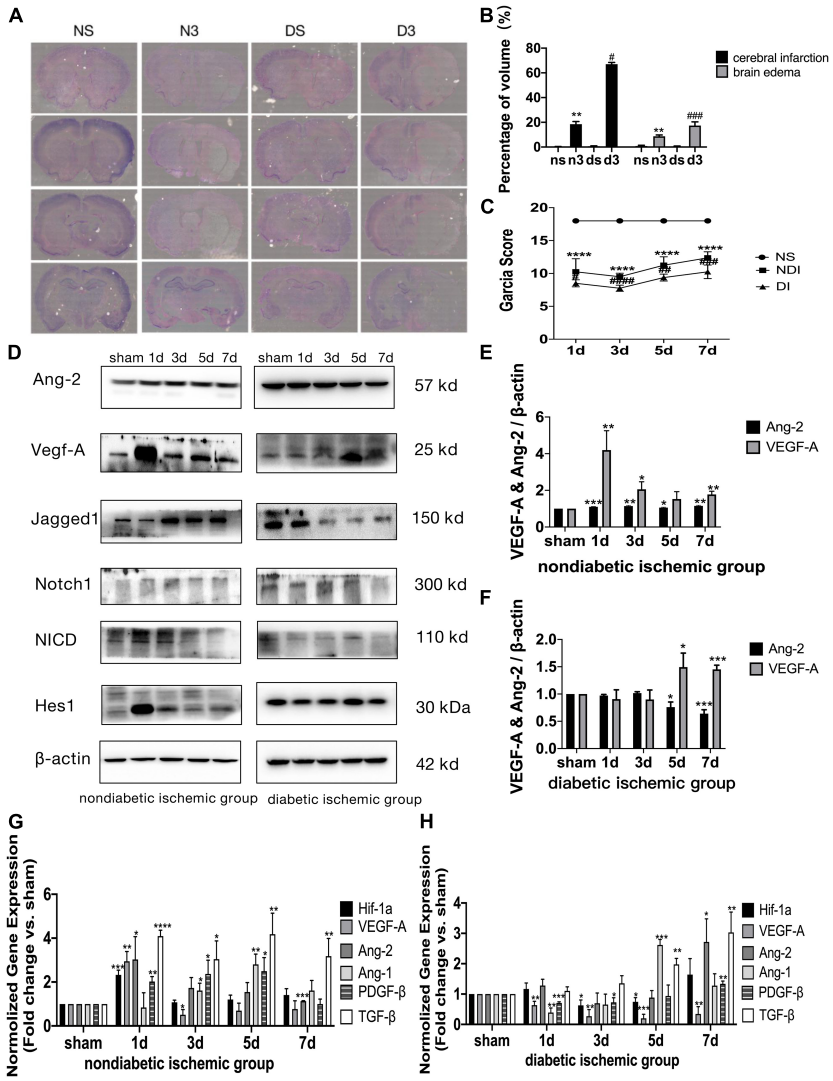

FIGURE 3 | Delayed angiogenesis after acute ischemic stroke in T2DM. **(A)** Cresyl violet (CV) staining on day 3. NS, non-diabetic sham group (Day 3); N3, non-diabetic cerebral ischemic group (Day 3); DS, diabetic sham group (Day 3); D3, diabetic cerebral ischemic group (Day 3). The unstained area was the infarction area. **(B)** The volume of cerebral infarction and brain edema was calculated by CV staining on day 3. **(C)** Garcia score was evaluated on D1–D7 after cerebral ischemia (n = 8 per group). **(D)** The expression of VEGF-A, Ang-2, Jagged1, Notch1, NICD, and Hes1 in ischemic penumbra was assessed by Western blot (n = 3 per group). **(E,F)** The expression of VEGF-A and Ang-2 protein were calculated in NDI group and DI group. **(G,H)** The gene expression of Hif-1a, VEGF-A, Ang-2, Ang-1, TGF-β, and PDGF-β was showed in NDI group and DI group. $^{*}p < 0.05$ vs. sham group, $^{**}p < 0.01$ vs. sham group, $^{***}p < 0.001$ vs. sham group, $^{****}p < 0.0001$ vs. sham group; $^{\#}p < 0.05$ vs. NDI group, $^{\#\#}p < 0.01$ vs. NDI group, $^{\#\#\#}p < 0.001$ vs. NDI group, $^{\#\#\#\#}p < 0.0001$ vs. NDI group.

to 7 ($p < 0.0001$), while DI group scored significantly lower than NDI group ($p < 0.05$) (**Figure 3C**).

Delayed Angiogenesis After Acute Ischemic Stroke in T2DM

At D1 after ischemic stroke, EC proliferation was significantly detected in NDI group, while there wasn't a significant increase until D7 in DI group (**Figures 4A–C**). Meanwhile, Ang-2, Ang-1, TGF-β, and PDGF-β mRNA levels weren't increased until D7 in DI group compared with DS group (**Figure 3H**). In contrast, at D1 after ischemic stroke, Hif-1a, VEGF-A, Ang-2, TGF-β, and PDGF-β mRNA were significantly increased in NDI group compared with NS group (**Figure 3G**). Similar changes exist in the protein expression of VEGF-A and Ang-2 in two groups (**Figures 3D–F**).

Suppressed Jagged1-Notch1 Signaling With Hampered Angiogenesis After Acute Ischemic Stroke in T2DM

The expression of Jagged1 and Notch 1 was significantly upregulated on ECS in the peri-infarct region of NDI group at D1 than the sham group (**Figures 5A**, **6A**) ($P < 0.05$). Moreover, Hes1, a downstream target of Notch1, was expressed on ECS

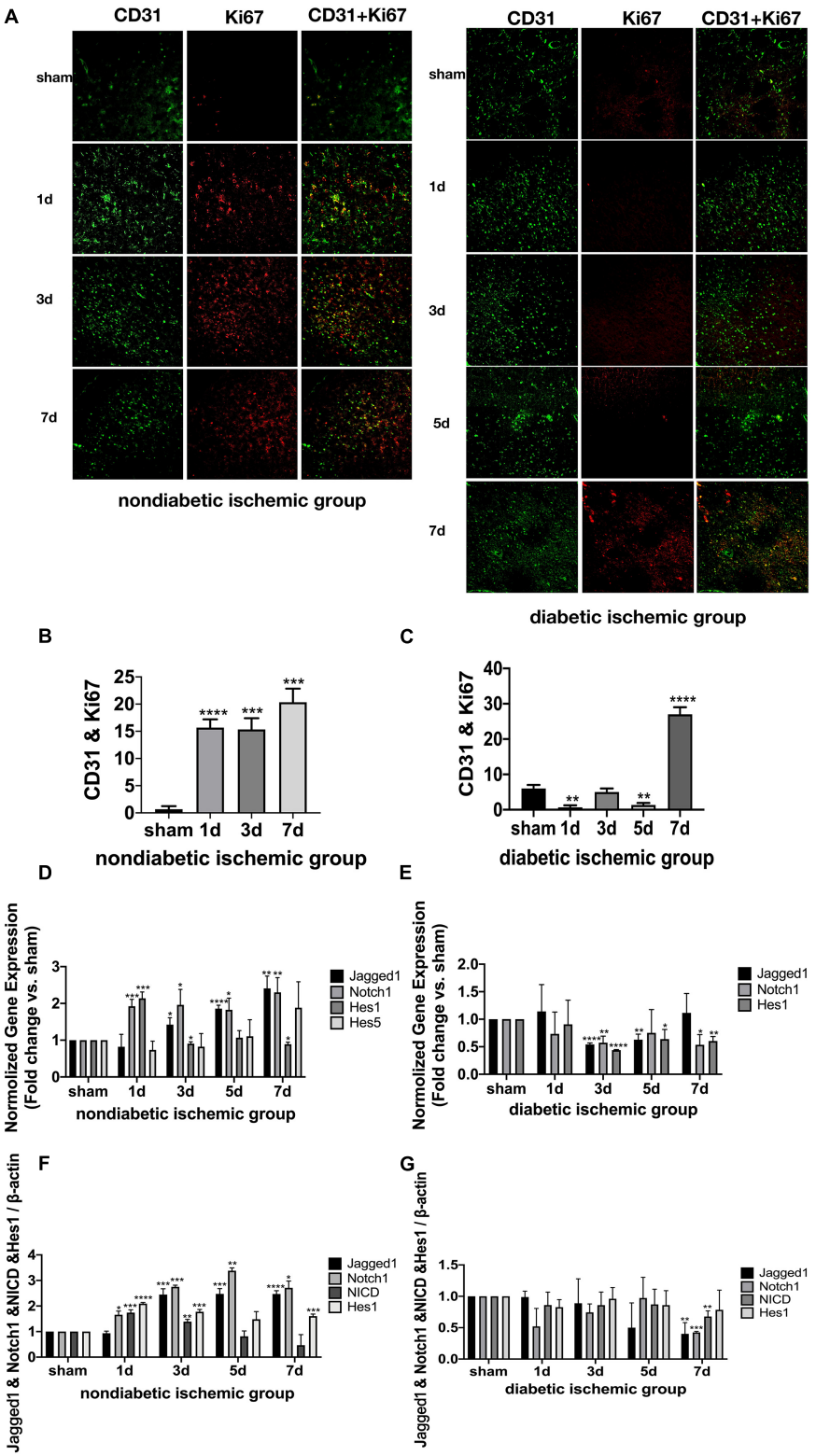

FIGURE 4 | Suppressed Jagged1-Notch1 signaling with hampered angiogenesis after acute ischemic stroke in T2DM. **(A–C)** The expression of Ki67 and CD31 was assessed by immunofluorescence staining in ischemic penumbra (Magnification * 200. Scale bar = 100 μm) and the positive cells of Ki67 and CD31 were calculated (n = 3 per group). **(D,E)** The gene expression of Jagged1, Notch1, Hes1, and Hes5 was showed in NDI and DI group. **(F,G)** The expression of Jagged1, Notch1, NICD, and Hes1 protein were calculated in NDI group and DI group. *$p < 0.05$ vs. sham group, **$p < 0.01$ vs. sham group, ***$p < 0.001$ vs. sham group, ****$p < 0.0001$ vs. sham group.

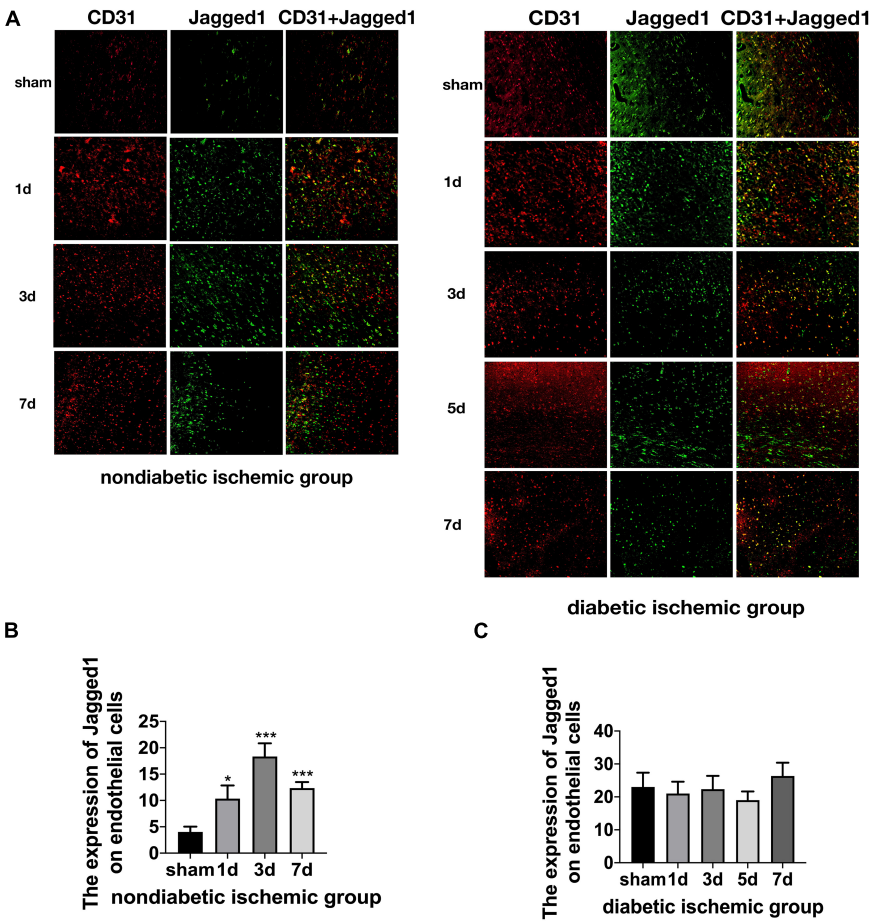

FIGURE 5 | Suppressed Jagged1-Notch1 signaling after acute ischemic stroke in T2DM. **(A–C)** The expression of Jagged1 and CD31 was assessed by immunofluorescence staining in ischemic penumbra (Magnification ×200. Scale bar = 100 μm) and the positive cells of Jagged1 and CD31 were calculated (n = 3 per group). *$p < 0.05$ vs. sham group, ***$p < 0.001$ vs. sham group.

in NDI group at D1, but rarely detected in the sham group (**Figure 7A**) ($P < 0.01$). However, the expression of Jagged1, Notch1, and Hes1 on ECS failed to elevate in DI group compared with DS group (**Figures 5–7**). In addition, qPCR (**Figures 4D,E**) and western blot (**Figure 3D**) revealed that after ischemic stroke, the expression of Notch1, Jagged1, and Hes1 mRNA (**Figure 4D**) and Notch1, Jagged1, NICD, and HES1 protein (**Figures 3D**, **4F**) was significantly increased at D1 and D3 in NDI group. In contrast, the expression of the Jagged1-Notch1 signaling pathway was not upregulated in diabetic group (**Figures 3D**, **4E,G**).

DISCUSSION

In the present study, we provided novel evidence of increased yet dysfunctional baseline neovascularization in the cerebrovasculature of HFD/STZ rats accompanying with the activated Jagged1-Notch1 signaling. Furthermore, we observed delayed angiogenesis after cerebral ischemia as well as suppressed Jagged1-Notch1 signaling in T2DM rats compared with non-diabetic rats.

The impact of diabetes on cerebral vasculature has not been investigated until recent years (Li et al., 2010; Prakash et al., 2012, 2013a) and various models of diabetes have been utilized. There is enhanced arteriogenesis and angiogenesis in the brain of GK rats (Li et al., 2010). Similar changes were observed in another model of T2DM, db/db mice (Prakash et al., 2013a). Our study focused on a unique T2DM model—HFD/STZ rats, an animal model not predominantly genetically determined. This model combines HFD and pancreatic β-cell toxin STZ (Reed et al., 2000), making it a more suitable animal model because it can not only mimic the natural history of T2DM but include the large heterogeneity which commonly exists in human population. We found that in HFD/STZ rats, there was enhanced baseline neovascularization in the cerebrovasculature, which is similar to other reports (Li et al., 2010; Prakash et al., 2012, 2013a). The fact that these animal models of T2DM are made from various strains with different disease duration evidently indicates that T2DM has a broad impact on the microvasculature of the brain.

Our study examined the expression of Hif-1a and VEGF-A in the cortex of diabetic group and non-diabetic controls. While physiologic angiogenesis depends on a tightly

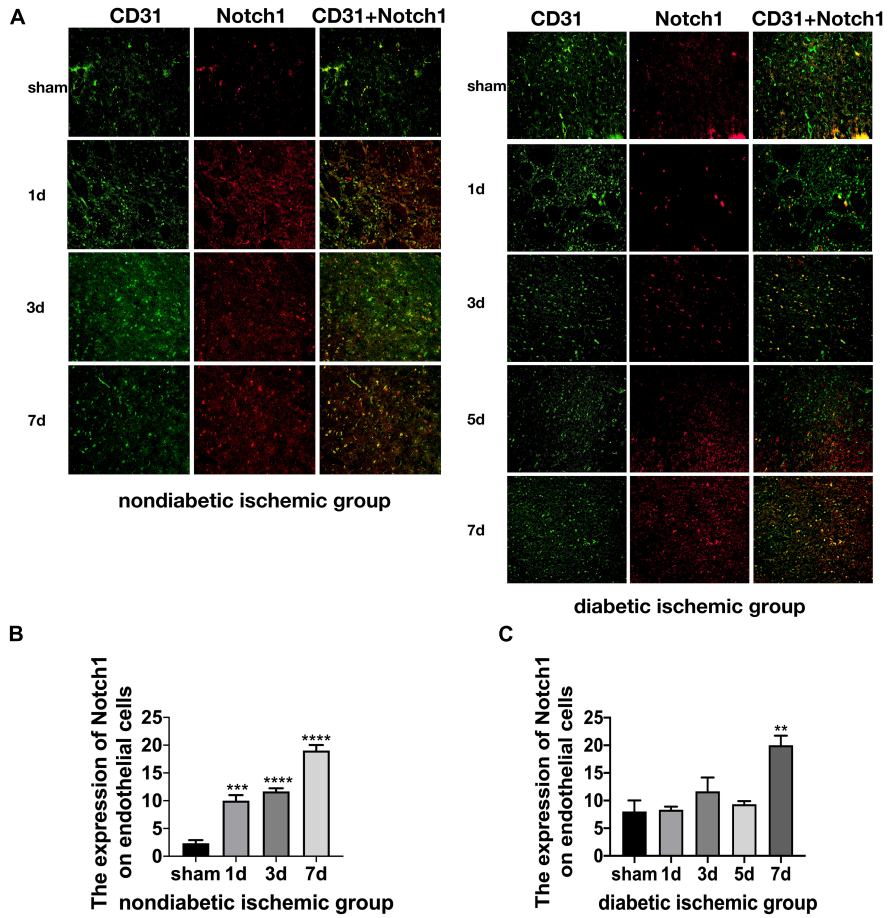

FIGURE 6 | Suppressed Jagged1-Notch1 signaling after acute ischemic stroke in T2DM. **(A–C)** The expression of Notch1 and CD31 was assessed by immunofluorescence staining in ischemic penumbra (Magnification ×200. Scale bar = 100 μm) and the positive cells of Notch1 and CD31 were calculated (n = 3 per group). $^{**}p < 0.01$ vs. sham group, $^{***}p < 0.001$ vs. sham group, $^{****}p < 0.0001$ vs. sham group.

coordinated balance between considerable anti-angiogenic and pro-angiogenic factors, it is well recognized that VEGF-A plays a pivotal role in this equilibrium (Ferrara, 2004). Substantial evidence also implicates VEGF as a mediator of pathological angiogenesis in diabetic retinopathy (Nakagawa et al., 2009; Wang et al., 2009; Advani and Gilbert, 2012). Furtherly, Hif-1 has been proposed to be a major stimulus to the activation of VEGF gene transcription (Forsythe et al., 1996). In our study, we found increased levels of both Hif-1a and VEGF-A in diabetes, which may imply that in diabetes early vascular dysfunction and decreased blood flow (Kelly-Cobbs et al., 2012) generate a hypoxic milieu that may be the initial incentive for enhanced cerebral microvasculature.

Except for Hif-1a/VEGF levels, an intact neovascularization process is controlled by the delicate balance between proangiogenic growth factors (VEGF-A and Ang-2) and stabilization and maturation factors (TGF-β, Ang-1, and PDGF-β) which is crucial to the blood vessel stabilization. The increased ratio of Ang-2/Ang-1 was found to be related to pro-angiogenic activity (Watanabe et al., 2005) and immature nature of vasculature (Pfister et al., 2010) in diabetic retinopathy. Meanwhile, increased Ang-2 but reduced Ang-1 expression may contribute to cerebral vascular damage after stroke in T2DM mice (Cui et al., 2011). In our study, we have shown that prior to cerebral ischemia, VEGF-A mRNA and Ang-2 mRNA were significantly increased in the cortex in the diabetic group compared with the non-diabetic group, while mRNAs for Ang-1, TGF-β, and PDGF-β were slightly increased, which may suggest the brain microvasculature in diabetic rat is immature. This is in conformity with another model of T2DM, the GK rat, in which augmented cerebral microvasculature was related to poor vascular mural maturity as revealed by less pericyte support and more non-perfused new vessel formation (Prakash et al., 2012). Interestingly, increased cerebral microvasculature of a mice model of type 1 diabetes with a longer duration is immature with a decrease in VEGF-A, Ang-1, PDGF-β, and TGF-β mRNA levels (Poittevin et al., 2015), which is in contrast to our findings. In our study, increased yet immature microvessels was accompanied by the upregulation of VEGF-A and Ang-2 mRNA and protein levels. Several factors including the different animal models of diabetes, the specific strains, and the severity of diabetes may explain the distinctions between the two studies.

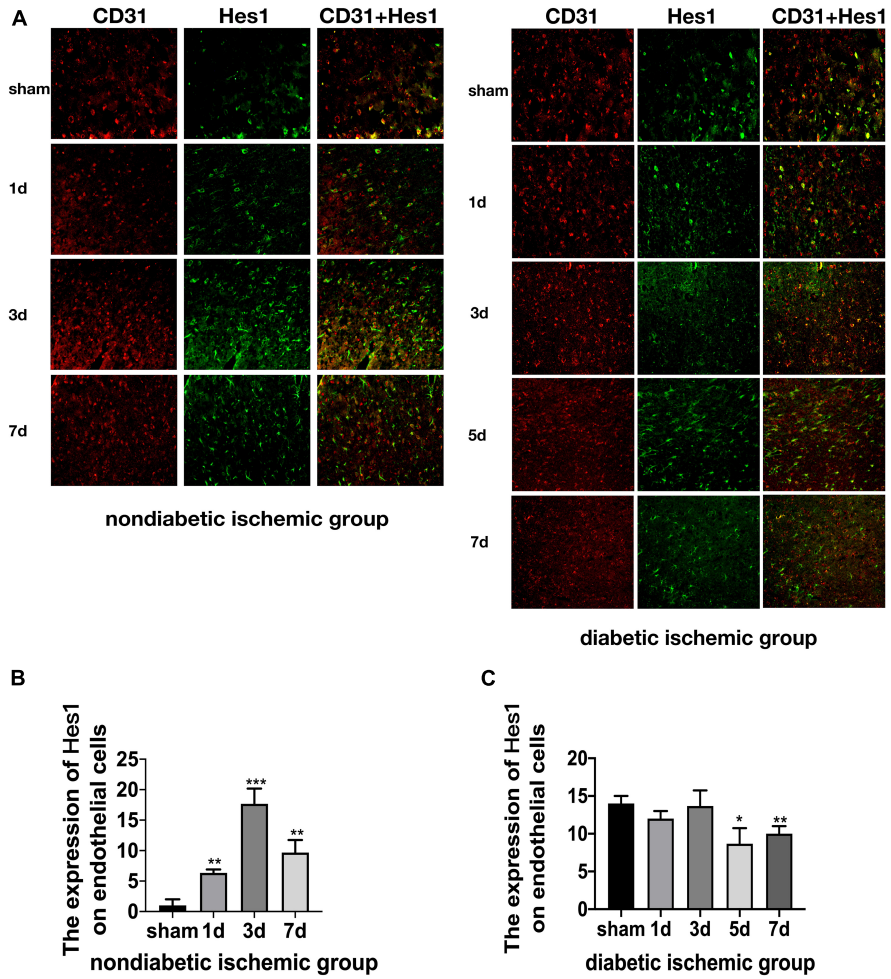

FIGURE 7 | Suppressed Jagged1-Notch1 signaling after acute ischemic stroke in T2DM. **(A–C)** The expression of Hes1 and CD31 was assessed by immunofluorescence staining in ischemic penumbra (Magnification ×200. Scale bar = 100 μm) and the positive cells of Hes1 and CD31 were calculated (n = 3 per group). *p < 0.05 vs. sham group, **p < 0.01 vs. sham group, ***p < 0.001 vs. sham group.

During acute ischemic stroke, insufficient blood flow to the brain and the poor tissue oxygen tension often results in reparative neovascularization in order to attend the instant needs of brain high metabolism. It is evident that numerous proangiogenic growth factors are upregulated as early as hours after the onset of cerebral ischemia in rodents (Hayashi et al., 2003). In our study, we have shown that at D1 after cerebral ischemia, there was a significant upregulation of VEGF-A, Ang-2, TGF-β, and PDGF-β mRNA in NDI group compared with NS group. Moreover, it has been reported that poststroke triggered angiogenesis leads to increased vessel density from D1 to D21 (Hayashi et al., 2003). In the current study, EC proliferation was significantly observed in the NDI group from D1 to D7, which is also consistent with the above previous study. And we know that there was a significant correlation between the number of blood vessels in the peri-infarct regions and survival time (Krupinski et al., 1993, 1994), indicating that angiogenesis stimulation may have a beneficial effect on the damaged brain after ischemic stroke. However, we observed that diabetes impaired the recovery process by delaying angiogenesis after stroke, which is similar with the type 1 diabetes model (Poittevin et al., 2015). In our study, Ang-2, Ang-1, TGF-β, and PDGF-β mRNA levels were not increased until D7 in DI group compared with DS group. VEGF-A and Ang-2 protein followed the same time course. Furthermore, there wasn't a significant increase of ECs until D7 in DI group, which is consistent with a previous study where while control animals displayed reparative neovascularization in both ischemic and non-ischemic hemispheres compared with the sham group, vascular density in the peri-infarct area was significantly reduced in diabetes mellitus (Prakash et al., 2013b). Collectively, impaired angiogenesis after cerebral ischemia in diabetic models may underlie why T2DM aggravates the ischemic brain injury.

The mechanisms of how diabetes leads to the dysfunctional neovascularization and impaired repair process after stroke are unclear and likely to contribute to assorted factors. Here we examined if the Jagged1-Notch1 pathway is involved in the impaired angiogenesis in diabetes. Accumulating evidences

in vascular biosciences has shown that intrinsic signaling interactions between ECs play vital roles in the physiology and pathology of blood vessels (Potente et al., 2011). Furthermore, the movement of a single EC integrated into the vascular morphology is regulated by these intercellular signaling (Arima et al., 2011). Notch receptors and their ligands, delta-like ligand 4 (Dll4), and Jagged1, underlie the dynamic and transient regulation. Dll4-Notch1 signaling between neighboring ECs within the sprouting angiogenesis serves to restrict tip-cell formation in adjacent (stalk) ECs (Hellström et al., 2007). The vessel-stabilizing activity of the Dll4-Notch1 interaction is antagonized by Jagged1, which is proangiogenic and functions by downregulating Dll4-Notch1 signaling and leads to the excessive but immature vessel plexus (Benedito et al., 2009). In our study, numbers of $Notch1^{+}CD31^{+}$, $Jagged1^{+}CD31^{+}$ cells, and $Hes1CD31^{+}$ cells were significantly increased in the diabetic group compared with the non-diabetic group. In addition, the mRNA of Jagged1, Notch1 and Hes5 and protein of Jagged1, Notch1, NICD, and Hes1 were increased in the diabetic group. Based on that, we have discovered that Jagged1-Notch1 signaling in adult rat was activated in diabetes mellitus associated with enhanced yet maybe immature cerebral neovascularization, a potentially novel mechanism of cerebral microvascular complications of diabetes. Intrudingly, when these diabetic rats were subjected to ischemic stroke, the Jagged1-Notch1 signaling pathway couldn't be further stimulated by the ischemic event while it has been activated in the non-diabetic ischemic group (Ren et al., 2018). Our study has shown that after ischemic stroke the expression of Notch1, Jagged1 and HES1 on ECs at D1, D3, and D7 in NDI group was significantly increased, while in DI group, the expressions of Notch1, Jagged1, and Hes1 in the peri-infarct region were not increased where there was delayed angiogenesis at acute phase. Therefore, although the causality cannot be strictly verified, we highly suspect that the baseline cerebral microvasculopathy and activated Jagged1-Notch1 signaling in T2DM before ischemic stroke is at least partly responsible for the delayed angiogenesis as well as suppressed Jagged1-Notch1 signaling which cannot be further stimulated after pMCAO.

There are a few limitations in this study. Firstly, we chose to develop a chronic induced T2DM rat model in order to better mimic clinical pathology yet with confounding factors. However, since dyslipidemia is also responsible for vascular impairment (Zechariah et al., 2013), it might be difficult to attribute the microvascular impairment solely to hyperglycemia. Secondly, although HFD/STZ induction is a recognized model of T2DM, it cannot totally involve the complex pathophysiology observed in T2DM patients. Furthermore, whether there is a causal relationship between the impaired cerebral microvasculature and altered Jagged1-Notch1 signaling pathway needs to be further verified.

In conclusion, our study investigated the cerebral microvascular impairment before and after ischemic stroke in T2DM rats and the altered expression of Jagged1-Notch1 signaling pathway, a potentially novel mechanism of diabetes-related cerebral microvasculature dysfunction. Our findings may provide a basis for the development of novel treatment as management of diabetic stroke patients.

DATA AVAILABILITY STATEMENT

The datasets presented in this study can be found in online repositories. The names of the repository/repositories and accession number(s) can be found in the article/ **Supplementary Material**.

ETHICS STATEMENT

The animal study was reviewed and approved by the guidelines of animal care and use established by Shanghai Fudan University.

AUTHOR CONTRIBUTIONS

XQW, WF, and HFB conceived and designed the experiments. ZHG, JJ, YLT, CJ, CG, and FFS performed the experiments. ZHG and XQW wrote the manuscript. All authors confirm that they are the original contributors of this work and approved it for its submission.

FUNDING

This work was supported by project grants from the National Natural Science Foundation of China (Grant No. 81901313).

ACKNOWLEDGMENTS

We thank other lab members for their continued help and support.

SUPPLEMENTARY MATERIAL

The Supplementary Material for this article can be found online at: https://www.frontiersin.org/articles/10.3389/fphys.2021.687947/full#supplementary-material

REFERENCES

Advani, A., and Gilbert, R. E. (2012). The endothelium in diabetic nephropathy. *Semin. Nephrol.* 32, 199–207. doi: 10.1016/j.semnephrol.2012.02.006

Arima, S., Nishiyama, K., Ko, T., Arima, Y., Hakozaki, Y., Sugihara, K., et al. (2011). Angiogenic morphogenesis driven by dynamic and heterogeneous collective endothelial cell movement. *Development* 138, 4763–4776. doi: 10.1242/dev.068023

Ashwal, S., Tone, B., Tian, H. R., Cole, D. J., and Pearce, W. J. (1998). Core and penumbral nitric oxide synthase activity during cerebral ischemia and reperfusion. *Stroke* 29, 1037–1046;discussion 1047.

Benedito, R., Roca, C., Sörensen, I., Adams, S., Gossler, A., Fruttiger, M., et al. (2009). The notch ligands Dll4 and Jagged1 have opposing effects on angiogenesis. *Cell* 137, 1124–1135. doi: 10.1016/j.cell.2009.03.025

Cannon, A., Handelsman, Y., Heile, M., and Shannon, M. (2018). Burden of illness in type 2 diabetes mellitus. *J. Manag. Care Spec. Pharm.* 24(9–a Suppl.), S5–S13. doi: 10.18553/jmcp.2018.24.9-a.s5

Cui, X., Chopp, M., Zacharek, A., Ye, X., Roberts, C., and Chen, J. (2011). Angiopoietin/Tie2 pathway mediates type 2 diabetes induced vascular damage after cerebral stroke. *Neurobiol. Dis.* 43, 285–292. doi: 10.1016/j.nbd.2011.04.005

Cui, Y., Liang, X., Gu, H., Hu, Y., Zhao, Z., Yang, X. Y., et al. (2017). Cerebral perfusion alterations in type 2 diabetes and its relation to insulin resistance and cognitive dysfunction. *Brain Imaging Behav.* 11, 1248–1257. doi: 10.1007/s11682-016-9583-9

Ergul, A., Elgebaly, M. M., Middlemore, M. L., Li, W., Elewa, H., Switzer, J. A., et al. (2007). Increased hemorrhagic transformation and altered infarct size and localization after experimental stroke in a rat model type 2 diabetes. *BMC Neurol.* 7:33. doi: 10.1186/1471-2377-7-33

Ferrara, N. (2004). Vascular endothelial growth factor: basic science and clinical progress. *Endocr. Rev.* 25, 581–611. doi: 10.1210/er.2003-0027

Forsythe, J. A., Jiang, B. H., Iyer, N. V., Agani, F., Leung, S. W., Koos, R. D., et al. (1996). Activation of vascular endothelial growth factor gene transcription by hypoxia-inducible factor 1. *Mol. Cell Biol.* 16, 4604–4613. doi: 10.1128/mcb.16.9.4604

Garcia, J. H., Wagner, S., Liu, K. F., and Hu, X. J. (1995). Neurological deficit and extent of neuronal necrosis attributable to middle cerebral artery occlusion in rats. statistical validation. *Stroke* 26, 627–634;discussion635. doi: 10.1161/01.str.26.4.627

Gheibi, S., Kashfi, K., and Ghasemi, A. (2017). A practical guide for induction of type-2 diabetes in rat: incorporating a high-fat diet and streptozotocin. *Biomed. Pharmacother.* 95, 605–613. doi: 10.1016/j.biopha.2017.08.098

Guo, Z., Wu, X., and Fan, W. (2021). Clarifying the effects of diabetes on the cerebral circulation: implications for stroke recovery and beyond. *Brain Res. Bull.* 171, 67–74. doi: 10.1016/j.brainresbull.2021.02.025

Hayashi, T., Noshita, N., Sugawara, T., and Chan, P. H. (2003). Temporal profile of angiogenesis and expression of related genes in the brain after ischemia. *J. Cereb. Blood Flow Metab.* 23, 166–180. doi: 10.1097/01.Wcb.0000041283.53351.Cb

Hellström, M., Phng, L. K., Hofmann, J. J., Wallgard, E., Coultas, L., Lindblom, P., et al. (2007). Dll4 signalling through Notch1 regulates formation of tip cells during angiogenesis. *Nature* 445, 776–780. doi: 10.1038/nature05571

Kelly-Cobbs, A. I., Prakash, R., Coucha, M., Knight, R. A., Li, W., Ogbi, S. N., et al. (2012). Cerebral myogenic reactivity and blood flow in type 2 diabetic rats: role of peroxynitrite in hypoxia-mediated loss of myogenic tone. *J. Pharmacol. Exp. Ther.* 342, 407–415. doi: 10.1124/jpet.111.191296

Krupinski, J., Kaluza, J., Kumar, P., Kumar, S., and Wang, J. M. (1994). Role of angiogenesis in patients with cerebral ischemic stroke. *Stroke* 25, 1794–1798. doi: 10.1161/01.str.25.9.1794

Krupinski, J., Kaluza, J., Kumar, P., Wang, M., and Kumar, S. (1993). Prognostic value of blood vessel density in ischaemic stroke. *Lancet* 342:742. doi: 10.1016/0140-6736(93)91734-4

Last, D., Alsop, D. C., Abduljalil, A. M., Marquis, R. P., de Bazelaire, C., Hu, K., et al. (2007). Global and regional effects of type 2 diabetes on brain tissue volumes and cerebral vasoreactivity. *Diabetes Care* 30, 1193–1199. doi: 10.2337/dc06-2052

Li, W., Prakash, R., Kelly-Cobbs, A. I., Ogbi, S., Kozak, A., El-Remessy, A. B., et al. (2010). Adaptive cerebral neovascularization in a model of type 2 diabetes: relevance to focal cerebral ischemia. *Diabetes* 59, 228–235. doi: 10.2337/db09-0902

Megherbi, S. E., Milan, C., Minier, D., Couvreur, G., Osseby, G. V., Tilling, K., et al. (2003). Association between diabetes and stroke subtype on survival and functional outcome 3 months after stroke: data from the European BIOMED Stroke Project. *Stroke* 34, 688–694. doi: 10.1161/01.Str.0000057975.15221.40

Nakagawa, T., Kosugi, T., Haneda, M., Rivard, C. J., and Long, D. A. (2009). Abnormal angiogenesis in diabetic nephropathy. *Diabetes* 58, 1471–1478. doi: 10.2337/db09-0119

Palacio, S., McClure, L. A., Benavente, O. R., Bazan, C. III, Pergola, P., and Hart, R. G. (2014). Lacunar strokes in patients with diabetes mellitus: risk factors, infarct location, and prognosis: the secondary prevention of small subcortical strokes study. *Stroke* 45, 2689–2694. doi: 10.1161/strokeaha.114.005018

Pan, Y., Wang, Y., Li, H., Gaisano, H. Y., Wang, Y., and He, Y. (2016). Association of diabetes and prognosis of minor stroke and its subtypes: a prospective observational study. *PLoS One* 11:e0153178. doi: 10.1371/journal.pone.0153178

Pfister, F., Wang, Y., Schreiter, K., vom Hagen, F., Altvater, K., Hoffmann, S., et al. (2010). Retinal overexpression of angiopoietin-2 mimics diabetic retinopathy and enhances vascular damages in hyperglycemia. *Acta Diabetol.* 47, 59–64. doi: 10.1007/s00592-009-0099-2

Phng, L. K., and Gerhardt, H. (2009). Angiogenesis: a team effort coordinated by notch. *Dev. Cell* 16, 196–208. doi: 10.1016/j.devcel.2009.01.015

Poittevin, M., Bonnin, P., Pimpie, C., Riviere, L., Sebrie, C., Dohan, A., et al. (2015). Diabetic microangiopathy: impact of impaired cerebral vasoreactivity and delayed angiogenesis after permanent middle cerebral artery occlusion on stroke damage and cerebral repair in mice. *Diabetes* 64, 999–1010. doi: 10.2337/db14-0759

Potente, M., Gerhardt, H., and Carmeliet, P. (2011). Basic and therapeutic aspects of angiogenesis. *Cell* 146, 873–887. doi: 10.1016/j.cell.2011.08.039

Prakash, R., Johnson, M., Fagan, S. C., and Ergul, A. (2013a). Cerebral neovascularization and remodeling patterns in two different models of type 2 diabetes. *PLoS One* 8:e56264. doi: 10.1371/journal.pone.0056264

Prakash, R., Li, W., Qu, Z., Johnson, M. A., Fagan, S. C., and Ergul, A. (2013b). Vascularization pattern after ischemic stroke is different in control versus diabetic rats: relevance to stroke recovery. *Stroke* 44, 2875–2882. doi: 10.1161/strokeaha.113.001660

Prakash, R., Somanath, P. R., El-Remessy, A. B., Kelly-Cobbs, A., Stern, J. E., Dore-Duffy, P., et al. (2012). Enhanced cerebral but not peripheral angiogenesis in the Goto-Kakizaki model of type 2 diabetes involves VEGF and peroxynitrite signaling. *Diabetes* 61, 1533–1542. doi: 10.2337/db11-1528

Reed, M. J., Meszaros, K., Entes, L. J., Claypool, M. D., Pinkett, J. G., Gadbois, T. M., et al. (2000). A new rat model of type 2 diabetes: the fat-fed, streptozotocin-treated rat. *Metabolism* 49, 1390–1394. doi: 10.1053/meta.2000.17721

Ren, C., Yao, Y., Han, R., Huang, Q., Li, H., Wang, B., et al. (2018). Cerebral ischemia induces angiogenesis in the peri-infarct regions via Notch1 signaling activation. *Exp. Neurol.* 304, 30–40. doi: 10.1016/j.expneurol.2018.02.013

Saeedi, P., Petersohn, I., Salpea, P., Malanda, B., Karuranga, S., Unwin, N., et al. (2019). Global and regional diabetes prevalence estimates for 2019 and projections for 2030 and 2045: results from the international diabetes federation diabetes Atlas, 9(th) edition. *Diabetes Res. Clin. Pract.* 157:107843. doi: 10.1016/j.diabres.2019.107843

Sima, A. A. (2010). Encephalopathies: the emerging diabetic complications. *Acta Diabetol.* 47, 279–293. doi: 10.1007/s00592-010-0218-0

Srinivasan, K., Viswanad, B., Asrat, L., Kaul, C. L., and Ramarao, P. (2005). Combination of high-fat diet-fed and low-dose streptozotocin-treated rat: a model for type 2 diabetes and pharmacological screening. *Pharmacol. Res.* 52, 313–320. doi: 10.1016/j.phrs.2005.05.004

Swanson, R. A., Morton, M. T., Tsao-Wu, G., Savalos, R. A., Davidson, C., and Sharp, F. R. (1990). A semiautomated method for measuring brain infarct volume. *J. Cereb. Blood Flow Metab.* 10, 290–293. doi: 10.1038/jcbfm.1990.47

Tu, Y., Guo, C., Song, F., Huo, Y., Geng, Y., Guo, M., et al. (2019). Mild hypothermia alleviates diabetes aggravated cerebral ischemic injury via activating autophagy and inhibiting pyroptosis. *Brain Res. Bull.* 150, 1–12. doi: 10.1016/j.brainresbull.2019.05.003

Tun, N. N., Arunagirinathan, G., Munshi, S. K., and Pappachan, J. M. (2017). Diabetes mellitus and stroke: a clinical update. *World J. Diabetes* 8, 235–248. doi: 10.4239/wjd.v8.i6.235

van Sloten, T. T., Sedaghat, S., Carnethon, M. R., Launer, L. J., and Stehouwer, C. D. A. (2020). Cerebral microvascular complications of type 2 diabetes: stroke, cognitive dysfunction, and depression. *Lancet Diabetes Endocrinol.* 8, 325–336. doi: 10.1016/s2213-8587(19)30405-x

Wang, X., Wang, G., and Wang, Y. (2009). Intravitreous vascular endothelial growth factor and hypoxia-inducible factor 1a in patients with proliferative diabetic retinopathy. *Am. J. Ophthalmol.* 148, 883–889. doi: 10.1016/j.ajo.2009.07.007

Wardlaw, J. M., Smith, C., and Dichgans, M. (2019). Small vessel disease: mechanisms and clinical implications. *Lancet Neurol.* 18, 684–696. doi: 10.1016/s1474-4422(19)30079-1

Watanabe, D., Suzuma, K., Suzuma, I., Ohashi, H., Ojima, T., Kurimoto, M., et al. (2005). Vitreous levels of angiopoietin 2 and vascular endothelial growth factor in patients with proliferative diabetic retinopathy. *Am. J. Ophthalmol.* 139, 476–481. doi: 10.1016/j.ajo.2004.10.004

Ye, X., Chopp, M., Cui, X., Zacharek, A., Cui, Y., Yan, T., et al. (2011). Niaspan enhances vascular remodeling after stroke in type 1 diabetic rats. *Exp. Neurol.* 232, 299–308. doi: 10.1016/j.expneurol.2011.09.022

Yoon, C. H., Choi, Y. E., Cha, Y. R., Koh, S. J., Choi, J. I., Kim, T. W., et al. (2016). Diabetes-induced jagged1 overexpression in endothelial cells causes retinal capillary regression in a murine model of diabetes mellitus: insights into diabetic retinopathy. *Circulation* 134, 233–247. doi: 10.1161/circulationaha.116.014411

Yu, X., Xu, X., Jackson, A., Sun, J., Huang, P., Mao, Y., et al. (2016). Blood Brain barrier disruption in diabetic stroke related to unfavorable outcome. *Cerebrovasc. Dis.* 42, 49–56. doi: 10.1159/000444809

Zechariah, A., ElAli, A., Hagemann, N., Jin, F., Doeppner, T. R., Helfrich, I., et al. (2013). Hyperlipidemia attenuates vascular endothelial growth factor-induced angiogenesis, impairs cerebral blood flow, and disturbs stroke recovery via decreased pericyte coverage of brain endothelial cells. *Arterioscler. Thromb. Vasc. Biol.* 33, 1561–1567. doi: 10.1161/atvbaha.112.300749

Zhu, M., Bi, X., Jia, Q., and Shangguan, S. (2010). The possible mechanism for impaired angiogenesis after transient focal ischemia in type 2 diabetic GK rats: different expressions of angiostatin and vascular endothelial growth factor. *Biomed. Pharmacother.* 64, 208–213. doi: 10.1016/j.biopha.2009.08.005

Conflict of Interest: The authors declare that the research was conducted in the absence of any commercial or financial relationships that could be construed as a potential conflict of interest.

frontiers in Physiology

ORIGINAL RESEARCH
published: 22 July 2021
doi: 10.3389/fphys.2021.696163

Serum Adropin as a Potential Biomarker for Predicting the Development of Type 2 Diabetes Mellitus in Individuals With Metabolic Dysfunction-Associated Fatty Liver Disease

Na Li[1], Guomin Xie[2,3], Biao Zhou[4], Aijuan Qu[2,3], Hua Meng[4], Jia Liu[1]* and Guang Wang[1]**

[1] Department of Endocrinology, Beijing Chao-Yang Hospital, Capital Medical University, Beijing, China, [2] Department of Physiology and Pathophysiology, School of Basic Medical Sciences, Capital Medical University, Beijing, China, [3] Key Laboratory of Remodeling-Related Cardiovascular Diseases, Ministry of Education, Beijing, China, [4] General Surgery Department and Obesity and Metabolic Disease Center, China-Japan Friendship Hospital, Beijing, China

OPEN ACCESS

Edited by:
Dechun Feng,
National Institute on Alcohol Abuse and Alcoholism (NIAAA), United States

Reviewed by:
Grace L. Guo,
Rutgers, The State University of New Jersey, United States
Huichang Bi,
Sun Yat-Sen University, China

***Correspondence:**
Guang Wang
drwg6688@126.com
Jia Liu
liujia0116@126.com
Hua Meng
menghuade@hotmail.com

Specialty section:
This article was submitted to Clinical and Translational Physiology, a section of the journal Frontiers in Physiology

Received: 16 April 2021
Accepted: 29 June 2021
Published: 22 July 2021

Citation:
Li N, Xie G, Zhou B, Qu A, Meng H, Liu J and Wang G (2021) Serum Adropin as a Potential Biomarker for Predicting the Development of Type 2 Diabetes Mellitus in Individuals With Metabolic Dysfunction-Associated Fatty Liver Disease. Front. Physiol. 12:696163. doi: 10.3389/fphys.2021.696163

Background: Adropin, a peptide translated from the *Energy Homeostasis Associated gene* (*ENHO*), was mainly expressed in the liver and was a regulator in metabolic and energy homeostasis. This study aims to investigate the correlation between adropin and histological characteristics of the liver, and the clinical relevance of adropin in patients with metabolic dysfunction-associated fatty liver disease (MAFLD).

Methods: A total of 62 subjects, including 32 healthy controls and 30 MAFLD patients, were enrolled in this case-control study. The MAFLD patients were further divided into two subgroups, including NGT-M group and T2DM-M group. Serum adropin levels, metabolic parameters and intrahepatic lipids, the liver *ENHO* mRNA expressions and histological characteristics were investigated.

Results: MAFLD patients showed significantly lower circulating adropin compared with healthy controls (2.02 ± 2.92 vs. 5.52 ± 0.65 ng/mL, $P < 0.0001$). Subgroup analysis exhibited dramatically declined serum adropin levels in T2DM-M patients compared with NGT-M group (0.51 ± 0.73 vs. 4.00 ± 3.52 ng/mL, $P < 0.001$). H&E and Oil Red O staining show exacerbated steatohepatitis in T2DM-M patients in contrast with NGT-M group. Furthermore, serum adropin concentrations were negatively correlated with intrahepatic triglyceride (TG), total cholesterol (TC), and NAFLD activity score (NAS) (TG: $r = -0.495$; TC: $r = -0.392$; NAS: $r = -0.451$; all $P < 0.05$).

Conclusions: MAFLD patients showed significantly lower adropin levels than the healthy controls, especially in T2DM patients. Adropin maybe a potential biomarker for predicting the development of MAFLD, especially in T2DM individuals.

Keywords: metabolic dysfunction-associated fatty liver disease, adropin, triglyceride, steatohepatitis, type 2 diabetes mellitus

INTRODUCTION

Metabolic dysfunction-associated fatty liver disease (MAFLD), formerly named non-alcoholic fatty liver disease (NAFLD), affecting a quarter of the general population, which has become the most common liver disease (Sarin et al., 2020; Eslam et al., 2020b). The newly proposed diagnostic criteria for MAFLD irrespective of alcohol intake or other concomitant liver diseases. The criteria are principally based on an evidence of hepatic steatosis and include one of the following three criteria: overweight/obesity, presence of type 2 diabetes mellitus (T2DM), or evidence of metabolic dysfunction (Eslam et al., 2020a). The fundamental pathophysiological change of hepatic steatosis is accumulated free fatty acids (FFAs) and triglycerides (TGs) in hepatocytes. Steatohepatitis is the severely advanced stage of hepatic steatosis and is typically characterized by steatosis, lobular inflammation, and ballooning with or without peri-sinusoidal fibrosis (Castera et al., 2019). Many biomarkers which can be used to predict steatohepatitis in patients with MAFLD have been reported. However, considering the invasiveness and expensive cost of liver biopsy, a noninvasive, economical, easily accessible, highly sensitive, and specific biomarker is urgently needed to predict the development of MAFLD.

Adropin, a secreted peptide encoded by the *Energy Homeostasis Associated* (*ENHO*) gene (Kumar et al., 2008), was mainly expressed in the brain and liver. Recent studies showed beneficial effects of adropin on improving glucose homeostasis, dyslipidemia, obesity-associated hyperinsulinemia, and energy homeostasis. Clinical studies suggested that serum adropin was reduced in many diseases, such as NAFLD, T2DM, diabetic nephropathies, coronary atherosclerosis, hypertension, and polycystic ovary disease (Jasaszwili et al., 2020; Ye et al., 2021). Nevertheless, the correlation between adropin and different glucose tolerance in MAFLD patients remains unclear. On the basis of previous findings, we hypothesized that adropin might be involved in the pathogenesis of MAFLD and the serum adropin could be served as a predictive factor of MAFLD. Thus, this study was designed to investigate the correlation between adropin and histological characteristics of the liver, and the clinical relevance of adropin in MAFLD patients.

MATERIALS AND METHODS

Study Design

From July 2019 to January 2020, 30 MAFLD patients were histologically confirmed with hepatic steatosis, which were enrolled in China-Japan Friendship Hospital. MAFLD patients were divided into two subgroups, including NGT-M group (13 normal glucose tolerance, NGT) and T2DM-M group (17 type 2 diabetes mellitus patients, T2DM). No drug intervention was given in patients with T2DM. We enrolled 32 sex and age matched healthy controls who were free from diagnosed hepatic steatosis based on the results of upper abdomen ultrasonography and routine physical examination at Beijing Chao-yang Hospital Affiliated to Capital Medical University from June 2018 to October 2019. All subjects had to meet the following exclusion criteria: alcohol consumption ($\geq$140 g/wk in men and $\geq$70 g/wk in women), chronic viral hepatitis, autoimmune hepatitis, drug-induced liver disease, primary biliary cirrhosis, biliary obstruction, Wilson's disease, and α-1 antitrypsin deficiency-associated liver disease. All participants completed a uniform questionnaire containing questions about the histories of present and past illnesses and medical therapy. Thirty MAFLD patients were asked to undergo intra-operative liver biopsy at the time of admission. The study was approved by the human research ethics committee of the China-Japan Friendship Hospital (2019-103-K71-1), according to the principles of the Declaration of Helsinki. Written informed consent was obtained from all subjects.

Human Liver Tissues and Serum

MAFLD patients ($n = 30$) from the department of general surgery collaboration with China-Japan Friendship Hospital underwent intra-operative liver biopsies during sleeve gastrectomy intervention, following the recommendations by the American Association for the Study of Liver Diseases (Rockey et al., 2009). The histological characteristics of the liver were graded according to a histological scoring system for NAFLD (Kleiner et al., 2005). NAFLD activity score (NAS) was calculated by adding these three items. Serum samples were centrifuged at 3,000 rpm for 15 min, and the obtained serum and liver tissues were immediately snap-frozen and stored at −80°C until use.

Anthropometric and Biochemical Measurements

Height, weight and waist/hip circumference were measured light clothes on and without shoes, and the body mass index (BMI, kg/m^2) was calculated. Fasting blood samples were obtained after overnight fast for the measurement of plasma glucose, C-peptide, insulin, alanine aminotransferase (ALT), aspartate aminotransferase (AST), gamma-glutamyl transferase (GGT), total cholesterol (TC), triglyceride (TG), high-density lipoprotein-cholesterol (HDL-c), low-density lipoprotein cholesterol (LDL-c) levels, apoprotein A1 (Apo-A1), apoprotein B (Apo-B), non-esterified fatty acid (NEFA), small dense-low-density lipoprotein cholesterol (sd-LDL). Homeostasis model assessment insulin resistance index (HOMA-IR) was calculated according to the following formula: FINS (μIU/mL) × FBG (mmol/L)/22.5. A 75-g oral glucose tolerance test (OGTT) was performed, plasma glucose levels were measured at 30, 60, 120, and 180 min after oral glucose, the levels of C-peptide and insulin were also detected at 60, 120, and 180 min after oral glucose. Human serum adropin was measured with an enzyme-linked immunosorbent assay (ELISA) kit (Phoenix

Abbreviations: Apo-A1, apoprotein A1; Apo-B, apoprotein B; BMI, body mass index; ELISA, enzyme-linked immunosorbent assay; ENHO, energy homeostasis associated gene; FBG, fasting blood glucose; FINS, fasting insulin; FFAs, free fatty acids; HbA1c, glycated hemoglobin; HDL-C, high-density lipoprotein cholesterol; HOMA-IR, homeostasis model assessment of insulin resistance; LDL-C, low-density lipoprotein cholesterol; MAFLD, metabolic dysfunction-associated fatty liver disease; MCD, methionine-choline deficient; NAFLD, nonalcoholic fatty liver disease; NAS, NAFLD activity score; NEFA, non-esterified fatty acid; NGT, normal glucose tolerance; OGTT, oral glucose tolerance test; sd-LDL, small dense-low-density lipoprotein cholesterol; T2DM, type 2 diabetes mellitus; TG, triglycerides; TC, total cholesterol; WHR, waist to hip ratio.

Pharmaceuticals, Belmont, CA, USA, EK-032-35), according to the manufacturer's protocol.

Histological Staining

Fresh liver tissue was immediately fixed in 10% phosphate-buffered formalin and 4% neutral-buffered formalin solution for 24 h, embedded in paraffin, sectioned at 6 μm, and then deparaffinized in xylene and rehydrated through a series of decreasing concentrations of ethanol. The sections were prepared for hematoxylin and eosin (H&E) staining, which demarcates fat degeneration. Oil Red O staining was conducted on frozen-sections embedded in OCT to determine hepatic steatosis. Images were captured with a light microscope (Olympus, Tokyo, Japan).

Liver Lipid Analysis

Hepatic triglycerides and cholesterol, free cholesterol was extracted in 50 mM Tris buffer, homogenized, and incubated at 37°C with shaking overnight. The triglyceride and cholesterol, free cholesterol measurement kit (Solarbio, Beijing, China) were used following the manufacturer's instruction to measure lipid contents.

RNA Extraction and qRT-PCR

Total RNA was extracted from human liver tissues using Trizol Reagent (Life Technologies, Carlsbad, CA), then reverse transcripted into cDNA with GoScript reverse transcriptase (Promega, Madison, WI), and prepared for RT-qPCR analysis with SYBR green premix (TaKaRa, Nojihigashi, Kusatsu, Shiga, Japan). RT-qPCR assays were performed on CFX Connect Real-Time System (BIO-RAD, CA). Values are expressed as fold change over control, *β-Actin* (*Actb*) was used for normalization to quantify relative mRNA expression levels, relative changes in mRNA expression were calculated using the comparative cycle method ($2^{-\Delta\Delta Ct}$). Real-time PCR primer sequences are shown in **Supplementary Table 1**.

TABLE 1 | Anthropometric parameters and biochemical indexes in healthy controls and MAFLD patients.

	Control (*n* = 32)	MAFLD (*n* = 30)	*P*-value
Sex (male), *n* (%)	11 (34)	10 (33)	0.931
Age (years)	35.1 ± 4.8	35.1 ± 9.5	0.989
BMI (Kg/m^2)	21.46 ± 1.61	36.88 ± 5.79	**<0.001**
Waist circumference (cm)	75.47 ± 8.41	115.30 ± 12.67	**<0.001**
WHR	0.91 ± 0.02	0.95 ± 0.07	**<0.01**
HbA_1c (%)	5.10 ± 0.44	6.54 ± 1.93	**<0.001**
FBG (mM)	4.74 ± 0.49	7.11 ± 2.84	**<0.001**
FINS (μU/mL)	5.50 (4.90–8.00)	15.89 (12.94–20.32)	**<0.001**
HOMA-IR	1.27 (0.87–1.85)	4.28 (3.76–5.57)	**<0.001**
TC (mM)	4.68 ± 0.59	4.67 ± 0.73	0.950
TG (mM)	0.90 (0.68–1.18)	1.88 (0.94–2.41)	**<0.001**
LDL-C (mM)	2.61 ± 0.56	2.78 ± 0.55	0.307
HDL-C (mM)	1.56 ± 0.33	0.91 ± 0.17	**<0.001**
Apo-A1 (g/L)	1.41 ± 0.23	1.37 ± 0.23	0.592
Apo-B (g/L)	0.78 ± 0.13	0.79 ± 0.15	0.916
sd-LDL (mM)	0.83 ± 0.25	0.79 ± 0.45	0.638
NEFA (mM)	0.49 (0.30–0.57)	0.50 (0.40–0.55)	0.219
ALT (IU/L)	16.75 ± 6.91	51.00 ± 30.52	**<0.001**
AST (IU/L)	19.56 ± 5.00	49.79 ± 25.79	**<0.001**
GGT (IU/L)	15.56 ± 6.20	44.88 ± 37.15	**<0.001**
Adropin (ng/ml)	5.52 ± 0.65	2.02 ± 2.92	**<0.001**

Values are presented as mean ± SD (standard deviation of mean) for normally distributed data or medians (25th, 75th percentiles) for non-normally distributed data.
Apo-A1, apoprotein A1; Apo-B, apoprotein B; BMI, body mass index; FBG, fasting blood glucose; FINS, fasting insulin; HDL-C, high-density lipoprotein cholesterol; HOMA-IR, homeostasis model assessment of insulin resistance; LDL-C, low-density lipoprotein cholesterol; NEFA, non-esterified fatty acid; sd-LDL, small dense-low-density lipoprotein cholesterol; TG, triglycerides; TC, total cholesterol; WHR, waist to hip ratio.
P-values in bold indicate significance. The P-value was assessed using Student's t-test or Mann–Whitney U-test.

TABLE 2 | Anthropometric parameters and biochemical indexes among NGT and T2DM groups in MAFLD patients.

	MAFLD		*P*-value
	NGT (*n* = 13)	T2DM (*n* = 17)	NGT vs. T2DM
Sex (male), *n* (%)	5 (38)	5 (29)	0.602
Age (years)	32.2 ± 9.5	37.3 ± 9.1	0.150
Weight (Kg)	110.90 ± 21.97	99.89 ± 17.09	0.132
BMI (Kg/m^2)	38.66 ± 6.76	35.51 ± 4.67	0.133
Waist circumference (cm)	121.20 ± 12.9	110.9 ± 10.85	**0.025**
WHR	0.97 ± 0.06	0.94 ± 0.08	0.266
HbA_1c (%)	5.36 ± 0.26	7.48 ± 2.18	**0.015**
FBG (mM)	5.54 ± 1.87	8.49 ± 2.86	**0.003**
FINS (μU/mL)	15.89 (12.09–19.47)	15.69 (13.23–23.90)	0.439
HOMA-IR	3.69 (2.20–4.38)	5.21 (4.18–9.64)	**0.020**
TC (mM)	4.62 ± 0.69	4.70 ± 0.79	0.820
TG (mM)	0.96 (0.78–1.86)	2.11 (1.83–3.69)	**0.037**
LDL-C (mM)	2.73 ± 0.57	2.81 ± 0.56	0.769
HDL-C (mM)	0.98 ± 0.21	0.85 ± 0.10	0.116
Apo-A1 (g/L)	1.46 ± 0.32	1.30 ± 0.09	0.138
Apo-B (g/L)	0.77 ± 0.19	0.85 ± 0.14	0.335
sd-LDL (mM)	0.68 ± 0.44	0.86 ± 0.46	0.415
NEFA (mM)	0.50 (0.40–0.50)	0.50 (0.48–0.63)	0.632
ALT (IU/L)	37.50 ± 14.85	65.40 ± 33.98	**0.047**
AST (IU/L)	47.25 ± 25.58	52.33 ± 26.88	0.640
GGT (IU/L)	41.43 ± 19.82	50.88 ± 49.86	0.647
Adropin (ng/ml)	4.00 ± 3.52	0.51 ± 0.73	**<0.001**
NAS	6.68 ± 1.61	6.94 ± 1.77	0.681

Values are presented as mean ± SD (standard deviation of mean) for normally distributed data or medians (25th, 75th percentiles) for non-normally distributed data.
Apo-A1, apoprotein A1; Apo-B, apoprotein B; BMI, body mass index; FBG, fasting blood glucose; FINS, fasting insulin; HDL-C, high-density lipoprotein cholesterol; HOMA-IR, homeostasis model assessment of insulin resistance; LDL-C, low-density lipoprotein cholesterol; NAS, NAFLD activity score; NEFA, non-esterified fatty acid; sd-LDL, small dense-low-density lipoprotein cholesterol; TG, triglycerides; TC, total cholesterol; WHR, waist to hip ratio.
P-values in bold indicate significance. The P-value was assessed using Student's t-test or Mann–Whitney U-test.

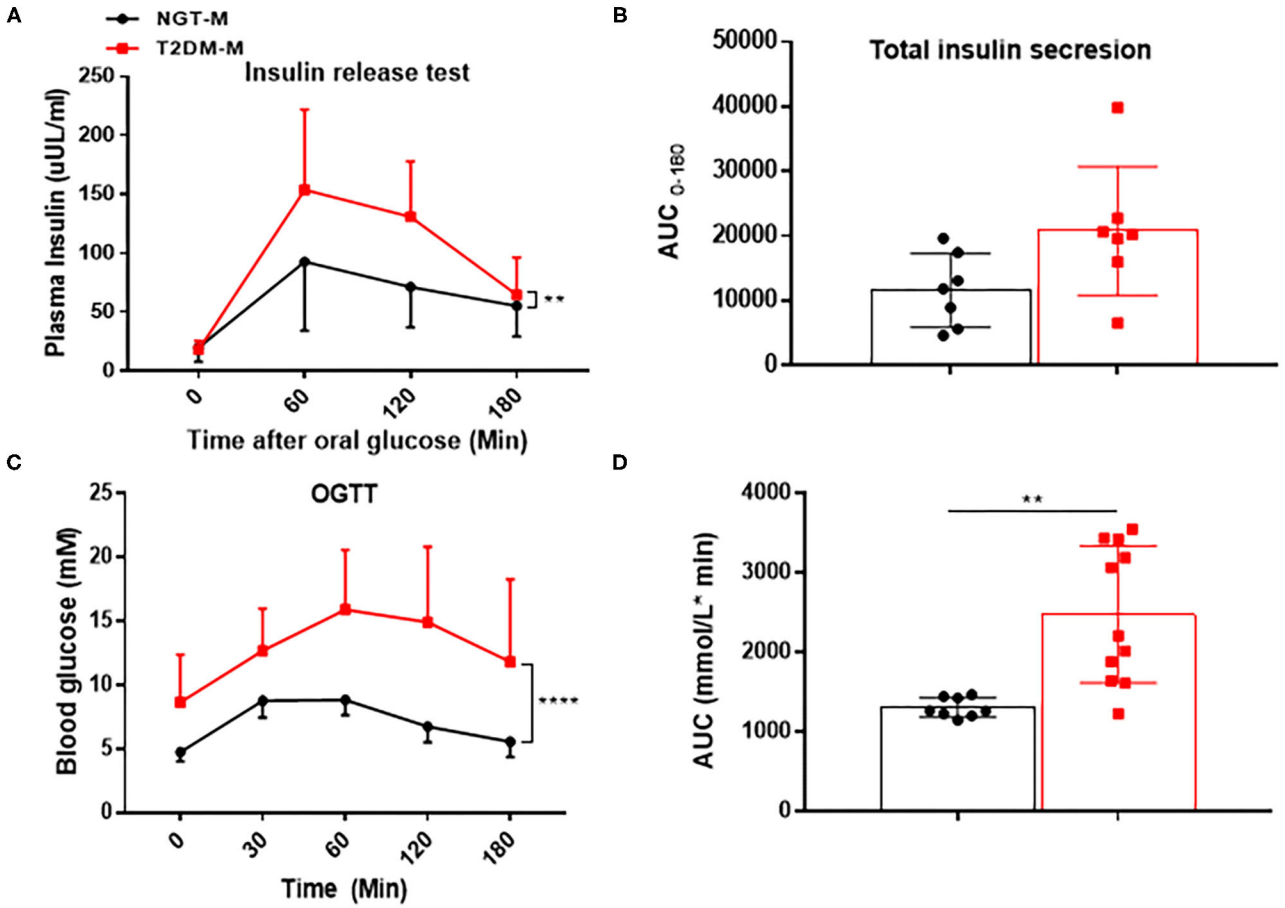

FIGURE 1 | The indicators of insulin resistance in MAFLD patients. **(A,B)** Insulin release test and the respective analysis of the area under the curve (AUC) ($n = 7$). **(C,D)** Oral glucose tolerance test (OGTT) and the respective analysis of the area under the curve (AUC) ($n = 8$–11). The data are expressed as the mean ± SD, $^{**}P < 0.01$, $^{****}P < 0.0001$.

Statistical Analysis

Normally distributed variables were expressed as mean values ± standard deviation of mean (SD). Non-normally distributed variables were described as medians (25th, 75th percentiles), including TG, FINS and HOMA-IR, NEFA. Categorical variables are expressed as *n* (number) with percentage (%). Comparisons between two groups were performed by Student's *t*-test for continuous variables and χ^2 analyses for categorical variables. The correlations between adropin and other parameters were analyzed by Pearson's or Spearman's coefficient. Data were analyzed using the IBM SPSS statistical software (version 24.0; SPSS Inc., Chicago, IL, USA) and GraphPad Prism software (version 7.0; CA, USA). Statistically significant was considered at $p < 0.05$ (two-tailed).

RESULTS

Clinical Characteristics of the Study Participants

Clinical characteristics including anthropometric parameters and biochemical indexes in both control subjects and MAFLD patients are shown in **Table 1**. The MAFLD patients had significantly higher levels of BMI, WHR, HbA_1c, FBG, FINS, HOMA-IR, TG, ALT, AST, and GGT but a lower level of HDL-c compared with healthy controls (All $p < 0.01$). The serum adropin level of MAFLD patients was significantly lower than that of control subjects (2.02 ± 2.92 ng/ml vs. 5.52 ± 0.65 ng/ml, $p < 0.001$).

Subgroup Analysis in MAFLD Patients With Different Glucose Tolerance

To investigate the effect of abnormal glucose metabolism on adropin in MAFLD patients, we performed a subgroup analysis. As **Table 2** showed, the two subgroups were similar in terms of age, BMI and WHR (All $p > 0.05$). However, the T2DM-M group had significantly higher levels of HbA_1c, FBG, HOMA-IR, TG, and ALT than those of NGT-M group (All $p < 0.05$). Insulin release test and AUC suggested that insulin release peak at 1 h but not return to fasting level at 3 h in T2DM-M group (**Figures 1A,B**). OGTT and AUC showed that glucose tolerance was severely impaired in T2DM-M group compared with NGT-M subjects (**Figures 1C,D**). Notably, serum adropin level was

significantly reduced in T2DM-M group compared with NGT-M group (0.51 ± 0.73 vs. 4.00 ± 3.52 ng/ml, $p < 0.001$).

Correlations of Serum Adropin Levels and Liver *ENHO* Expressions With Metabolic Parameters in MAFLD Subjects

To investigated the relationship between adropin and metabolic parameters in MAFLD patients, a linear correlation analysis was performed. As summarized in **Table 3**, serum adropin levels were negatively correlated with BMI, FBG, FINS, HbA1c and HOMA-IR, TG, Apo-B, NEFA, ALT, AST, and GTT, in spite of these differences did not reach the statistical significance. Interestingly, serum adropin levels were positively correlated with HDL-C and Apo-A1 (All $p < 0.001$). Furthermore, liver *ENHO* mRNA expression was obviously downregulated in T2DM-M group compared with NGT-M group (0.63 ± 0.06 vs. 1.00 ± 0.11, $p < 0.01$) (**Figure 2A**). Liver *ENHO* mRNA expression was positively correlated with Apo-A1 ($r = 0.497$, $p < 0.05$). Circulating adropin level was positively associated with liver *ENHO* mRNA expression ($r = 0.637$, $p < 0.001$; **Figure 2B**).

Histological Features of the Liver in Patients With MAFLD

T2DM-M patients exhibited more severe hepatic macrosteatosis, inflammation, and ballooning (**Figure 3A**), concurrent with a higher NAS and inflammation score (**Figure 3B**). Oil Red O staining demonstrated a more lipid accumulation in the T2DM-M patients (**Figure 3A**). Hepatic TG and free cholesterol were significantly higher in the T2DM-M group than those in the NGT-M group (**Figure 3C**). Moreover, the pro-inflammation genes (*TNF*, *IL1B*, and *IL6*) mRNA expression in the liver were higher in the T2DM-M group compared with NGT-M group (**Figure 3D**). Besides, serum adropin levels were significantly inverse correlated with intrahepatic TG ($r = -0.495$, $p = 0.006$; **Figure 4A**), TC ($r = -0.392$, $p = 0.036$; **Figure 4B**), and NAS ($r = -0.451$, $p = 0.018$; **Figure 4C**). Liver adropin levels were negatively correlated with intrahepatic TG ($r = -0.430$, $p = 0.025$; **Figure 4D**), TC ($r = -0.303$, $p = 0.124$; **Figure 4E**), and NAS ($r = -0.325$, $p = 0.105$; **Figure 4F**). We have analyzed the association between adropin and liver pro-inflammation genes. As shown in **Supplementary Figures 1A–F**, the mRNA expressions of *IL6* and *IL1B* were negatively correlated with adropin, but there were no statistically difference.

TABLE 3 | Correlation of serum adropin level and liver *ENHO* mRNA expression with metabolic indicators in MAFLD patients.

Variables	Serum adropin level (ng/ml)		Liver *ENHO* mRNA expression (A.U)	
	r	*P*	*r*	*P*
BMI (Kg/m^2)	−0.014	0.940	−0.016	0.937
Waist circumference (cm)	0.044	0.817	0.106	0.590
WHR	0.057	0.765	0.149	0.746
HbA_1c (%)	−0.318	0.198	−0.218	0.385
FBG (mM)	−0.358	0.052	−0.152	0.439
FINS (μU/mL)	−0.166	0.510	−0.247	0.323
HOMA-IR	−0.308	0.215	−0.310	0.211
TC (mM)	0.190	0.450	−0.237	0.344
TG (mM)	−0.244	0.362	−0.352	0.182
LDL-C (mM)	0.018	0.944	−0.348	0.157
HDL-C (mM)	0.785	**0.000**	0.380	0.119
Apo-A1 (g/L)	0.780	**0.000**	0.497	**0.036**
Apo-B (g/L)	−0.007	0.976	−0.283	0.256
sd-LDL (mM)	0.128	0.625	−0.189	0.484
NEFA (mM)	−0.256	0.322	0.058	0.838
ALT (IU/L)	−0.369	0.131	−0.336	0.187
AST (IU/L)	−0.067	0.754	−0.008	0.971
GGT (IU/L)	−0.028	0.918	0.280	0.311

Correlations between serum adropin or liver ENHO mRNA expression and anthropomorphic, blood chemistry data were calculated by Pearson's or Spearman's coefficient (r).

Apo-A1, apoprotein A1; Apo-B, apoprotein B; BMI, body mass index; FBG, fasting blood glucose; FINS, fasting insulin; HDL-C, high-density lipoprotein cholesterol; HOMA-IR, homeostasis model assessment of insulin resistance; LDL-C, low-density lipoprotein cholesterol; NEFA, non-esterified fatty acid; sd-LDL, small dense-low-density lipoprotein cholesterol; TG, triglycerides; TC, total cholesterol; WHR, waist to hip ratio.

P-values in bold indicate significance.

DISCUSSION

Our results indicate that serum adropin levels and liver *ENHO* mRNA expressions were significantly decreased in T2DM-M patients. These data verified the inverse association between circulating adropin and intrahepatic TG, TC, and NAS. As far as we known, few researches have been done to investigate the association of adropin with intrahepatic lipid contents in adult MAFLD patients. Overall, lower serum level of adropin may be a practical biomarker that can be used to detect the progression of MAFLD.

Several previous studies consistently showed that adropin played a critical role in maintaining glucose homeostasis, increasing the glucose utilization, improving glucose tolerance, and reducing insulin resistance (Butler et al., 2019; Jasaszwili et al., 2020). Adropin deficiency exacerbated the dysregulated glucose homeostasis and insulin resistance in diet-induced obesity (DIO) mice. Adropin injection significantly reduced fasting blood glucose, inhibited hepatic glucose production, lowered fasting insulin level, and improved insulin resistance in high-fat diet mice. *In vitro* study showed that adropin effects on glucose production were restricted in insulin resistance hepatocytes induced by palmitic acid or high glucose (Chen et al., 2017, 2020). Chronic consumption of high fat/high sucrose diets resulting in hepatic insulin resistance suppressed liver adropin expression, and could contribute to the dysregulation of glucose metabolism (Banerjee et al., 2020). Most clinical studies confirmed a dramatically decline of adropin in patients with T2DM when compared with healthy subjects (Wu et al., 2014; Chen et al., 2017). In accordance with prior studies, we found that serum adropin level and liver adropin expression was significantly decreased in T2DM-M patients. Moreover, serum adropin levels were positively correlated with liver adropin expression. Therefore, the lower serum adropin level of MAFLD patients may indicate more serious insulin resistance and glucose intolerance. All these data imply a closely connection between adropin and glucose homeostasis in MAFLD patients.

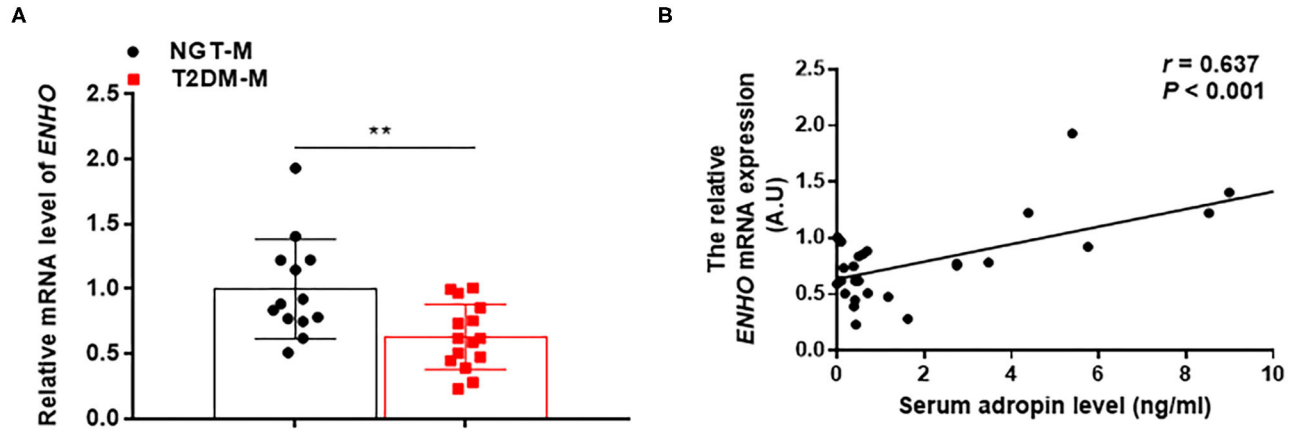

FIGURE 2 | Adropin expression in the liver was lower in MAFLD subjects. **(A)** Quantitative real-time RT-PCR analysis of *ENHO* mRNA expression in the liver from MAFLD patients ($n = 13$–15). **(B)** Correlations of liver *ENHO* mRNA expression with serum adropin levels. The data are expressed as the mean ± SD, $^{**}P < 0.01$.

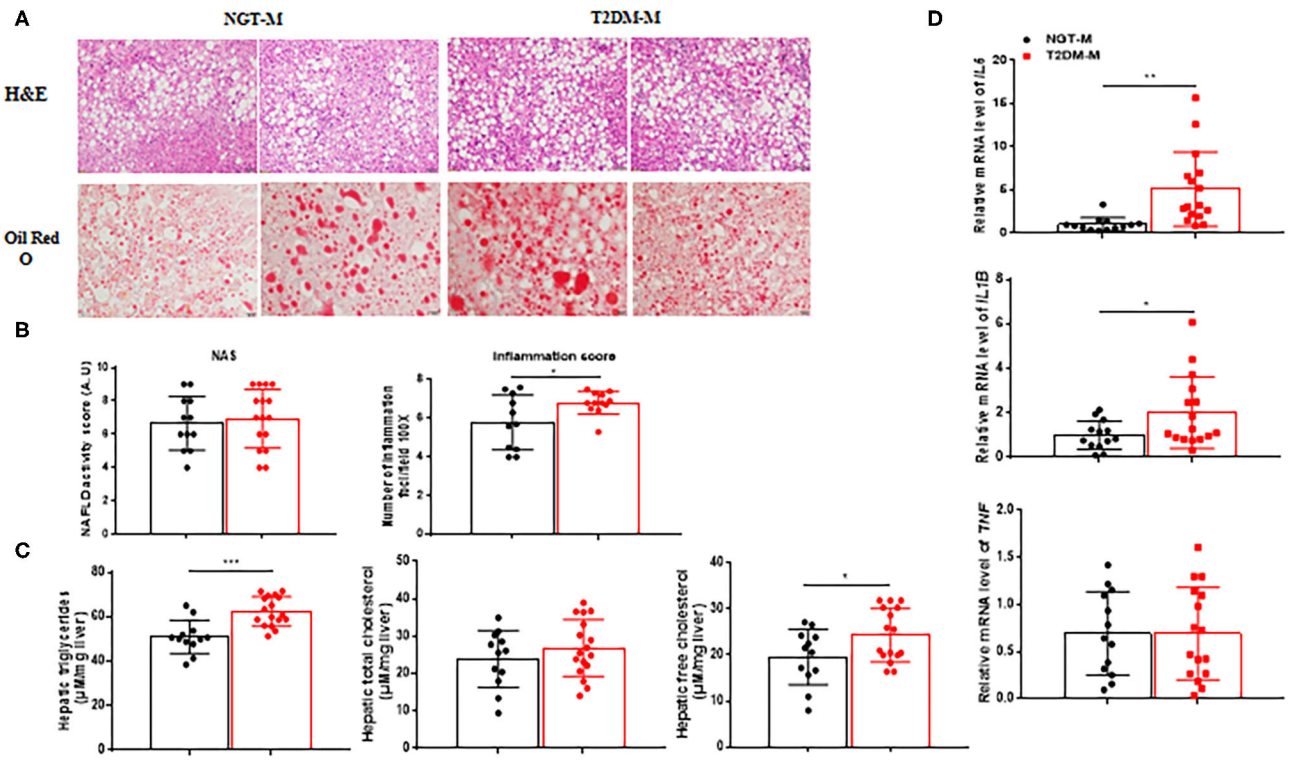

FIGURE 3 | Steatohepatitis was exacerbated in T2DM-M group compared with NGT-M group. **(A)** Representative liver HandE staining (magnification, ×200; scale bar: 50 μm) and Oil Red O staining (magnification, ×400; scale bar: 20 μm) ($n = 13$–17). **(B)** Hepatic histological analysis of HandE staining (NAS and lobular inflammation score) ($n = 11$–16). **(C)** Hepatic triglycerides and (free) cholesterol levels ($n = 12$–17). **(D)** Quantitative real-time RT-PCR analysis of *TNF IL1B IL6* mRNA expressions in the liver from MAFLD patients ($n = 13$–16). The data are expressed as the mean ± SD, $^{*}P < 0.05$, $^{**}P < 0.01$, and $^{***}P < 0.001$.

Adropin is required for metabolic homeostasis and is involved in preventing dyslipidaemia (Kumar et al., 2008). Animal studies suggested that adropin could suppress fatty acid oxidation (Gao et al., 2014). In human subjects, circulating adropin was negatively correlated with the levels of plasma TG, apolipoprotein B, and LDL-c and was positively correlated with the HDL-c level (Butler et al., 2012). Our findings are consistent with previous studies that serum adropin concentrations were inversely associated with these indices of blood lipid. It is important to note that liver TG and TC was inversely correlated with serum adropin level, but only liver TG was significantly negative correlated with liver *ENHO* mRNA expression. We

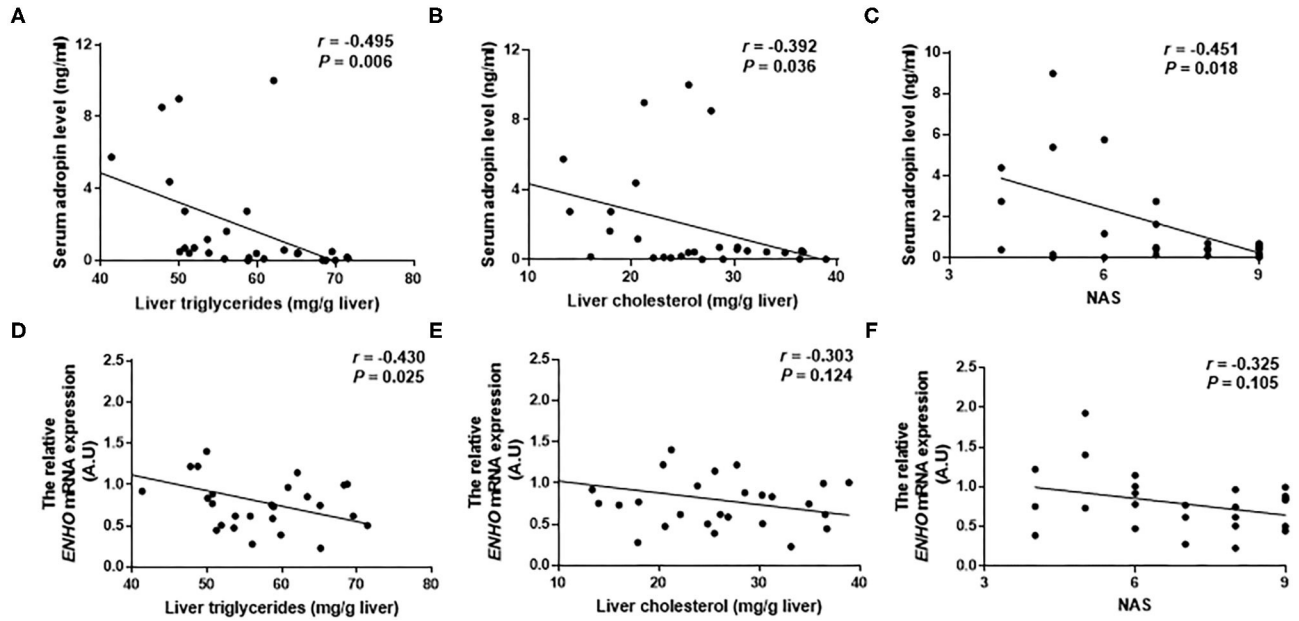

FIGURE 4 | The correlation between serum adropin/liver adropin levels and the level of liver triglycerides **(A,D)**, and liver cholesterol **(B,E)**, and NAFLD activity score **(C,F)** in MAFLD patients.

believed that two reasons might explain these differences. On the one hand, circulating adropin levels may associate with the discrepancy of the equilibrium between cholesterol synthesis and processing of circulating lipoprotein particles (Ghoshal et al., 2018). On the other hand, liver *ENHO* mRNA expression is regulated by the biological clock and nutrition status. Experiments based on mice overexpressing adropin unable to prove the role for adropin in regulating cholesterol uptake from the diet, clearance from the circulation or cholesterol biosynthesis (Ghoshal et al., 2018). The precise effect of adropin in lipid metabolism is still unclear. Further studies examining the relationship between adropin expression in liver tissues and intrahepatic TG and TC are required. Our study showed that circulating adropin was negatively correlated with intrahepatic TG and TC.

Genetically engineered animals provided strong evidence indicating that adropin contributes to the modulation of inflammation. Chen et al. (2019) demonstrated that serum adropin concentrations were obviously decreased in steatohepatitis, adropin deficient mice showed exacerbated hepatic steatosis, inflammation and fibrosis when fed methionine-choline deficient (MCD) or western diets. Serum adropin level was lower in B-ultrasound or liver biopsy diagnosed NAFLD patients, and was associated with the severity of NAFLD (Sayin et al., 2014; Kutlu et al., 2019). Adropin treatment decreased the expression of the proinflammatory cytokines *Il1b*, *Il6*, and *Tnfa* in mice with MCD diet-induced steatohepatitis (Chen et al., 2019). Thus, adropin as a potential anti-inflammatory factor plays an important role in the process of steatohepatitis. Herein, we included patients with biopsy-proven hepatic steatosis to explore the association between adropin and liver injury. We found that both serum adropin level and liver *ENHO* mRNA expression were negatively associated with ALT and NAS. The proinflammatory genes (*TNF*, *IL6*, and *IL1B*) were increased in T2DM-M patients compared with those in NGT-M group. In addition, the serum adropin levels and liver *ENHO* mRNA expressions were dramatically decreased in T2DM-M patients compared with NGT-M group. Thus, our findings pointed out the potential of adropin in identifying MAFLD, especially in T2DM individuals.

A limitation of this study is the cross-sectional design which harbored a small sample size, and the liver samples from patients who volunteered to have a liver biopsy, which may lead to selection bias. Hence, more large and random liver-biopsy hepatic steatosis populations are needed to further confirm our results and conclusions.

CONCLUSIONS

To sum up, the current findings provide further indication of the significance of adropin in maintaining metabolic homeostasis. Adropin may participate in the pathogenesis of MAFLD and can be served as a predictive biomarker of MAFLD. Nevertheless, more *in vivo* experiments and a large-scale clinical trial is required to confirm these data in MAFLD.

DATA AVAILABILITY STATEMENT

The original contributions presented in the study are included in the article/**Supplementary Material**, further inquiries can be directed to the corresponding author/s.

ETHICS STATEMENT

The studies involving human participants were reviewed and approved by the Ethics Committee of the China-Japan Friendship Hospital (2019-103-K71). The patients/participants provided their written informed consent to participate in this study.

AUTHOR CONTRIBUTIONS

GW, JL, HM, and AQ: conceived and designed the experiments. NL, GX, and AQ: analyzed the data. NL, GX, AQ, and BZ: contributed reagents materials analysis tools. NL: wrote the paper. GW, JL, and AQ: revised and adapted the manuscript. All authors read and approved the final manuscript.

FUNDING

The Chinese National Natural Science Foundation (No. 81770792, 81972137) and Beijing Municipal Natural Science Foundation (No. Z201810025038) to GW.

SUPPLEMENTARY MATERIAL

The Supplementary Material for this article can be found online at: https://www.frontiersin.org/articles/10.3389/fphys.2021.696163/full#supplementary-material

REFERENCES

Banerjee, S., Ghoshal, S., Stevens, J. R., McCommis, K. S., Gao, S., Castro-Sepulveda, M., et al. (2020). Hepatocyte expression of the micropeptide adropin regulates the liver fasting response and is enhanced by caloric restriction. *J. Biol. Chem.* 295, 13753–13768. doi: 10.1074/jbc.RA120.014381

Butler, A. A., Tam, C. S., Stanhope, K. L., Wolfe, B. M., Ali, M. R., O'Keeffe, M., et al. (2012). Low circulating adropin concentrations with obesity and aging correlate with risk factors for metabolic disease and increase after gastric bypass surgery in humans. *J. Clin. Endocrinol. Metab.* 97, 3783–3791. doi: 10.1210/jc.2012-2194

Butler, A. A., Zhang, J., Price, C. A., Stevens, J. R., Graham, J. L., Stanhope, K. L., et al. (2019). Low plasma adropin concentrations increase risks of weight gain and metabolic dysregulation in response to a high-sugar diet in male nonhuman primates. *J. Biol. Chem.* 294, 9706–9719. doi: 10.1074/jbc.RA119.007528

Castera, L., Friedrich-Rust, M., and Loomba, R. (2019). Noninvasive assessment of liver disease in patients with nonalcoholic fatty liver disease. *Gastroenterology* 156, 1264–1281.e1264. doi: 10.1053/j.gastro.2018.12.036

Chen, S., Zeng, K., Liu, Q. C., Guo, Z., Zhang, S., Chen, X. R., et al. (2017). Adropin deficiency worsens HFD-induced metabolic defects. *Cell Death Dis.* 8:e3008. doi: 10.1038/cddis.2017.362

Chen, X., Chen, S., Shen, T., Yang, W., Chen, Q., Zhang, P., et al. (2020). Adropin regulates hepatic glucose production *via* PP2A/AMPK pathway in insulin-resistant hepatocytes. *FASEB J.* 34, 10056–10072. doi: 10.1096/fj.202000115RR

Chen, X., Xue, H., Fang, W., Chen, K., Chen, S., Yang, W., et al. (2019). Adropin protects against liver injury in nonalcoholic steatohepatitis via the Nrf2 mediated antioxidant capacity. *Redox Biol.* 21:101068. doi: 10.1016/j.redox.2018.101068

Eslam, M., Newsome, P. N., Sarin, S. K., Anstee, Q. M., Targher, G., Romero-Gomez, M., et al. (2020a). A new definition for metabolic dysfunction-associated fatty liver disease: an international expert consensus statement. *J. Hepatol.* 73, 202–209. doi: 10.1016/j.jhep.2020.07.045

Eslam, M., Sanyal, A. J., George, J., and International Consensus, P. (2020b). MAFLD: a consensus-driven proposed nomenclature for metabolic associated fatty liver disease. *Gastroenterology.* 158, 1999–2014.e1991. doi: 10.1053/j.gastro.2019.11.312

Gao, S., McMillan, R. P., Jacas, J., Zhu, Q., Li, X., Kumar, G. K., et al. (2014). Regulation of substrate oxidation preferences in muscle by the peptide hormone adropin. *Diabetes* 63, 3242–3252. doi: 10.2337/db14-0388

Ghoshal, S., Stevens, J. R., Billon, C., Girardet, C., Sitaula, S., Leon, A. S., et al. (2018). Adropin: an endocrine link between the biological clock and cholesterol homeostasis. *Mol. Metab.* 8, 51–64. doi: 10.1016/j.molmet.2017.12.002

Jasaszwili, M., Billert, M., Strowski, M. Z., Nowak, K. W., and Skrzypski, M. (2020). Adropin as a fat-burning hormone with multiple functions-review of a decade of research. *Molecules* 25:549. doi: 10.3390/molecules25030549

Kleiner, D. E., Brunt, E. M., Van Natta, M., Behling, C., Contos, M. J., Cummings, O. W., et al. (2005). Design and validation of a histological scoring system for nonalcoholic fatty liver disease. *Hepatology* 41, 1313–1321. doi: 10.1002/hep.20701

Kumar, K. G., Trevaskis, J. L., Lam, D. D., Sutton, G. M., Koza, R. A., Chouljenko, V. N., et al. (2008). Identification of adropin as a secreted factor linking dietary macronutrient intake with energy homeostasis and lipid metabolism. *Cell Metab.* 8, 468–481. doi: 10.1016/j.cmet.2008.10.011

Kutlu, O., Altun, O., Dikker, O., Aktas, S., Ozsoy, N., Arman, Y., et al. (2019). Serum adropin levels are reduced in adult patients with nonalcoholic fatty liver disease. *Med. Princ. Pract.* 28, 463–469. doi: 10.1159/000500106

Rockey, D. C., Caldwell, S. H., Goodman, Z. D., Nelson, R. C., Smith, A. D., and American Association for the Study of Liver, D. (2009). Liver biopsy. *Hepatology* 49, 1017–1044. doi: 10.1002/hep.22742

Sarin, S. K., Kumar, M., Eslam, M., George, J., Al Mahtab, M., Akbar, S. M. F., et al. (2020). Correction to lancet gastroenterol hepatol 2020; 5: 167–228. *Lancet Gastroenterol. Hepatol.* 5:e2. doi: 10.1016/S2468-1253(19)30342-5

Sayin, O., Tokgoz, Y., and Arslan, N. (2014). Investigation of adropin and leptin levels in pediatric obesity-related nonalcoholic fatty liver disease. *J. Pediatr. Endocrinol. Metab.* 27, 479–484. doi: 10.1515/jpem-2013-0296

Wu, L., Fang, J., Chen, L., Zhao, Z., Luo, Y., Lin, C., et al. (2014). Low serum adropin is associated with coronary atherosclerosis in type 2 diabetic and non-diabetic patients. *Clin. Chem. Lab. Med.* 52, 751–758. doi: 10.1515/cclm-2013-0844

Ye, Z., Zhang, C., and Zhao, Y. (2021). Potential effects of adropin on systemic metabolic and hormonal abnormalities in polycystic ovary syndrome. *Reprod. Biomed. Online* 42,1007–1014. doi: 10.1016/j.rbmo.2021.01.020

Conflict of Interest: The authors declare that the research was conducted in the absence of any commercial or financial relationships that could be construed as a potential conflict of interest.

frontiers in Physiology

ORIGINAL RESEARCH
published: 26 July 2021
doi: 10.3389/fphys.2021.659211

The G2A Receptor Deficiency Aggravates Atherosclerosis in Rats by Regulating Macrophages and Lipid Metabolism

Xueqin Cui[1†], Roumei Xing[1†], Yue Tian[1], Man Wang[1], Yue Sun[1], Yongqian Xu[1], Yiqing Yang[1], Yongliang Zhao[1], Ling Xie[1], Yufang Xiao[1], Dali Li[1], Biao Zheng[1,2], Mingyao Liu[1*] and Huaqing Chen[1*]*

[1] Shanghai Key Laboratory of Regulatory Biology, School of Life Sciences, Institute of Biomedical Sciences, East China Normal University, Shanghai, China, [2] Department of Pathology & Immunology, Baylor College of Medicine, Houston, TX, United States

OPEN ACCESS

Edited by:
Jiqiu Wang,
Shanghai Jiao Tong University, China

Reviewed by:
Andreas Daiber,
Johannes Gutenberg University Mainz, Germany
Howard Prentice,
Florida Atlantic University, United States

***Correspondence:**
Biao Zheng
bzheng@bio.ecnu.edu.cn
Mingyao Liu
myliu@bio.ecnu.edu.cn
Huaqing Chen
hqchen@bio.ecnu.edu.cn

[†] These authors have contributed equally to this work and share first authorship

Specialty section:
This article was submitted to Clinical and Translational Physiology, a section of the journal Frontiers in Physiology

Received: 27 January 2021
Accepted: 13 April 2021
Published: 26 July 2021

Citation:
Cui X, Xing R, Tian Y, Wang M, Sun Y, Xu Y, Yang Y, Zhao Y, Xie L, Xiao Y, Li D, Zheng B, Liu M and Chen H (2021) The G2A Receptor Deficiency Aggravates Atherosclerosis in Rats by Regulating Macrophages and Lipid Metabolism. Front. Physiol. 12:659211. doi: 10.3389/fphys.2021.659211

The orphan G protein-coupled receptor G2A has been linked to atherosclerosis development. However, available data from mouse models are controversial. Rat G2A receptor bears more similarities with its human homolog. We proposed that the atherosclerosis model established from *Ldlr*$^{-/-}$ rat, which has been reported to share more similar phenotypes with the human disease, may help to further understand this lipid receptor. G2A deletion was found markedly aggravated in the lipid disorder in the rat model, which has not been reported in mouse studies. Examination of aortas revealed exacerbated atherosclerotic plaques in G2A deficient rats, together with increased oxidative stress and macrophage accumulation. In addition, consistently promoted migration and apoptosis were noticed in G2A deficient macrophages, even in macrophages from G2A single knockout rats. Further analysis found significantly declined phosphorylation of PI3 kinase (PI3K) and AKT, together with reduced downstream genes Bcl2 and Bcl-xl, suggesting possible involvement of PI3K/AKT pathway in G2A regulation to macrophage apoptosis. These data indicate that G2A modulates atherosclerosis by regulating lipid metabolism and macrophage migration and apoptosis. Our study provides a new understanding of the role of G2A in atherosclerosis, supporting it as a potential therapeutic target.

Keywords: G2A, atherosclerosis, LDLR deficient rat, lipid disorder, macrophage

INTRODUCTION

As a chronic disease affecting arteries, atherosclerosis is characterized by lumen narrowing progressively developed from gradual expansion of lesions, which may eventually lead to myocardial infarction or stroke. It has been largely accepted that both lipid disorder and chronic inflammation are involved in atherosclerosis. The complicated interplay between inflammation and

Abbreviations: LDLR, low-density lipoprotein receptor; LRP, LDLR-related protein; oxLDL, oxidized low-density lipoprotein; LPC, lysophosphatidylcholine; 9-HODE, 9-hydroxyoctadecadienoic acid; ROS, reactive oxygen species; WT, wild type; MMP, matrix metalloproteinase.

lipid metabolism leads to immune cell infiltration and aggravated lesions in the arterial wall (Moore and Tabas, 2011; Shalhoub et al., 2011; Fogelstrand and Boren, 2012; van Diepen et al., 2013).

As the predominant immune cell type, macrophages around lesions are thought to originate from bone marrow; in which hematopoietic stem cells give rise to circulating monocytes (Tabas and Lichtman, 2017). It is believed that macrophage accumulation in the intima and subintima of arteries is vital for the formation of obstructive atherosclerotic plaques. The number of infiltrated macrophages and their location at plaque rupture-sensitive sites is related to plaque vulnerability (Davies et al., 1993). As part of their general homeostatic scavenging function, macrophages could consume toxic lipids, such as oxidized low-density lipoproteins (oxLDL) (Acton et al., 1996). Increased oxLDL is associated with the formation of lipid-laden macrophages-foam cells in lesional sites, which is critical in atherosclerosis development (Kadl et al., 2010; Chinetti-Gbaguidi and Staels, 2011). The pathological mechanism of atherosclerosis suggest that, although lipid-lowering therapy represents the mainstream strategy at the moment, the possible combination of restoring imbalanced immunity could become a promising new goal for combating the disease.

The orphan G protein-coupled receptor G2A (GPR132) got its name because it induces G2 cell cycle arrest (Weng et al., 1998). It is activated by lysophospholipids and free fatty acids including lysophosphatidylcholine (LPC) and 9-hydroxyoctadecadienoic acid (9-HODE), which related to oxLDL (Obinata et al., 2005; Yang et al., 2005; Frasch et al., 2007; Foster et al., 2019). G2A is highly expressed in immune tissues, also on immune cells including macrophages and lymphocytes. It is also expressed in endothelium (Rikitake et al., 2002; Parks et al., 2005). In addition to modifying cell cycle and oncogenesis, research data about G2A mainly concentrated on its function in immunity and inflammation (Peter et al., 2008; Bolick et al., 2009; Frasch et al., 2011; Qin et al., 2014), though a few suggested its involvement in hepatic lipid metabolism (Johnson et al., 2008).

In humans or mice, G2A was found predominantly expressed in monocytes/macrophages within plaques, suggesting its involvement in atherosclerosis initiation or progression (Rikitake et al., 2002). Quite a few studies had been conducted in mouse atherosclerotic models and found that G2A showed regulatory effects on atherosclerosis development through alterations of macrophages, endothelium, or other factors. However, both proatherogenic and atheroprotective actions of G2A had been described (Parks et al., 2005, 2006, 2009; Bolick et al., 2009). Some stated that G2A deletion led to macrophage activation and less apoptosis which was associated with more macrophages in aortas and increased atherosclerosis (Bolick et al., 2009). Others found G2A deficiency attenuated atherosclerosis owing to HDL increase, independent of macrophages (Parks et al., 2006, 2009). By bone marrow transplantation, bone marrow-derived cells were found both participated and not participated in G2A regulating atherosclerosis (Bolick et al., 2009; Parks et al., 2009). The difference reported in these articles was not related to background variation since they used the same mouse strain. As for G2A's role on blood lipid profiles, studies from mice usually described no significant effect, but some reported HDL modulation in $Ldlr^{-/-}$ model after prolonged diet intervention (Parks et al., 2005, 2009; Bolick et al., 2009). The above information indicates that mouse study alone is not sufficient to elucidate G2A's impact on atherosclerosis. New animal systems are hence required to help to clarify G2A mediated effects on different aspects of atherosclerosis including macrophages and lipid metabolism.

Rats have been used extensively as human disease models with their advantages. When we looked at the amino acid sequence of rat G2A, it shares more similarity with human G2A than the mouse homolog does: 60 vs. 21% similarity in the N-terminal extracellular domain and 73 vs. 41% in C-terminal cytoplasmic tail (Obinata and Izumi, 2009). Moreover, we have developed genetically modified rat models of atherosclerosis and found that they share more closely related human phenotype than mice in certain aspects, including heavier plaques in males (Zhao et al., 2018). Thus in this study, we assessed the role of G2A in atherosclerosis using the rat model to get a better understanding of the receptor. Our results showed that G2A deletion greatly aggravated dyslipidemia, potentiated macrophage migration and apoptosis in LDLR deficient rats, and eventually led to more macrophage accumulation and lesion development in the aortic wall.

MATERIALS AND METHODS

Animals

The total *Ldlr* gene knockout ($Ldlr^{-/-}$) rat was previously established by the CRISPR/Cas9 system and maintained in our laboratory (Zhao et al., 2018). In the current study, a heritable total *G2a* knockout ($G2a^{-/-}$) rat was generated in the same way. Briefly, two sgRNAs targeting the exon 3 of *G2a*, CTGCCACACGTTGTCCTACGAGG, and CGGCGAGCACGTTTCTCTGTAGG, were constructed by overlapping PCR. The transcribed sgRNA and Cas9 mRNA were purified and a mixture of them was microinjected into zygotes of Sprague Dawley rats (SLAC Laboratory Animal Co., Ltd., Shanghai, China). Three pups (founder 1–3) were born after 50 injected zygotes were transferred to 1 pseudopregnant female rat. All three pups carried *G2a* deletion. Sequence analysis revealed that these three founders had frameshift mutations (**Supplementary Figures 1A,B**). In the end, founder one was chosen and a stable colony of $G2a^{-/-}$ rat was established, which carried 199-bp deletion from No. 137654370bp to 137654379bp and No. 137654088bp to 137654276bp in the genome (NC_005105.4), and resulted in a termination codon TAA and deletion of 346 amino acids. Rat tail clips were used for genotyping as usual (**Supplementary Figure 1C**). PCR primers for identifying *G2a* mutation were 5′- CCTCATCTTGTCAGGGTC -3′ (sense) and 5′- CCGCAGGTAGTAGTAGCC -3′ (antisense). Homozygous $G2a^{-/-}$ rats showed a markedly reduced *G2a* expression in related tissues (**Supplementary Figure 1D**).

Genetically matched $Ldlr^{-/-}$ and $Ldlr^{-/-}G2a^{-/-}$ rats were derived from cross-breeding $G2a^{-/-}$ and $Ldlr^{-/-}$ rats. Both male and female animals were maintained and monitored as

described previously, in a SPF facility on 12 h light/12 h dark cycles. All rats were supplied water and a normal diet freely accessible. Animals were transferred to Western Diet at 8 week-old to induce atherosclerosis (Zhao et al., 2018). All animal procedures and techniques were approved by the Animal Ethics Committee of East China Normal University with a permit number (R20170202). A mix of male and female rats was used in this study. Most animal experiments were originally conducted by dividing male and female rats. As both genders displayed similar results, they were combined. Representative images of histological analysis and immunoblotting were from male rats. A scheme depicting the time protocol of rat treatments and time points of measuring various parameters was provided in **Supplementary Figure 2**.

Bone Marrow-Derived Macrophages and Foam Cell Induction

Bone Marrow-Derived Macrophages (BMDMs) were induced from bone marrow derived cells of 8 or 36 week-old animals as previously described (Weischenfeldt and Porse, 2008; Muschter et al., 2015), and about 90% of the resulted cells were CD68 positive. For foam cell induction, macrophages were incubated with 10 μg/ml oxLDL for 24–48 h. In some experiments, macrophages were stimulated with 100 ng/ml LPS (Sigma) or 20 ng/ml IL-4 (PeproTech) and their expression of inflammatory or anti-inflammatory cytokines were then evaluated by quantitative real-time PCR.

Cell Migration Assay

Migration assay was performed using the transwell chamber (Corning Falcon) in a 24-well cell culture plate. Cell suspensions containing 1×10^5 cells in 500 μl serum-free DMEM medium with 10 μg/ml oxLDL were placed in the top chamber. The lower chamber was filled with 500 μl complete DMEM medium containing 10 μg/ml oxLDL and 10% FBS. After 36 h incubation in a 37°C, 5% CO_2 incubator, migrated cells were fixed with 4% paraformaldehyde, washed then stained with 0.1% crystal violet for 30 min. Images were captured through an inverted microscope (Olympus), and cells counted with the ImageJ software.

ROS Detection in HUVEC Cells

The primary human umbilical vein endothelial cell (HUVEC) was from Dr. Xinli Wang (Baylor College of Medicine, Houston, TX), and cultured as described previously (Wu et al., 2016). Expression of G2A in the cells was knocked down by siRNA (about 60% knockdown assessed by real-time PCR). ROS was detected by means of an oxidation-sensitive fluorescent probe (DCFH-DA) (ROS Assay Kit, S0033S, Beyotime Biotechnology, China). After treated with 20 μg/ml oxLDL for 36 h, cells were washed then incubated with 10 μmol/L DCFH-DA according to the manufacturer's instructions. The dichlorofluorescein (DCF) fluorescence was detected by FlexStation 3 (Molecular Devices) at an excitation wavelength of 488 nm and emission wavelength of 525 nm. The oxidative stress marker, malondialdehyde (MDA) in serum was conducted by a plate reader assay, based on reaction between MDA and thiobarbituric acid, as described in Lipid Peroxidation MDA assay kit (S0131S, Beyotime Biotechnology, China). OD535nm was detected by Cytation 5 imaging reader (BioTek, United States).

Detection of Serum Lipids

At 8, 24, and 36 week-old, rats were fastened overnight. Blood samples were collected under anesthesia through intraperitoneal injection of 1.25% (m/v) avertin (Sigma-Aldrich). Serum was obtained by centrifugation at 3,000 rpm for 15 min at 4°C, and then kept at −80°C until analysis. Lipids including total cholesterol (TC), triglyceride (TG), low-density lipoprotein cholesterol (LDL-c) and high-density lipoprotein cholesterol (HDL-c) were analyzed using AU680 Automatic Biochemistry Analyzer (Beckman Coulter, United States). For atherosclerosis risk prediction, the atherosclerotic index was calculated as (TC-HDL-c)/HDL-c (Zhao et al., 2018; Zhang et al., 2020). Levels of oxLDL, free fatty acid, insulin and leptin were determined by respective ELISA assays from Shanghai Hengyuan Biological Technology Co., Ltd. (Shanghai, China).

Quantitative Real-Time PCR Analysis

Total RNA was extracted from cells or tissues using Trizol (Invitrogen). Reverse transcription was performed with the cDNA Prime Script Reverse Transcription kit (Takara) according to the manufacturer's instructions. Real-time PCR was performed in triplicate by SYBR Green PCR Master Mix (Takara) on a MX3005p system (Stratagene, United States). 500 ng RNA was used for the reverse transcription, and 500 ng cDNA for real-time PCR. The expression of target genes was normalized to the house keeping gene β-actin.

Histological Analysis

The histological analysis was performed as previously published (Zhao et al., 2018). Briefly, rats were sacrificed at 36 or 54 weeks old by CO_2 asphyxiation under avertin anesthesia. Whole aortas were excised and adipose tissue and adhesion tissue around the arteries were removed. Aortas were fixed in 4% paraformaldehyde at 4°C overnight. The fixed tissues were paraffin-embedded, and sections were prepared using a paraffin slicer (Leica) then subjected to hematoxylin-eosin (H&E) staining. The *en face* aortas or frozen sections were subjected to Oil red O staining, Masson staining or immunohistochemical staining. Stained sections were photographed by an inverted microscope (Leica) or Caseviewer2.0 (3D HISTECH), and the resulted images were analyzed by Image-Pro® Plus version 6.0 software.

Immunoblotting

Ice-cold SDS lysis buffer (0.08 mM Tris–HCl, 10 SDS, 0.25% bromophenol blue, 50% glycerol and 25% β-mercaptoethanol) was used to collect proteins from cells. Heat denatured proteins were equally loaded and fractionated by 12% SDS-PAGE, then transferred to a nitrocellulose membrane (Schleicher and Schuell MicroScience). According to the target protein, membranes were incubated with the following respective primary antibodies:

rabbit anti-PI3K (1:1,000 dilution, Cat. No. 4257), rabbit anti-phospho-PI3K (1:1,000, Cat. No. 4228), rabbit anti-AKT (1:1,000, Cat. No. 9272), rabbit anti-phospho-AKT (1:2,000, Cat. No. 4060), and rabbit anti-Bcl-xL (1:1,000, Cat. No. 2764) from Cell Signaling Technology (CST), rabbit anti-Bcl-2 (1:1,000, sc-56015) from Santa Cruz and mouse anti-β-actin (1:1,000, A5441) from Sigma. Secondary antibodies were donkey anti-mouse or donkey anti-rabbit (1:2,000) from Thermo-Invitrogen. Detection of positive bands were conducted using fluorescence labeled secondary antibodies IRDye® 800CW goat anti-mouse IgG (Cat. No. 926-32210) and IRDye® 800CW goat anti-rabbit IgG (Cat. No. 926-32211) from Li-COR. Images of the blots were analyzed on the Odyssey Infra-Red Imaging System (Li-COR).

Statistical Analysis

All data are expressed as mean ± SD. Statistical analysis was performed by Graphpad prism 6 software. Differences between two groups were determined by an unpaired Student's *t*-test. For multiple comparisons, two-way ANOVA with Tukey's multiple comparison test was used. Values of $p < 0.05$ were considered statistically significant.

RESULTS

G2A Single Deficiency Did Not Alter Lipid Metabolism in WT Rats but Promoted Macrophage Migration and Apoptosis

To evaluate its possible involvement in atherosclerosis, G2A expression in atherosclerosis related tissues and cells were first analyzed in WT rats. Similar to mice G2A, rat G2A was found highly expressed in immune organs including thymus and spleen, and widely expressed in immune cells, such as lymphocytes and different subpopulations of macrophage, with the bone marrow cells showed the highest expression. There was also some G2A expression in the visceral adipose tissue (VAT) and aorta (**Supplementary Figure 3**).

Next, phenotypes associated with atherosclerosis development including lipid metabolism, oxidative stress and macrophages were compared between $G2a^{-/-}$ and WT rats. Serum lipid profile analysis did not show a significant difference in the two genotypes in either normal diet or Western diet-fed groups (**Supplementary Figure 4**). Neither was an obvious change discovered in cytokines secreted by macrophages, except a minor increase in the inflammatory cytokine TNFα by LPS stimulated $G2a^{-/-}$ macrophages (**Figures 1A,B**). However, consistent enhancement was detected in macrophage migration. As shown in **Figure 1C**, bone marrow derived macrophages from 8 week-old $G2a^{-/-}$ rats displayed enhanced migration when induced by ox-LDL. Moreover, the reactive oxygen species (ROS) producing enzyme nitric oxide synthase 2 (iNOS) was markedly increased in arteries of G2A deficient rats (**Figure 1D**), indicating oxidative stress and cell injury. The expression of apoptotic genes was significantly enhanced while survival genes were reduced in $G2a^{-/-}$ macrophages (**Figure 1E**).

We further analyzed the effects of G2A deficiency on ATP binding cassette transporters and lipid scavenger receptors. ABCA1 did not show significant change, but a decreased ABCG1 mRNA level was noticed in $G2a^{-/-}$ macrophages (**Figure 1F**). No significant difference in LDLR-related proteins (LRP1, LRP5, and LRP6) was detected. There were some changes in the expression of lipid scavenger receptors (SRs), though, with increases in SRB1 and lectin-like oxidized LDL receptor-1 (LOX-1) but a reduction in SRA1 (**Figure 1G**). Taken together, G2A knockout in WT rats did not affect lipid metabolism but led to arterial oxidative stress as well as enhancement in macrophage migration and apoptosis.

G2A Deficiency Exacerbated Lipid Disorder in the $Ldlr^{-/-}$ Atherosclerotic Model

Although G2A deficiency did not alter lipid profiles in WT rats, an apparent difference was observed between sera from 24 week-old $Ldlr^{-/-}$ and $Ldlr^{-/-}G2a^{-/-}$ rats with the former clearer and the latter more turbid (**Figure 2A**). Not surprisingly, greatly augmented TC and TG were detected in $Ldlr^{-/-}G2a^{-/-}$ rats. A significant increase for TC even began at 8 week-old, before Western diet induction (**Figure 2B**). The HDL-c level did not show significant change, but a marked elevation of LDL-c was detected at 36 week-old, along with a trend of increase in LDL/HDL ratio (**Figure 2C**). Interestingly, a greatly up-regulated atherosclerotic index was manifested in 24 and 36 week-old $Ldlr^{-/-}G2a^{-/-}$ rats as compared to respective $Ldlr^{-/-}$ controls (**Figure 2D**), predicting higher atherosclerosis risk. No significant alteration was noticed in free fatty acids, but a very consistent increase was found in the serum level of oxLDL, even at 8 weeks old before the Western diet intervention (**Figures 2E,F**). To analyze whether the aggravated lipid disorder had anything to do with food intake and body weight, we checked the two indexes, as well as water intake, leptin, and insulin. Only water intake in male $Ldlr^{-/-}G2a^{-/-}$ displayed a moderate enhancement as compared to the male $Ldlr^{-/-}$ counterpart (**Supplementary Figure 5**). No significant difference in these indexes was detected between female rats of the two genotypes (data not shown). Therefore, G2A deficiency severely aggravated lipid disorder in $Ldlr^{-/-}$ rats which had no apparent relation to food intake or body weight.

G2A Deletion Aggravated Atherosclerosis in the $Ldlr^{-/-}$ Rat Model

After finding the exacerbated dyslipidemia in $Ldlr^{-/-}G2a^{-/-}$ rats, we next examined the direct effect of G2A deficiency on atherosclerosis development. Not surprisingly, male and female Western diet-fed $Ldlr^{-/-}G2a^{-/-}$ rats at 36 and 54 weeks of age showed significantly more aortic plaques by *en face* analysis, as compared to $Ldlr^{-/-}$ rats. Representative *en face* aortic images were presented in **Figure 3A** and lesion areas accounted for 7.2–15.4% of total aortic intima in 36 week-old and 15.3–17.3% in 54 week-old $Ldlr^{-/-}G2a^{-/-}$ rats, average 1.9 and 1.5-fold increase of lesion area in respective $Ldlr^{-/-}$ counterparts. Besides, histological analysis showed more lipid deposition in different segments of the $Ldlr^{-/-}G2a^{-/-}$ aorta, especially in

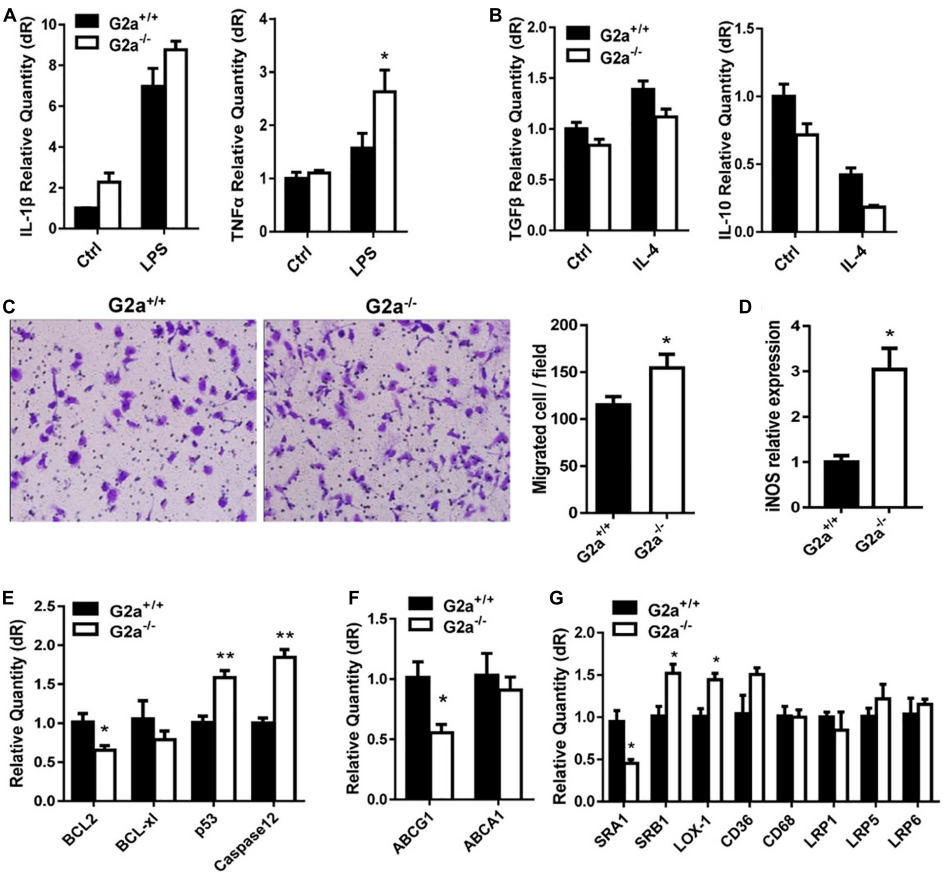

FIGURE 1 | Effect of G2A single knockout on WT rats. Real-time analysis of **(A)** inflammatory cytokines expressed by LPS stimulated macrophages, and **(B)** anti-inflammatory cytokines by IL-4 stimulated macrophages from 8 week-old WT and *G2a*$^{-/-}$ rats. **(C)** Transwell migration assay for 10 μg/ml ox-LDL stimulated macrophages. **(D)** The mRNA level of iNOS in arteries from WT and *G2a*$^{-/-}$ rats. **(E–G)** Real-time PCR analysis of indicated genes in macrophages induced for 24 h by ox-LDL. Data are expressed as mean ± SD. $n = 3$–9. $^{*}p < 0.05$, $^{**}p < 0.01$ vs. WT littermates (Student's *t*-test).

the aortic sinus and coronary arterial orifice (**Figures 3B,C**). To analyze whether G2A deficiency affected other tissues, we examined the liver, spleen, heart, kidney, visceral adipose tissue (VAT), and lung. No significant change was discovered in their relative tissue weight (data not shown). However, there was more lipid deposit in the *Ldlr*$^{-/-}$*G2a*$^{-/-}$ liver without significant change in aspartate aminotransferase (AST) or alanine aminotransferase (ALT) levels. A similar result was noticed in the kidney of *Ldlr*$^{-/-}$*G2a*$^{-/-}$ rats, with more lipid deposits but no significant difference in uric acid or creatinine level. Moreover, no apparent histological change was found in the liver or kidney (**Supplementary Figure 6**). The collective data means G2A deficiency in *Ldlr*$^{-/-}$ rats led to increased atherosclerosis development, and enhanced lipid deposition in the liver and kidney.

Increased Macrophage Recruitment and Vascular Fibrosis in Aortas of G2A Deficient *Ldlr*$^{-/-}$ Rats

As macrophage infiltration plays an important role in atherosclerosis development (Martens et al., 1998), we proceeded to perform immunohistochemical analysis to see whether there is any change in aortic macrophages. Indeed, increased macrophage content was found in the aortic sinus of *Ldlr*$^{-/-}$*G2a*$^{-/-}$ as compared to *Ldlr*$^{-/-}$ rats (**Figure 4A**), together with markedly elevated CD68 mRNA level (**Figure 4C**). In addition, increased staining of the adhesion molecule VCAM1 was also found in the aortic sinus of *Ldlr*$^{-/-}$*G2a*$^{-/-}$ rats, together with increased mRNA levels of VCAM1, ICAM1, and E-selectin, although the VCAM1 change did not reach significance (**Figures 4B,D**). Moreover, Masson staining revealed more collagen deposition in the vessel wall of *Ldlr*$^{-/-}$*G2a*$^{-/-}$ rats (**Figure 4E**). Hence the aggravated atherosclerosis in G2A deficient *Ldlr*$^{-/-}$ rats was accompanied by increased macrophage recruitment and vascular fibrosis.

Enhancement of Macrophage Migration and Apoptosis in the G2A Deficient Atherosclerotic Rats

The above results and G2A single deletion's effect on macrophages prompted us to analyze functional changes in monocytes and macrophages. Both bone marrow-derived

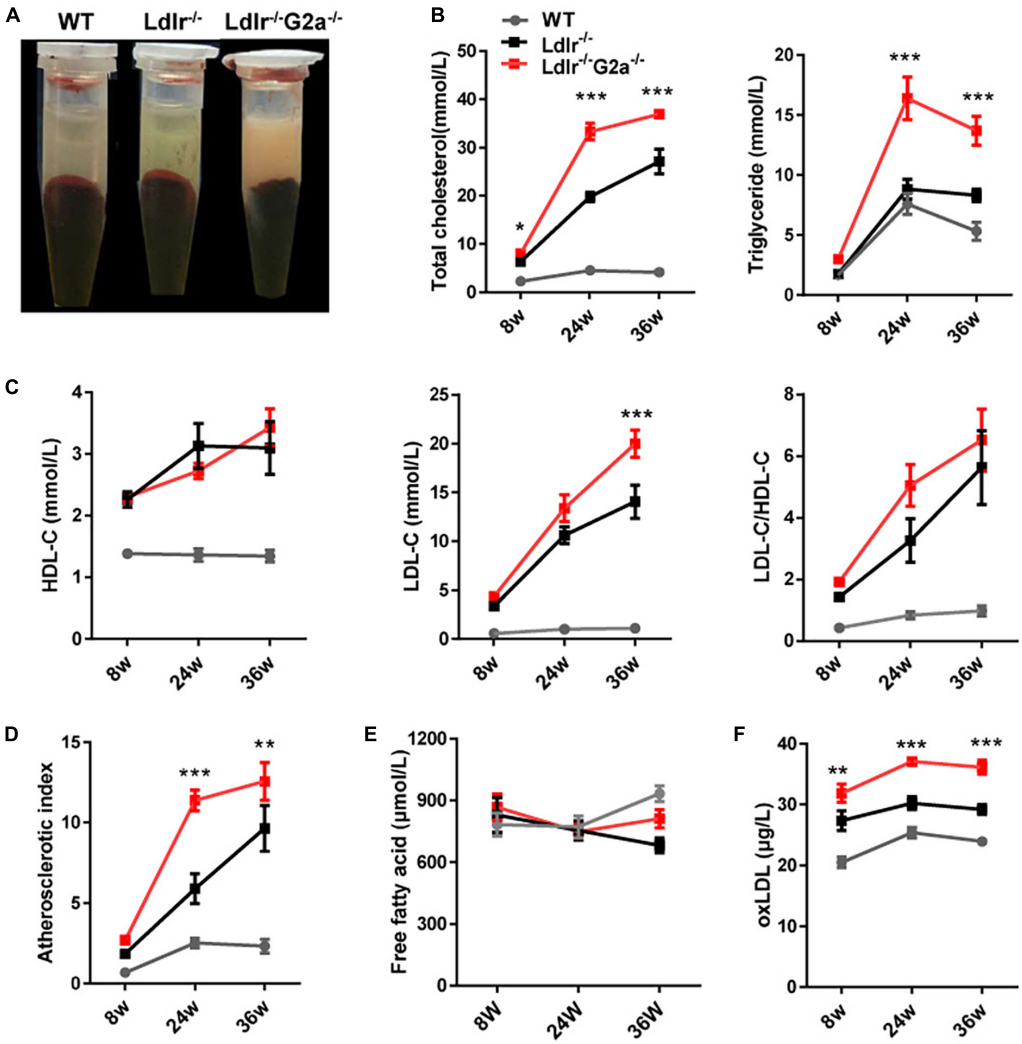

FIGURE 2 | Lipid profile of WT, *Ldlr*$^{-/-}$and *Ldlr*$^{-/-}$*G2a*$^{-/-}$ rats. **(A)** Typical appearance of sera from the three genotypes. **(B)** Total cholesterol (TC) and triglyceride (TG) level. **(C)** High density lipoprotein cholesterol (HDL-c), Low-density lipoprotein cholesterol (LDL-c), and LDL-c/HDL-c ratio. **(D)** The atherosclerosis predictor atherosclerotic index, calculated as (TC- HDL-c)/HDL-c. **(E)** Serum level of free fatty acid. **(F)** Oxidized low-density lipoprotein (oxLDL) level. Data are shown as mean ± SD and combined from male and female rats (they showed a similar pattern). n = 10–15. *$p < 0.05$, **$p < 0.01$, ***$p < 0.001$ vs. *Ldlr*$^{-/-}$ rats (two-way ANOVA with Tukey's multiple comparisons test).

monocytes and macrophages from *Ldlr*$^{-/-}$*G2a*$^{-/-}$ rats exhibited a higher migration ability than those from *Ldlr*$^{-/-}$ rats (**Figures 5A,B**). Concomitantly, there were consistently and significantly increased aortic chemokines related to monocyte and macrophage recruitment (**Figure 5C**), indicating increased interactions between these cells and endothelium. The increased macrophage chemotaxis may also attribute to matrix metalloproteinase (MMP) enhancement, as increased expression of MMP1 and MMP9 was found in *Ldlr*$^{-/-}$*G2a*$^{-/-}$ macrophages (**Figure 5D**). Since the significantly increased CCL2 is related to inflammation, the inflammatory phenotype of macrophages was also examined. After 24 h stimulation by oxLDL, *Ldlr*$^{-/-}$*G2a*$^{-/-}$ macrophages displayed a minor increase in inflammatory IL-1β and reduction in anti-inflammatory IL-10 as compared to *Ldlr*$^{-/-}$ macrophages. In polarization conditions, G2A deficient macrophages showed a significant increase of IL-1β when stimulated by LPS, and decreased TGF and IL-10 when stimulated with IL-4 (**Supplementary Figure 7**).

The expression of genes encoding ATP-binding cassette transporters, responsible for cholesterol efflux, was unaffected by G2A deficiency as examined by real-time PCR (**Figure 5E**). However, the expression of scavenger receptors (SRs) including LOX1, CD36, SRA1, and SRB1 were all significantly increased (**Figure 5F**). Among them, LOX-1 displayed the greatest elevation. SRs mediated oxLDL internalization was also enhanced by G2A deletion (**Figure 5G**). Intriguingly, the cell number was declined when macrophages were incubated with Dil-oxLDL for 24 h, as compared to 18 h incubation (data not shown), implying possible cell apoptosis.

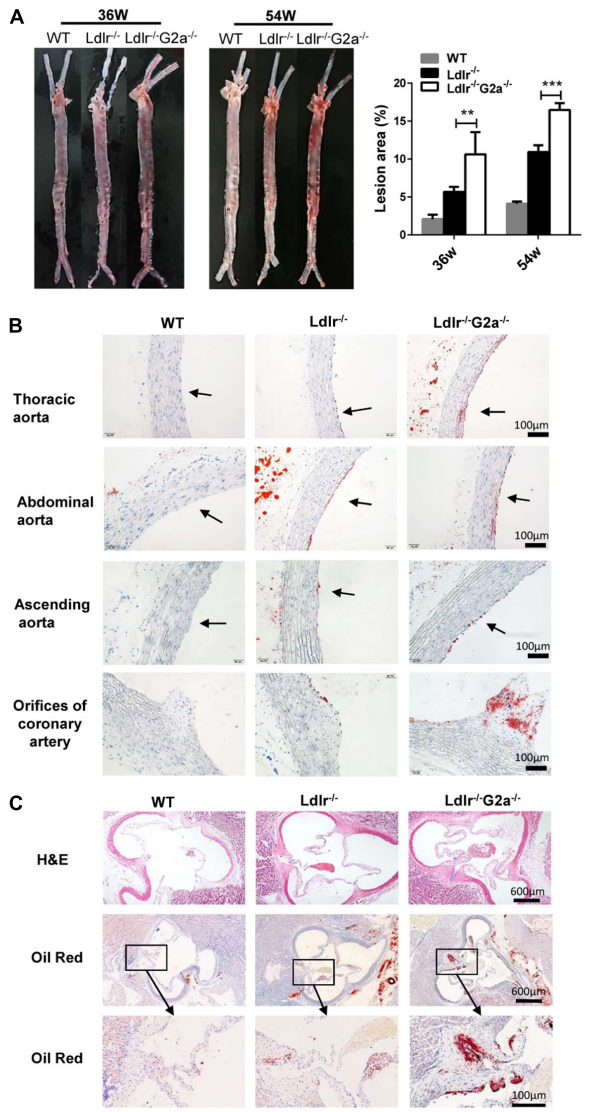

FIGURE 3 | Representative images and lesion quantification of atherosclerosis in the Western diet-fed rats. **(A)** Oil Red O staining of *en face* aortas, and quantification for their lesion area (% total aorta) in 36 and 54 week-old male rats. **(B)** Oil Red O staining of aortic segments in 36 week-old rats. **(C)** H&E and Oil Red O staining of aortic sinuses from different genotypes at 36 weeks of age. Data are shown as mean ± SD ($n = 6$). $^{**}p < 0.01$ and $^{***}p < 0.001$ vs. $Ldlr^{-/-}$ rats (two-way ANOVA with Tukey's multiple comparisons test).

Further examination revealed G2A regulating macrophage apoptosis which is related with oxidative stress. As in WT, the absence of G2A in $Ldlr^{-/-}$ rats greatly up-regulated iNOS mRNA expression, both in the aorta and oxLDL stimulated macrophages, suggesting stress associated with increased blood oxLDL and oxLDL uptake. This was confirmed by the elevated serum MDA level in $Ldlr^{-/-}G2a^{-/-}$ rats and ROS generation in G2A knockdown HUVEC cells (**Figures 6A,B**). As shown in **Figure 6C**, the expression of apoptotic genes p53 and caspase 12 was enhanced while survival genes (Bcl2, Dad, and Bcl-xl) were reduced in $Ldlr^{-/-}G2a^{-/-}$ macrophages. In addition, flow cytometry analysis (FACSCalibur, Becton Dickinson, United States) manifested significantly elevated Annexin V-positive apoptotic cells (**Figure 6D**). The result was corroborated by *in situ* TUNEL assay which showed increased corresponding fluorescence in section preparations of $Ldlr^{-/-}G2a^{-/-}$ aortas (**Supplementary Figure 8**). Apoptotic pathway-related genes were then probed by immunoblotting. There was significantly reduced phosphorylation of PI3 kinase (PI3K) and AKT (**Figure 6E** and **Supplementary Figure 9**), as well as a decrease of downstream gene expression including Bcl2 and Bcl-xl. The data suggested possible participation of PI3K/AKT signaling pathway in G2A regulation to macrophage apoptosis. Finally, to examine whether there was any alteration in efferocytosis, the clearance of apoptotic cells, LDLR-related proteins in macrophages were analyzed significantly suppressed expression of LRP1 and LRP2 was detected. Moreover, Gas6 and Mfge8 were inhibited although only the latter reached significance (**Figure 6F**). Altogether, the above results indicate that G2A deletion induced atherosclerosis aggravation was associated with macrophage changes including increased chemotaxis and apoptosis.

DISCUSSION

In the present study, we found a protective effect mediated by G2A in the atherosclerosis model established from LDLR deficient rats. As reported in $Ldlr^{-/-}$ mice, rat G2A deficiency did not significantly alter body weight. Very different from mice, though, the absence of G2A in the rat model markedly exacerbated lipid disorder. In addition, rat G2A deficiency promoted oxidative stress and secretion of aortic chemokines and adhesive molecules which attracted macrophages, eventually led to aggravated atherosclerosis. Our data indicate that G2A not only participates in regulating macrophage apoptosis and accumulation but is also involved in lipid metabolism. Intriguingly, the effects of G2A on macrophage and lipid were noticed as early as 8 week-old, before the induction of atherosclerosis. While the major functions of G2A on macrophages were regulating migration and apoptosis as G2A deficiency in both WT and $Ldlr^{-/-}$ led to obvious changes in these two phenotypes, G2A deletion aggravated lipid disorder only became eminent in $Ldlr^{-/-}$ rats. A scheme summarizing the potential mechanism of G2A deficiency in atherosclerosis development by regulating macrophages has been provided in **Figure 7**.

Previous reports about G2A regulation to immune cells were mostly based on *in vitro* experiments, stimulated by different lipid activators like LPC and 9-HODE (Radu et al., 2004; Wang et al., 2005; Yang et al., 2005; Frasch et al., 2007). Whether one of these ever-growing activators could become the specific agonist for G2A is debated. Additionally, data from murine models about G2A's role in atherosclerosis are conflicting. While comparing to mice G2A receptor, the rat homolog bears more similarities with human G2A. Above considerations prompted us to use the rat atherosclerosis model which has been reported to share a more similar phenotype to the human disease (Zhao et al., 2018;

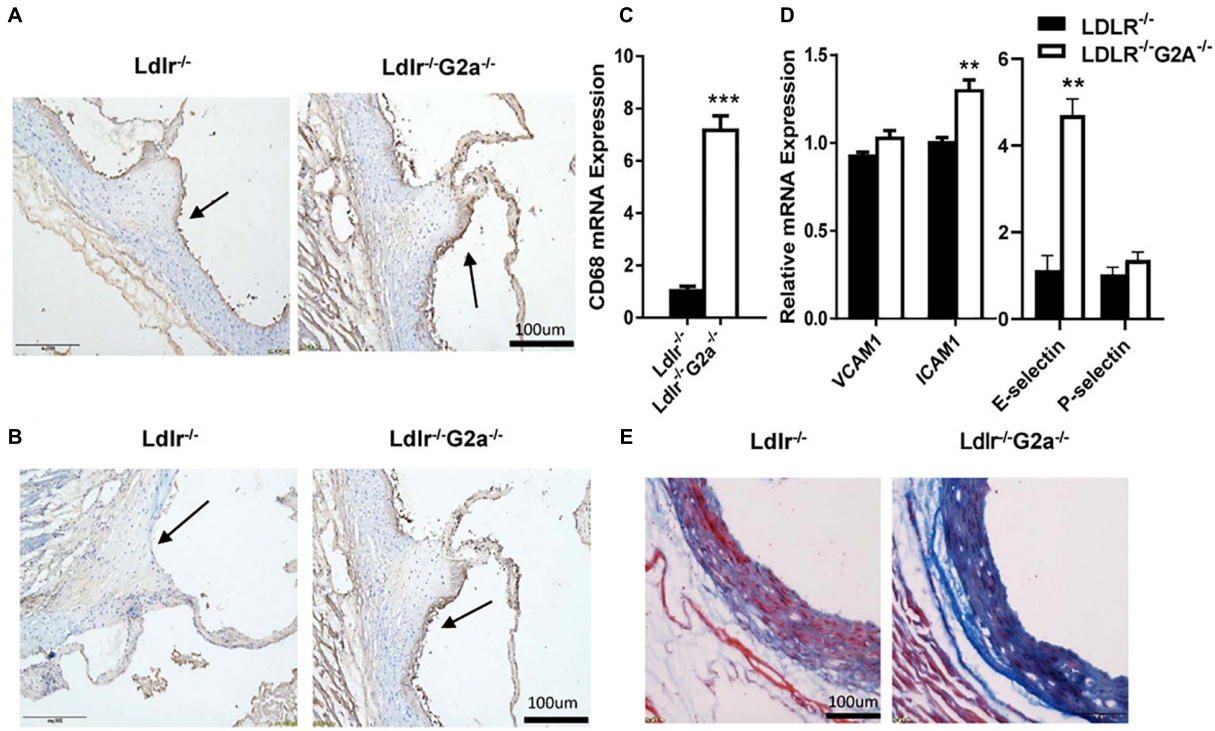

FIGURE 4 | Lesional macrophage accumulation and vascular fibrosis in 36 week-old rats. **(A)** Macrophages in aortic sinus of the two indicated genotypes, identified by immunohistochemical staining with anti-CD68 antibody (Bio-Rad AbD Sereotec, Cat. No. MCA341PE). **(B)** Detection of VCAM1 in aortic sinus by immunohistochemical staining with anti-VCAM1 antibody (Proteintech, Cat. No. 11444-I-AP). **(C,D)** The mRNA level of CD68, VCAM1, ICAM1, E-selectin, and P-selectin in aortas. **(E)** Masson staining of aortic sinuses. Data are shown as mean ± SD. $n = 4–8$. $^{**}p < 0.01$ and $^{***}p < 0.001$ (Student's *t*-test).

Lee et al., 2019). Our investigation in the $Ldlr^{-/-}$ rat model found that knockout of G2A exacerbated atherosclerosis. This result agrees with the mice report which described that G2A deletion on $Apoe^{-/-}$ or $Ldlr^{-/-}$ background contributed to aortic macrophage accumulation and increased atherosclerotic plaques (Bolick et al., 2009), but it is in contrast to the other two in $Ldlr^{-/-}$ model which found that mice G2A deficiency attenuated atherosclerosis (Parks et al., 2006, 2009). It is expected that our study may take advantage of the benefits from the rat model and provide new clues for interpreting the role of G2A. Interestingly in this study, the rat G2A was found to strongly modify the lipid profile.

This dramatic impact of G2A on lipid profile in LDLR deficient rats was completely different from mouse studies. Although a few reports suggested G2A may participate in homeostasis of hepatobiliary bile salt and phospholipid that is important for gallstone formation (Johnson et al., 2008), analysis of blood lipid profiles usually presented no significant change in G2A deficient atherosclerotic mice (Parks et al., 2005; Bolick et al., 2009). Some studies observed HDL elevation only after extended treatment with Western diet or high-cholesterol diet in $Ldlr^{-/-}$ mice (Parks et al., 2006, 2009). It is well-known that dyslipidemia could lead to inflammation. Here the intriguing result that G2A deficiency in $Ldlr^{-/-}$ rats induced a marked elevation of dyslipidemia implied that aberrant lipid metabolism may cross-regulate with macrophages and endothelium in atherosclerosis development. Especially, the enhanced inflammatory phenotype in macrophages might attribute to hypercholesteremia induced by G2A depletion, as obvious inflammatory macrophages were only observed in $Ldlr^{-/-}G2a^{-/-}$ rats along with the elevated lipid disorder, not in single G2A knockouts.

As a stress sensor that monitors oxidative state (Obinata and Izumi, 2009), G2A deletion in rats led to arterial stress with increased ROS and oxLDL levels, thus contributed to more macrophage accumulation. Here macrophages may promote atherosclerosis progression through different aspects including migration and apoptosis. The enhanced monocyte and macrophage migration due to G2A deletion brought about elevated macrophage recruitment to the vessel wall, as previously reported in $Ldlr^{-/-}G2a^{-/-}$ mice (Bolick et al., 2007). G2A knockdown had also been reported to increase macrophages in mouse neurons and prolong inflammatory hyperalgesia (Su et al., 2018). However, some mice reports stated no change in macrophage chemotaxis by G2A deletion in *Ldlr* knockouts (Parks et al., 2005). In addition to elevated aortic chemokines and adhesion molecules, the increased macrophage migration in our study may also be attributable to MMP1 and MMP9 enhancement. The oxLDL up-regulates MMPs production from macrophages (Chase et al., 2002). Among them, MMP9 is well-known for its induction of cell migration including macrophages and vascular smooth muscle cells, as well as its promotion to macrophage invasion

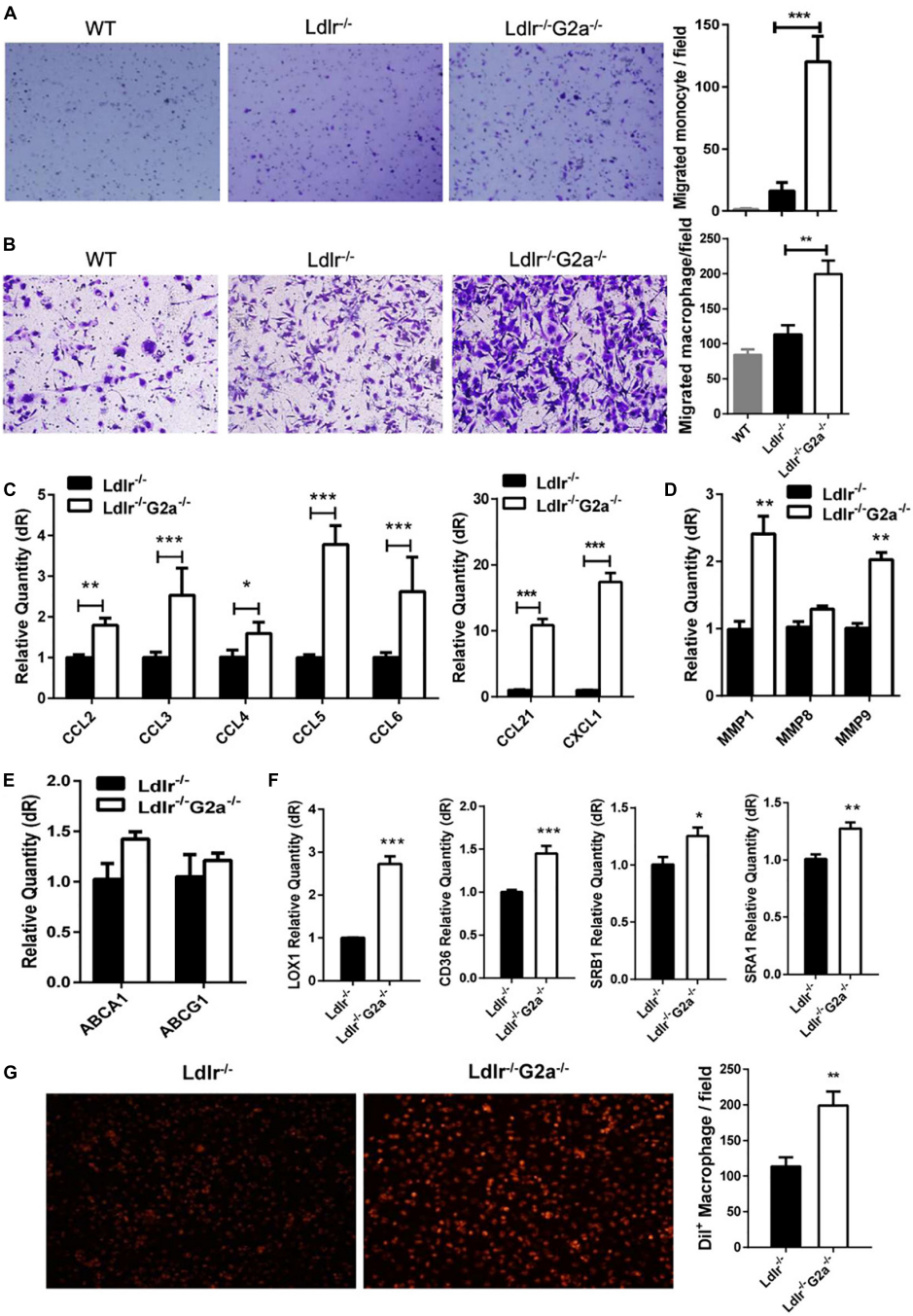

FIGURE 5 | Effect of G2A deficiency on macrophage migration and lipid transportation. **(A,B)** Migration assay for oxLDL stimulated monocytes and macrophages from different genotypes of rats. **(C)** The mRNA level of aortic chemokines. **(D)** Relative expression of MMPs in macrophages. **(E)** Expression of ATP binding cassette transporters in macrophages. **(F)** Expression of different scavenger receptors. **(G)** Dil-oxLDL uptake by *Ldlr*$^{-/-}$ and *Ldlr*$^{-/-}$*G2a*$^{-/-}$ macrophages. Cells were incubated with 10 μg/ml Dil-oxLDL for 18 h in the dark, then washed and examined under a microscope. Fluorescence was analyzed by Image J. Data are shown as mean ± SD. $n = 3$–9. $^{*}p < 0.05$, $^{**}p < 0.01$ and $^{***}p < 0.001$.

through the intima (Newby, 2007; Yang et al., 2015; Webb et al., 2017). Recently a study found that both MMP1 and MMP9 were closely linked with aldosterone-induced macrophage migration and infiltration in the myocardium (Liao et al., 2020). MMP9 is also known to associate with collagen accumulation in hypertensive arterial walls (Wang et al., 2015).

Apart from migration, macrophage apoptosis also participates in G2A regulating atherosclerosis, which seems related to PI-3K/Akt pathway. However, there may be other pathways or

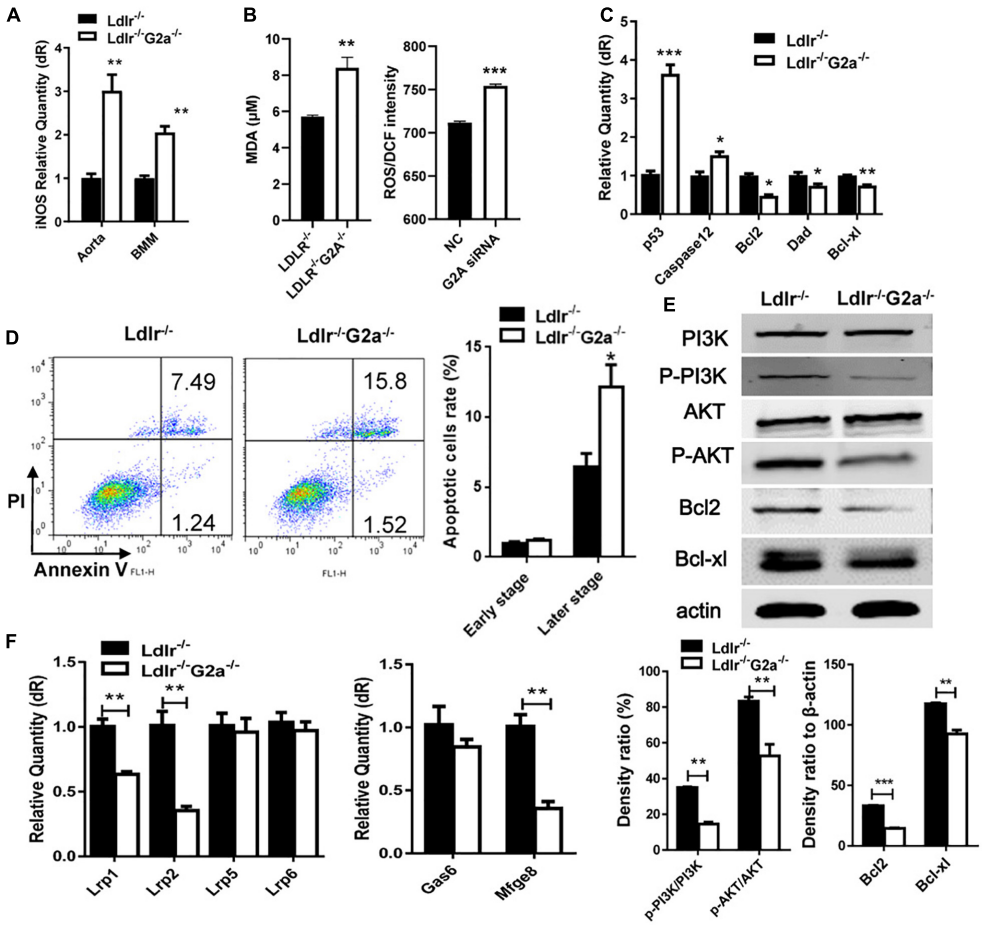

FIGURE 6 | Macrophage apoptosis and efferocytosis in *Ldlr*$^{-/-}$ and *Ldlr*$^{-/-}$*G2a*$^{-/-}$ rats. **(A)** iNOS expression in aortas and oxLDL-induced macrophages. **(B)** The serum MDA level of the two genotypes, and ROS generation in G2A knockdown HUVEC cells (NC, scrambled siRNA). **(C)** Relative expression of apoptotic genes and survival genes. **(D)** Flow cytometry analysis for Annexin V positive macrophages. **(E)** Immunoblot analysis of proteins of PI3K/AKT pathway in macrophages. The β-actin was used as a control for protein loading. **(F)** Relative expression of efferocytosis related genes. Data are representative of three or more independent experiments and shown as mean ± SD. *$p < 0.05$, **$p < 0.01$ and ***$p < 0.001$ (Student's *t*-test).

components involved. As shown in **Figure 7**, G2A deficiency-induced elevation in LDL and ox-LDL intake leads to lipid accumulation in macrophages, which may cause activation of the ER stress-mediated pathway and promote apoptosis (Chistiakov et al., 2016; Sukhorukov et al., 2020). The increased accumulation of apoptotic cells further enhanced lesion development and macrophage content. Here decreased efferocytosis may also contribute to the accumulating process, as previous reports suggested G2A mediate efferocytosis following tissue injury (Kabarowski, 2009; Frasch et al., 2011; Kern et al., 2018). Since macrophage death is often observed in rupture-prone human and mice plaques (Johnson and Jackson, 2001), increased macrophage apoptosis together with increased MMPs is frequently linked with plaque instability. Moreover, formerly MMP1 was reported to enhance the senescence of endothelial cells via p53 activation (Struewing et al., 2009). In this study we found both increased MMP1 and p53 expression in G2A deficient macrophages, implying G2A deletion may exert an effect on macrophage senescence, which might eventually lead to autophagy. Moreover, one of the downstream genes of the PI3K/Akt pathway, mTOR, inhibits autophagy (Glick et al., 2010), so the inhibited PI3K/Akt pathway by G2A deletion implies possible autophagy involvement. Considering the current study and previous rat atherosclerotic investigations (Wei et al., 2015; Sithu et al., 2017; Zhao et al., 2018), we suspect rats may more accurately model macrophage functions involved in atherosclerosis.

While plaque formation is a consequence of immune cell migration, the initiation of atherosclerosis is thought to relate to endothelial dysfunction. Although more work needs to be done, we did find that G2A in the endothelium may play an important role in atherosclerosis regulation. In addition to the elevated expression of adhesion molecules in G2A deficient aortic sinus, aortic chemokines were also markedly enhanced. These led to macrophage recruitment, indicating promoted endothelial-monocyte/macrophage interaction. We also found that G2A knockdown in HUVEC cells promoted ROS generation. These data support endothelial G2A's anti-atherosclerosis effect (Bolick et al., 2007), and may partially

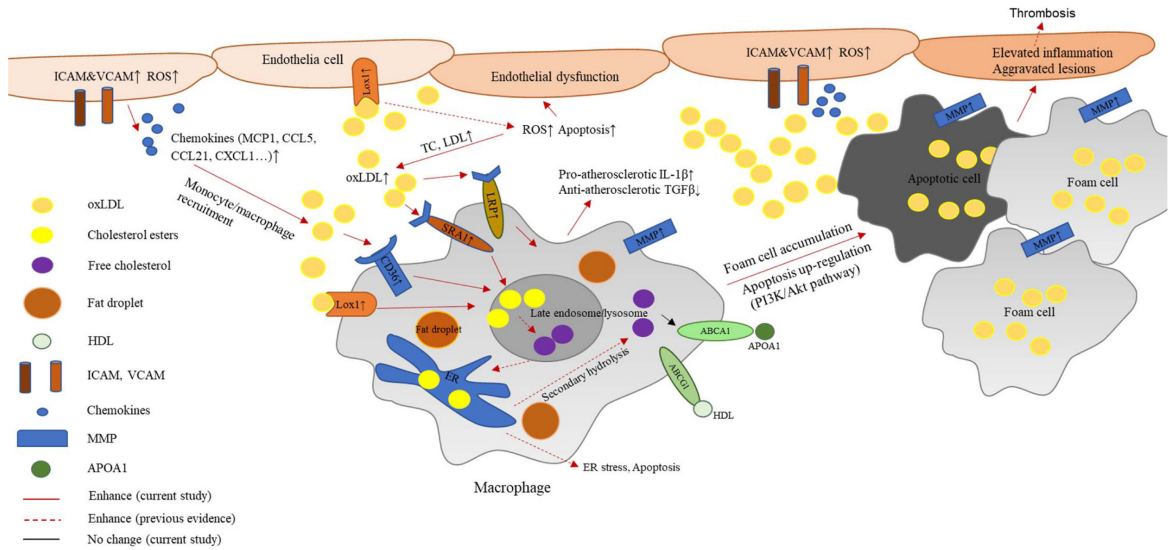

FIGURE 7 | Potential mechanism of G2A deficiency in atherosclerosis development by regulating macrophages. G2A knockout in LDLR deficient background leads to an exaggerated lipid disorder and pro-atherosclerosis phenotype. The latter associates with oxidative stress and endothelial dysfunction. Increased expression of adhesion molecules and chemokines recruits more macrophages to the intima. These macrophages engulf oxidized cholesterol (oxLDL) through scavenger receptors including LOX-1, CD36, and SR-A1. However, ABCA1 and ABCG1 which participate in cholesterol efflux did not change. The disruption of lipid homeostasis in macrophages leads to cholesterol accumulation and formation of foam cells. In addition, inflammatory cytokine production by macrophages shifts them to a more pro-atherosclerosis phenotype. Moreover, PI-3K/AKT signaling pathway was found to participate in the up-regulated apoptosis. All these changes eventually contribute to aggravated aortic lesions.

explain why macrophage changes were noticed even before the induction of atherosclerosis.

In the future, more solid investigation is essential to elucidate functions of endothelial G2A. For macrophage, a rat model with specific G2A deficiency in this cell type might be more useful to determine the exact effect of macrophage G2A on atherosclerosis. Other immune cells, such as T cells may also play their parts in G2A mediated atherosclerosis development (Radu et al., 2004). In addition, it is not certain how much of these rat data could be translated to human disease. Despite these limitations, the present research offers a new angle to look at the function of G2A in atherosclerosis initiation and development.

In summary, this study enriched our understanding of G2A in atherosclerosis development. The rat data demonstrate G2A regulating atherosclerosis by modifying lipid disorder and macrophage functions. Increased atherosclerosis in $Ldlr^{-/-}G2a^{-/-}$ rats may partially attribute to multiple alterations in macrophages including up-regulated migration and apoptosis. More importantly, the marked regulation of lipid disorder presents a new dimension about the role of G2A. It is possible that by modulating G2A signaling in both lipid metabolism and macrophages, we may find a way to develop more powerful therapies for atherosclerosis.

DATA AVAILABILITY STATEMENT

The original contributions presented in the study are included in the article/ **Supplementary Material**, further inquiries can be directed to the corresponding author/s.

ETHICS STATEMENT

The animal study was reviewed and approved by the Animal Ethics Committee of East China Normal University.

AUTHOR CONTRIBUTIONS

HC, BZ, ML, and DL conceived the experiments. XC, RX, YT, MW, YS, YXu, YY, YZ, LX, and YXi conducted the experiments. XC, RX, YT, MW, YS, YXu, and DL analyzed the results. XC, RX, and YXi drafted the work. HC, BZ, and ML wrote and revised the manuscript. All authors reviewed and approved the manuscript.

FUNDING

This work was supported by grants from the National Natural Science Foundation of China (81830083), the Innovation Program of Shanghai Municipal Education Commission (2017-01-07-00-05-E00011), and ECNU Multifunctional Platform for Innovation (011).

SUPPLEMENTARY MATERIAL

The Supplementary Material for this article can be found online at: https://www.frontiersin.org/articles/10.3389/fphys.2021.659211/full#supplementary-material

REFERENCES

Acton, S., Rigotti, A., Landschulz, K. T., Xu, S., Hobbs, H. H., and Krieger, M. (1996). Identification of scavenger receptor SR-BI as a high density lipoprotein receptor. *Science* 271, 518–520. doi: 10.1126/science.271.5248.518

Bolick, D. T., Skaflen, M. D., Johnson, L. E., Kwon, S. C., Howatt, D., Daugherty, A., et al. (2009). G2A deficiency in mice promotes macrophage activation and atherosclerosis. *Circ. Res.* 104, 318–327. doi: 10.1161/circresaha.108.181131

Bolick, D. T., Whetzel, A. M., Skaflen, M., Deem, T. L., Lee, J., and Hedrick, C. C. (2007). Absence of the G protein-coupled receptor G2A in mice promotes monocyte/endothelial interactions in aorta. *Circ. Res.* 100, 572–580. doi: 10.1161/01.res.0000258877.57836.d2

Chase, A. J., Bond, M., Crook, M. F., and Newby, A. C. (2002). Role of nuclear factor-kappa B activation in metalloproteinase-1, -3, and -9 secretion by human macrophages in vitro and rabbit foam cells produced in vivo. *Arterioscler. Thromb. Vasc. Biol.* 22, 765–771. doi: 10.1161/01.atv.0000015078.09208.92

Chinetti-Gbaguidi, G., and Staels, B. (2011). Macrophage polarization in metabolic disorders: functions and regulation. *Curr. Opin. Lipidol.* 22, 365–372. doi: 10.1097/mol.0b013e32834a77b4

Chistiakov, D. A., Bobryshev, Y. V., and Orekhov, A. N. (2016). Macrophage-mediated cholesterol handling in atherosclerosis. *J. Cell Mol. Med.* 20, 17–28. doi: 10.1111/jcmm.12689

Davies, M. J., Richardson, P. D., Woolf, N., Katz, D. R., and Mann, J. (1993). Risk of thrombosis in human atherosclerotic plaques: role of extracellular lipid, macrophage, and smooth muscle cell content. *Br. Heart J.* 69, 377–381. doi: 10.1136/hrt.69.5.377

Fogelstrand, P., and Boren, J. (2012). Retention of atherogenic lipoproteins in the artery wall and its role in atherogenesis. *Nutr. Metab. Cardiovasc. Dis.* 22, 1–7. doi: 10.1016/j.numecd.2011.09.007

Foster, J. R., Ueno, S., Chen, M. X., Harvey, J., Dowell, S. J., Irving, A. J., et al. (2019). N-Palmitoylglycine and other N-acylamides activate the lipid receptor G2A/GPR132. *Pharmacol. Res. Perspect.* 7:e00542.

Frasch, S. C., Fernandez-Boyanapalli, R. F., Berry, K. Z., Leslie, C. C., Bonventre, J. V., Murphy, R. C., et al. (2011). Signaling via macrophage G2A enhances efferocytosis of dying neutrophils by augmentation of RAC activity. *J. Biol. Chem.* 286, 12108–12122. doi: 10.1074/jbc.m110.181800

Frasch, S. C., Zemski-Berry, K., Murphy, R. C., Borregaard, N., Henson, P. M., and Bratton, D. L. (2007). Lysophospholipids of different classes mobilize neutrophil secretory vesicles and induce redundant signaling through G2A. *J. Immunol.* 178, 6540–6548. doi: 10.4049/jimmunol.178.10.6540

Glick, D., Barth, S., and Macleod, K. F. (2010). Autophagy: cellular and molecular mechanisms. *J. Pathol.* 221, 3–12. doi: 10.1002/path.2697

Johnson, J. L., and Jackson, C. L. (2001). Atherosclerotic plaque rupture in the apolipoprotein E knockout mouse. *Atherosclerosis* 154, 399–406. doi: 10.1016/s0021-9150(00)00515-3

Johnson, L. E., Elias, M. S., Bolick, D. T., Skaflen, M. D., Green, R. M., and Hedrick, C. C. (2008). The G protein-coupled receptor G2A: involvement in hepatic lipid metabolism and gallstone formation in mice. *Hepatology* 48, 1138–1148. doi: 10.1002/hep.22433

Kabarowski, J. H. (2009). G2A and LPC: regulatory functions in immunity. *Prostaglandins Other Lipid Mediat.* 89, 73–81. doi: 10.1016/j.prostaglandins.2009.04.007

Kadl, A., Meher, A. K., Sharma, P. R., Lee, M. Y., Doran, A. C., Johnstone, S. R., et al. (2010). Identification of a novel macrophage phenotype that develops in response to atherogenic phospholipids via Nrf2. *Circ. Res.* 107, 737–746. doi: 10.1161/circresaha.109.215715

Kern, K., Schafer, S. M. G., Cohnen, J., Pierre, S., Osthues, T., Tarighi, N., et al. (2018). The G2A receptor controls polarization of macrophage by determining their localization within the inflamed tissue. *Front. Immunol.* 9:2261. doi: 10.3389/fimmu.2018.02261

Lee, J. G., Ha, C. H., Yoon, B., Cheong, S. A., Kim, G., Lee, D. J., et al. (2019). Knockout rat models mimicking human atherosclerosis created by Cpf1-mediated gene targeting. *Sci. Rep.* 9:2628.

Liao, C. W., Chou, C. H., Wu, X. M., Chen, Z. W., Chen, Y. H., Chang, Y. Y., et al. (2020). Interleukin-6 plays a critical role in aldosterone-induced macrophage recruitment and infiltration in the myocardium. *Biochim. Biophys. Acta Mol. Basis Dis.* 1866:165627. doi: 10.1016/j.bbadis.2019.165627

Martens, J. S., Reiner, N. E., Herrera-Velit, P., and Steinbrecher, U. P. (1998). Phosphatidylinositol 3-kinase is involved in the induction of macrophage growth by oxidized low density lipoprotein. *J. Biol. Chem.* 273, 4915–4920. doi: 10.1074/jbc.273.9.4915

Moore, K. J., and Tabas, I. (2011). Macrophages in the pathogenesis of atherosclerosis. *Cell* 145, 341–355. doi: 10.1016/j.cell.2011.04.005

Muschter, D., Gottl, C., Vogel, M., Grifka, J., Straub, R. H., and Grassel, S. (2015). Reactivity of rat bone marrow-derived macrophages to neurotransmitter stimulation in the context of collagen II-induced arthritis. *Arthrit. Res. Ther.* 17:169.

Newby, A. C. (2007). Metalloproteinases and vulnerable atherosclerotic plaques. *Trends Cardiovasc. Med.* 17, 253–258. doi: 10.1016/j.tcm.2007.09.001

Obinata, H., Hattori, T., Nakane, S., Tatei, K., and Izumi, T. (2005). Identification of 9-hydroxyoctadecadienoic acid and other oxidized free fatty acids as ligands of the G protein-coupled receptor G2A. *J. Biol. Chem.* 280, 40676–40683. doi: 10.1074/jbc.m507787200

Obinata, H., and Izumi, T. (2009). G2A as a receptor for oxidized free fatty acids. *Prostaglandins Other Lipid Mediat.* 89, 66–72. doi: 10.1016/j.prostaglandins.2008.11.002

Parks, B. W., Gambill, G. P., Lusis, A. J., and Kabarowski, J. H. (2005). Loss of G2A promotes macrophage accumulation in atherosclerotic lesions of low density lipoprotein receptor-deficient mice. *J. Lipid Res.* 46, 1405–1415. doi: 10.1194/jlr.m500085-jlr200

Parks, B. W., Lusis, A. J., and Kabarowski, J. H. (2006). Loss of the lysophosphatidylcholine effector, G2A, ameliorates aortic atherosclerosis in low-density lipoprotein receptor knockout mice. *Arterioscler. Thromb. Vasc. Biol.* 26, 2703–2709. doi: 10.1161/01.atv.0000246774.02426.71

Parks, B. W., Srivastava, R., Yu, S., and Kabarowski, J. H. (2009). ApoE-dependent modulation of HDL and atherosclerosis by G2A in LDL receptor-deficient mice independent of bone marrow-derived cells. *Arterioscler. Thromb. Vasc. Biol.* 29, 539–547. doi: 10.1161/atvbaha.108.179937

Peter, C., Waibel, M., Radu, C. G., Yang, L. V., Witte, O. N., Schulze-Osthoff, K., et al. (2008). Migration to apoptotic "find-me" signals is mediated via the phagocyte receptor G2A. *J. Biol. Chem.* 283, 5296–5305. doi: 10.1074/jbc.m706586200

Qin, X., Qiu, C., and Zhao, L. (2014). Lysophosphatidylcholine perpetuates macrophage polarization toward classically activated phenotype in inflammation. *Cell Immunol.* 289, 185–190. doi: 10.1016/j.cellimm.2014.04.010

Radu, C. G., Yang, L. V., Riedinger, M., Au, M., and Witte, O. N. (2004). T cell chemotaxis to lysophosphatidylcholine through the G2A receptor. *Proc. Natl. Acad. Sci. U.S.A.* 101, 245–250. doi: 10.1073/pnas.2536801100

Rikitake, Y., Hirata, K., Yamashita, T., Iwai, K., Kobayashi, S., Itoh, H., et al. (2002). Expression of G2A, a receptor for lysophosphatidylcholine, by macrophages in murine, rabbit, and human atherosclerotic plaques. *Arterioscler. Thromb. Vasc. Biol.* 22, 2049–2053. doi: 10.1161/01.atv.0000040598.18570.54

Shalhoub, J., Falck-Hansen, M. A., Davies, A. H., and Monaco, C. (2011). Innate immunity and monocyte-macrophage activation in atherosclerosis. *J. Inflamm.* 8:9. doi: 10.1186/1476-9255-8-9

Sithu, S. D., Malovichko, M. V., Riggs, K. A., Wickramasinghe, N. S., Winner, M. G., Agarwal, A., et al. (2017). Atherogenesis and metabolic dysregulation in LDL receptor-knockout rats. *JCI Insight.* 2:e86442.

Struewing, I. T., Durham, S. N., Barnett, C. D., and Mao, C. D. (2009). Enhanced endothelial cell senescence by lithium-induced matrix metalloproteinase-1 expression. *J. Biol. Chem.* 284, 17595–17606. doi: 10.1074/jbc.m109.001735

Su, Y. S., Huang, Y. F., Wong, J., Lee, C. W., Hsieh, W. S., and Sun, W. H. (2018). G2A as a threshold regulator of inflammatory Hyperalgesia modulates chronic Hyperalgesia. *J. Mol. Neurosci.* 64, 39–50. doi: 10.1007/s12031-017-1000-3

Sukhorukov, V. N., Khotina, V. A., Bagheri Ekta, M., Ivanova, E. A., Sobenin, I. A., and Orekhov, A. N. (2020). Endoplasmic reticulum stress in macrophages: the vicious circle of lipid accumulation and pro-inflammatory response. *Biomedicines* 8:434.

Tabas, I., and Lichtman, A. H. (2017). Monocyte-Macrophages and T Cells in Atherosclerosis. *Immunity* 47, 621–634. doi: 10.1016/j.immuni.2017.09.008

van Diepen, J. A., Berbee, J. F., Havekes, L. M., and Rensen, P. C. (2013). Interactions between inflammation and lipid metabolism: relevance for efficacy of anti-inflammatory drugs in the treatment of atherosclerosis. *Atherosclerosis* 228, 306–315. doi: 10.1016/j.atherosclerosis.2013.02.028

Wang, L., Radu, C. G., Yang, L. V., Bentolila, L. A., Riedinger, M., and Witte, O. N. (2005). Lysophosphatidylcholine-induced surface redistribution regulates signaling of the murine G protein-coupled receptor G2A. *Mol. Biol. Cell* 16, 2234–2247. doi: 10.1091/mbc.e04-12-1044

Wang, M., Kim, S. H., Monticone, R. E., and Lakatta, E. G. (2015). Matrix metalloproteinases promote arterial remodeling in aging, hypertension, and atherosclerosis. *Hypertension* 65, 698–703. doi: 10.1161/hypertensionaha.114.03618

Webb, A. H., Gao, B. T., Goldsmith, Z. K., Irvine, A. S., Saleh, N., Lee, R. P., et al. (2017). Inhibition of MMP-2 and MMP-9 decreases cellular migration, and angiogenesis in in vitro models of retinoblastoma. *BMC Cancer* 17:434. doi: 10.1186/s12885-017-3418-y

Wei, S., Zhang, Y., Su, L., He, K., Wang, Q., Zhang, Y., et al. (2015). Apolipoprotein E-deficient rats develop atherosclerotic plaques in partially ligated carotid arteries. *Atherosclerosis* 243, 589–592. doi: 10.1016/j.atherosclerosis.2015.10.093

Weischenfeldt, J., and Porse, B. (2008). Bone marrow-derived macrophages (BMM): isolation and applications. *CSH Protoc.* 2008:pdb prot5080.

Weng, Z., Fluckiger, A. C., Nisitani, S., Wahl, M. I., Le, L. Q., Hunter, C. A., et al. (1998). A DNA damage and stress inducible G protein-coupled receptor blocks cells in G2/M. *Proc. Natl. Acad. Sci. U.S.A.* 95, 12334–12339. doi: 10.1073/pnas.95.21.12334

Wu, Y., Wang, X., Chang, S., Lu, W., Liu, M., and Pang, X. (2016). beta-Lapachone induces NAD(P)H:Quinone Oxidoreductase-1- and oxidative stress-dependent heat shock protein 90 cleavage and inhibits tumor growth and angiogenesis. *J. Pharmacol. Exp. Ther.* 357, 466–475. doi: 10.1124/jpet.116.232694

Yang, L. V., Radu, C. G., Wang, L., Riedinger, M., and Witte, O. N. (2005). Gi-independent macrophage chemotaxis to lysophosphatidylcholine via the immunoregulatory GPCR G2A. *Blood* 105, 1127–1134. doi: 10.1182/blood-2004-05-1916

Yang, Y. H., Li, D. L., Bi, X. Y., Sun, L., Yu, X. J., Fang, H. L., et al. (2015). Acetylcholine inhibits LPS-induced MMP-9 production and cell migration via the alpha7 nAChR-JAK2/STAT3 pathway in RAW264.7 cells. *Cell Physiol. Biochem.* 36, 2025–2038. doi: 10.1159/000430170

Zhang, H., Wang, D., Ma, H., Ren, Y., Li, C., Zheng, Y., et al. (2020). Increased atherogenic index in the general hearing loss population. *Open Med.* 15, 349–357. doi: 10.1515/med-2020-0003

Zhao, Y., Yang, Y., Xing, R., Cui, X., Xiao, Y., Xie, L., et al. (2018). Hyperlipidemia induces typical atherosclerosis development in Ldlr and Apoe deficient rats. *Atherosclerosis* 271, 26–35. doi: 10.1016/j.atherosclerosis.2018.02.015

Conflict of Interest: The authors declare that the research was conducted in the absence of any commercial or financial relationships that could be construed as a potential conflict of interest.

Publisher's Note: All claims expressed in this article are solely those of the authors and do not necessarily represent those of their affiliated organizations, or those of the publisher, the editors and the reviewers. Any product that may be evaluated in this article, or claim that may be made by its manufacturer, is not guaranteed or endorsed by the publisher.

frontiers in Physiology

REVIEW
published: 09 September 2021
doi: 10.3389/fphys.2021.732929

Liver Zonation – Revisiting Old Questions With New Technologies

*Rory P. Cunningham and Natalie Porat-Shliom**

Thoracic and GI Malignancies Branch, Center for Cancer Research, National Cancer Institute, NIH, Bethesda, MD, United States

Despite the ever-increasing prevalence of non-alcoholic fatty liver disease (NAFLD), the etiology and pathogenesis remain poorly understood. This is due, in part, to the liver's complex physiology and architecture. The liver maintains glucose and lipid homeostasis by coordinating numerous metabolic processes with great efficiency. This is made possible by the spatial compartmentalization of metabolic pathways a phenomenon known as liver zonation. Despite the importance of zonation to normal liver function, it is unresolved if and how perturbations to liver zonation can drive hepatic pathophysiology and NAFLD development. While hepatocyte heterogeneity has been identified over a century ago, its examination had been severely hindered due to technological limitations. Recent advances in single cell analysis and imaging technologies now permit further characterization of cells across the liver lobule. This review summarizes the advances in examining liver zonation and elucidating its regulatory role in liver physiology and pathology. Understanding the spatial organization of metabolism is vital to further our knowledge of liver disease and to provide targeted therapeutic avenues.

Keywords: liver, physiology, zonation, architecture, technologies

OPEN ACCESS

Edited by:
Jiqiu Wang,
Shanghai Jiao Tong University, China

Reviewed by:
Savneet Kaur,
Institute of Liver and Biliary Sciences (ILBS), India
Francisco Westermeier,
FH Joanneum, Austria

****Correspondence:***
Natalie Porat-Shliom
poratshliomn@nih.gov

Specialty section:
This article was submitted to Integrative Physiology, a section of the journal Frontiers in Physiology

Received: *29 June 2021*
Accepted: *10 August 2021*
Published: *09 September 2021*

Citation:
Cunningham RP and Porat-Shliom N (2021) Liver Zonation – Revisiting Old Questions With New Technologies. Front. Physiol. 12:732929. doi: 10.3389/fphys.2021.732929

INTRODUCTION

One of the central roles of the liver is maintaining energy homeostasis by preserving blood glucose levels. It does this by storing carbohydrates in the form of glycogen when nutrients are available, and then releasing it back into the blood stream during periods of fasting (Trefts et al., 2017). Facilitating this, the liver alternates between oxidizing fat or glucose for energy, depending on fuel availability. Additionally, the liver is one of the central hubs for protein synthesis – contributing to a wide array of circulating proteins such as albumin, and blood clotting factors. The liver also forms the first line of defense for drug and alcohol detoxification and is an important immunological organ. With these diverse functions in mind, the pertinent question remains – how can these varied and divergent processes coincide simultaneously in the liver?

These multi-faceted, vital physiological roles are enabled by the liver's complex architecture. The liver contains a vast array of cell types all interacting with each other, of which hepatocytes make up ∼60%. Spatially, hepatocytes are arranged into hexagonal units called lobules, made up of around 15 concentric layers of cells. Oxygen, hormone, and nutrient rich blood arrives through the hepatic artery and portal vein and enters at the periphery of the lobule, flowing toward a single central vein (**Figure 1**). Conversely, bile flows outward from the center of the lobule and drains in the peripheral portal bile duct. The regions surrounding the hepatic arteries and portal veins are known as periportal (zone 1), while those adjacent to the central vein are called the pericentral areas of the lobule (zone 3), with the cells in between these regions, referred to as mid-lobular hepatocytes

(zone 2). As blood flows directionally toward the central vein, hepatocytes take up oxygen, nutrients, and metabolize hormones, actively shaping their microenvironment by creating a gradient along the periportal-pericentral axis. In turn, this gradient is one of the primary drivers of differential gene expression and the subsequent functional heterogeneity of cells within the lobule. As a result, the spatial metabolic compartmentalization allows opposing metabolic functions to operate simultaneously. For example, through non-uniform expression of the enzymes, glutamine synthesis is confined to only two layers of hepatocytes surrounding the central vein, whereas ureagenesis exclusively restricted to periportal areas (Gebhardt, 1992). Any ammonia escaping ureagenesis in periportal cells is consumed and converted to glutamine in pericentral cells, thereby maintaining low levels of ammonia. In addition to this binary (on/off) zonated pattern, other enzymes have a graded expression pattern across the lobule. For example, enzymes involved in lipid synthesis are expressed predominantly in the pericentral region and expression gradually diminishes toward the periphery of the lobule, while β-oxidation enzymes in periportal cells decrease in expression in a graded manner toward the central vein (Gebhardt, 1992). These two patterns of gene expression highlight the complexity and specificity of spatially separated functions in the lobule.

Examining liver zonation is vital for our understanding of liver disease, of which many develop non-uniformly across the lobule. One example is non-alcoholic fatty liver disease (NAFLD), a spectrum of liver disease, encompassing hepatic steatosis, steatohepatitis (NASH), cirrhosis, and its end stage of hepatocellular carcinoma (HCC), with disease progression often occurring in a zonated pattern. NAFLD and NASH/cirrhosis initially develop with hepatic steatosis and inflammation, respectively, in the pericentral cells and progresses outward (Chalasani et al., 2008; Yeh and Brunt, 2014). Similarly, drug and alcohol-induced hepatotoxicity (Gebhardt, 1992) as well as parasite infection-induced hepatic fibrosis (Loose et al., 1978) initiates in the pericentral area. Conversely, many liver injuries are restricted to or at least begin in periportal areas, such as autoimmune hepatitis (Sahebjam and Vierling, 2015), primary biliary cirrhosis (Lindor et al., 2009), and iron overload-induced injury (Mori et al., 2020). Moreover, patients with HCC display disrupted Wnt/β-catenin signaling (Tian et al., 2016), key regulators of liver zonation. Aside for non-uniform injury of hepatocytes, other hepatic cell types also display zonated pathology during disease progression to cirrhosis. A mouse model of fibrosis revealed that pericentral hepatic stellate cells differentiate to become the dominant pathogenic collagen-producing cells across the lobule (Dobie et al., 2019). Similarly, liver sinusoidal endothelial cells (LSECs) in pericentral regions are more susceptible to damage associated with liver cirrhosis compared to periportal LSECs, with increased capillarization and decreased regulation of endocytosis (Su et al., 2021). These zonated pathologies of various hepatic cell types reveal differential vulnerabilities which may conceal important underlying mechanisms. In other words, understanding why a disease develops in a certain region or zone may provide new details of its pathophysiology. Examination the non-uniform onset of liver disease, and liver zonation overall, is still in its infancy. Increasing our understanding of the spatial dependence of disease development and progression is crucial for creating targeted treatment approaches.

The concept of hepatic functional heterogeneity is gaining much attention, with several excellent reviews previously published on liver zonation (Jungermann and Katz, 1982; Gebhardt, 1992; Jungermann and Kietzmann, 1996; Gebhardt and Matz-Soja, 2014; Ben-Moshe and Itzkovitz, 2019). In this review, we highlight fundamental questions in liver biology and how addressing them provided insights into liver zonation. In parallel, we will explore how technological advances over the years and the bounds made in recent ones open new opportunity to investigate how zonation supports complex liver metabolism. While embracing technological advancements to further this exciting field, many of the questions raised a century ago are still not fully answered which will be underscored. Ultimately, an integrated understanding of the spatial and temporal regulation of liver function are urgently needed to deepen our knowledge of liver physiology and disease etiology that will enable more efficacious avenues of future treatment.

HEPATOCYTE CELL BIOLOGY ACROSS THE LOBULE

Cell biologists in the early 1900s were fueled purely by a passion for knowledge in the face of limited technology. Unperturbed by this lack of technological advancement, the study of hepatocyte cell biology in the lobule was initially based exclusively on electron microscopy in the early to mid 1900s. Noël (1923) divided the rat liver lobule into three zones of what he eloquently described as the zones of permanent activity (periportal), the intermediary zone (mid lobular), and the zone of permanent repose (pericentral). It was observed that hepatic mitochondria were larger and more spherical in the periportal zone and became elongated toward the central vein (Noël, 1923). Smith (1931) observed no lobular variation in rats with respect to mitochondria morphology, although pericentral cells tended to have less in number. Further, he described the deposition of glycogen after feeding starting from the periphery of the lobule toward the central vein, with its withdrawal during fasting in the opposite order. Kater (1933) used several animal models, including mice, rats, dogs, and birds, to describe the accumulation of glycogen and fat across the lobule, as well as alterations in mitochondria morphology. Deane (1944) showed larger mitochondria, Golgi, bile granules, glycogen, and less lipids in mouse periportal hepatocytes, while Novikoff (1959) described the heterogeneity of enzymes across the rat lobule. Indeed, Dean was the first to coin the term "zonation" when referring to hepatocyte heterogeneity as early as 1944 (Deane, 1944). These scientists were the pioneers of cellular biology at the time, and their work has spawned countless lines of research from these fascinating discoveries, not least being liver zonation. While astute observations for their time, they were limited to individual cell imaging and 2D rendering. This latter consideration may be of particular importance to mitochondrial morphology since a section through the middle of a slender mitochondrion would

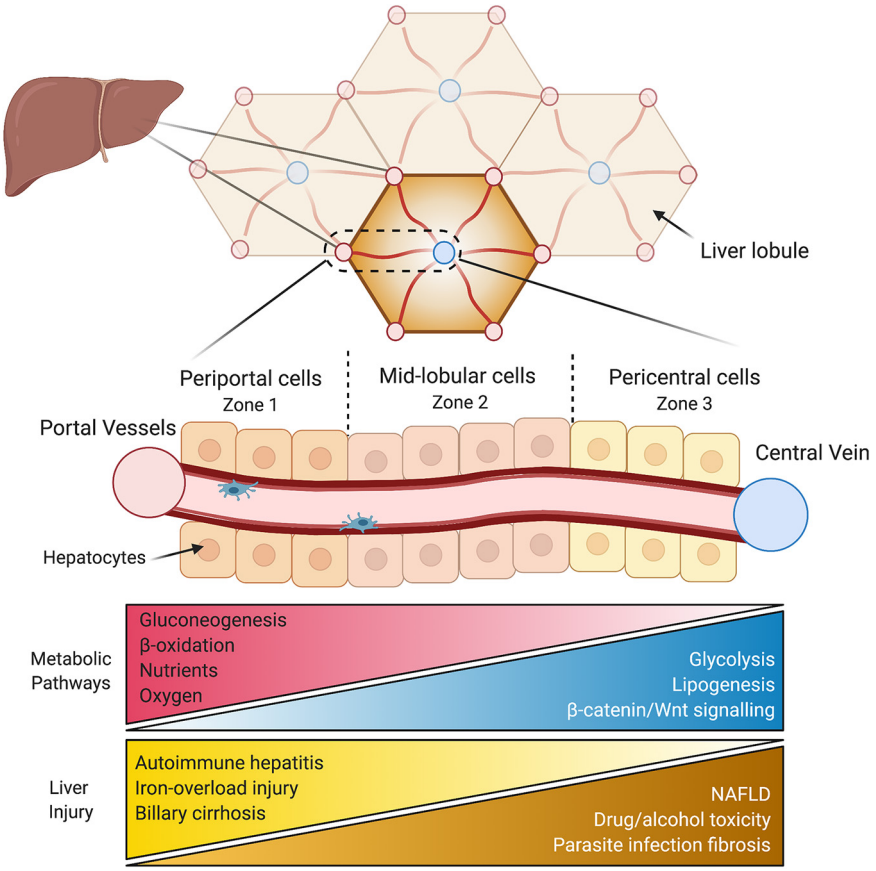

FIGURE 1 | Liver anatomy and the hepatic lobule. The liver is composed of hexagonal units called lobules. Oxygen and nutrient rich blood flows directionally from the hepatic vessels (red) in the corners of the lobule toward a central vein in the middle (blue). Periportal hepatocytes (zone 1) are at the periphery of the lobule, followed by mid-lobular cells, and finally pericentral hepatocytes surround the central vein (zone 3). The variable microenvironment along the periportal-pericentral axis results in graded gene expression and the spatial separation of certain metabolic processes to periportal (red) and pericentral (blue) regions. Certain liver injuries are also zone-dependent, with some originating or confined to periportal (yellow) regions and some to pericentral regions of the lobule (brown). NAFLD, non-alcoholic fatty liver disease.

falsely give it a round and spherical shape. Given that many of the processes that are zonated in the lobule are mitochondria related, β-oxidation and oxidative phosphorylation to name two, examining the structural differences in this organelle and others would further the understanding of the spatial metabolic compartmentalization in the liver.

Recent improvements in imaging and mathematical modeling technology have overcome the limitation of 2D imaging of subcellular organelles. Using a combination of array tomography, transmission electron tomography, and 3D modeling technology, the ultrastructure and morphology of giant mitochondria were analyzed in livers from NAFLD patients (Shami et al., 2021). This analysis revealed the decreased surface area to volume ratio and disorganized cristae contribute to the mitochondrial dysfunction during NAFLD development, but unfortunately authors did not make comparisons between zones in the lobule. Another recent imaging innovation that can be utilized for the study of subcellular heterogeneity in the liver is focused ion beam scanning electron microscopy (FIB-SEM). This utilizes scanning electron microscopy to scan the surface of the sample, then the focused ion beam then "mills" the surface with nanometer precision. As a result, the increased resolution in the *Z*-axis allows examination of subcellular structure in great details. Recently, Parlakgül et al. (2020) resolved the three-dimensional organization of subcellular organelles using FIB-SEM imaging in conjunction with deep-learning-based image segmentation in the intact murine liver. Advancements made to FIB-SEM in recent years have increased imaging volume, allowing them to image large intact livers from both lean and obese mice to the scale of 15 full or partial hepatocytes. This analysis revealed that the hepatocyte endoplasmic reticulum undergoes significant structural re-organization during the transition from lean to NAFLD. The results underscore the dynamic nature of cellular organelles and their central role in metabolic adaptation and homeostasis. While authors used transmission electron microscopy to ensure that all hepatocytes were from the mid-lobular zone, using this sub-cellular resolution to examine periportal versus pericentral hepatocytes during NAFLD progression warrants further attention moving forward. These new imaging technologies allow for multi-scale imaging at high

resolution from the subcellular to the lobule level that will surely yield new perspective to the century old questions.

HEPATOCYTE HETEROGENEITY – FROM DISCOVERY TO PRESENT

Early reports of hepatocyte heterogeneity were made in the first part of the 1900s and were purely observational and qualitative in nature (Noël, 1923; Smith, 1931; Kater, 1933; Deane, 1944). A seminal paper by Novikoff (1959) quantitatively described elevated gluconeogenic and mitochondrial respiratory enzymes in rat periportal cells via histochemistry, giving an early indication of functional heterogeneity across the lobule. As technological advances occurred, including the ability to separate the zones of the lobule, this proposed zonation of hepatocyte function was confirmed. Enzymatic assays and use of radiolabeled isolated sub-populations of hepatocytes isolated from rat livers revealed higher activity of gluconeogenesis and fatty acid oxidation in periportal hepatocytes, and elevated glycolysis and drug metabolism in pericentral cells (Nauck et al., 1981; Jungermann, 1983, 1988; Bengtsson et al., 1987; Guzmán et al., 1995). This functional heterogeneity and separation of periportal and pericentral cells are discussed in more detail in the next section.

These initial experiments were limited to investigating only a select few specific proteins and enzymatic activities at a time and did not shed light into the molecular basis underlying the heterogeneity. The ability to profile hepatocytes gene expression through mRNA analysis, enabled a higher throughput examination. In 2006, the gene expression profiles of isolated mouse periportal and pericentral cells examined via microarray analysis (Braeuning et al., 2006). These revealed for the first time, that 198 genes were differentially expressed in periportal and pericentral hepatocytes and supported previous findings of spatial separation of lipid and glucose utilization and synthesis. This study also revealed that transcriptional regulation is a major contributor to hepatocyte heterogeneity and further investigation is warranted to gain insight into the molecular makeup of different hepatocytes. The introduction of genome-wide RNA profiling known as bulk RNA sequencing (RNA-seq), enabled vastly higher throughputs – detecting thousands of gene transcripts. These datasets made it possible to aggregate cells into clusters based on their similarity in gene expression patterns. This advancement has paved the way for examination of hepatocyte heterogeneity and other cell types within the liver. Using bulk RNA-seq, human hepatocyte gene expression profiles have been created showing that periportal and pericentral zones are regulated in part, by gut derived toxins and xenobiotic metabolisms, respectively (McEnerney et al., 2017).

Single cell (sc) RNA-seq technologies now allow a window into hepatocytes differential gene expression at an even greater resolution. Halpern et al. (2017) performed scRNA-seq on dissociated hepatocytes from murine livers. Next, they utilized established zonated landmark genes to create a map, where hepatocytes can be retrospectively returned to their spatial position/layer within the lobule (Halpern et al., 2017). This allows for the high throughput of RNA sequencing while maintaining precise coordinates of gene expression distribution in the lobule. While increasing the spatial resolution of gene expression profiles, it is important to note that this is done retrospectively, *in silico*. Strikingly, they demonstrated that half of liver genes are non-uniformly expressed, namely zonated. Interestingly, the increased single cell resolution allowed the identification of genes that are highly expressed in mid-lobule layers. Two examples are *hamp* and *hamp2* that regulate hepatic iron levels, that would have otherwise been lost using binary periportal/pericentral classifications or investigating whole liver homogenate. Validation of the scRNA seq results were confirmed by smFISH to locate the spatial position of hepatocytes expressing the gene. In subsequent recent studies of human livers, scRNA-seq were performed on whole liver (Aizarani et al., 2019), malignant and non-malignant liver tumors (Massalha et al., 2020), and hepatic non-parenchymal cells (MacParland et al., 2018), revealing intricate zonated profiles of gene expression and the impact of cell-to-cell interactions has on gene expression. The use of scRNA seq provides the fundamental basis to understand gene expression patterns as the foundation underlying hepatocyte heterogeneity on which deeper understanding can be gained through the regulation at the protein level and interactions between different cells.

RNA-seq technologies allowed greater throughput than previous methods; however, the exact location/origin of the cell is lost during sample preparation and the dissociation process can introduce changes to gene expression (van den Brink et al., 2017; Saviano et al., 2020). To overcome these challenges, examining hepatic zonation in intact liver tissue would allow maximal preservation of the cellular metabolic state while maintaining spatial resolution. Filling this methodology gap, spatial transcriptomics expands upon traditional single cell or bulk sequencing, where cells lose their positional information once they are collected for cell-based RNA seq techniques. Spatial transcriptomics allows for the investigation of cells and tissues gene expression be examined while maintaining their spatial positioning. Particularly, *in situ* spatial transcriptomics has been developed to create a map of the cells' location within the tissue prior to lysing (Rodriques et al., 2019; Vickovic et al., 2019). Here, tissue is placed on a slide with unique barcodes to define the cells' position on the slide. After a standard hematoxylin and eosin-stained image, the tissue is lysed for scRNA-seq, and then the transcription profile of each cell is repositioned in space to its spatial barcoded position based on the original H&E image. This new technique has not yet been performed on liver sections, despite its great potential for investigation of liver zonation. This may be particularly useful for investigating heterogeneity in small sections of tissue, a common occurrence with human liver biopsies, where both transcriptomics and spatial positioning can be derived from a single tissue section without material loss.

Examining liver zonation using RNA-seq approaches allow high-throughput but are limited to transcriptional messaging. Expanding on their previous work of scRNA-seq, the Itzkovitz group developed spatial sorting of murine hepatocytes based on differential expression of cell surface markers, followed by proteomic analysis (Ben-Moshe et al., 2019). They created a

comprehensive proteomic map and found a strong correlation between gene and protein expression. This indicates the prevailing regulation of hepatocyte heterogeneity occurs at the transcriptional level. However, several genes displayed conflicting expression between mRNA and protein – some genes were zonated at mRNA but not protein levels (*A1cf*, *Clmn*, and *Lsr*), while some were zonated at the protein but not the mRNA level (Rpb4, Idh3, and Mrpl43). Arguably, zonation at the protein level has a greater impact on hepatocyte function and dysfunction; therefore, examining mRNA only may cause important regulatory proteins to be missed. One of the challenges in high throughput evaluation of protein expression via Mass Spectrometry is sample size and sensitivity that may cause low abundance proteins to remained undiscovered. Beyond gene or protein expression, changes to post translational modifications likely come into play, adding an additional layer of regulation. Indeed, these are significantly harder to measure and would require further technological advancements. To fully understand the molecular basis of heterogeneity across the lobule, all dimensions of regulation must be considered and integrated. Moving forward, investigating how proteomics and post translation modifications shape the spatial compartmentalization of metabolic functions should help to fill any knowledge gaps left by examining transcriptional regulation only.

LOCATION, LOCATION, LOCATION – SPATIAL DIVISION OF LABOR IN THE LOBULE

The phrase "divide and conquer" succinctly describes the liver's unique ability to spatially separate opposing functions for increased metabolic efficiency. Examining this division of labor across the lobule was made possible through extensive technological advances. Initial observations were made by immunohistochemical studies, where the expression of certain enzymes served as a proxy for function. Specifically, the pioneering work by Jungermann demonstrated the spatial division of carbohydrate metabolism across the rat liver lobule, with gluconeogenic enzymes predominantly localized in periportal regions and glycolytic enzymes located in pericentral regions (Katz et al., 1977a,b). However, the mere expression of an enzyme does not necessarily translate into activity. This was addressed by elegant radiolabeling and flux rate studies confirming the dominance of gluconeogenesis and glycolysis in rat periportal and pericentral hepatocytes, respectively (Katz and Jungermann, 1976; Jungermann et al., 1982). The ability to separate hepatocytes into their respective zones was paramount in assessing differences in hepatocyte function and to move away from purely observational distribution of enzymes. One of the earliest attempts was made by Shank et al. (1959) using a dissecting microscope. Guided by the portal tracks as a landmark, they dissected periportal, midlobular, and pericentral hepatocytes from frozen sections of rat liver followed by biochemical analysis (Shank et al., 1959). The measured higher activity of glucose-6-phosphate dehydrogenase and lactate dehydrogenase periportal areas, while isocitric and glutamic dehydrogenase activity were elevated in pericentral cells. This method was the foundation on which laser capture microdissection (LCM) was developed, which utilizes a laser beam instead of a dissecting microscope for increased precision to isolated and classify certain zones of the liver (Saito et al., 2013; McEnerney et al., 2017). Using LCM to separate zones and pathway analysis with RNA sequencing data, McEnerney et al. (2017) demonstrated in human liver lobules that immune response pathways were localized to periportal regions while xenobiotic metabolism is predominantly in pericentral cells. One caveat of this approach is the inability to distinguish between hepatocytes and non-parenchymal cells. As such, Kupffer cells, stellate cells, and liver sinusoidal endothelial cell (LSECs), all of which display non-uniform distribution (Halpern et al., 2018; Gola et al., 2021), may confound the results.

Selective zonal damage has also been used to isolate hepatocytes form different zones for functional analysis using ortho (perfusion via portal vein) and retrograde (perfusion via central vein) delivery of harmful agents. Perfusion of the detergent digitonin via the portal vein, will result in selective damage to periportal cells while retrograde perfusion of collagenase will dissociate and release pericentral cells that can be functionally analyzed *in vitro*. Similarly, digitonin perfusion via the vena cava maintains viable periportal cells. First described in rats in 1985 (Lindros and Penttilä, 1985; Quistorff, 1985), the digitonin-collagenase perfusion technique has been used to evaluate enzymatic activity in the isolated cells that demonstrated that drug metabolism is restricted to pericentral cells (Bengtsson et al., 1987). Further, radiolabeled fatty acid oxidation experiments in rats revealed profound zone flexibility in fatty acid oxidation in response to a variety of conditions (Guzmán et al., 1995). Specifically, fatty acid oxidation was higher in periportal hepatocytes compared to pericentral cells under both fed and fasted conditions, confirming previous reports of higher β-oxidation in periportal hepatocytes. Additionally, pericentral hepatocytes relied on non-mitochondrial fatty acid oxidation, as peroxisomal fatty acid oxidation was elevated in these cells across all conditions. Unfortunately, digitonin-collagenase perfusion relies on damaging one cell population while recovering another, forcing the comparison between zones to be made between separate animals and increasing variability. Further, isolation may take several hours, resulting in one population of cells to be *ex vivo* several hours longer. These limitations were demonstrated when periportal and pericentral cells were isolated from two different lobes from the same rat liver at the same time (Tordjmann et al., 1997). Here, authors showed that sensitivity to angiotensin II was up to 80% higher in pericentral cells versus periportal, whereas no differences between zones had been recorded previously. Further, albumin mRNA was only 35% higher in periportal cells, as opposed to previously larger reported differences from cells isolated from separate animals. These data reveal that periportal and pericentral cells isolated from two different livers increase further variability between the zones and may significantly mask or alter zonated markers.

Separating periportal and pericentral cells via fluorescent-activated cell sorting (FACS) has also been used for decades (Gumucio et al., 1981; Thalhammer et al., 1989). In this form

of flow cytometry, proximal and distal zones of the lobule are stained via ortho and retrograde perfusion before this homogenate of isolated hepatocytes are separated by FACS based on their fluorescent zone-specific labeling. Using this method, Thalhammer et al. (1989) demonstrated that succinate dehydrogenase and β-glucuronidase activity (related to oxidative phosphorylation and carbohydrate breakdown, respectively) were elevated in periportal cells compared to pericentral cells in rats. While this method allowed comparisons of hepatocyte subpopulations in the same liver, it was still constrained to the accuracy and the length of time it required for forward and backward perfusions. Greatly enhancing the separation efficiency of hepatocyte sub-types via FACS has been the identification of bona fide periportal and pericentral protein markers. Using perfused murine livers to dissociate cells, isolated hepatocytes stained with pericentral (CD73 or glutamine synthetase) and periportal (E-cadherin) were categorized into periportal or pericentral zones based on their positive cell populations for certain zonated markers (Halpern et al., 2017; Ben-Moshe et al., 2019; Berndt et al., 2021). The Itzkovitz group further stratified these hepatocytes into eight layers by defining "gates" based on their combined fluorescence of their pericentral or periportal markers (CD73 and e-cadherin) (Ben-Moshe et al., 2019). These gates were then validated against their spatially resolved scRNA-seq map (Halpern et al., 2017). Notably, this method increases the spatial resolution of protein expression profile by stratifying hepatocytes across different layers of the lobule instead of the binary classification of periportal and pericentral cells. Combining FACS, proteomics and pathway analysis, the Itzkovitz group colleagues demonstrated in mice that energetically demanding tasks such as plasma protein production and oxidative phosphorylation pathways were elevated in periportal regions, while xenobiotic and glutathione metabolism were pericentrally located (Ben-Moshe et al., 2019). Despite this advancement, *in vivo* functional relevance can be difficult to infer from gene and protein expression only. Addressing this, a shotgun proteomic approach on zone-specific hepatocytes isolated via immunostaining and subsequent FACS was used to explore the proteome map of the mouse liver lobule (Berndt et al., 2021). Relative protein abundance of enzymes and membrane transporters in pericentral and periportal hepatocytes were quantified to infer the functional significance using biochemistry-based kinetic model of hepatocyte metabolism (Berndt et al., 2018). This model demonstrated that proteins and enzymes related to glycolysis were elevated in pericentral cells, whereas periportal cells had a higher gluconeogenic capacity. Periportal hepatocytes also had elevated respiratory chain complexes, indicating a higher capacity for ATP generation, confirmed by the model demonstrating higher ATP/ADP rations in periportal versus pericentral cells.

Overall, the ability to examine the spatial division of labor across the lobule had made significant strides in the last century (**Figure 2**). This is due, in part, to improved ability to separate periportal and pericentral cells from the same animal at the same time. Further, proteomic analysis with increased spatial resolution now allows high throughput investigation of enzyme expression which is relevant to the functional capacities in different zones. Moving forward, *in vivo* models to measure metabolic functions in intact livers, and how they change in response to perturbation will shed light on the spatial and temporal regulation of liver function.

WHAT REGULATES LIVER ZONATION?

Hepatocytes are organized in an assembly-line-like structure giving rise to speculations regarding the role liver anatomy fulfills in zonation. Specifically, periportal and pericentral regions of the lobule are exposed to different environments: blood entering at the periphery of the lobule is rich in oxygen and nutrients, whereas pericentral cells are exposed to more hypoxic and nutrient sparce conditions (Rappaport et al., 1954). Deane (1944) intuitively speculated that many of the changes in glycogen storage and organelle morphology she observed, were due to the higher levels of oxygen in periportal regions of mice. In depth analysis of the liver anatomy by Rappaport in the 1950's elegantly described how the hepatic vascular framework plays a major role in dictating both the structure and function of the mammalian liver (Rappaport, 1958, 1973). This vascular architecture is regulated by a multitude of factor such as hydrostatic pressure and the microvasculature smooth muscle contractility which respond to nervous stimuli, hormones and metabolites, among others. Indeed, the regulation of carbohydrate metabolism across the lobule by oxygen and the glucagon/insulin ratio was elegantly demonstrated by Jungermann both *in vitro* and perfused rat livers (Nauck et al., 1981; Wölfle et al., 1983; Wölfle and Jungermann, 1985; Jungermann and Kietzmann, 1997, 2000), supporting the role of nutrient and metabolic hormone gradients in the regulation of hepatocyte gene expression and functions.

The introduction of transgenic mouse lines has greatly increased the ability to examine factors regulating liver zonation through tissue-specific loss- and gain-of function studies. Conditional knockout of β-catenin and its negative regulator adenomatous polyposis coli (APC), demonstrated the essential role of β-catenin/Wnt signaling in liver zonation (Benhamouche et al., 2006; Sekine et al., 2006). Interestingly, β-catenin and its negative regulator APC were shown to be expressed in pericentral and periportal regions, respectively (Benhamouche et al., 2006). Knockout of APC, which activates β-catenin, imposed a pericentral like phenotype across the lobule as identified by immunohistochemistry and microarray analysis of zonated pathways. Conversely, β-catenin KO mice displayed elevated periportal features in the lobule and loss of pericentral ones including disrupted ammonia and xenobiotic metabolism. Remarkably, blocking upstream Wnt signaling via *Lpr5* knockout mice resulted in the same disruption of hepatocyte heterogeneity as β-catenin knockout mice (Yang et al., 2014), indicating that β-catenin is regulated by Wnt signaling. Instead of hepatocytes, Kupffer cells and endothelial cells surrounding the central vein were found to be the source of Wnt ligand secretion, highlighting the complex intracellular crosstalk required for maintaining liver zonation (Preziosi et al., 2018). Counterbalancing pericentral zonation phenotype of β-catenin/Wnt signaling, bloodborne molecule/s activate Ras signaling that in turn promote the

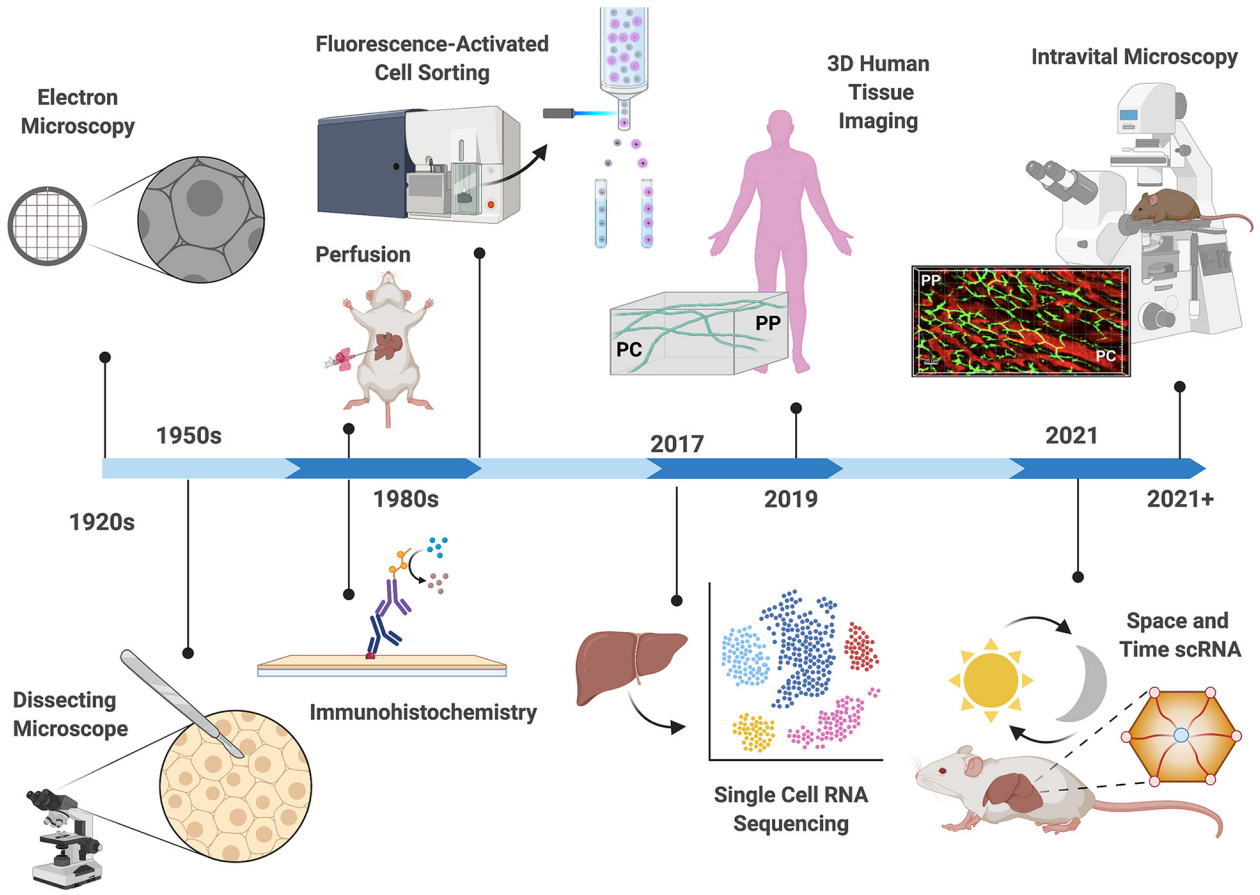

FIGURE 2 | Technological advances in the study of liver zonation. Over the past century, technological advances have driven discoveries related to hepatocyte organization and function. Early observations describing structural heterogeneity were confined to microscopy techniques (Noël, 1923; Kater, 1933; Shank et al., 1959). The development of hepatocyte separation approaches (1950–1980), including perfusion techniques, fluorescent activated cell sorting (FACS), and immunohistochemistry allowed biochemical classification of hepatocyte activities (Baron et al., 1981; Gumucio et al., 1981; Lindros and Penttilä, 1985). Deep insight into the differential gene expression patterns in the hepatic lobule was accomplished in 2017, where single cell RNA sequencing revealed that fifty percent of liver genes are non-uniformly distributed (Halpern et al., 2017). The first three-dimensional (3D) multiphoton microscopy of the human liver lobule reveled disrupted bile canalicular network in nonalcoholic fatty liver disease patients in 2019 (Segovia-Miranda et al., 2019). Recently (2021), changes in gene expression patterns across the lobule were examined in different times of the day revealing yet another layer of complexity in the regulation of compartmentalization (Droin et al., 2021). Advances in mouse genetics and light microscopy now allow the use of Intravital microscopy for examination of the hepatic lobule in real time. Depicted is a projection of 3D volume of the murine lobule acquired with intravital confocal microscopy (PP, periportal; PC, pericentral; bile canaliculi in green, sinusoids in red).

expression of periportal genes while suppressing pericentral associated genes (Braeuning et al., 2007). Another antagonist to the β-catenin/Wnt signaling pathway is glucagon, which exhibits a declining concentration gradient like that of oxygen along the periportal to pericentral axis. Glucagon deficient mice exhibit perturbed zonation profiles with dampened periportal gene expression and extended glutamine synthase expression, indicating a shift toward a more pericentral like phenotype (Cheng et al., 2018). Moreover, reinfusion of glucagon in deficient mice restored liver zonation profiles. This push and pull relationship between glucagon/Ras and β-catenin/Wnt signaling create a fine balancing act that shape metabolic compartmentalization across the lobule. The fact that glucagon is secreted in response to fasting underlines the livers' ability to quickly alter its zonation profile in order to adapt to substrate availability.

Oxygen gradient across the lobule drive transcriptional responses that are regulated by hypoxia-induced transcription factors (HIFs). Those are predominantly active in pericentral regions where oxygen concentrations are markedly lower (Kietzmann et al., 2001). HIFs provide another layer of regulation for liver zonation and patterned gene expression profiles due to their crosstalk with other important factors governing heterogeneity (Kietzmann, 2019). For example, ablation of the *hif-1a* gene in stem cells reduced β-catenin/Wnt gene expression in hypoxic conditions (Mazumdar et al., 2010), and β-catenin's negative regulator, APC, directly represses HIF-1α (Newton et al., 2010). This interplay between factors regulating liver zonation underlines the complexity of this process but also highlight critical regulatory junctions that warrants further investigation in liver pathophysiology.

These earlier discoveries of factors that regulate liver zonation were examined using new technologies. Single cell RNA-seq revealed Wnt signaling, and low oxygen are drivers of pericentral zonation profiles, while Ras signaling being a key inducer of periportal zonation, and pituitary hormones repress pericentral genes (Halpern et al., 2017). Notably, two thirds of zonated genes were not targets of Wnt, hypoxia, Ras signaling, or pituitary hormones, indicating that a combination of these factors or other unknown factors are at play highlighting how much more there is to be discovered. For example, exercise and physical activity is known to improve NAFLD outcomes and increase hepatic metabolic efficiency (Rector et al., 2008; Stevanović et al., 2020; Thyfault and Rector, 2020). Whether the effect of exercise is ubiquitous across the lobule or whether it induces a zone-specific phenotype are not known.

Indeed, new technologies now allow the discovery of new factors that shape liver zonation. Recently, the microbiome was shown to help establish a periportal dominant immune zonation in the mammalian lobule (Gola et al., 2021). Here, LSECs sensed gut derived bacteria which in turn triggered a signaling cascade and chemokine secretion which ultimately orchestrated immune cell localization to periportal regions. This novel discovery was made possible via a combination of advanced techniques such as multiplex imaging of human tissue, transgenic mouse lines, and transcriptomics. This finding opens the door for further investigation as to additional factors of liver zonation that may not have been previously considered and exemplifies the complex interplay that regulates hepatic heterogeneity.

DO NON-PARENCHYMAL CELLS ALSO DISPLAY HETEROGENEITY WITHIN THE LOBULE?

Like hepatocytes, non-parenchymal cells are also exposed to distinct microenvironments created by gradient of factors across the lobule. It is therefore likely that these gradients shape their gene expression, morphology, and function. One example is zonation of LSECs morphology which shows larger and more porous cells in the pericentral zone of rats, potentially facilitating filtration of toxins (Blouin et al., 1977; Gebhardt, 1992). A second example is related to enrichment of immune cells in periportal regions and the important central role this fulfills in proper immunological response. Indeed, initial histological and microscopy reports in rodents observed the liver's resident macrophage, Kupffer cells, to be predominantly located in periportal regions of the rat lobule (Bouwens et al., 1986; Lough et al., 1987). These qualitative reports were confirmed and expanded upon by the use of scRNA-seq and immunohistochemistry, demonstrating that Kupffer cell gene expression was upregulated in periportal areas in mice (Halpern et al., 2017) and humans (MacParland et al., 2018). Advancements in imaging technology has allowed further characterization of hepatic immune cell heterogeneity – two-photon intravital microscopy revealed natural killer T cells to be concentrated around periportal areas (Geissmann et al., 2005). In an elegant study by Gola et al. (2021), clearing-enhanced 3D imaging showed Kupffer cells and natural killer T cells enriched in periportal regions of mice and human lobules. Further, they demonstrated that this immune cell zonation was driven by the exposure of gut derived bacteria sensed by LSECs and the formation of chemokine gradients across the lobule, rather than classic Wnt signaling. When immune cell positioning and zonation was disrupted, authors observed increased bacterial spread toward pericentral regions and inflammatory damage, highlighting the importance of the non-uniform distribution of resident immune cells across the lobule. Collectively, these data indicate that hepatic immune cell heterogeneity is centralized in periportal zones of the lobule to prevent bacteria from reaching pericentral regions and entering the blood stream.

One of the difficulties in mapping any potential zonation profile of non-parenchymal cells in the liver is due in part, to the high abundance of hepatocytes masking any heterogeneity of less abundant cell types. LSECs are one such cell type, and often lack sufficient material for RNA-seq techniques or well-established landmark zonation genes. Gola et al. (2021) mapped the location of LSECs across the lobule using only the expression of CD117, with higher gradient of expression from periportal to pericentral regions. However, using hepatocyte zonation markers to help guide the zonation of LSECs would give a more comprehensive zonation map. Applying this concept, Halpern et al. (2018) developed paired-cell RNA sequencing (pcRNA-seq), where the zonation profile of LSECs is based on the profile of the hepatocyte that is attached to it from the previously established hepatocyte scRNA-seq data (Halpern et al., 2017). This approach revealed that approximately 35% of LSECs genes in mice were zonated, a fact that would be otherwise masked by the significantly more abundant hepatocyte gene expression. Interestingly, the authors demonstrated that pericentral LSECs expressed both Wnt ligands and the Wnt antagonist Dkk3, indicating a fine balancing act in the pericentral region of both positive and negative Wnt regulators. These data suggest that LSECs, like hepatocytes, are highly zonated, and that pcRNA-seq is a viable method for examining low abundant cells populations across tissues. Supporting these findings, recent pathway analysis on RNA-seq data and immunohistochemistry from human liver samples have identified distinct sub-population of LSECs across the liver lobule with functional heterogeneity depending on their location (Strauss et al., 2017; MacParland et al., 2018). Strauss et al. (2017) referred to periportal LSECs as type 1 and LSECs in midlobular and pericentral zones as type 2. In addition to having a different molecular phenotype, type 1 LSECs had a wider luminal space than type 2 LSECs to facilitate a reduction in blood flow velocity into the lobule. Non-parenchymal cells also display spatially dependent pathologies during progression to cirrhosis. Single cell analysis revealed that in a mouse model of liver cirrhosis, LSECs in pericentral areas are more susceptible to damage than periportal LSECs, and displayed increased capillarization and impaired regulation of endocytosis (Su et al., 2021). Further, pericentral hepatic stellate cells were identified as key collagen producing cells during liver fibrosis in mice (Dobie et al., 2019). This spatial zonation of hepatic stellate cells during cirrhosis development was due to only pericentral stellate cells differentiating into pathogenic collagen producing

cells. Mapping out the spatial heterogeneity of all hepatic cell types is important to understand the full picture of metabolic compartmentalization in the liver, and whether disruption of non-parenchymal cell zonation is a significant contributor to disease development and progression.

HOW DOES LIVER ZONATION CHANGE OVER TIME?

It is well established that hepatocyte function is altered by their position within the lobule, but is it also dependent on time of day? One of the earliest observations supporting this idea was made by Deane (1944). She excised mouse livers every 3 h for a 24 h period (Deane, 1944) and describes changes to mitochondrial morphologies in the periportal region in different times of the day. Consistently, other cellular components show zonal distribution that changes during the day. For example, bile granules were more numerous in periportal regions and peaked during the fasting hours. In contrast, lipid droplets are concentrated in pericentral cells but become more abundant and widely spread during fasting. Glycogen was deposited initially in the periportal areas in the hours post feeding, and then along the lobule toward the center (Uchiyama, 1990). Subsequently, extended fasting led to the depletion of glycogen storages from pericentral cells first. While these studies described important observations, they were limited by the temporal resolution (∼3 h intervals) and confined to qualitative data. Assessing gene and protein expression as well as organelle composition is vital to understanding how temporal parameters such as feeding/fasting cycles and circadian rhythms regulate liver zonation.

In recent years, circadian rhythm has been recognized as a robust driver of hepatic function and gene expression (Rey et al., 2011; Atger et al., 2015). However, the interaction between spatial and temporal aspects in liver physiology and pathophysiology is relatively unknown. Is liver zonation dependent on time of day? To answer these questions and expand on previous studies that were limited to qualitative analysis, the Itzkovitz group added another dimension to their spatial analysis of liver zonation – time. In collaboration with chronobiologist Felix Naef, scRNA-seq was performed on mouse hepatocytes across four different time points in a 24-h period with a 12/12 light/dark cycle (Droin et al., 2021). The authors found 30% of hepatocyte genes were regulated by space only, while some (20%) were affected only by time of day. For example, the core clock genes (*bmal1*, *dbp*) were unsurprisingly strongly regulated by temporal rhythms and expressed ubiquitously across the different zones, visually confirmed using smFISH. Interestingly, 7% of all genes displayed effects of both space and time; for example, the fatty acid synthesis and mitophagy genes *elovl3* and *bnip3,* respectively, both had higher expression in pericentral cells, whereas *elovl3* peaked in expression during the fed period and *bnip3* peaked during the fasting cycle. This dual regulation of expression in both time and space allows the liver to appropriately respond to metabolic demands and substrate availability during the diurnal feeding and fasting cycles. Further, key regulators of liver zonation – Wnt and hypoxia signaling, also displayed dual regulation, with targets of both peaking in expression in pericentral cells at the end of the fasting period. This indicates that temporal rhythm may also regulate hepatocyte heterogeneity, and that the metabolic switch between the feeding and fasting cycle may be an important consideration when examining liver zonation. While 7% of genes displayed effects of both space and time, only a minute fraction displayed interactions between these two variables. In other words, a small subset of zonated genes (either high pericentral or periportal expression) flipped their location depending on the time of day, or genes with strong temporal rhythms (high expression during the day, low at night) were reversed in different zones of the lobule. Whether these interactions between space and time gene regulation in the lobule are exacerbated in the setting of liver disease is unknown but warrants further investigation.

The advances of high throughput technology as well as the deeper understanding of the factors regulating temporal and diurnal rhythms have shown the complexity of the interactions between spatial and temporal regulation of liver zonation. While these studies demonstrate that liver zonation changes during the day, methods that allow high temporal resolution are lacking. Advances in light microscopy, such as intravital microscopy (IVM) has made it possible to examine cells in live tissue to provide spatial and temporal accuracy for physiological events *in vivo*. Recent advances in methodology to reduce motion artifact such as respiration and heartbeat have enabled examination of live tissue phenomena that would otherwise confined to *in vitro* (Weigert et al., 2013). Taking advantage of these improvements in imaging methods, fluorescence probes, and mouse genetics, Porat-Shliom et al. (2016) used IVM to demonstrate *in vivo* hepatic glucose uptake (Stefkovich et al., 2021), and how liver kinase B1 (LKB1) is a vital regulator of hepatocyte tight junctions. Mice lacking LKB1 had impaired hepatocyte transport kinetics and increased cellular permeability resulting from junctional disruption, all of which was visualized in real time using IVM. Moving forward, methods that can track *in vivo* processes across time such as IVM, will be vital for encompassing both spatial and temporal regulation of liver zonation.

THE IMPACT OF LIVER ZONATION ON DETOXIFICATION

Drug detoxification and metabolism, also known as xenobiotic metabolism, is one of the liver's most vital functions for removing foreign chemicals (i.e., drugs, alcohol, and toxins). This has been one obstacle in developing drugs for treating liver disease, including NAFLD. Therefore, it is critical to understand hepatocytes that specialize in drug metabolism with the long-term goal to improve drug treatment efficiency. Initially described in the late 1970s and early 80s, hepatic detoxification was shown to be pericentrally localized via spectrophotometric and immunohistochemical analysis; higher expression of xenobiotic metabolizing enzymes, particularly cytochrome P-450, were in pericentral regions compared to periportal or mid-lobular in rat and human liver (Gooding et al., 1978;

Baron et al., 1981; Hall et al., 1989; Bühler et al., 1992). Additionally, flow cytometry has been used to determine rat hepatocyte subpopulations based on the ability of cytochrome P-450 to metabolize ethoxy fluorescein ethyl ester to fluorescein (Miller, 1983; Black et al., 1993). Selective zonal damage has been particularly useful for examination of detoxification zonation, as acetaminophen overdose induce necrosis of pericentral regions only (Anundi et al., 1993; Ben-Shachar et al., 2012). In periportal and pericentral cells isolated via digitonin perfusion, pericentral cells exhibited higher cytochrome P-450 levels in response to acetaminophen, as well as increased vulnerability to drug induced injury when isolated from ethanol pre-treated rats (Anundi et al., 1993). Further, pericentral regions have higher markers of tissue damage after carbon tetrachloride-induced liver injury in mice (Abdel-Bakky et al., 2015). More recently, the use of scRNA-seq and smFISH confirmed these earlier reports, demonstrating that genes related to detoxification and drug metabolisms had elevated expression in pericentral regions in mice (Halpern et al., 2017). Similarly, pathway analysis of human hepatocyte gene expression cross referenced with established mouse zonation markers revealed an increase in detoxification related genes in pericentral zones suggesting that this spatial positioning is evolutionary conserved (MacParland et al., 2018).

To circumvent the challenges of using *in vivo* mouse models, mathematical and virtual models have been attempted to examine the heterogeneity of drug-induced liver injury. Robust pericentral accumulation of the N-acetyl-p-benzoquinone imine (NAPQI), a toxic byproduct of acetaminophen metabolism, explained the early pericentral necrosis during drug induced liver injury using virtual mice (Smith et al., 2016). A more recent mathematical model of acetaminophen induced liver injury suggested intrahepatocyte communication contributed to this explanation of pericentral dominant necrosis during drug induced injury (Kennedy et al., 2019). This intrahepatic communication suggested exosomes, gap junctions, and connexin hemichannels play an essential role in the toxic effect of chemicals, including facilitating or counteracting cell death processes.

Mathematical modeling has enabled the integration of multiple factors to identify testable hypotheses. However, the spatial and temporal complexity of xenobiotic metabolism make *in vivo* studies the gold standard. Tavakoli et al. (2019) used IVM to track the transport kinetics of fluorescein, a surrogate drug molecule; enabling the examination of live hepatic drug metabolism in the different zones of the rat liver and its interaction with hepatocytes, sinusoids, and bile canaliculi. The combination of IVM and mathematical modeling allowed the authors to accurately track and infer the kinetics of fluorescein across the different compartments in the liver. This novel technology has allowed for the first time, *in vivo* tracking of drug metabolism across the liver lobule – an enormous leap from the methods of 50 years ago. With hepatotoxicity the primary reason for failed phase I drug development (Larrey, 2002), the use of IVM for understanding how liver zonation affects the pharmokinetics of new therapeutics is an important and timely advancement. Further, using IVM avoids the issue of other cell types becoming damaged and compensatory changes to other zones of the liver during selective zonal damage techniques. Further investigation of hepatocytes that specialize in drug metabolism will greatly enhance our ability to design more effective and accurate pharmacological treatments for liver disease.

IS LIVER REGENERATION ZONE SPECIFIC?

The liver has the remarkable capacity of self-regeneration, however, the source of the new cells in hepatic homeostasis and regeneration is one of the unresolved mysteries in liver biology. Initial models addressing this question were of liver streaming – where new hepatocytes were generated in the periportal regions and slowly migrated toward the central vein (Zajicek et al., 1985; Lee et al., 1998). This concept has been controversial, with evidence suggesting that proliferating hepatocytes were distributed evenly across the lobule (Bralet et al., 1994). The introduction of Cre-loxP technology which allows gene editing, has greatly enhanced the ability to examine the process of regeneration. Transgenic mouse lines tracking hepatic *Lgr5*, a stem cell marker, revealed that hepatocytes around the central vein give rise to their own lineage and are self-sustaining during liver injury (Ang et al., 2019). *Lgr5* positive hepatocytes overlapped with hepatocytes expressing glutamine synthetase (pericentral marker), but not e-cadherin (periportal marker). In addition, the *Lgr5* positive cells were also found to be the source for HCC development. Supporting this, pericentral hepatocytes in mice have increased expression of liver progenitor markers and can support and replace most hepatocytes in the lobule during homeostatic renewal (Wang et al., 2015). In direct discordance with this, lineage tracing indicated that liver regeneration after partial hepatectomy in mice is carried out uniformly throughout the liver, as opposed to being driven by those in pericentral regions (Sun et al., 2020). Conversely still, periportal hepatocytes were found to drive regeneration and proliferation following liver injury in chronic HCC murine models (Font-Burgada et al., 2015). These discrepancies could indicate that distinct population of hepatocyte are responsible for renewal in response to different forms of injury.

The controversy surrounding hepatic regeneration may have been born out of methodological shortcomings. These studies typically rely on tracing of a single marker gene to trace the lineage of the cells resulting in a partial or skewed view of the process. Recently, new methods have enabled the unbiased tracing of multiple hepatocyte population with high temporal and spatial accuracy during regeneration. Incorporating dual recombinase genetic-mediated murine models and hepatocyte-specific promotors, He et al. (2021) were able to non-invasively monitor long-term hepatocyte proliferation in live mice by constitutively activating a recombinase that permanently records hepatocyte transcription. This genetic proliferation lineage tracing method (Protrace) along with light-sheet microscopy, identified midzonal hepatocytes to be the major contributors of proliferation during liver homeostasis, without having to rely on individual lineage tracing genes. Furthering this comprehensive

examination of regeneration heterogeneity in the liver, 11 conditional Cre knock-in murine strains were generated to enable inducible fluorescent labeling of hepatocytes across zones of the lobule to compare the regenerative capacity (Wei et al., 2021). Like He et al. (2021), authors demonstrated that midlobular hepatocytes were the main source of hepatocyte regeneration during liver homeostasis. Single-cell and bulk RNA sequencing, as well as CRISPER knockout models were used to identify genes and pathways regulating this increased proliferative capacity of mid lobular hepatocytes. These methods identified insulin-like growth factor binding protein 2, mammalian target of rapamycin, and cyclin d1 as the major regulators of mid lobular regeneration. Moreover, it was demonstrated that regeneration in response to chronic biliary (periportal) and centrilobular injury is dependent on the damaged area; damage to periportal areas increases regeneration in mid lobular and pericentral cells, while damage to the pericentral area increases regeneration in periportal and midlobular areas.

These two groundbreaking studies challenge the notion that midlobular cells are merely a transition zone between periportal and pericentral hepatocytes and identify them as the main contributor to liver regeneration. It was speculated that this may be due in part, to their spatial protection from toxic injuries at either end of the lobule and are appropriately positioned to initiate regeneration to replenish both periportal and pericentral hepatocytes. Indeed, identifying the mechanisms underlying the regenerative capacity of mid-lobular cells is vital for our ability to restore function following liver injury and disease.

EXAMINING THE BILE CANALICULAR NETWORK ACROSS THE LIVER LOBULE

Bile acids are produced and secreted from the liver to emulsify dietary lipids and act as signaling molecules, before being recycled and reabsorbed by hepatocytes. They flow directionally from pericentral toward periportal which is in the opposite direction of blood flow. The bile canalicular network also display structural and functional heterogeneity along the liver lobule. Specifically, variations in canalicular size and branching were observed via electron microscopy (Layden and Boyer, 1978; Baumgartner et al., 1987). Functionally, uneven bile acid uptake and excretion across the lobule was observed by infusion of bile-acid analogs and autoradiography (Jones et al., 1980; Groothuis et al., 1982). In a series of experiments by Baumgartner et al. (1986, 1987), retrograde perfusions in rats showed labeled taurocholate to be excreted slower than during orthograde, indicating greater uptake in periportal hepatocytes. Experiments of selective damage to pericentral hepatocytes in rats confirmed that pericentral hepatocytes contributed only a small fraction of uptake, with the vast majority occurring in periportal and midlobular cells (Gumucio et al., 1979), and that the pericentral region is the prime area for bile acid synthesis (Dionne et al., 1990). While these studies demonstrated initial structural and functional canalicular heterogeneity, examining dynamic properties of the biliary fluid network were limited by technology at the time.

Significant strides in imaging, particularly multiphoton IVM, have allowed for in depth analysis of the biliary network. Meyer *at al.* performed IVM of the mouse biliary network and mathematical modeling to demonstrate that bile flow increases in speed from the central vein to the bile ducts in the periportal regions, while biliary pressure decreases in the same direction (Meyer et al., 2017). These data indicate that both bile canalicular contractility and osmotic pressure display important heterogeneity across the liver lobule to maintain bile flow dynamics. Furthering the understanding of bile canaliculi structure in human NAFLD patients, multiphoton microscopy and 3D tissue reconstruction was used to identify the pathologic adaptation of hepatic architecture and function across the spectrum of NAFLD development (Segovia-Miranda et al., 2019). Multiphoton microscopy has advantages over other forms of light microscopy modalities due to its deep tissue penetration and limited photodamage, making it an ideal method for imaging the complex, three-dimensional organization of intact tissue. Here, human liver samples were obtained from patients with varying degrees of NAFLD – healthy control, healthy obese, steatosis, and NASH. To determine different zone of the liver, the lobule was computationally divided into 10 equidistance regions along the pericentral to periportal region. 3D spatially resolved analysis revealed that lipid droplets were typically pericentrally located but expanded to periportal regions upon NASH progression. Further, the bile canaliculi network presented with disrupted integrity with NAFLD onset, an interesting observation that would otherwise have been lost with a 2D rendering. The complexity of bile fluid dynamics and biliary network architecture make it difficult to study without the appropriate tools. These advances in light microscopy technologies now allow exciting questions of the biliary network to be addressed dynamically, *in vivo* and extend this examination to human samples.

IS HEPATIC SPATIAL HETEROGENEITY CONSERVED FROM RODENT TO HUMANS?

Most liver zonation studies were performed in rodent models (mice and rats). However, whether the findings are relevant to human hepatic physiology is a critically important question. Examination of human liver zonation was confined to light microscopy and immunohistochemistry in the 1980s (Horn et al., 1988; Hall et al., 1989). Those directly comparing human and rodent lobules observed similar heterogeneity in terms of glycogen deposits (Chamlian et al., 1989), pericentral drug-induced injury (Birge et al., 1990), and pericentral apoptotic bodies (Benedetti et al., 1988). More recently, immunofluorescence revealed that Kupffer cells were localized in periportal areas of both mice and humans, indicating the non-uniform distribution of immune cells is conserved (Gola et al., 2021). However, given the differences in metabolic demands between human and

rodents, it is reasonable to speculate that some variations in metabolic compartmentalization will arise. Indeed, while certain enzymes maintain a similar lobular distribution in both human and rodents, there are multiple examples where a different pattern of expression emerges. One example is glutamine synthetase and carbamoylphosphate synthetase that participate in nitrogen metabolism, that overlap in pericentral and periportal regions, respectively, in rat liver (Gebhardt and Mecke, 1983; Moorman et al., 1989). However, the human liver contains an intermediate zone where neither enzyme is present (Multhaupt et al., 1987; Moorman et al., 1989). Similarly, the gluconeogenesis enzyme phosphoenolpyruvate carboxykinase (PEPCK) is periportally located rats (Wimmer et al., 1990b), where in humans it appears to be ubiquitous across the lobule highlighting important differences in regulation of these pathways across species (Wimmer et al., 1990a).

The apparent discrepancies between humans and rodents may also be methodological rather than physiological. Limited access to human samples introduces inherent variability that is otherwise absent in tightly controlled rodent studies; variations in sex, body composition, age, as well as samples obtained from deceased or surgical patients introduce disease/ischemia to the long list of variables. Further, older methods examining human liver heterogeneity have been limited by the throughput. Single cell and bulk RNA sequencing has allowed a vast array of genes involved in liver zonation to be examined, which is particularly pertinent for human tissues where the amount of sample obtained can often be a limiting factor in the type analyses ran. Maximizing the obtainable information from these limited samples, McEnerney et al. (2017) performed RNA-seq on human livers obtained from lean patients undergoing hepatectomy surgery, where zones of the lobule were separated via laser capture microdissection. They observed robust overlap of zone-dependent gene expression profiles between human and mice (Braeuning et al., 2006), with hypoxia and Wnt signaling pathways being key regulators of pericentral zonation. While processes such as ammonia detoxification and xenobiotic metabolism were similarly zonated for humans and rodents, aldehyde dehydrogenase (an enzyme involved in alcohol metabolism) was upregulated in periportal regions of mice but pericentral regions in humans. Expanding on this, scRNA-seq was applied to dissociated healthy human liver samples (MacParland et al., 2018), and the subsequent datasets were cross-referenced with the single cell gene expression map established in mice (Halpern et al., 2017). This provided a zonated map of both hepatocytes and non-parenchymal cells in human liver, demonstrating significant human and rodent overlap of zonation profiles. Notably, pathway analysis revealed that not all gene expression clusters had strong correlation with the established murine zonation profiles, with authors suggesting that these differences may be due to different landmark genes that define human and rodent heterogeneity. Based on scRNA-seq data, Aizarani et al. (2019) suggested there is limited evolutionary conservation of hepatic zonated gene expression between human and mice (only 68% positively correlated), despite similar zonation of well-established zonated genes such as *PCK1* (gluconeogenesis) and *CYP2A1* (drug metabolism). Similarly, single cell analysis revealed both discordant and concordant hepatic zonation profiles were found between human and rodents; genes related to drug metabolism were both pericentrally located in humans and rodents, but lipogenic genes were pericentrally located in humans and periportally located in mice (Massalha et al., 2020). However, there is discordance between functional activity and genetic expression; functional assays have demonstrated lipogenesis to be a pericentral dominant process in rats (Guzmán and Castro, 1989). This highlights potential divergent zonation gene expression profiles among species, revealing that gene expression does not always align with function, underscoring the need for more functional assessments of zonated processes, particularly in the mouse liver. The higher resolution of single cell transcriptomics may further highlight the conflicting zonation profiles between species and underlines the need for further comparisons to be made.

The paucity of human liver zonation studies is further compounded by the lack of human disease samples. The limited number of studies examining human liver zonation are typically not directly comparing NAFLD vs. non-NAFLD subjects, making it difficult to identify how liver zonation is affected by disease progression in humans. Addressing this, spatially resolved lobules were examined from liver biopsies obtained from patients undergoing oncologic or bariatric surgeries with varying degrees of severity on the NAFLD to NASH spectrum (Segovia-Miranda et al., 2019). Confirming histological observations from rodent studies, multiphoton microscopy and 3D reconstruction demonstrated that lipid accumulated in pericentral regions during early stages of NAFLD development but expanded toward periportal regions during disease progression. Additionally, disruption in nuclear texture and the bile canaliculi were observed across the lobule with NASH development. These structural alterations are indicative of dysfunction; however, further mechanistic studies are necessary to fully understand whether those are primary or secondary to NAFLD pathophysiology. An additional challenge lays in the fact that mouse models of NAFLD and NASH are unable to replicate the human disease (Takahashi et al., 2012; Van Herck et al., 2017). Therefore, identifying the differences between human and rodent metabolic compartmentalization would allow us to; (1) be aware of the caveats of extrapolating rodent results to humans, and (2) design better and more comparable rodent models to study liver zonation.

Collectively, the gross similarities between rodent and human liver zonation merit the continued use of rodent models for examining the factors regulating metabolic compartmentalization in the lobule (**Figure 3**). However, the subtle differences described here indicate that a push for examining human liver lobules should supplement the foundational knowledge that rodent studies have provided. The coupling of mechanistic animal studies and observational human samples are important for furthering our understanding of the effects of disease progression on liver zonation and vice versa.

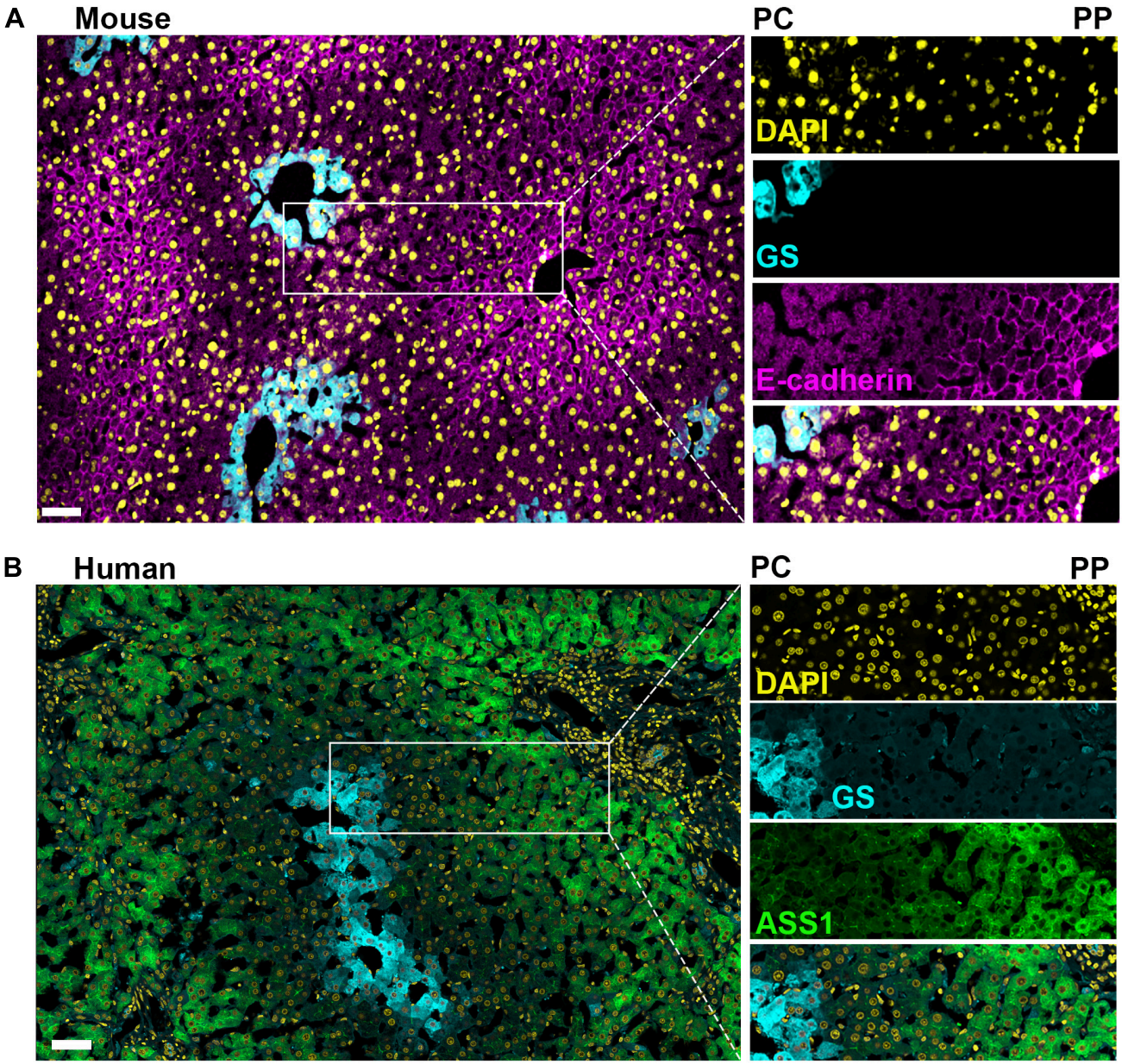

FIGURE 3 | Comparison of mouse and human liver lobules. Confocal microscopy image of immunofluorescence-stained mouse and human liver sections illustrate the conservation and differences between species regarding markers of hepatocyte heterogeneity. **(A)** Mouse liver section with a pericentral (PC) to periportal (PP) axis highlighted showing; a uniform nuclei distribution across the axis (DAPI in yellow), glutamine synthetase (GS) is selectively expressed in pericentral hepatocytes (cyan), and E-cadherin is enriched in periportal hepatocytes (magenta). **(B)** Human liver section with a pericentral (PC) to periportal (PP) axis highlighted showing; a uniform nuclei distribution across the axis (DAPI in yellow) and glutamine synthetase selectively expressed in pericentral hepatocytes (cyan), while argininosuccinate synthase 1 (ASS1, green) is expressed predominantly in periportal hepatocytes. Pericentral expression of glutamine synthetase is conserved between murine and human. Scale bar = 50 μm.

CONCLUSION

The liver's complex architecture gives rise to the profound heterogeneity seen among hepatocytes. This heterogeneity was astutely observed by pioneers in cell biology, whose findings have stood the test of time close to a century later. Their seminal work has created a strong foundation for hepatic physiology upon which the current body of knowledge is built.

As of late, researchers are lending more credence to this heterogeneity recognizing that investigation of the homogenized liver undermines its complexity, causing the loss of vital information. The introduction of omic approaches have vastly increased both transcriptional and translational throughput,

and advancements in high resolution *in vivo* imaging has brought the study of liver heterogeneity to exciting new heights (**Figure 2**). Despite these advances, there are still significant gaps in our knowledge that require further investigation. While transcriptional regulation of hepatic gene expression may provide the central basis to liver zonation, additional, less explored mechanisms may be at play; these include regulation at the protein expression level and protein post-translational modifications. Although measuring protein expression and post-translational modifications requires significant larger samples, up and coming technologies such as Mass Spectrometry Imaging (MSI) address these issues and allow spatial detection of proteins, metabolites, lipids and glycans in intact tissues (Buchberger et al., 2018). Additionally, Mass Spectrometry metabolomics has recently advanced to permit analysis of single cells (Duncan et al., 2019; Thiele et al., 2019), making this the next frontier for studies of liver zonation. Notably, technologies with increased spatial and temporal resolution that do not require tissue dissociation will be superior to those that require dissociation. In this sense, light microscopy modalities and IVM would enable deep tissue 3D reconstruction and time-dependent physiological processes across the different zones of the intact liver. Importantly, microscopy permits the interrogation of the interactions between non-parenchymal cells and hepatocytes which are only starting to be resolved. Further studies are required to unravel the complex interplay between LSECs, immune cells and the microbiome in determining hepatic compartmentalization. Ultimately, advancing our understanding of metabolic compartmentalization will allow us to examine these questions in the context of liver disease that will increase both the accuracy and efficacy of future treatments.

AUTHOR CONTRIBUTIONS

Both authors listed have made a substantial, direct and intellectual contribution to the work, and approved it for publication.

FUNDING

This work was supported by the National Cancer Institute Division of Intramural Research 1ZIABC011828-01.

ACKNOWLEDGMENTS

Images in **Figure 3** were approved and conducted according to the animal protocols approved by the National Cancer Institute (NCI)-Bethesda Animal Care and Use Committee (ACUC) under animal protocol LCMB037 and Human tissue was obtained through collaboration with Jonathan Hernandez on a NIH IRB-approved protocol 13-C-0076. We thank members of the NP-S lab, Will Printz, Win Arias, and Snorri Thorgeirsson for critical reading of the manuscript. **Figures 1**, **2** were created using BioRender.com.

REFERENCES

Abdel-Bakky, M. S., Helal, G. K., El-Sayed, E. M., and Saad, A. S. (2015). Carbon tetrachloride-induced liver injury in mice is tissue factor dependent. *Environ. Toxicol. Pharmacol.* 39, 1199–1205. doi: 10.1016/j.etap.2015.02.012

Aizarani, N., Saviano, A., Sagar, Mailly, L., Durand, S., Herman, J. S., et al. (2019). A human liver cell atlas reveals heterogeneity and epithelial progenitors. *Nature* 572, 199–204. doi: 10.1038/s41586-019-1373-2

Ang, C. H., Hsu, S. H., Guo, F., Tan, C. T., Yu, V. C., Visvader, J. E., et al. (2019). Lgr5(+) pericentral hepatocytes are self-maintained in normal liver regeneration and susceptible to hepatocarcinogenesis. *Proc. Natl. Acad. Sci. U.S.A.* 116, 19530–19540. doi: 10.1073/pnas.1908099116

Anundi, I., Lähteenmäki, T., Rundgren, M., Moldeus, P., and Lindros, K. O. (1993). Zonation of acetaminophen metabolism and cytochrome P450 2E1-mediated toxicity studied in isolated periportal and perivenous hepatocytes. *Biochem. Pharmacol.* 45, 1251–1259. doi: 10.1016/0006-2952(93)90277-4

Atger, F., Gobet, C., Marquis, J., Martin, E., Wang, J., Weger, B., et al. (2015). Circadian and feeding rhythms differentially affect rhythmic mRNA transcription and translation in mouse liver. *Proc. Natl. Acad. Sci. U.S.A.* 112, E6579–E6588.

Baron, J., Redick, J. A., and Guengerich, F. P. (1981). An immunohistochemical study on the localization and distributions of phenobarbital- and 3-methylcholanthrene-inducible cytochromes P-450 within the livers of untreated rats. *J. Biol. Chem.* 256, 5931–5937. doi: 10.1016/s0021-9258(19)69299-9

Baumgartner, U., Miyai, K., and Hardison, W. G. (1986). Greater taurodeoxycholate biotransformation during backward perfusion of rat liver. *Am. J. Physiol.* 251(Pt 1), G431–G435.

Baumgartner, U., Miyai, K., and Hardison, W. G. (1987). Modulation of hepatic biotransformation and biliary excretion of bile acid by age and sinusoidal bile acid load. *Am. J. Physiol.* 252(Pt 1), G114–G119.

Benedetti, A., Jézéquel, A. M., and Orlandi, F. (1988). Preferential distribution of apoptotic bodies in acinar zone 3 of normal human and rat liver. *J. Hepatol.* 7, 319–324. doi: 10.1016/s0168-8278(88)80004-7

Bengtsson, G., Julkunen, A., Penttilä, K. E., and Lindros, K. O. (1987). Effect of phenobarbital on the distribution of drug metabolizing enzymes between periportal and perivenous rat hepatocytes prepared by digitonin-collagenase liver perfusion. *J. Pharmacol. Exp. Ther.* 240, 663–667.

Benhamouche, S., Decaens, T., Godard, C., Chambrey, R., Rickman, D. S., Moinard, C., et al. (2006). Apc tumor suppressor gene is the "zonation-keeper" of mouse liver. *Dev. Cell* 10, 759–770. doi: 10.1016/j.devcel.2006.03.015

Ben-Moshe, S., and Itzkovitz, S. (2019). Spatial heterogeneity in the mammalian liver. *Nat. Rev. Gastroenterol. Hepatol.* 16, 395–410. doi: 10.1038/s41575-019-0134-x

Ben-Moshe, S., Shapira, Y., Moor, A. E., Manco, R., Veg, T., Bahar Halpern, K., et al. (2019). Spatial sorting enables comprehensive characterization of liver zonation. *Nat. Metab.* 1, 899–911. doi: 10.1038/s42255-019-0109-9

Ben-Shachar, R., Chen, Y., Luo, S., Hartman, C., Reed, M., and Nijhout, H. F. (2012). The biochemistry of acetaminophen hepatotoxicity and rescue: a mathematical model. *Theor. Biol. Med. Model.* 9:55. doi: 10.1186/1742-4682-9-55

Berndt, N., Bulik, S., Wallach, I., Wünsch, T., König, M., Stockmann, M., et al. (2018). HEPATOKIN1 is a biochemistry-based model of liver metabolism for applications in medicine and pharmacology. *Nat. Commun.* 9:2386.

Berndt, N., Kolbe, E., Gajowski, R., Eckstein, J., Ott, F., Meierhofer, D., et al. (2021). Functional consequences of metabolic zonation in murine livers: insights for an old story. *Hepatology* 73, 795–810. doi: 10.1002/hep.31274

Birge, R. B., Bartolone, J. B., Hart, S. G., Nishanian, E. V., Tyson, C. A., Khairallah, E. A., et al. (1990). Acetaminophen hepatotoxicity: correspondence of selective

protein arylation in human and mouse liver in vitro, in culture, and in vivo. *Toxicol. Appl. Pharmacol.* 105, 472–482. doi: 10.1016/0041-008x(90)90150-s

Black, K. A., Novicki, D. L., Vincent, J. L., and Smith, G. J. (1993). Flow cytometric analysis of xenobiotic metabolism activity in isolated rat hepatocytes. *Cytometry* 14, 334–338. doi: 10.1002/cyto.990140314

Blouin, A., Bolender, R. P., and Weibel, E. R. (1977). Distribution of organelles and membranes between hepatocytes and nonhepatocytes in the rat liver parenchyma. A stereological study. *J. Cell Biol.* 72, 441–455. doi: 10.1083/jcb.72.2.441

Bouwens, L., Baekeland, M., De Zanger, R., and Wisse, E. (1986). Quantitation, tissue distribution and proliferation kinetics of Kupffer cells in normal rat liver. *Hepatology* 6, 718–722. doi: 10.1002/hep.1840060430

Braeuning, A., Ittrich, C., Köhle, C., Hailfinger, S., Bonin, M., Buchmann, A., et al. (2006). Differential gene expression in periportal and perivenous mouse hepatocytes. *FEBS J.* 273, 5051–5061. doi: 10.1111/j.1742-4658.2006.05503.x

Braeuning, A., Menzel, M., Kleinschnitz, E. M., Harada, N., Tamai, Y., Köhle, C., et al. (2007). Serum components and activated Ha-ras antagonize expression of perivenous marker genes stimulated by beta-catenin signaling in mouse hepatocytes. *FEBS J.* 274, 4766–4777. doi: 10.1111/j.1742-4658.2007.06002.x

Bralet, M. P., Branchereau, S., Brechot, C., and Ferry, N. (1994). Cell lineage study in the liver using retroviral mediated gene transfer. Evidence against the streaming of hepatocytes in normal liver. *Am. J. Pathol.* 144, 896–905.

Buchberger, A. R., DeLaney, K., Johnson, J., and Li, L. (2018). Mass spectrometry imaging: a review of emerging advancements and future insights. *Anal. Chem.* 90, 240–265. doi: 10.1021/acs.analchem.7b04733

Bühler, R., Lindros, K. O., Nordling, A., Johansson, I., and Ingelman-Sundberg, M. (1992). Zonation of cytochrome P450 isozyme expression and induction in rat liver. *Eur. J. Biochem.* 204, 407–412. doi: 10.1111/j.1432-1033.1992.tb16650.x

Chalasani, N., Wilson, L., Kleiner, D. E., Cummings, O. W., Brunt, E. M., and Unalp, A. (2008). Relationship of steatosis grade and zonal location to histological features of steatohepatitis in adult patients with non-alcoholic fatty liver disease. *J. Hepatol.* 48, 829–834. doi: 10.1016/j.jhep.2008.01.016

Chamlian, A., Benkoel, L., Minko, D., Njee, T., and Gulian, J. M. (1989). Ultrastructural heterogeneity of glycogen in human liver. *Liver* 9, 346–350. doi: 10.1111/j.1600-0676.1989.tb00422.x

Cheng, X., Kim, S. Y., Okamoto, H., Xin, Y., Yancopoulos, G. D., Murphy, A. J., et al. (2018). Glucagon contributes to liver zonation. *Proc. Natl. Acad. Sci. U.S.A.* 115, E4111–E4119.

Deane, H. W. (1944). A cytological study of the diurnal cycle of the liver of the mouse in relation to storage and secretion. *Anat. Rec.* 88, 39–65. doi: 10.1002/ar.1090880104

Dionne, S., Russo, P., Tuch-Weber, B., Plaa, G. L., and Yousef, I. M. (1990). The role of acinar zone 3 hepatocytes in bile formation: influence of bromobenzene treatment on bile formation in the rat. *Liver* 10, 85–93. doi: 10.1111/j.1600-0676.1990.tb00441.x

Dobie, R., Wilson-Kanamori, J. R., Henderson, B. E. P., Smith, J. R., Matchett, K. P., Portman, J. R., et al. (2019). Single-Cell Transcriptomics Uncovers Zonation of Function in the Mesenchyme during Liver Fibrosis. *Cell Rep.* 29, 1832–1847e8.

Droin, C., Kholtei, J. E., Bahar Halpern, K., Hurni, C., Rozenberg, M., Muvkadi, S., et al. (2021). Space-time logic of liver gene expression at sub-lobular scale. *Nat. Metab.* 3, 43–58. doi: 10.1038/s42255-020-00323-1

Duncan, K. D., Fyrestam, J., and Lanekoff, I. (2019). Advances in mass spectrometry based single-cell metabolomics. *Analyst* 144, 782–793. doi: 10.1039/c8an01581c

Font-Burgada, J., Shalapour, S., Ramaswamy, S., Hsueh, B., Rossell, D., Umemura, A., et al. (2015). Hybrid periportal hepatocytes regenerate the injured liver without giving rise to cancer. *Cell* 162, 766–779. doi: 10.1016/j.cell.2015.07.026

Gebhardt, R. (1992). Metabolic zonation of the liver: regulation and implications for liver function. *Pharmacol. Ther.* 53, 275–354. doi: 10.1016/0163-7258(92)90055-5

Gebhardt, R., and Matz-Soja, M. (2014). Liver zonation: Novel aspects of its regulation and its impact on homeostasis. *World J. Gastroenterol.* 20, 8491–8504. doi: 10.3748/wjg.v20.i26.8491

Gebhardt, R., and Mecke, D. (1983). Heterogeneous distribution of glutamine synthetase among rat liver parenchymal cells in situ and in primary culture. *EMBO J.* 2, 567–570. doi: 10.1002/j.1460-2075.1983.tb01464.x

Geissmann, F., Cameron, T. O., Sidobre, S., Manlongat, N., Kronenberg, M., Briskin, M. J., et al. (2005). Intravascular immune surveillance by CXCR6+ NKT cells patrolling liver sinusoids. *PLoS Biol.* 3:e113. doi: 10.1371/journal.pbio.0030113

Gola, A., Dorrington, M. G., Speranza, E., Sala, C., Shih, R. M., Radtke, A. J., et al. (2021). Commensal-driven immune zonation of the liver promotes host defence. *Nature* 589, 131–136. doi: 10.1038/s41586-020-2977-2

Gooding, P. E., Chayen, J., Sawyer, B., and Slater, T. F. (1978). Cytochrome P-450 distribution in rat liver and the effect of sodium phenobarbitone administration. *Chem. Biol. Interact.* 20, 299–310. doi: 10.1016/0009-2797(78)90108-4

Groothuis, G. M., Hardonk, M. J., Keulemans, K. P., Nieuwenhuis, P., and Meijer, D. K. (1982). Autoradiographic and kinetic demonstration of acinar heterogeneity of taurocholate transport. *Am. J. Physiol.* 243, G455–G462.

Gumucio, J. J., Katz, M. E., Miller, D. L., Balabaud, C. P., Greenfield, J. M., and Wagner, R. M. (1979). Bile salt transport after selective damage to acinar zone 3 hepatocytes by bromobenzene in the rat. *Toxicol. Appl. Pharmacol.* 50, 77–85. doi: 10.1016/0041-008x(79)90494-0

Gumucio, J. J., Miller, D. L., Krauss, M. D., and Zanolli, C. C. (1981). Transport of fluorescent compounds into hepatocytes and the resultant zonal labeling of the hepatic acinus in the rat. *Gastroenterology* 80, 639–646. doi: 10.1016/0016-5085(81)90119-0

Guzmán, M., and Castro, J. (1989). Zonation of fatty acid metabolism in rat liver. *Biochem. J.* 264, 107–113. doi: 10.1042/bj2640107

Guzmán, M., Bijleveld, C., and Geelen, M. J. (1995). Flexibility of zonation of fatty acid oxidation in rat liver. *Biochem. J.* 311(Pt 3), 853–860. doi: 10.1042/bj3110853

Hall, P. M., Stupans, I., Burgess, W., Birkett, D. J., and McManus, M. E. (1989). Immunohistochemical localization of NADPH-cytochrome P450 reductase in human tissues. *Carcinogenesis* 10, 521–530. doi: 10.1093/carcin/10.3.521

Halpern, K. B., Shenhav, R., Massalha, H., Toth, B., Egozi, A., Massasa, E. E., et al. (2018). Paired-cell sequencing enables spatial gene expression mapping of liver endothelial cells. *Nat. Biotechnol.* 36, 962–970. doi: 10.1038/nbt.4231

Halpern, K. B., Shenhav, R., Matcovitch-Natan, O., Toth, B., Lemze, D., Golan, M., et al. (2017). Single-cell spatial reconstruction reveals global division of labour in the mammalian liver. *Nature* 542, 352–356. doi: 10.1038/nature21065

He, L., Pu, W., Liu, X., Zhang, Z., Han, M., Li, Y., et al. (2021). Proliferation tracing reveals regional hepatocyte generation in liver homeostasis and repair. *Science* 371:6532.

Horn, T., Junge, J., Nielsen, O., and Christoffersen, P. (1988). Light microscopical demonstration and zonal distribution of parasinusoidal cells (Ito cells) in normal human liver. *Virchows Arch. A Pathol. Anat. Histopathol.* 413, 147–149. doi: 10.1007/bf00749676

Jones, A. L., Hradek, G. T., Renston, R. H., Wong, K. Y., Karlaganis, G., and Paumgartner, G. (1980). Autoradiographic evidence for hepatic lobular concentration gradient of bile acid derivative. *Am. J. Physiol.* 238, G233–G237.

Jungermann, K. (1983). Functional significance of hepatocyte heterogeneity for glycolysis and gluconeogenesis. *Pharmacol. Biochem. Behav.* 18(Suppl. 1), 409–414. doi: 10.1016/0091-3057(83)90208-3

Jungermann, K. (1988). Metabolic zonation of liver parenchyma. *Semin. Liver Dis.* 8, 329–341. doi: 10.1055/s-2008-1040554

Jungermann, K., and Katz, N. (1982). Functional hepatocellular heterogeneity. *Hepatology.* 2, 385–395.

Jungermann, K., and Kietzmann, T. (1996). Zonation of parenchymal and nonparenchymal metabolism in liver. *Annu. Rev. Nutr.* 16, 179–203. doi: 10.1146/annurev.nu.16.070196.001143

Jungermann, K., and Kietzmann, T. (1997). Role of oxygen in the zonation of carbohydrate metabolism and gene expression in liver. *Kidney Int.* 51, 402–412. doi: 10.1038/ki.1997.53

Jungermann, K., and Kietzmann, T. (2000). Oxygen: modulator of metabolic zonation and disease of the liver. *Hepatology* 31, 255–260. doi: 10.1002/hep.510310201

Jungermann, K., Heilbronn, R., Katz, N., and Sasse, D. (1982). The glucose/glucose-6-phosphate cycle in the periportal and perivenous zone of rat liver. *Eur. J. Biochem.* 123, 429–436. doi: 10.1111/j.1432-1033.1982.tb19786.x

Kater, J. M. (1933). Comparative and experimental studies on the cytology of the liver. *Zeitschrift für Zellforschung Mikroskopische Anat.* 17, 217–246. doi: 10.1007/bf00374042

Katz, N., and Jungermann, K. (1976). [Autoregulatory shift from fructolysis to lactate gluconeogenisis in rat hepatocyte suspensions. The problem of metabolic zonation of liver parenchyma]. *Hoppe Seylers Z Physiol. Chem.* 357, 359–375. doi: 10.1515/bchm2.1976.357.1.359

Katz, N., Teutsch, H. F., Jungermann, K., and Sasse, D. (1977a). Heterogeneous reciprocal localization of fructose-1,6-bisphosphatase and of glucokinase in microdissected periportal and perivenous rat liver tissue. *FEBS Lett.* 83, 272–276. doi: 10.1016/0014-5793(77)81021-1

Katz, N., Teutsch, H. F., Sasse, D., and Jungermann, K. (1977b). Heterogeneous distribution of glucose-6-phosphatase in microdissected periportal and perivenous rat liver tissue. *FEBS Lett.* 76, 226–230. doi: 10.1016/0014-5793(77)80157-9

Kennedy, R. C., Smith, A. K., Ropella, G. E. P., McGill, M. R., Jaeschke, H., and Hunt, C. A. (2019). Propagation of pericentral necrosis during acetaminophen-induced liver injury: evidence for early interhepatocyte communication and information exchange. *Toxicol. Sci.* 169, 151–166. doi: 10.1093/toxsci/kfz029

Kietzmann, T. (2019). Liver zonation in health and disease: hypoxia and hypoxia-inducible transcription factors as concert masters. *Int. J. Mol. Sci.* 20:2347. doi: 10.3390/ijms20092347

Kietzmann, T., Cornesse, Y., Brechtel, K., Modaressi, S., and Jungermann, K. (2001). Perivenous expression of the mRNA of the three hypoxia-inducible factor alpha-subunits, HIF1alpha, HIF2alpha and HIF3alpha, in rat liver. *Biochem. J.* 354(Pt 3), 531–537. doi: 10.1042/0264-6021:3540531

Larrey, D. (2002). Epidemiology and individual susceptibility to adverse drug reactions affecting the liver. *Semin. Liver. Dis.* 22, 145–155. doi: 10.1055/s-2002-30105

Layden, T. J., and Boyer, J. L. (1978). Influence of bile acids on bile canalicular membrane morphology and the lobular gradient in canalicular size. *Lab. Invest.* 39, 110–119.

Lee, V. M., Cameron, R. G., and Archer, M. C. (1998). Zonal location of compensatory hepatocyte proliferation following chemically induced hepatotoxicity in rats and humans. *Toxicol. Pathol.* 26, 621–627. doi: 10.1177/019262339802600505

Lindor, K. D., Gershwin, M. E., Poupon, R., Kaplan, M., Bergasa, N. V., and Heathcote, E. J. (2009). Primary biliary cirrhosis. *Hepatology.* 50, 291–308.

Lindros, K. O., and Penttilä, K. E. (1985). Digitonin-collagenase perfusion for efficient separation of periportal or perivenous hepatocytes. *Biochem. J.* 228, 757–760. doi: 10.1042/bj2280757

Loose, L. D., Silkworth, J. B., Pittman, K. A., Benitz, K. F., and Mueller, W. (1978). Impaired host resistance to endotoxin and malaria in polychlorinated biphenyl- and hexachlorobenzene-treated mice. *Infect. Immun.* 20, 30–35. doi: 10.1128/iai.20.1.30-35.1978

Lough, J., Rosenthall, L., Arzoumanian, A., and Goresky, C. A. (1987). Kupffer cell depletion associated with capillarization of liver sinusoids in carbon tetrachloride-induced rat liver cirrhosis. *J. Hepatol.* 5, 190–198. doi: 10.1016/s0168-8278(87)80572-x

MacParland, S. A., Liu, J. C., Ma, X. Z., Innes, B. T., Bartczak, A. M., Gage, B. K., et al. (2018). Single cell RNA sequencing of human liver reveals distinct intrahepatic macrophage populations. *Nat. Commun.* 9: 4383.

Massalha, H., Bahar Halpern, K., Abu-Gazala, S., Jana, T., Massasa, E. E., Moor, A. E., et al. (2020). A single cell atlas of the human liver tumor microenvironment. *Mol. Syst. Biol.* 16:e9682.

Mazumdar, J., O'Brien, W. T., Johnson, R. S., LaManna, J. C., Chavez, J. C., Klein, P. S., et al. (2010). O2 regulates stem cells through Wnt/β-catenin signalling. *Nat. Cell Biol.* 12, 1007–1013. doi: 10.1038/ncb2102

McEnerney, L., Duncan, K., Bang, B. R., Elmasry, S., Li, M., Miki, T., et al. (2017). Dual modulation of human hepatic zonation via canonical and non-canonical Wnt pathways. *Exp. Mol. Med.* 49:e413. doi: 10.1038/emm.2017.226

Meyer, K., Ostrenko, O., Bourantas, G., Morales-Navarrete, H., Porat-Shliom, N., Segovia-Miranda, F., et al. (2017). A predictive 3D multi-scale model of biliary fluid dynamics in the liver lobule. *Cell Syst.* 4, 277–290.e9.

Miller, A. G. (1983). Ethylated fluoresceins: assay of cytochrome P-450 activity and application to measurements in single cells by flow cytometry. *Anal. Biochem.* 133, 46–57. doi: 10.1016/0003-2697(83)90220-8

Moorman, A. F., Vermeulen, J. L., Charles, R., and Lamers, W. H. (1989). Localization of ammonia-metabolizing enzymes in human liver: ontogenesis of heterogeneity. *Hepatology* 9, 367–372. doi: 10.1002/hep.1840090305

Mori, M., Izawa, T., Inai, Y., Fujiwara, S., Aikawa, R., Kuwamura, M., et al. (2020). Dietary Iron Overload Differentially Modulates Chemically-Induced Liver Injury in Rats. *Nutrients* 12, 2784. doi: 10.3390/nu12092784

Multhaupt, H., Fritz, P., and Schumacher, K. (1987). Immunohistochemical localisation of arginase in human liver using monoclonal antibodies against human liver arginase. *Histochemistry* 87, 465–470. doi: 10.1007/bf00496818

Nauck, M., Wolfle, D., Katz, N., and Jungermann, K. (1981). Modulation of the glucagon-dependent induction of phosphoenolpyruvate carboxykinase and tyrosine aminotransferase by arterial and venous oxygen concentrations in hepatocyte cultures. *Eur. J. Biochem.* 119, 657–661. doi: 10.1111/j.1432-1033.1981.tb05658.x

Newton, I. P., Kenneth, N. S., Appleton, P. L., Näthke, I., and Rocha, S. (2010). Adenomatous polyposis coli and hypoxia-inducible factor-1{alpha} have an antagonistic connection. *Mol. Biol. Cell.* 21, 3630–3638. doi: 10.1091/mbc.e10-04-0312

Noël, R. (1923). *Recherches Histo-Physiologiques sur la Cellule Hépatique des Mammifères*. Paris: University of Paris.

Novikoff, A. B. (1959). Cell heterogeneity within the hepatic lobule of the rat: staining reactions. *J. Histochem. Cytochem.* 7, 240–244. doi: 10.1177/7.4.240

Parlakgül, G., Arruda, A. P., Cagampan, E., Pang, S., Güney, E., Lee, Y., et al. (2020). High resolution 3D imaging of liver reveals a central role for subcellular architectural organization in metabolism. *Preprint bioRxiv [Preprint]* doi: 10.1101/2020.11.18.387803

Porat-Shliom, N., Tietgens, A. J., Van Itallie, C. M., Vitale-Cross, L., Jarnik, M., Harding, O. J., et al. (2016). Liver kinase B1 regulates hepatocellular tight junction distribution and function in vivo. *Hepatology* 64, 1317–1329. doi: 10.1002/hep.28724

Preziosi, M., Okabe, H., Poddar, M., Singh, S., and Monga, S. P. (2018). Endothelial Wnts regulate β-catenin signaling in murine liver zonation and regeneration: a sequel to the Wnt–Wnt situation. *Hepatol. Commun.* 2, 845–860. doi: 10.1002/hep4.1196

Quistorff, B. (1985). Gluconeogenesis in periportal and perivenous hepatocytes of rat liver, isolated by a new high-yield digitonin/collagenase perfusion technique. *Biochem. J.* 229, 221–226. doi: 10.1042/bj2290221

Rappaport, A. M. (1958). The structural and functional unit in the human liver (liver acinus). *Anat. Rec.* 130, 673–689. doi: 10.1002/ar.1091300405

Rappaport, A. M. (1973). The microcirculatory hepatic unit. *Microvasc. Res.* 6, 212–228. doi: 10.1016/0026-2862(73)90021-6

Rappaport, A. M., Borowy, Z. J., Lougheed, W. M., and Lotto, W. N. (1954). Subdivision of hexagonal liver lobules into a structural and functional unit; role in hepatic physiology and pathology. *Anat. Rec.* 119, 11–33. doi: 10.1002/ar.1091190103

Rector, R. S., Thyfault, J. P., Morris, R. T., Laye, M. J., Borengasser, S. J., Booth, F. W., et al. (2008). Daily exercise increases hepatic fatty acid oxidation and prevents steatosis in Otsuka Long-Evans Tokushima Fatty rats. *Am. J. Physiol. Gastrointest. Liver Physiol.* 294, G619–G626.

Rey, G., Cesbron, F., Rougemont, J., Reinke, H., Brunner, M., and Naef, F. (2011). Genome-wide and phase-specific DNA-binding rhythms of BMAL1 control circadian output functions in mouse liver. *PLoS. Biol.* 9:e1000595. doi: 10.1371/journal.pbio.1000595

Rodriques, S. G., Stickels, R. R., Goeva, A., Martin, C. A., Murray, E., Vanderburg, C. R., et al. (2019). Slide-seq: a scalable technology for measuring genome-wide expression at high spatial resolution. *Science* 363, 1463–1467. doi: 10.1126/science.aaw1219

Sahebjam, F., and Vierling, J. M. (2015). Autoimmune hepatitis. *Front. Med.* 9:187–219. doi: 10.1007/s11684-015-0386-y

Saito, K., Negishi, M., and James Squires, E. (2013). Sexual dimorphisms in zonal gene expression in mouse liver. *Biochem. Biophys. Res. Commun.* 436, 730–735. doi: 10.1016/j.bbrc.2013.06.025

Saviano, A., Henderson, N. C., and Baumert, T. F. (2020). Single-cell genomics and spatial transcriptomics: discovery of novel cell states and cellular interactions in liver physiology and disease biology. *J. Hepatol.* 73, 1219–1230. doi: 10.1016/j.jhep.2020.06.004

Segovia-Miranda, F., Morales-Navarrete, H., Kücken, M., Moser, V., Seifert, S., Repnik, U., et al. (2019). Three-dimensional spatially resolved geometrical and functional models of human liver tissue reveal new aspects of NAFLD progression. *Nat. Med.* 25, 1885–1893. doi: 10.1038/s41591-019-0660-7

Sekine, S., Lan, B. Y., Bedolli, M., Feng, S., and Hebrok, M. (2006). Liver-specific loss of beta-catenin blocks glutamine synthesis pathway activity and cytochrome p450 expression in mice. *Hepatology* 43, 817–825. doi: 10.1002/hep.21131

Shami, G. J., Cheng, D., Verhaegh, P., Koek, G., Wisse, E., and Braet, F. (2021). Three-dimensional ultrastructure of giant mitochondria in human non-alcoholic fatty liver disease. *Sci. Rep.* 11:3319.

Shank, R. E., Morrison, G., Cheng, C. H., Karl, I., and Schwartz, R. (1959). Cell heterogeneity within the hepatic lobule: quantitative histochemistry. *J. Histochem. Cytochem.* 7, 237–239. doi: 10.1177/7.4.237

Smith, A. K., Petersen, B. K., Ropella, G. E., Kennedy, R. C., Kaplowitz, N., Ookhtens, M., et al. (2016). Competing mechanistic hypotheses of acetaminophen-induced hepatotoxicity challenged by virtual experiments. *PLoS. Comput. Biol.* 12:e1005253. doi: 10.1371/journal.pcbi.1005253

Smith, D. M. (1931). The ontogenetic history of the mitochondria of the hepatic cell of the white rat. *J. Morphol.* 52, 485–511.

Stefkovich, M. L., Kang, S. W. S., and Porat-Shliom, N. (2021). Intravital microscopy for the study of hepatic glucose uptake. *Curr. Protoc.* 1:e139.

Stevanović, J., Beleza, J., Coxito, P., Ascensão, A., and Magalhães, J. (2020). Physical exercise and liver "fitness": Role of mitochondrial function and epigenetics-related mechanisms in non-alcoholic fatty liver disease. *Mol. Metab.* 32, 1–14.

Strauss, O., Phillips, A., Ruggiero, K., Bartlett, A., and Dunbar, P. R. (2017). Immunofluorescence identifies distinct subsets of endothelial cells in the human liver. *Sci. Rep.* 7:44356.

Su, T., Yang, Y., Lai, S., Jeong, J., Jung, Y., McConnell, M., et al. (2021). Single-Cell Transcriptomics Reveals Zone-Specific Alterations of Liver Sinusoidal Endothelial Cells in Cirrhosis. *Cell. Mol. Gastroenterol. Hepatol.* 11, 1139–1161. doi: 10.1016/j.jcmgh.2020.12.007

Sun, T., Pikiolek, M., Orsini, V., Bergling, S., Holwerda, S., Morelli, L., et al. (2020). AXIN2(+) pericentral hepatocytes have limited contributions to liver homeostasis and regeneration. *Cell Stem. Cell* 26, 97–107.e6.

Takahashi, Y., Soejima, Y., and Fukusato, T. (2012). Animal models of nonalcoholic fatty liver disease/nonalcoholic steatohepatitis. *World J. Gastroenterol.* 18, 2300–2308. doi: 10.3748/wjg.v18.i19.2300

Tavakoli, M., Tsekouras, K., Day, R., Dunn, K. W., and Pressé, S. (2019). Quantitative kinetic models from intravital microscopy: a case study using hepatic transport. *J. Phys. Chem. B* 123, 7302–7312. doi: 10.1021/acs.jpcb.9b04729

Thalhammer, T., Gessl, A., Braakman, I., and Graf, J. (1989). Separation of hepatocytes of different acinar zones by flow cytometry. *Cytometry* 10, 772–778. doi: 10.1002/cyto.990100615

Thiele, C., Wunderling, K., and Leyendecker, P. (2019). Multiplexed and single cell tracing of lipid metabolism. *Nat. Methods* 16, 1123–1130. doi: 10.1038/s41592-019-0593-6

Thyfault, J. P., and Rector, R. S. (2020). Exercise combats hepatic steatosis: potential mechanisms and clinical implications. *Diabetes* 69, 517–524. doi: 10.2337/dbi18-0043

Tian, Y., Mok, M. T. S., Yang, P., and Cheng, A. S. L. (2016). Epigenetic Activation of Wnt/β-Catenin Signaling in NAFLD-Associated Hepatocarcinogenesis. *Cancers (Basel)* 8, 76. doi: 10.3390/cancers8080076

Tordjmann, T., Berthon, B., Lardeux, B., Moreau, A., Jacquemin, E., Combettes, L., et al. (1997). An improved digitonin-collagenase perfusion technique for the isolation of periportal and perivenous hepatocytes from a single rat liver: physiological implications for lobular heterogeneity. *Hepatology* 26, 1592–1599. doi: 10.1002/hep.510260630

Trefts, E., Gannon, M., and Wasserman, D. H. (2017). The liver. *Curr. Biol.* 27, R1147–R1151.

Uchiyama, Y. (1990). Rhythms in morphology and function of hepatocytes. *J. Gastroenterol. Hepatol.* 5, 321–333. doi: 10.1111/j.1440-1746.1990.tb01634.x

van den Brink, S. C., Sage, F., Vértesy, Á, Spanjaard, B., Peterson-Maduro, J., Baron, C. S., et al. (2017). Single-cell sequencing reveals dissociation-induced gene expression in tissue subpopulations. *Nat. Methods* 14, 935–936. doi: 10.1038/nmeth.4437

Van Herck, M. A., Vonghia, L., and Francque, S. M. (2017). Animal models of nonalcoholic fatty liver disease-a starter's guide. *Nutrients* 9:1072. doi: 10.3390/nu9101072

Vickovic, S., Eraslan, G., Salmén, F., Klughammer, J., Stenbeck, L., Schapiro, D., et al. (2019). High-definition spatial transcriptomics for in situ tissue profiling. *Nat. Methods* 16, 987–990. doi: 10.1038/s41592-019-0548-y

Wang, B., Zhao, L., Fish, M., Logan, C. Y., and Nusse, R. (2015). Self-renewing diploid Axin2(+) cells fuel homeostatic renewal of the liver. *Nature* 524, 180–185. doi: 10.1038/nature14863

Wei, Y., Wang, Y. G., Jia, Y., Li, L., Yoon, J., Zhang, S., et al. (2021). Liver homeostasis is maintained by midlobular zone 2 hepatocytes. *Science* 371:6532.

Weigert, R., Porat-Shliom, N., and Amornphimoltham, P. (2013). Imaging cell biology in live animals: ready for prime time. *J. Cell. Biol.* 201, 969–979. doi: 10.1083/jcb.201212130

Wimmer, M., Luttringer, C., and Colombi, M. (1990a). Enzyme activity patterns of phosphoenolpyruvate carboxykinase, pyruvate kinase, glucose-6-phosphate-dehydrogenase and malic enzyme in human liver. *Histochemistry* 93, 409–415. doi: 10.1007/bf00315859

Wimmer, M., Luttringer, C., and Colombi, M. (1990b). The development of the acinar heterotopic pattern of phosphoenolpyruvate carboxykinase activity in the newborn rat. *Histochemistry* 94, 55–59.

Wölfle, D., and Jungermann, K. (1985). Long-term effects of physiological oxygen concentrations on glycolysis and gluconeogenesis in hepatocyte cultures. *Eur. J. Biochem.* 151, 299–303. doi: 10.1111/j.1432-1033.1985.tb09100.x

Wölfle, D., Schmidt, H., and Jungermann, K. (1983). Short-term modulation of glycogen metabolism, glycolysis and gluconeogenesis by physiological oxygen concentrations in hepatocyte cultures. *Eur. J. Biochem.* 135, 405–412. doi: 10.1111/j.1432-1033.1983.tb07667.x

Yang, J., Mowry, L. E., Nejak-Bowen, K. N., Okabe, H., Diegel, C. R., Lang, R. A., et al. (2014). β-catenin signaling in murine liver zonation and regeneration: a Wnt-Wnt situation! *Hepatology* 60, 964–976. doi: 10.1002/hep.27082

Yeh, M. M., and Brunt, E. M. (2014). Pathological features of fatty liver disease. *Gastroenterology* 147, 754–764. doi: 10.1053/j.gastro.2014.07.056

Zajicek, G., Oren, R., and Weinreb, M. Jr. (1985). The streaming liver. *Liver* 5, 293–300. doi: 10.1111/j.1600-0676.1985.tb00252.x

Conflict of Interest: The authors declare that the research was conducted in the absence of any commercial or financial relationships that could be construed as a potential conflict of interest.

Publisher's Note: All claims expressed in this article are solely those of the authors and do not necessarily represent those of their affiliated organizations, or those of the publisher, the editors and the reviewers. Any product that may be evaluated in this article, or claim that may be made by its manufacturer, is not guaranteed or endorsed by the publisher.

Frontiers in Physiology

Understanding how an organism's components work together to maintain a healthy state

The second most-cited physiology journal, promoting a multidisciplinary approach to the physiology of living systems - from the subcellular and molecular domains to the intact organism and its interaction with the environment.

Discover the latest Research Topics

See more →

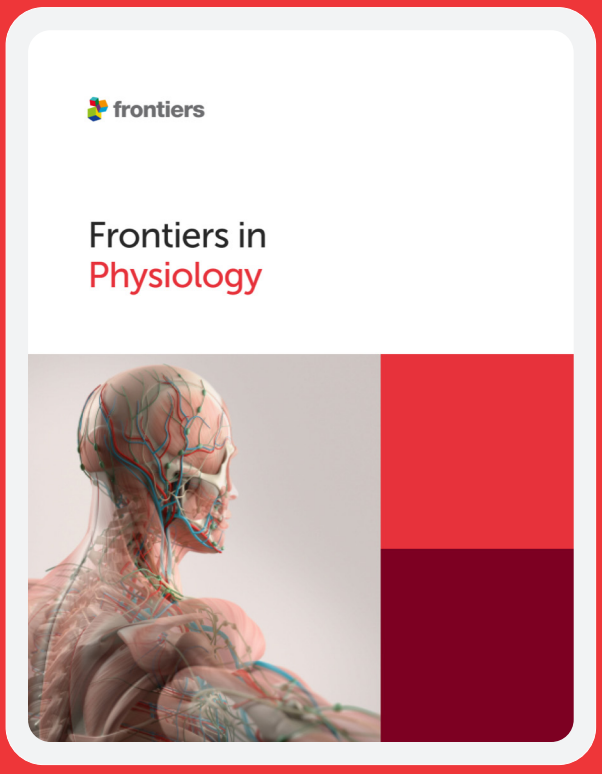

Frontiers

Avenue du Tribunal-Fédéral 34
1005 Lausanne, Switzerland
frontiersin.org

Contact us

+41 (0)21 510 17 00
frontiersin.org/about/contact